SP-1296

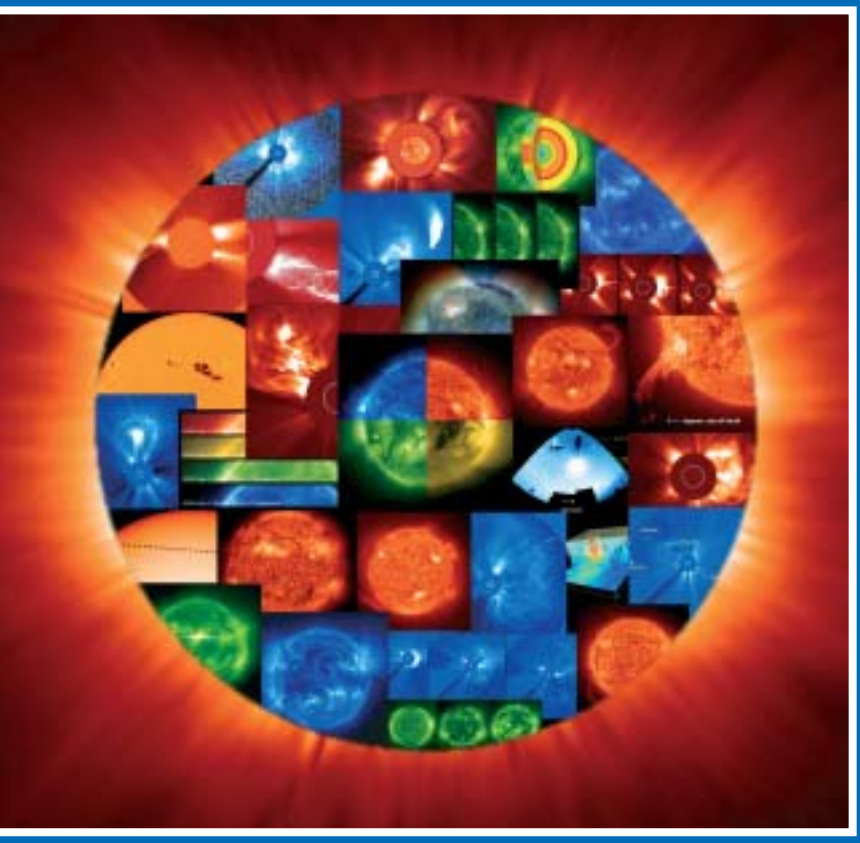

# ESA's Report to the 36th COSPAR Meeting

Beijing, China
July 2006

European Space Agency
Agence spatiale européenne

**SP-1296**
June 2006

# ESA's Report to the 36th COSPAR Meeting

Beijing, China
July 2006

*European Space Agency*
*Agence spatiale européenne*

# Contributors

This report on the scientific missions of the European Space Agency was written by:


| | | | |
|---|---|---|---|
| L. Cacciapuoti | A. Gimenez | P. McNamara | N. Schartel |
| A. Chicarro | F. Jansen | A. Nota | R. Schulz |
| J. Clavel | P. Jakobsen | H. Opgenoorth | G. Schwehm |
| C.P. Escoubet | O. Jennrich | A. Parmar | H. Svedhem |
| F. Favata | J.-P. Lebreton | M. Perryman | J. Tauber |
| B. Foing | D. Macchetto | G. Pilbratt | C. Winkler |
| M. Fridlund | R. Marsden | A. Salama | K. Wirth |



The authors acknowledge the use of published and unpublished material supplied by experimenters, observers and colleagues.

The report was completed on 10 April 2006.


Communications should be addressed to the scientific editor:


R. Marsden
ESA Research and Scientific Support Department
European Space Research and Technology Centre (ESTEC)
Postbus 299
NL-2200 AG Noordwijk
The Netherlands
Tel: +31 71 565-3583
Email: richard.marsden@esa.int


*Cover:*
A collage of the 30 best images from SOHO selected by its scientists, against a backdrop of the solar corona taken by its UVCS instrument. The 10th anniversary of the launch of the highly successful observatory was celebrated in December 2005. (S. Hill, SOHO, NASA/ESA)


Edited by: A. Wilson
Printed in The Netherlands
Published and distributed by: ESA Publications Division
ESTEC, Noordwijk, The Netherlands



ISBN 92-9092-995-2
ISSN 0379-6566
Price: EUR 40

# Contents


1. Introduction . . . . . .1

2. Missions in Operation
   - 2.1 Hubble Space Telescope . . . . . .9
   - 2.2 Ulysses . . . . . .15
   - 2.3 SOHO . . . . . .21
   - 2.4 Cassini/Huygens . . . . . .27
   - 2.5 XMM-Newton . . . . . .35
   - 2.6 Cluster . . . . . .41
   - 2.7 Integral . . . . . .47
   - 2.8 Mars Express . . . . . .55
   - 2.9 SMART-1 . . . . . .61
   - 2.10 Double Star . . . . . .67
   - 2.11 Rosetta . . . . . .69
   - 2.12 Venus Express . . . . . .75

3. Mission in Post-Operations/Archival Phase
   - 3.1 ISO . . . . . .83

4. Projects under Development
   - 4.1 Herschel . . . . . .93
   - 4.2 Planck . . . . . .99
   - 4.3 LISA Pathfinder . . . . . .103
   - 4.4 Gaia . . . . . .107
   - 4.5 JWST . . . . . .111
   - 4.6 BepiColombo . . . . . .115
   - 4.7 Contributions to Nationally-led Missions
     - 4.7.1 COROT . . . . . .119
     - 4.7.2 Microscope . . . . . .120
     - 4.7.3 Akari . . . . . .121
     - 4.7.4 Suzaku . . . . . .121
     - 4.7.5 Solar-B . . . . . .122

5. Missions under Definition
   - 5.1 LISA . . . . . .125
   - 5.2 Solar Orbiter . . . . . .129

6. Missions under Study
   - 6.1 Darwin . . . . . .133
   - 6.2 XEUS . . . . . .137
   - 6.3 ROSITA/Lobster . . . . . .139
   - 6.4 ACES . . . . . .141

Acronyms . . . . . .145

# 1. Introduction

**Table 1.1. ESRO/ESA scientific spacecraft.**

| | *Launch date* | *End of operational life* | *Mission* |
|---|---|---|---|
| *Launched* | | | |
| ESRO-II | 17 May 1968 | 9 May 1971 | Cosmic rays, solar X-rays |
| ESRO-IA | 3 October 1968 | 26 June 1970 | Auroral and polar-cap phenomena, ionosphere |
| HEOS-1 | 5 December 1968 | 28 October 1975 | Interplanetary medium, bow shock |
| ESRO-IB | 1 October 1969 | 23 November 1969 | As ESRO-IA |
| HEOS-2 | 31 January 1972 | 2 August 1974 | Polar magnetosphere, interplanetary medium |
| TD-1 | 12 March 1972 | 4 May 1974 | Astronomy (UV, X- and gamma-ray) |
| ESRO-IV | 26 November 1972 | 15 April 1974 | Neutral atmosphere, ionosphere, auroral particles |
| Cos-B | 9 August 1975 | 25 April 1982 | Gamma-ray astronomy |
| Geos-1 | 20 April 1977 | 23 June 1978 | Dynamics of the magnetosphere |
| ISEE-2 | 22 October 1977 | 26 September 1987 | Sun/Earth relations and magnetosphere |
| IUE | 26 January 1978 | 30 September 1996 | Ultraviolet astronomy |
| Geos-2 | 24 July 1978 | October 1985 | Magnetospheric fields, waves and particles |
| Exosat | 26 May 1983 | 9 April 1986 | X-ray astronomy |
| FSLP | 28 November 1983 | 8 December 1983 | Multi-disciplinary; First Spacelab Payload |
| Giotto | 2 July 1985 | 23 July 1992 | Comet Halley and Comet Grigg-Skjellerup encounters |
| Hipparcos | 8 August 1989 | 15 August 1993 | Astrometry |
| HST | 24 April 1990 | | UV/optical/near-IR astronomy |
| Ulysses | 6 October 1990 | March 2008 | Heliosphere |
| Eureca | 31 July 1992 | 24 June 1993 | Multi-disciplinary |
| ISO | 17 November 1995 | 8 April 1998 | Infrared astronomy |
| SOHO | 2 December 1995 | March 2007 | Sun (including interior) and heliosphere |
| Huygens/Cassini | 15 October 1997 | 14 January 2005 | Titan probe/Saturn orbiter |
| XMM-Newton | 10 December 1999 | March 2010 | X-ray spectroscopy |
| Cluster | 16 July/9 August 2000 | December 2009 | 3-D space plasma investigation |
| Integral | 17 October 2002 | December 2010 | Gamma-ray astronomy |
| Mars Express | 2 June 2003 | 31 October 2007 | Mars exploration |
| SMART-1 | 27 September 2003 | September 2006 | Navigation with solar-electric propulsion |
| Rosetta | 2 March 2004 | December 2015 | Comet rendezvous |
| Venus Express | 9 November 2005 | August 2007 | Venus exploration |
| *Planned launches* | | | |
| Planck | February 2008 | | Cosmic microwave background |
| Herschel | February 2008 | | Far-infrared and submillimetre astronomy |
| LISA Pathfinder | October 2009 | | LISA Technology Package |
| Gaia | 2011 | | Galaxy mapper |
| JWST | 2013 | | Next-generation space telescope |
| BepiColombo | 2013 | | Mission to Mercury |
| LISA | 2015 | | Search for gravitational waves |
| Solar Orbiter | 2015 | | Sun (including polar regions) and inner heliosphere |

# 1. Introduction

The report for the 36th COSPAR Meeting covers, as in previous issues, the missions of the Scientific Programme of ESA in the areas of astronomy, Solar System science and fundamental physics. This year's COSPAR meeting will take place only weeks before the end of the SMART-1 mission to the Moon, a technology project that provided the first European look at our natural satellite from lunar orbit. In October of this year, a new mission will be launched: COROT. ESA, together with a number of countries, is contributing to this unique, French-led project that will provide an insight into the interior of the stars, by means of the asteroseismology technique successfully applied by SOHO. COROT will also perform a systematic search for new extrasolar planets using photometric transits.

The record number of ESA Science Programme missions in operation established at the time of the last report was maintained in 2006 (Huygens having been replaced in the list by Venus Express). Eleven different missions, involving 14 operating spacecraft, are providing excellent science to the worldwide scientific community. The Research and Scientific Support Department (RSSD) is responsible for the science operations of these missions and makes every effort to ensure the best possible science return. The Department also supports the realisation of approved projects in all phases of their development.

Cassini/Huygens arrived at Saturn in June 2004, after having visited Jupiter en route. The release of the European Huygens probe towards the atmosphere of Titan occurred, exactly as planned, at Christmas 2005. Its purpose was to investigate the physical nature of, and conditions at, Titan that were expected to provide important insights into the early evolution of our own atmosphere. The Titan atmospheric descent took place on 14 January 2005, with astonishing results from the probe, including its landing on the surface of a new world.

Since the 35th COSPAR report, a mission has been launched that represents a significant step forward for European participation in the exploration of different bodies of the Solar System. In November 2005, Venus Express was sent on its way to Earth's sister planet; insertion into orbit around Venus took place in April 2006 and scientific operations began. The mission will provide the clues to understand why the planet is so different from Earth, despite being the most similar in mass and size. The atmosphere of Venus will be fully analysed, as will as its structure and dynamics, and some surface features.

In July 2004, the second of the two satellites of the Double Star mission (a cooperative effort between the Chinese National Space Administration and ESA) was launched, completing the polar and equatorial set of spacecraft working together with the European 4-satellite Cluster mission. The scientific results obtained by this constellation have clearly demonstrated the advantages of multi-satellite missions in understanding the physics of the magnetosphere. In the meantime, Cluster's operational life was extended to end-2009, while Double Star's nominal mission will be completed at the end of 2006.

Last year, one of the missions launched during the period of the previous report reached an important milestone. Mars Express, launched from Baikonur in June 2003, has been providing excellent scientific data and astonishing three-dimensional views of the Red Planet. A key instrument, the MARSIS radar, was not brought in operation, however, because of the risk associated with its deployment. After detailed studies and simulations, the antennas were successfully deployed in 2005; the planet's subsurface is now open to exploration by the first European Mars orbiter.

The prime objective of SMART-1, launched in 2003, is to test solar electric propulsion systems for navigating the Solar System. Starting at the end of 2004, however, its path towards lunar orbit has also permitted new observations of the

Moon. As a result, new, close-up views of our neighbour in the Solar System are now available. Unfortunately, the current orbit around the Moon cannot be held forever. Propellant depletion will mark the end of the mission, ending in impact with the lunar surface at the beginning of September 2006. It is planned for this to happen on the visible face of the Moon.

The most recent launch, that of the Japanese Astro-F mission, occurred in February 2006. The project includes significant operational support by ESA, and is open to scientific exploitation by European scientists. Now called Akari, this is an IR astronomical observatory that will pave the way for ESA's Herschel telescope, while complementing ESA's earlier Infrared Space Observatory (ISO) mission.

The next challenge for ESA's Science Programme, in addition to the scientific exploitation of in-orbit missions, is the launch of a number of astronomy missions, including the Herschel sub-mm observatory, and Planck, the explorer of the Cosmic Microwave Background radiation that will provide data of unique quality for understanding the origin of our Universe.

In the meantime, older missions in orbit have continued to provide excellent scientific results. XMM-Newton, launched in 1999, continues to deliver new views of our Universe at X-ray energies, thanks to its large photon-collection capability and throughput. It is well into the phase of routine scientific operations as an observatory, and has proved able to react rapidly to targets of opportunity showing short-lived, high-energy bursts. The operation of XMM-Newton, together with the Integral higher-energy observatory, has proved to be a scientific bonus. Integral also entered routine operations and provided new views of the galactic centre region, as well as close interacting binaries hosting compact objects. The quality of the scientific results obtained with XMM-Newton and Integral is demonstrated by the increasing number of scientific papers being published, and was the main reason for extending their operations into 2010, well beyond their nominal lives.

At lower energies, the Hubble Space Telescope (HST) continues to give exciting results in almost all areas of astronomy, contributing particularly to our understanding of the extragalactic cosmos. The totally unexpected determination, through very distant supernovae, of the acceleration of the expansion of the Universe, is an example. The announcement of the cancellation of a future servicing mission (SM4) to HST during the last reporting period was received as a major setback to the continuation of the mission. Fortunately, the situation was reversed last year. Preparations for SM4, including the installation of two new instruments, are now at an advanced stage.

ESA's missions studying the Sun-Earth connection have also retained their leading role. SOHO, which celebrated its 10th anniversary of launch in December 2005, continues its comprehensive study of the Sun's interior, outer atmosphere and the solar wind, even under the constraints imposed by problems with the high-gain antenna. The four Cluster satellites, together with the Chinese-led Double Star mission, are contributing in a fundamental way to our understanding of the magnetosphere and its connection to the Sun. Ulysses, now in its 16th year, has continued its journey outside the plane of the ecliptic and will fly over the poles of the Sun for a third time in 2007 and 2008. This will enable Ulysses to search for differences in behaviour of the interplanetary medium related to the solar magnetic field reversal that occurred in 2000/2001, and will allow comparison of the measurements during solar minimum concurrent with data from SOHO and Cluster.

Work is continuing on missions in their post-operational phase, i.e. after switch-off of the respective satellites. These activities are aimed at obtaining a full, homogeneous recalibration of the observations and the delivery of a final archive to

the scientific community. In the case of the International Ultraviolet Explorer, the final archive was delivered some time ago and handed over to national organisations. For the ISO, the active archive phase continues to improve the quality and accessibility of the data by improving the previous global pipeline analyses that populated the existing archive. This effort will culminate within the current year.

Concerning missions under development, activities now centre on the preparation of Planck, which will investigate the fine spatial variation of the cosmic background radiation, and Herschel, a powerful far-IR and sub-mm observatory. These satellites are to be launched together in early 2008 and delivered to the L2 Lagrangian point on the Earth-Sun line for their operational phases. LISA Pathfinder, designed to test the technologies for measuring gravitational waves in space, is now planned for launch in late 2009. This delay has, of course, implications for the full development of LISA, which can started at industrial level only be after the tests have been successfully carried out.

Work on the European contribution to the James Webb Space Telescope (JWST) has started at full speed, for delivery in 2010. The development phase at industrial level has been started for Gaia, with a launch in late 2011, and BepiColombo, to be launched in 2013. Gaia will conduct a three-dimensional study of the stellar content of our Galaxy of unprecedented quality, while BepiColombo, in cooperation with the Japanese space agency, will explore the intriguing characteristics of the innermost planet of the solar system, Mercury. Still in its study phase is the LISA gravitational wave observatory (a cooperative project with NASA), as is Solar Orbiter, a mission to study the Sun and inner heliosphere in detail, building on the experience gained with SOHO and Ulysses. Both have planned launch dates no earlier than 2015.

Looking further into the future of ESA's Scientific Programme, a Call for Proposals to the scientific community will soon be issued, following the earlier call for themes. This will form the basis for the definition of the Cosmic Vision plan for the 2015-2025 time period. It is expected that new, exciting proposals will be submitted, a small number of which will be selected for further study, leading to a renewed breadth of ideas and science in the European space science programme beyond Solar Orbiter and LISA.

# 2. Missions in Operation

# 2.1 Hubble Space Telescope

## Introduction

More than a decade after launch, the Hubble Space Telescope (HST) continues to produce excellent scientific results and stunning imagery. In the current cycle, 70% of HST observations use the third-generation Advanced Camera for Surveys (ACS), installed in April 2002. It consists of three independent cameras that provide wide-field, high-resolution and UV imaging, respectively, with a broad assortment of filters designed to address a wide range of scientific goals. Other active instruments are the Near-IR Camera and Multi-Object Spectrometer (NICMOS), the Wide Field Planetary Camera 2 (WFPC2) and the Fine Guidance Sensors (FGS). They are all performing nominally. Unfortunately, the Space Telescope Imaging Spectrograph (STIS), the only spectrograph on HST, ceased operating in August 2004.

Observations with HST have had an impact on every area of astronomical research. A few highlights of the results obtained during 2005 are presented here.

## Science achievements

**Star formation in the Milky Way**

One of the most stunning images delivered by HST in 2005 was the high-resolution map of the Orion Nebula (Fig. 2.1.1). This turbulent star-formation region is one of astronomy's most dramatic and photogenic celestial objects. Observations were carried out between September 2004 and May 2005, using 105 HST orbits. Astronomers used all of HST's cameras (ACS, WFPC2 and NICMOS-Camera 3) in parallel to observe a field 1/6th of a square degree, almost centred on the Trapezium stars. The survey covers this cornerstone region with unprecedented sensitivity (24 mag), dynamic range (~12 mag), spatial resolution (50 mas), and wide spectral coverage (9 filters from $U$ to $H$). A full resolution (3.3 x 3.6 $10^4$ pixels) colour mosaic was obtained from the combination of 520 ACS images, creating the largest HST picture ever produced.

The image reveals a tapestry of star formation, from the dense pillars of gas and dust that may be the homes of fledgling stars, to the hot, young, massive stars that have emerged from their gas-and-dust cocoons and are shaping the nebula with their powerful UV light. Because of its proximity, the Orion Nebula is a perfect laboratory for studying how stars are born. The data reveal for the first time a rich population of young substellar objects (brown dwarfs) at visible wavelengths, allowing their circumstellar discs, envelopes and occasionally their multiple nature to be resolved. The photometric database and the atlas of non-stellar objects are in preparation. The stellar photometry of the cluster, which spans a factor of $10^4$ in mass (from 40 solar masses to a few Jupiter masses) will provide the richest, most accurate and unbiased dataset of stellar parameters for pre-main-sequence objects ever obtained.

**Star formation in a neighbouring galaxy: the Small Magellanic Cloud**

The Small Magellanic Cloud's (SMC) subsolar present-day metallicity ($Z = 0.004$) makes it the best empirical laboratory to study star formation and evolution in an environment that most closely resembles the early Universe. Its proximity readily permits in-depth studies of its resolved stellar content with the HST. The SMC is characterised by a dust-to-gas mass ratio that is 30 times lower than that of the Milky Way. The combination of low metallicity and low dust content could influence the star-formation process. How does this environment affect the process for lower-mass star formation, given that the intense radiation field is much harsher than in the Milky Way? This question can only be answered by a systematic study of star formation in the SMC and a detailed comparison of its star formation properties with those of the Milky Way.

From HST/ACS deep $V$, $I$ and Hα images, astronomers have discovered pre-main

*For further information, see http://ecf.hq.eso.org/*

**Figure 2.1.1. HST colour composite map of the Orion Nebula.**

sequence populations in two young clusters of the SMC: NGC 346 (Fig. 2.1.2) and NGC 602 (Fig. 2.1.3). NGC 346 is the largest, most massive HII region in the SMC, and is considered to be an archetype of massive star formation in low-metallicity dwarf galaxies. It contains more than half of the known O stars in the SMC and associated CO clouds. NGC 602 is an extremely young cluster in the relatively isolated wing of the SMC, where the gas and stellar content are lower. The low-mass stars in NGC 346 have likely formed together with the cluster ~3–5 Myr ago, but have not yet reached the main sequence. Their magnitudes and colours are those of pre-main sequence stars in the mass range 0.6–3 $M_{Sun}$, mostly concentrated in the main cluster, but with secondary subclusters spread over a larger region. These subclusters appear to be spatially coincident with previously known knots of molecular gas identified in ground-based and ISO observations.

**Understanding the ages of galaxies**

SBS 1415+437 is a metal-poor ($Z \sim 1/11\ Z_{Sun}$) star-forming dwarf galaxy, regarded as a very young system in the nearby Universe that started to form stars less than 100 Myr ago. The presumed 'youth' of this galaxy is in contrast with the classical picture that dwarf galaxies are the first systems to collapse in an hierarchical scenario of galaxy formation, and supports the view that star formation in such systems may have been inhibited until the present epoch (for example, owing to ionisation).

**Figure 2.1.2. HST *V*, *I* colour composite image of the star-forming region NGC 346 in the Small Magellanic Cloud.**

**Figure 2.1.3. HST *V*, *I*, Hα colour composite image of the star-forming region NGC 602 in the Small Magellanic Cloud.**

**Figure 2.1.4. HST true-colour composite image of SBS 1415+437. North is at about –14.6º from horizontal.**

The most direct way to infer the age of a nearby galaxy is to resolve it into individual stars and study the colour-magnitude diagram. The red giant branch (RGB) sequence, formed by evolved stars with ages in excess of ~1 Gyr, is of particular interest. An unambiguous RGB detection implies that star formation was already active more than a Gyr ago, whereas absence of the RGB indicates that the system has started to form stars only recently. While SBS 1415+437 has already been resolved with HST/WFPC2 (but only the brightest young stars have been detected owing to the relatively short integration times of the observations), a new deep HST/ACS imaging study of this system (Fig. 2.1.4) found for the first time clear evidence of a conspicuous RGB stellar population (Fig. 2.1.5). While the brightness of the RGB tip in the new *I* versus *V-I* colour-magnitude diagram, yields a distance ~13.6 Mpc, the colour of the RGB implies that its stars must be older than ~1.3 Gyr, with the exact age depending on the assumed metallicity and dust extinction. The number of RGB stars also suggests that most of the stellar mass resides in this evolved population. In view of these and other HST results for metal-poor galaxies, it seems that the local Universe simply may not contain any galaxies that are currently undergoing their first burst of star formation.

**A very massive and evolved galaxy in the early Universe: a crisis in cosmology?**
A major aim of observational cosmology is to understand how and when stars are formed and how they assemble into galaxies. These questions are intimately related to the question of how the Universe became transparent to radiation; that is, how the vast amounts of gas residing between galaxies first became ionised. In order to pursue these aims, it is necessary to study the light from the first stars and galaxies at the very early stages of the evolution of the Universe, when visible light is shifted by the expansion of the Universe into IR and longer wavelengths. Recent developments have allowed us to push these types of studies to epochs when the Universe was only a fraction of its present age.

Recently, HST acquired the deepest images of the Universe ever made at optical and near-IR wavelengths, the Hubble Ultra Deep Field (HUDF). This is located

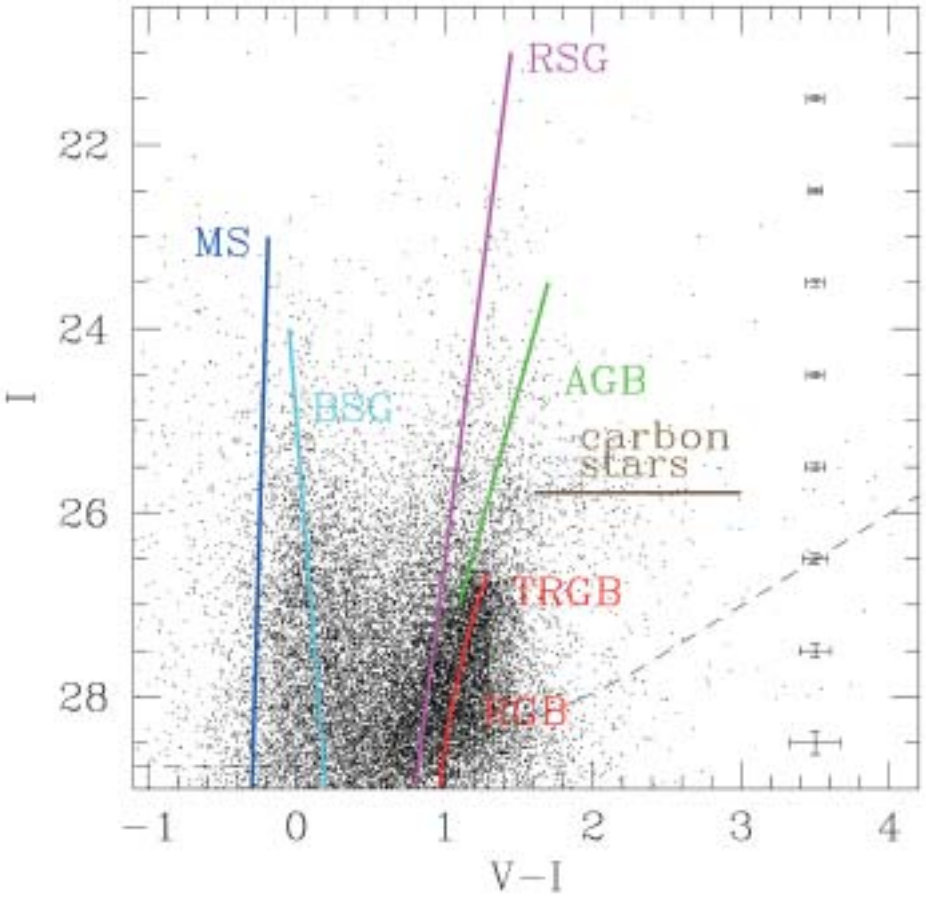


**Figure 2.1.5.** ***I*** **vs.** ***V-I*** **colour-magnitude diagram of the resolved stellar population of SBS 1415+437. The data are corrected for foreground extinction but not for possible internal extinction. The median photometric random error as a function of** ***I*****-band magnitude is indicated on the right. The dashed curve provides an estimate of the 50% completeness level. The detection of a red giant branch at** $I \sim 26.7$ **clearly reveals the presence of stars older than 1 Gyr. The main evolutionary sequences seen in the data are indicated in an approximate sense as coloured straight lines: main sequence (MS), blue supergiants (BSG), red supergiants (RSG), the red giant branch (RGB) with its tip (TRGB), the asymptotic giant branch (AGB), and carbon stars (AGB stars in which carbon has been dredged up to the surface).**

within the area covered by the Great Observatories Origins Deep Survey (GOODS), for which mid- and far-IR observations (3.6–8.0 $\mu$m) with the Spitzer Space Telescope are also available. Among approximately 10 000 galaxies detected in the HUDF, an extremely massive galaxy was found that is believed to be about as far away as the most distant galaxies and quasars now known.

The light reaching us today began its journey when the Universe was only about 800 million years old. ACS does not see the galaxy at all, despite the fact that the HUDF is the deepest image ever taken in optical light. This indicates that the galaxy's blue light has been absorbed by traveling billions of light-years through intervening hydrogen gas. The galaxy was detected using NICMOS, and also with an IR camera on the Very Large Telescope (VLT) at the European Southern Observatory, but at those wavelengths it is very faint and red (Fig. 2.1.6). However, the galaxy was found to be very bright at the longer wavelengths covered by Spitzer. At these wavelengths, light originates from older, redder stars that should make up most of the mass in a galaxy, and the brightness of the galaxy suggests that it is indeed quite massive. By combining the multi-wavelength information provided by HST, Spitzer and VLT, a stellar mass of $6 \times 10^{11}$ $M_{Sun}$ is calculated for this galaxy, at redshift $z = 6.5$, 800 Myr after the Big Bang.

Most galaxies are expected to have been built by the mergers of smaller galaxies. However, the discovery of this object suggests that at least a few galaxies formed

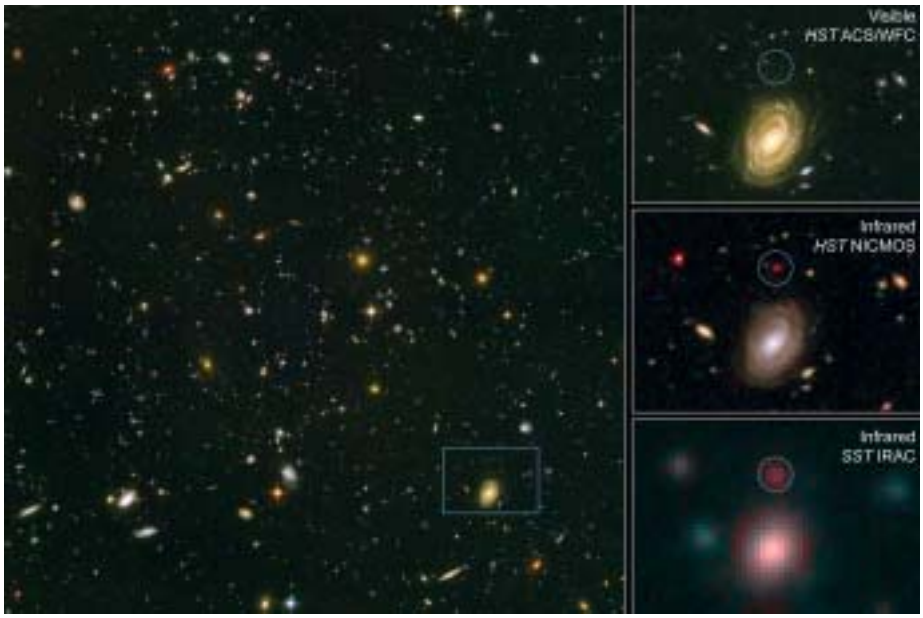


**Figure 2.1.6. Images of the massive galaxy at $z = 6.5$ from observations with HST ($B$, $V$, $I$, $z$), HST/NICMOS ($J$, $H$) VLT/ISAAC ($K$) and Spitzer (3.6–8.0 $\mu$m).**

rapidly (and in their entirety) long ago, as some older theories of 'monolithic' galaxy formation have suggested. For such a large galaxy, this would have been a tremendously explosive event, and the energy from the rapid emergence of those stars would have helped to reheat the Universe very shortly after it cooled following the Big Bang. This early epoch (the first 5% of the Universe's age) is fertile ground awaiting the James Webb Space Telescope, which will have the IR sensitivity possibly to look all the way back to the very first stars that ignited after the Big Bang.

# 2.2 Ulysses

## Introduction

Ulysses is an exploratory mission being carried out jointly by ESA and NASA. Its primary objective is to characterise the uncharted high-latitude regions of the heliosphere within 5 AU of the Sun, under a wide range of solar activity conditions. Ulysses has, for the first time, permitted *in situ* measurements to be made away from the plane of the ecliptic and over the poles of the Sun. Its unique trajectory (Fig. 2.2.1) has taken the spacecraft into the unexplored third dimension of the heliosphere.

The European contribution to the Ulysses programme consists of the provision and operation of the spacecraft and about half of the experiments. NASA provided the launch aboard Space Shuttle Discovery (together with the upper stage) and the spacecraft power generator, and is responsible for the remaining experiments. NASA also supports the mission using its Deep Space Network (DSN).

The broad range of phenomena being studied by Ulysses includes the solar wind, the heliospheric magnetic field, solar radio bursts and plasma waves, solar and interplanetary energetic particles, galactic cosmic rays, interstellar neutral gas, cosmic dust and gamma-ray bursts. A summary of the nine sets of instruments is presented in Table 2.2.1.

While the main focus of the mission is clearly the heliosphere and its variations in time and space, the investigations cover a wider range of scientific interest. Examples include studies related to Jupiter's magnetosphere (both *in situ* and via remote sensing), and radio-science investigations into the structure of the corona and a search for gravitational waves using the spacecraft and ground telecommunication systems. A major theme for Ulysses is the nature of the Local Interstellar Medium and its interface with the heliosphere; the mission continues to provide important contributions to our knowledge in this area, and to topics of a broad astrophysical nature.

In addition to the science teams selected at the start of the project, the group of

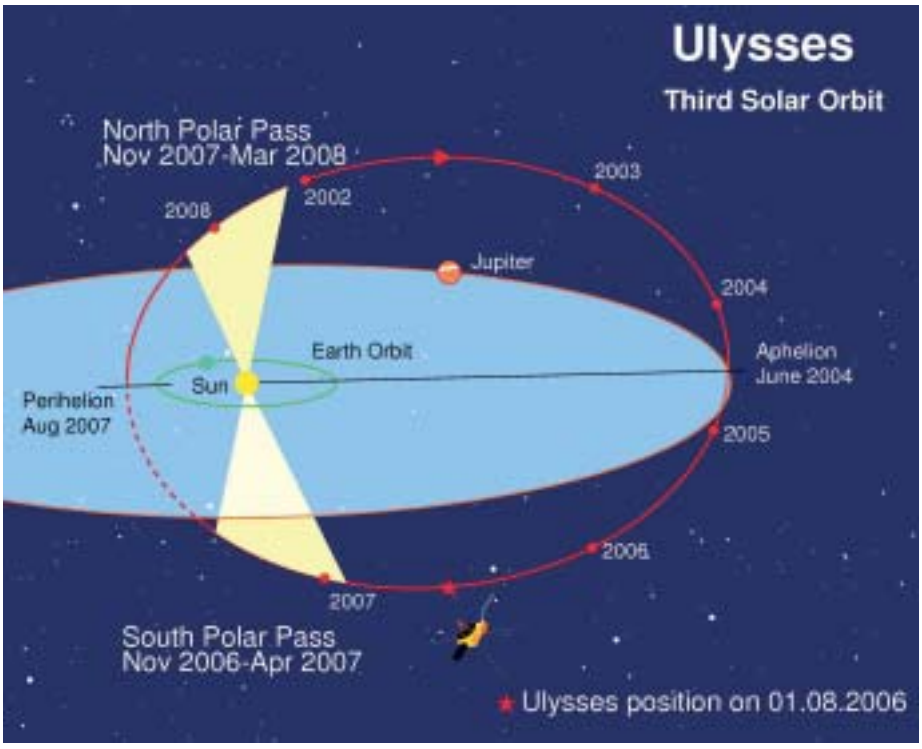


**Figure 2.2.1. The Ulysses orbit viewed from 15 deg above the ecliptic plane. Dots mark the start of each year.**

*For further information, see http://helio2.estec.esa.int/ulysses/*

**Table 2.2.1. The Ulysses scientific payload.**

| *Expt. Code* | *Investigation* | *Scientific Acronym* | *Principal Investigator* | *Collaborating Institutes* |
|---|---|---|---|---|
| HED | Magnetic field | VHM/FGM | A. Balogh, Imperial College London (UK) | JPL (USA) |
| BAM | Solar wind plasma | SWOOPS | D.J. McComas, Southwest Research Institute (USA) | Los Alamos National Lab (USA): Ames Research Center (USA); JPL (USA); HAO Boulder (USA): Univ of Boston (USA); MSFC (USA); MPS Lindau (D) |
| GLG | Solar wind ion composition | SWICS | J. Geiss, ISSI (CH); G. Gloeckler, Univ of Maryland (USA) | Univ of New Hampshire (USA); GSFC (USA); TU Braunschweig (D); MPS Lindau (D); Univ of Michigan (USA) |
| STO | Unified radio and plasma waves | URAP | R.J. MacDowall, GSFC (USA) | Obs de Paris Meudon (F); Univ of Minnesota (USA); CETP Velizy (F) |
| KEP | Energetic particles and interstellar neutral gas | EPAC/GAS | N. Krupp, MPS Lindau (D) | Imperial College (UK); Swedish Inst Space Physics Kiruna & Umeå (S); Aerospace Corp (USA); Univ of Bonn (D); MPE Garching (D); Polish Acad Sciences (P) |
| LAN | Low-energy ions and electrons | HI-SCALE | L.J. Lanzerotti, Bell Laboratories (USA) | APL Laurel (USA); UC Berkeley (USA); Univ of Kansas (USA); Obs de Paris Meudon (F): Univ of Thrace (Gr); Univ of Birmingham (UK) |
| SIM | Cosmic rays and solar particles | COSPIN | R.B. McKibben, Univ of New Hampshire (USA) | Imperial College (UK); ESA Research & Scientific Support Dept (NL); NRC Ottawa (Can); Univ of Kiel (D); CEN Saclay (F); Danish Space Research Inst (DK); NCR Milan (I); MPK Heidelberg (D); Univ of Maryland (USA); MPS Lindau (D) |
| HUS | Solar X-ray and cosmic gamma-ray bursts | GRB | K. Hurley, UC Berkeley (USA) M. Sommer (retired), Samerberg (D) | CESR Toulouse (F); SRON Utrecht (NL); Obs de Paris Meudon (F); GSFC (USA) |
| GRU | Cosmic dust | DUST | H. Krüger, MPS Lindau (D) | Univ of Canterbury (UK); ESA RSSD (NL); MPE Garching (D); JSC (USA); Univ of Florida (USA); MPK Heidelberg (D) |

scientists directly associated with the mission comprises nine European Guest Investigator (GI) teams, a number of NASA GIs, and the European Interdisciplinary Investigators who were selected together with the hardware teams.

## Mission status

The spacecraft was launched by the Space Shuttle on 6 October 1990, using a combined IUS/PAM-S upper-stage to inject it into a direct Earth/Jupiter transfer orbit. A gravity-assist manoeuvre at Jupiter in February 1992 placed Ulysses in its final

**Table 2.2.2. Key dates in the Ulysses mission.**

| *Event* | *Date* |
|---|---|
| Launch | 1990 10 06 |
| Jupiter flyby | 1992 02 08 |
| start | 1994 06 26 |
| maximum latitude (80.2°, 2.3 AU) | 1994 09 13 |
| end | 1994 11 05 |
| 1st Perihelion (1.34 AU) | 1995 03 12 |
| 2nd Polar Pass (north) | |
| start | 1995 06 19 |
| maximum latitude (80.2°, 2.0 AU) | 1995 07 31 |
| end | 1995 09 29 |
| Start of Solar Maximum Mission | 1995 10 01 |
| Aphelion (5.40 AU) | 1998 04 17 |
| 3rd Polar Pass (south) | |
| start | 2000 09 06 |
| maximum latitude (80.2°, 2.3 AU) | 2000 11 27 |
| end | 2001 01 16 |
| 2nd Perihelion (1.34 AU) | 2001 05 23 |
| 4th Polar Pass (north) | |
| start | 2001 08 31 |
| maximum latitude (80.2°, 2.0 AU) | 2001 10 13 |
| end | 2001 12 12 |
| Jupiter approach (0.8 AU) | 2004 02 04 |
| Aphelion | 2004 06 30 |
| 5th Polar Pass (south) | |
| start | 2006 11 17 |
| maximum latitude | 2007 02 07 |
| end | 2007 04 03 |
| 3rd Perihelion | 2007 08 18 |
| 6th Polar Pass (north) | |
| start | 2007 11 30 |
| maximum latitude | 2008 01 11 |
| end | 2008 03 15 |
| End of Mission | 2008 03 15 |

Sun-centred out-of-ecliptic orbit, which has a perihelion distance of 1.3 AU and an aphelion of 5.4 AU. The orbital period is 6.2 years. Key mission milestones, including details of the polar passes (defined to be the parts of the trajectory when the spacecraft is above 70° heliographic latitude in either hemisphere), are presented in Table 2.2.2.

The mission celebrated its 15th launch anniversary in October 2005, and all spacecraft systems and the nine sets of scientific instruments continue to function well. Spacecraft operations, conducted by the joint ESA-NASA Mission Operations Team at JPL have proceeded in a highly efficient and productive way, with no anomalies during the reporting period. Data coverage over the mission lifetime to date is an impressive 97%. The payload power-sharing strategy introduced in May 2002 to cope with the decreasing output of the Radioisotope Thermoelectric Generator (RTG) that provides onboard power has continued, albeit with a further restriction. Starting in October 2004, a fixed 'core payload' configuration (measuring magnetic field, solar wind ions, energetic particles and cosmic rays, radio waves and dust) was introduced. This configuration was chosen on scientific grounds, and because it provided the best compromise from the thermal and power standpoints. A fixed configuration was deemed necessary in order to avoid thermal and power transients at a time when critical areas of the spacecraft were colder than at any time in the mission to date. Maintaining the hydrazine fuel above its freezing point has been a high operational priority during the reporting period. This approach minimised both the risk to the spacecraft, and the impact on the scientific output of the mission. More flexible payload operations will be possible again starting in 2007, when Ulysses is close enough to the Sun that the Cold-Case Heater that warms the equipment platform is no longer required. It is anticipated that sufficient power will be available to operate the full payload complement during the majority of the third polar passes. Currently, the spacecraft continues its climb to high southern latitudes as it moves closer to the Sun, and will reach 50° south by mid-2006.

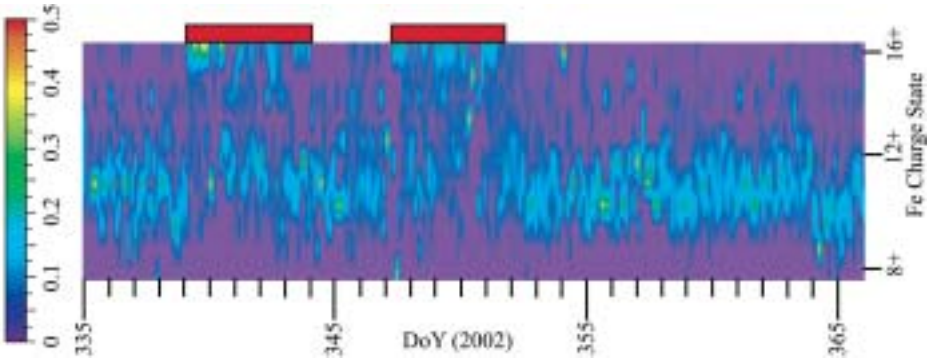


**Figure 2.2.2. Iron charge state vs. day-of-year (DOY) from Ulysses/SWICS, normalised to a total flux of unity for each data sample. The normal solar wind charge state is ~10–11. The red bars at the top draw attention to intervals of unusually large enhancements in the high iron charge state $Fe^{16+}$. (Courtesy S.T. Suess)**

In February 2004, the SPC agreed to extend the mission until March 2008. This third extension will enable the spacecraft to complete a third set of polar passes. On the NASA side, the 2005 Sun-Solar System Connections (S3C) Senior Review Panel also recommended that Ulysses be funded through its return to the north solar pole in 2008.

## Scientific highlights

The unique perspective offered by Ulysses' orbit naturally lends itself to multi-spacecraft studies of transient solar wind features. Examples are the SOHO-Ulysses 'quadrature' campaigns conducted when Ulysses is positioned off the solar limb as seen from Earth. Remote-sensing observations from SOHO can then be used to track disturbances leaving the Sun in the direction of Ulysses, and the *in situ* measurements at Ulysses reveal the evolution of these structures as they travel outwards in the heliosphere. A prerequisite is the ability to identify the same parcel of plasma at both locations. The quadrature campaign in November 2002, at which time Ulysses was at 4.3 AU and 27°N off the west limb of the Sun, was particularly successful. For the first time, it was possible to identify the same very hot plasma remotely at the Sun with SOHO and *in situ* at Ulysses. Four large coronal mass ejections (CMEs) were observed by SOHO leaving the Sun in the general direction of Ulysses over a period of several days at the end of November. By the time they reached Ulysses some 15 days later, the interplanetary counterparts of these CMEs (ICMEs) had apparently merged to form a single large solar wind structure that drove a strong interplanetary shock. The plasma of this merged structure contained unusually large enhancements in highly ionised iron ions (charge state $Fe^{16+}$), indicating a high-temperature source (Fig. 2.2.2). Such high-charge states are often seen in the solar wind and have been identified with ICMEs. The data from SOHO/UVCS also showed high Fe charge states, in particular in the aftermath of the 26 November 2002 CME. In this case, it was very hot plasma at 6-10x$10^6$K that was apparently produced high in the solar atmosphere, above 1.5 solar radii. The most likely source of such hot plasma was a reconnection event occurring in post-flare loops.

The major episode of solar activity in October/November 2003 (dubbed the 'Halloween' events) appeared to be the last in the present sunspot cycle. This proved not to be the case, however. In January and September 2005 the Sun, although rapidly approaching solar minimum, again produced displays of major activity. The latter period included one of the largest solar flares of cycle 23, an X17+ flare on 7 September, occurring as the active region responsible rotated into view of the Earth on the Sun's east limb. A very large and very fast CME was also associated with this

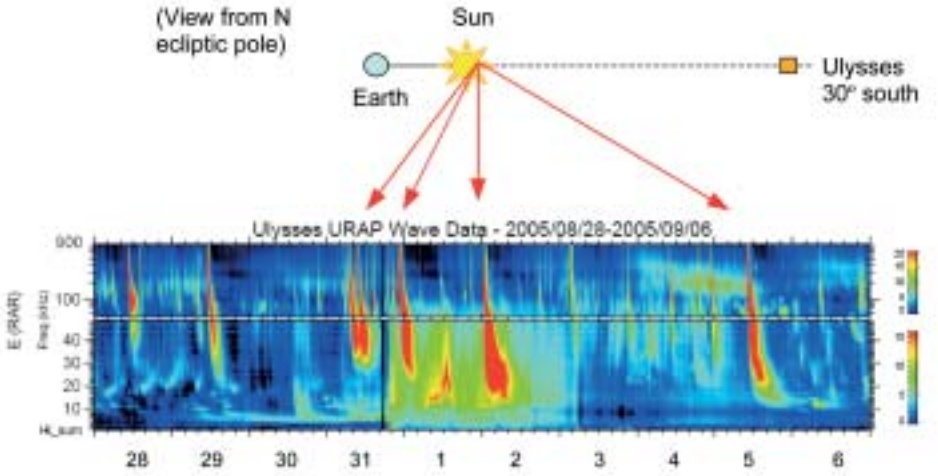


**Figure 2.2.3. Radio bursts from Active Region 10808, detected aboard Ulysses by URAP in August/September 2005. (Courtesy R.J. MacDowall)**

flare. At the time, Ulysses was positioned almost directly behind the Sun as seen from Earth, at 30ºS latitude and 4.8 AU from the Sun (Fig. 2.2.3). This geometry provided Ulysses with a unique view of the source of the activity for several days prior to its appearance on the visible (from Earth) solar disc. Based on observations from the Ulysses radio experiment, it is likely that region 10808 produced at least four intense flares while on the far side as viewed from Earth. The X17+ flare produced an unusually intense radio burst observed by Ulysses, and a shock was observed *in situ* at Ulysses on 14 September. Assuming the shock was driven by the disturbance associated with the X17+ flare, this implies a transit velocity of ~1210 km/s over a distance of almost 5 AU! The radio bursts associated with some of the X-class flares occurring after the X17+ flare had surprisingly low intensities. This is consistent with what was seen for the 2003 Halloween events. A possible explanation is that the entire inner heliosphere was filled with energetic electrons to a flux level sufficient to block the plasma instability that would otherwise initiate the radio emission process.

Like water droplets from a rotating garden sprinkler, the magnetic field carried away from the rotating Sun by the radially out-flowing solar wind is on average wound into a spiral pattern (an Archimedean spiral) in the heliosphere. A recurring theme in many of the results obtained by Ulysses, however, is the unexpectedly large degree to which the instantaneous heliospheric magnetic field direction measured at the spacecraft deviates from this pattern. Theories exist to explain such systematic deviations from the spiral pattern, but these require radial distances of several AU for a deviation of order 1 AU to develop. Observations of 'jets' of energetic electrons from Jupiter's magnetosphere, acquired by Ulysses during its distant encounter with the planet in 2003/2004, show that such deviations are common within a radial interval of as little as 0.1 AU, however. Electron jets were discovered during Ulysses' first Jupiter flyby in 1992, and were identified as brief (lasting minutes to hours), highly focused bursts of MeV electrons flowing away from Jupiter along the heliospheric magnetic field. Jets were observed up to distances of 1 AU from Jupiter and were interpreted as evidence for direct magnetic connection to Jupiter's magnetosphere. In the recent cases, the position of Ulysses relative to Jupiter was such that magnetic connection along the average spiral field could not have occurred, implying large deviations. If such large deviations are indeed common, they may play a significant role in the distribution of charged particles throughout the heliosphere.

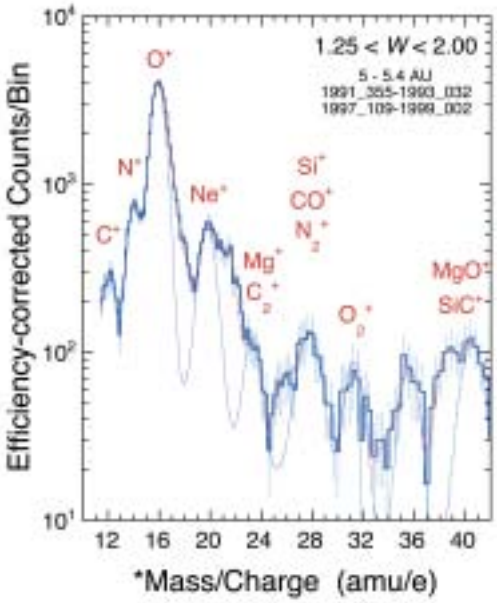


**Figure 2.2.4. Spectrum of 'inner-source' pick-up ions measured by Ulysses/SWICS. (Courtesy G. Gloeckler)**

It is not yet clear how or why such large-scale deviations develop, whether they are consistently present throughout the solar cycle, or how they can be incorporated into current theories of particle propagation.

Another topic of continuing interest, and one to which Ulysses is making unique contributions, is the study of 'inner-source' pick-up ions (Fig. 2.2.4). In contrast to pick-up ions of interstellar origin (created through ionisation of neutral interstellar gas that penetrates the heliosphere), the precise origin of the inner-source ions remains uncertain. Among the possible candidates are neutral solar wind atoms that are implanted in, and subsequently released from, dust grains close to the Sun. The composition of the inner source is certainly not cometary in nature, making Sun-grazing comets, for example, an unlikely progenitor. Ulysses measurements have demonstrated clearly that the population of inner-source ions extends out as far as the orbit of Jupiter, suggesting that several different sources may be contributing. In addition to the intrinsic interest in these ions, they also form a potentially important seed population for injection into shock acceleration processes that give rise to fluxes of energetic particles of non-solar origin found throughout the heliosphere.

## Ulysses data archive

Data from the Ulysses investigations and flight project are being archived and made accessible to the public through two channels: the ESA Ulysses Data Archive at ESTEC, and NASA's National Space Science Data Center (NSSDC). There is no formal proprietary period for Ulysses data, which are placed in the public archives immediately following verification by the PI teams. The ESA archive provides a number of on-line facilities to browse and download selected measurements made by the scientific instruments. The user is able to view 26-day and 1-year summary plots of the main parameters measured, and (if of interest) download ASCII data files and accompanying documentation for further analysis. A new plotting tool was introduced in 2005 that allows the user flexibility in defining start and end times and provides the capability to combine parameters from different experiments on the same plot. The ESA archive is accessible via the Ulysses homepage.

# 2.3 SOHO

## Introduction

Since its launch on 2 December 1995, the joint ESA/NASA SOHO mission has provided a wealth of information about the Sun, from its interior, through the hot and dynamic atmosphere, to the solar wind and its interaction with the interstellar medium. Research using SOHO observations has revolutionised our understanding of the Sun, and science teams from around the world have made great strides towards a better understanding of 'the big three' areas of research that SOHO set out to tackle: the structure and dynamics of the solar interior, the heating of the solar corona, and the acceleration of the solar wind. The findings have been documented in an impressive and growing body of scientific literature and popular articles. SOHO enjoys a remarkable 'market share' in the worldwide solar physics community, with over 2400 papers in refereed journals, representing the work of over 2300 scientists. At the same time, SOHO's easily accessible, spectacular data and basic science results have captured the imagination of the space science community and the general public alike.

SOHO's 12 instruments, which represent the most comprehensive set of solar and heliospheric instruments ever developed and carried on the same platform, are summarised in Table 2.3.1.

## Mission status

SOHO was launched by an Atlas IIAS from Cape Canaveral on 2 December 1995, and inserted into its halo orbit around the L1 Lagrangian point on 14 February 1996, 6 weeks ahead of schedule. A 5-year extension of the mission, to March 2003, was approved in 1997. A further extension until March 2007 was approved by ESA's SPC in February 2002, and a third extension until December 2009 is being considered.

Since June 2003, the east-west pointing mechanism of SOHO's high-gain antenna (HGA) has been parked. As a result, 'keyhole' periods of limited telemetry for 2-3 weeks occur every 3 months (half orbit). During the keyholes, data can be transmitted only through SOHO's low-gain antenna using the larger (and highly competed for) 34 m and 70 m DSN stations. To ensure continuity of the helioseismology and total solar irradiance data during long coverage holes, a Central On-Board Software patch was developed to make more efficient use of the solid-state recorder (SSR) by selectively recording only certain packets. The patch increases the nominal recording capacity of the SSR from 11 h to nearly 70 h of helioseismology and total solar irradiance data from GOLF, VIRGO and MDI, and to over 230 h if the medium bandwidth helioseismology (MDI) is excluded. The patch was uplinked and tested in September 2004 and has been used ever since with great success. VIRGO, GOLF and MDI low-bandwidth data were captured continuously throughout all subsequent keyholes, and LASCO and CELIAS telemetry was also recorded for most parts of the keyholes.

## Operations

The SOHO Experiment Operations Facility (EOF), located at NASA's Goddard Space Flight Center (GSFC), serves as the focal point for mission science planning and instrument operations. There, the experiment teams receive real-time and playback telemetry, process these data to determine instrument commands, and send commands directly from their workstations through the ground system to their instruments, both in near real-time and on a delayed execution basis.

From the very beginning of the mission, much of SOHO's observing time has been devoted to coordinated campaigns. As of the end of January 2006, the campaign database listed a total of 1142 coordinated campaigns. Of these, 373 involved ground-based observatories, 110 Yohkoh and 442 TRACE. On average, for more than 20 h

*For further information, see http://soho.estec.esa.nl*

per day during the last 2 years one or more instruments were explicitly collaborating with another instrument or observatory. In addition, the regular observing programmes of, for example, EIT and LASCO are designed to maximise the usefulness of both data sets taken together.

## 10 years of SOHO

On 2 December 2005 SOHO celebrated its 10th launch anniversary. The impressive statistics from SOHO's first decade include:

- 140 PhD theses were written using SOHO data;
- 289 scientific meetings on subjects related to SOHO were held;
- 944 news stories appeared on the SOHO Newsroom pages (recorded only between 1997 and 2005!);
- 1000 comets were found. SOHO is the most prolific comet-finder observatory of all time, and has identified almost half of all comets for which an orbit determination has been made;
- 2400 reviewed papers using SOHO data were published;
- about 2300 scientists appear in the author lists of those papers (every current solar scientist has had the chance to work with SOHO data);
- 3230 science planning meetings were held;
- 2 million command blocks were sent to the spacecraft by the ground system;
- 5 million distinct files were served by the web server;
- almost 10 million exposures were made by CDS;
- 16 million distinct hosts were served by the web server;
- 100 million exposures were taken by MDI;
- 266 million web page requests were served;
- 16 Tb of data are in the SOHO archive (including MDI data at Stanford);
- 85 Tb of web pages/data were downloaded from the SOHO archive at GSFC;
- 114 Tb of web pages/data were served over the internet, including the Stanford MDI archive. The total amount of data given to users is considerably higher when offline requests are accounted for.

## Scientific highlights

Polarisation analysis of single-view LASCO images has produced the first 3-D reconstructions of coronal mass ejections (CMEs; Fig. 2.3.1). The scattering point's distance from the plane-of-the-sky is determined by the ratio of polarised-to-unpolarised electron scattered emission. From the brightness ratio, the 3-D structure, position and velocity could be computed for several CMEs.

The SUMER team has presented a spectral atlas of solar coronal features (coronal holes, quiet corona, active corona and flares), covering the wavelength range 670-1609 Å and complementing the SUMER spectral atlas of solar disc features. It comprises 504 lines, 300 (60%) of which have been identified. The published line intensities provide a rich source for probing electron densities, electron temperatures, opacities and elemental abundances of the upper solar atmosphere. It also presents a powerful tool for the design of future instruments and the planning of future observations.

Active region NOAA 10720 (Fig. 2.3.2) turned out to be one of the most flaring regions of the last few years, with 15 M-class and five X-class flares during 14-22 January 2005. The energetic particle event associated with the X7.1 flare on 20 January was the strongest radiation storm since October 1989, based on the flux level of the highest-energy protons (>100 MeV). This event was covered in near real-

**Table 2.3.1. Instruments in the SOHO payload.**

| *Investigation* | *Principal Investigator* | *Collaborating Countries* | *Measurements* | *Technique* |
|---|---|---|---|---|
| *Helioseismology* | | | | |
| Global Oscillations at Low Frequencies (GOLF) | A. Gabriel, IAS, Orsay, F | F, ESA, DK, D, CH, UK, NL, E, USA | Global Sun velocity oscillations ($l$=0-3) | Na-vapour resonant scattering cell, Doppler shift and circular polarisation |
| Variability of solar IRradiance and Gravity Oscillations (VIRGO) | C. Fröhlich, PMOD/WRC, Davos, CH | CH, N, F, B, ESA, E | Low-degree ($l$=0-7) irradiance oscillations and solar constant | Global Sun and low-resolution (12-pixel) imaging and active cavity radiometers |
| Michelson Doppler Imager (MDI) | P.H. Scherrer, Stanford Univ, California, USA | USA, DK, UK | Velocity oscillations high-degree modes (up to $l$=4500) | Doppler shift with Fourier tachometer, 4 and 1.3 arcsec resolution |
| *Solar Atmosphere Remote Sensing* | | | | |
| Solar UV Measurements of Emitted Radiation (SUMER) | W. Curdt, MPAe, Lindau, D | D, F, CH, USA | Plasma flow characteristics (temperature, density, velocity); chromosphere through corona | Normal-incidence spectrometer, 50-160 nm, spectral resolution 20000-40000, angular resolution 1.2-1.5 arcsec |
| Coronal Diagnostic Spectrometer (CDS) | A. Fludra, RAL, Chilton, UK | UK, CH, D, USA, N, I | Temperature and density: transition region and corona | Normal and grazing-incidence spectrometers, 15-80 nm, spectral resolution 1000-10000, angular resolution 3 arcsec |
| Extreme-ultraviolet Imaging Telescope (EIT) | J-P Delaboudinière, IAS, Orsay, F | F, USA, B | Evolution of chromospheric and coronal structures | Full-disc images (1024×1024 pixels in 42×42 arcmin) at lines of HeII, FeIX, FeXII, FeXV |
| Ultraviolet Coronagraph Spectrometer (UVCS) | J.L. Kohl, SAO, Cambridge, MA, USA | USA, I, CH, D | Electron and ion temperature densities, velocities in corona (1.3-10 $R_S$) | Profiles and/or intensity of selected EUV lines between 1.3 and 10 $R_S$ |
| Large Angle and Spectrometric COronagraph (LASCO) | R. Howard NRL, Washington DC, USA | USA, D, F UK | Structures' evolution, mass, momentum and energy transport in corona (1.1-30 $R_S$) | One internally and two externally occulted coronagraphs. Spectrometer for 1.1-3 $R_S$ |
| Solar Wind ANisotropies (SWAN) | J.L. Bertaux, SA Verrières-le-Buisson, F | F, FIN, USA | Solar wind mass flux anisotropies. Temporal variations | Scanning telescopes with hydrogen absorption cell for Lyman-alpha |
| *Solar Wind 'in situ'* | | | | |
| Charge, ELement and Isotope Analysis System (CELIAS) | P. Bochsler, Univ. Bern, CH | CH, D, USA, Russia | Energy distribution and composition. (mass, charge, charge state) (0.1-1000 keV/e) | Electrostatic deflection, time-of-flight measurements and solid-state detectors |
| Comprehensive SupraThermal Energetic Particle analyser (COSTEP) | H. Kunow Univ. Kiel, D | D, USA, J, F, E, ESA, IRL | Energy distribution of ions (p, He) 0.04-53 MeV/n and electrons 0.04-5 MeV | Solid-state detector telescopes and electrostatic analysers |
| Energetic and Relativistic Nuclei and Electron experiment (ERNE) | J. Torsti, Univ. Turku, FIN | FIN, UK | Energy distribution and isotopic, composition of ions (p-Ni) 1.4-540 MeV/n and electrons 5-60 MeV | Solid-state and plastic scintillation detectors |

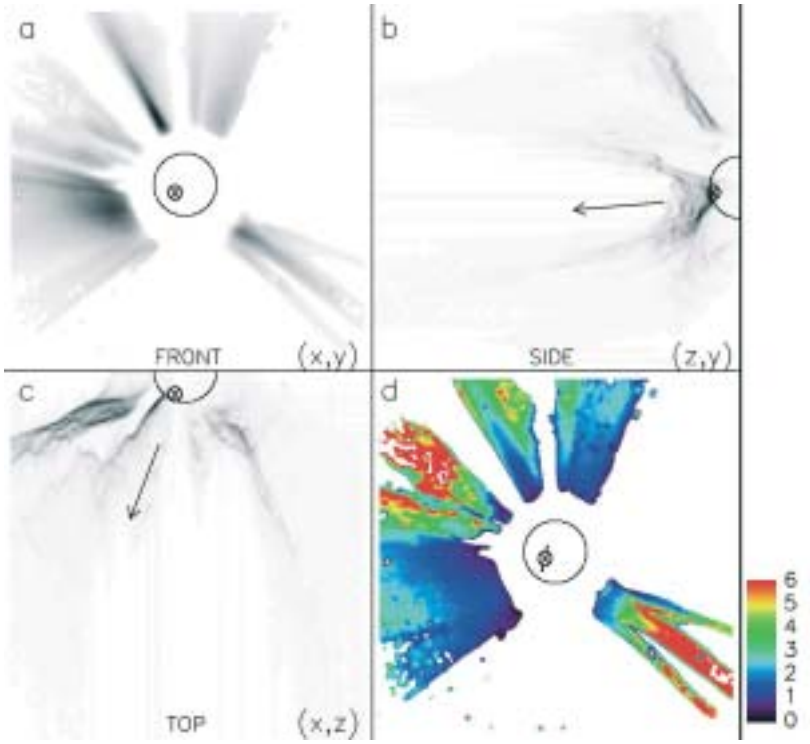


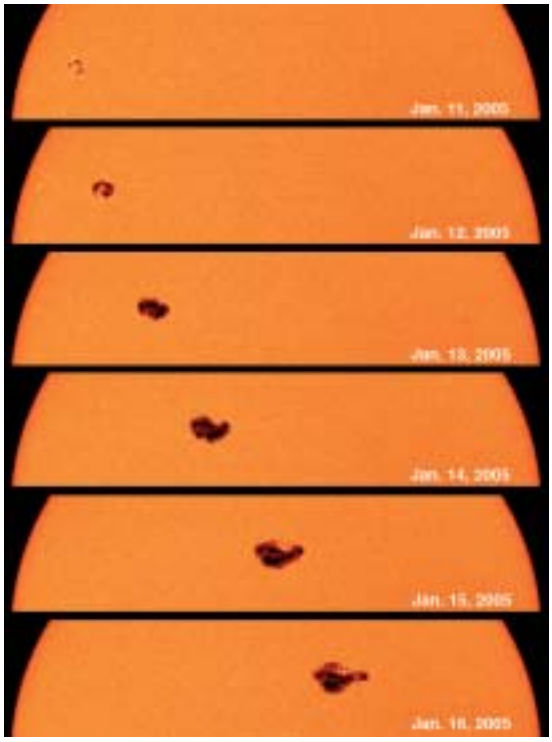


**Figure 2.3.1 (left). A CME heading almost directly towards Earth, observed by SOHO/LASCO C2. The size of the Sun is indicated by a circle, and the X-marked circle on the Sun shows the origin of the CME. Panel (a) shows the total intensity (darker means more intensity) as imaged directly by LASCO. Panel (d) is a topographic map of the material shown in (a). The distance from the plane of the Sun to the material is colour-coded; the scale in units of solar radii is shown on the side. Panels (b) and (c) show the intensity as it would have appeared to an observer positioned to the side of the Sun or directly above it, respectively.**
**Figure 2.3.2 (right). SOHO/MDI image of the growth of active region NOAA 10720 11-16 January 2005.**

time in a special feature on the SOHO home page and attracted considerable media attention.

The discovery of an interplanetary 'highway' for solar energetic particles (SEPs) was made possible by exceptionally accurate ERNE measurements of the proton flux anisotropy (Fig. 2.3.3). During most of the first 4 h of the SEP event of 2 May 1998 the proton intensity parallel to the magnetic field was ~1000 times higher than in the perpendicular direction. These observations indicate that the magnetic flux-rope structure of the CME provides a 'highway' for transport of solar energetic protons with a parallel mean free path of at least 10 AU.

New methods of local helioseismology (time-distance helioseismology, helioseismic holography, and ring-diagram analysis) provide a unique, 3-D view of the solar interior. Analysis of high-resolution MDI data has revealed a fascinating picture of the large-scale, subsurface dynamics of the Sun, with dramatic changes with the solar cycle. Zonal flows in the convection zone play an important role for solar activity because active regions tend to appear in the transition shear layers between faster and slower streams. MDI observations revealed the appearance of new branches at high latitude in 2002, indicating the onset of the next solar cycle well before the appearance of new cycle sunspot regions. The observations indicate that

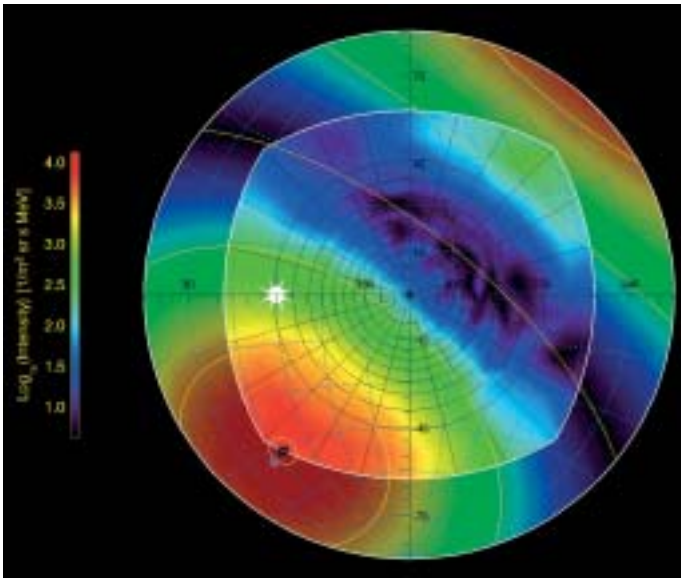

**Figure 2.3.3. High-energy proton directional intensity observed on 2 May 1998 by the ERNE/HED particle telescope. The particle event occurred inside the magnetic cloud of a previous CME, which formed an 'interplanetary highway' for particles from the Sun to the Earth. The image indicates that protons arrived in two exceptionally narrow beams from opposite directions along the interplanetary magnetic field line. The white asterisk shows the position of the Sun. The observed proton flux distribution (central part of the image) has been numerically extrapolated through the edge of the sky hemisphere that is about 27° beyond the ERNE/HED view cone.**

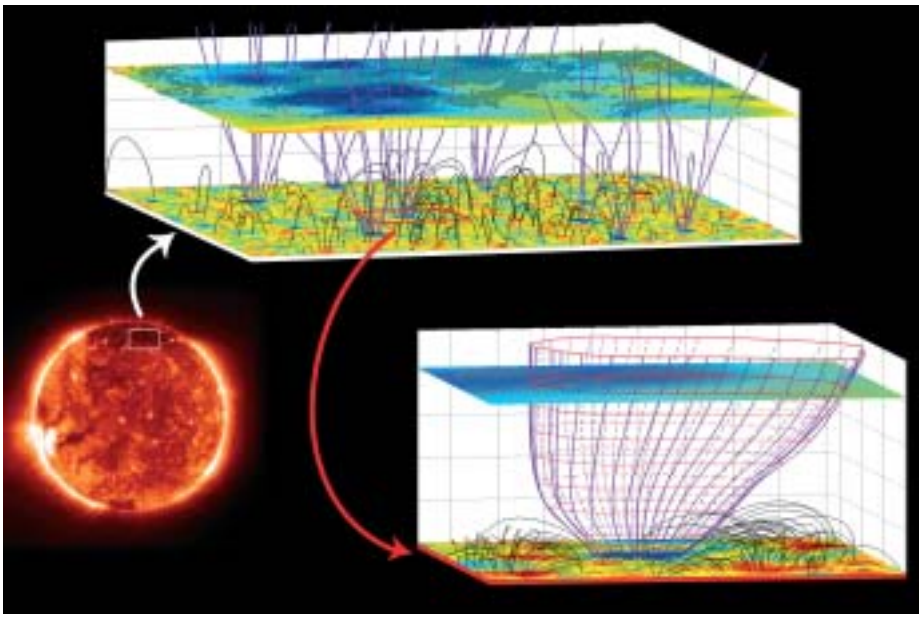

**Figure 2.3.3. Coronal funnels; the magenta curves illustrate open magnetic field lines, dark grey arches show closed ones. The lower plane shows the magnetic field vertical component measured by MDI (blue to red). The upper plane shows Ne VIII Doppler shifts from SUMER (hatched regions have large outflows), together with the inclination of the magnetic field (blue to red) as extrapolated from the MDI measurements.**

these new branches originate deep in the convection zone. The origin of the evolving zonal flows is not yet understood.

The SWAN team determined the direction of the interstellar neutral hydrogen flow as it enters the inner heliosphere: it is deflected relative to the helium flow by about 4°. The most likely explanation of this deflection is a distortion of the heliosphere under the action of an ambient interstellar magnetic field. In this case, the helium flow vector and the hydrogen flow vector constrain the direction of the magnetic field and act as an interstellar magnetic compass.

Using SUMER and MDI data, a Chinese-German team of scientists has located the

source region of the fast solar wind between 5000 km and 20 000 km above the surface in magnetic funnels (Fig. 2.3.4). According to their new model, the solar wind plasma is supplied by closed magnetic loops that are swept by convection to funnel regions where they undergo reconnection with existing open field lines. Thereby plasma previously confined within closed loops is released and accelerated to form the solar wind.

On 5 August 2005, Toni Scarmato, a high school teacher from San Costantino di Briatico, Calabria, Italy, discovered SOHO's 999th and 1000th cometas Nearly half of all comets for which orbital elements have been determined (since 1761) were discovered by SOHO, over two thirds of those by amateurs accessing LASCO data via the Web.

SOHO-14 was held jointly with the annual meeting of the Global Oscillation Network Group (GONG) 12–16 July 2004 at Yale University on the topic 'Helio- and Asteroseismology: Towards a Golden Future'. It focused on the study of the interior of the Sun from a seismic perspective and the prospects for similar study of solar-like stars. Nearly 120 participants discussed over 125 papers addressing a wide variety of topics, including the observational status of low-, medium-, and high-degree p-mode characterisation, low-frequency g-mode detection, solar structure and dynamics, mode excitation and damping, advances in local helioseismology, and first results from Canada's MOST asteroseismology mission. The proceedings were published by ESA as SP-559.

SOHO-15 was held 6–9 September 2004 at St. Andrews University, UK, on the topic 'Coronal Heating'. More than 130 participants presented and discussed over 140 papers addressing a wide variety of topics, including wave heating, the role of magnetic reconnection, and kinetic aspects of coronal heating. The proceedings were published by ESA as SP-575. A joint RHESSI, SOHO and TRACE workshop was held 8–11 December 2004 in Sonoma, California, on the topic 'Coordinated Observations of Flares and CMEs'. Solar Wind 11 / SOHO-16 'Connecting Sun and Heliosphere' was held 12–17 June 2005 in Whistler, Canada. It combined two of the most successful conference series in solar and heliospheric physics and attracted over 200 participants, who presented and discussed over 250 papers. The proceedings were published by ESA as SP-592.

# 2.4 Cassini/Huygens

## Introduction

Huygens is the element contributed by ESA to Cassini/Huygens, the joint NASA/ESA/ASI planetary mission to the Saturnian system. Titan, the largest moon of Saturn, is a central target of the mission. The Saturn Orbiter was provided by NASA, while ASI contributed its high-gain antenna and other radio subsystem equipment under a bilateral NASA/ASI agreement. JPL is managing the mission for NASA. The spacecraft was launched on 15 October 1997 by a Titan IVB-Centaur rocket from Cape Canaveral Air Force Station in Florida. The 5.6 t spacecraft was too heavy to be injected into a direct trajectory to Saturn, so the interplanetary voyage of about 6.7 years included gravity-assist manoeuvres at Venus, Earth and Jupiter (Fig. 2.4.1). It was inserted into orbit around Saturn on 1 July 2004. Titan observations were conducted before the release of Huygens, on 2 July, 26 October and 13 December 2004. They were key to confirming the properties of Titan's atmosphere and increasing confidence in the success of the Huygens entry. At the end of the third revolution, the Orbiter released Huygens for a successful entry and landing, on 14 January 2005. Following completion of the Probe mission, the Orbiter is continuing its exploration of the Saturnian system during 75 orbits around Saturn over 4 years. It is making repeated close flybys of Titan, both for data gathering about the moon and for gravity-assist orbit changes that are permitting it to make a tour of Saturn's satellites, reconnoitre the magnetosphere and obtain views of Saturn's higher latitudes. During its 4-year nominal mission, Cassini is making detailed observations of Saturn's atmosphere, magnetosphere, rings, icy satellites and Titan.

## Scientific objectives

The Cassini/Huygens mission is designed to explore the Saturnian system and all of its elements: the planet and its atmosphere, rings and magnetosphere, and a large number of its moons, particularly Titan and the icy satellites. Titan is the second largest moon in the Solar System after Jupiter's Ganymede. Its atmosphere resembles that of the Earth more closely than that of any other Solar System body. Nitrogen is the major constituent, at a surface pressure of 1.5 bar, compared with 1 bar on Earth. The other major constituent is methane: ~1.5% in the upper atmosphere, ~5% near the surface. Argon, which was speculated to be present with an upper limit of 1%, was

**Figure 2.4.1. Left: the interplanetary trajectory of the Cassini/Huygens spacecraft. Right: the trajectory upon arrival at Saturn; the Probe is released towards the end of the initial orbit around Saturn.**

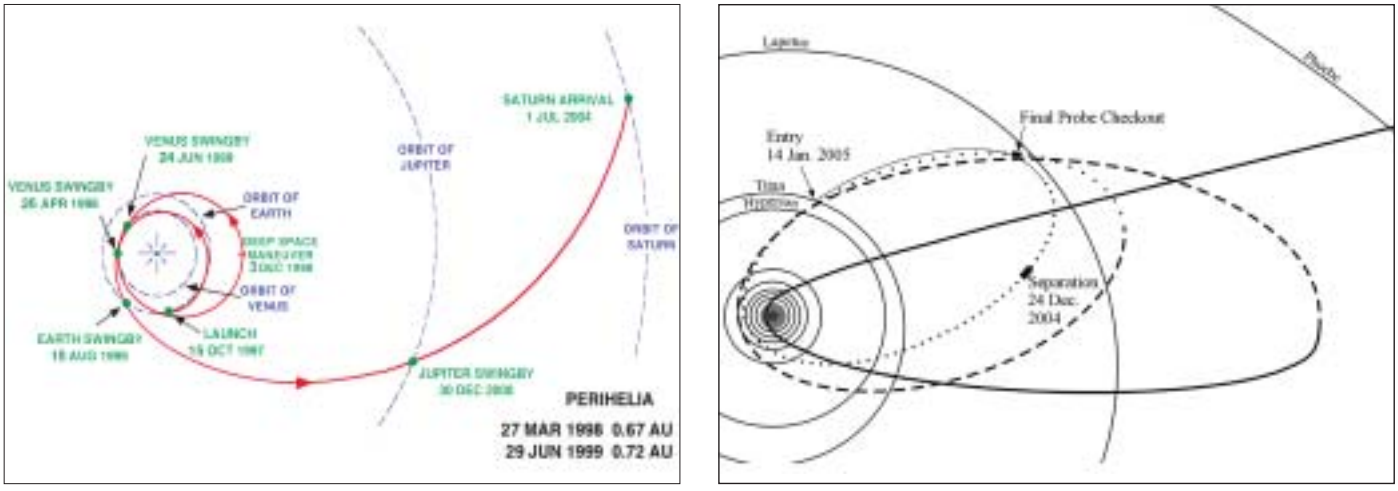


*For further information, see http://sci.esa.int/huygens*

**Table 2.4.1. The principal characteristics of the Huygens payload.**

| *Instrument/PI* | *Science objectives* | *Sensors/measurements* | *Mass (kg)* | *Power (typical/ peak, W)* | *Participating countries* |
|---|---|---|---|---|---|
| **Huygens Atmospheric Structure Instrument** (HASI)<br><br>M. Fulchignoni, University Paris 7/ Obs. Paris-Meudon (France) | Atmospheric temperature and pressure profile, winds and turbulence<br>Atmospheric conductivity.<br>Search for lightning.<br>Surface permittivity and radar reflectivity. | *T*: 50-300K, *P*: 0-2000 mbar<br>γ: 1 μ*g*-20 m*g*<br>AC *E*-field: 0-10 kHz ,<br>80 dB at 2 μV/m Hz<br>DC *E*-field: 50 dB at 40 mV/m<br>Conductivity $10^{-15}$ Ω/m to ∞<br>Relative permittivity: 1 to ∞<br>Acoustic: 0-5 kHz, 90 dB at 5 mPa | 6.3 | 15/85 | I, A, D, E, F, N, SF, USA, UK, ESA/RSSD, IS |
| **Gas Chromatograph Mass Spectrometer** (GCMS)<br><br>H.B. Niemann, NASA/GSFC, Greenbelt (USA) | Atmospheric composition profile. Aerosol pyrolysis products analysis. | Mass range: 2-146 dalton<br>Dynamic range: >$10^{8}$<br>Sensitivity: $10^{-10}$ mixing ratio<br>Mass resolution: $10^{-6}$ at 60 dalton<br>GC: 3 parallel columns, $H_2$ carrier gas<br>Quadropole mass filter<br>5 electron impact sources<br>Enrichment cells (×100-×1000) | 17.3 | 28/79 | USA, A, F |
| **Aerosol Collector and Pyrolyser** (ACP)<br><br>G.M. Israel, SA/CNRS Verriéres-le-Buisson (France) | Aerosol sampling in two layers – pyrolysis and injection to GCMS | 2 samples: 150-40 km; 23-17 km<br>3-step pyrolysis: 20°C, 250°C, 600°C | 6.3 | 3/85 | F, A, USA |
| **Descent Imager/Spectral Radiometer** (DISR)<br><br>M.G. Tomasko, University of Arizona, Tucson (USA) | Atmospheric composition and cloud structure.<br>Aerosol properties.<br>Atmospheric energy budget.<br>Surface imaging. | Upward and downward (480-960 nm) and IR (0.87-1.64 μm) spectrometers, res. 2.4/6.3 nm.<br>Downward and side looking imagers. (0.660-1 μm), res. 0.06-0.20°<br>Solar Aureole measurements: 550±5 nm, 939±6 nm.<br>Surface spectral reflectance with surface lamp. | 8.1 | 13/70 | USA, D, F |
| **Doppler Wind Experiment** (DWE)<br><br>M.K. Bird, University of Bonn (Germany) | Probe Doppler tracking from the Orbiter for zonal wind profile measurement. | (Allan Variance) : $10^{-11}$ (1 s); $5\times10^{-12}$ (10 s); $10^{-12}$ (100 s)<br>Wind measurements 2-200 m/s<br>Probe spin, signal attenuation | 1.9 | 10/18 | D, I, USA |
| **Surface Science Package** (SSP)<br><br>J.C. Zarnecki, Open University, Milton Keynes (UK) | Titan surface state and composition at landing site. Atmospheric measurements. | γ: 0-100 *g*; tilt ±60°; *T*: 65-110K;<br>$T_{th}$: 0-400 mW $m^{-1}$ $K^{-1}$<br>Speed of sound: 150-2000 m $s^{-1}$,<br>Liquid density: 400-700 kg $m^{-3}$<br>Refractive index: 1.25-1.45<br>Acoustic sounding, liquid relative permittivity | 3.9 | 10/11 | UK, F, USA, ESA/RSSD, PL |

**Table 2.4.2. The Huygens interdisciplinary scientists.**

| *Scientist/Affiliation* | *Field of Investigation* |
|---|---|
| *ESA Selection* | |
| D. Gautier, Obs. de Paris, Meudon, F | Titan aeronomy |
| J.I. Lunine, Univ. of Arizona, Tucson, USA | Titan atmosphere/surface interactions |
| F. Raulin, LPCE, Univ. Paris 12, Creteil, F | Titan chemistry and exobiology |
| *NASA Selection* | |
| M. Blanc, Observatoire Midi-Pyrénées, Toulouse, F | Plasma circulation and magnetosphere/ ionosphere coupling |
| J. Cuzzi, NASA Ames Research Center, Moffett Field, USA | Rings and dust within Saturnian system |
| T. Gombosi, Univ. of Michigan, Ann Arbor, USA | Plasma environment in Saturn's magnetosphere |
| T. Owen, Inst. for Astronomy, Honolulu, USA | Atmospheres of Titan and Saturn |
| J. Pollack (deceased), NASA Ames Research Center, Moffett Field, USA | Origin and evolution of Saturnian system |
| L. Soderblom, US Geological Survey, Flagstaff, USA | Satellites of Saturn |
| D. Strobel, Johns Hopkins University, Baltimore, USA | Titan's and Saturn's atmospheric aeronomy |

detected, but in small quantities (at the ppm level). At Titan, methane takes the role that water plays on Earth. The photolysis of methane in the atmosphere, owing mainly to the solar UV radiation but also to cosmic rays and precipitating energetic magnetospheric particles, gives rise to a complex organic chemistry. Chemical reactions taking place in the continuously evolving atmosphere provide possible analogues to some of the prebiotic organic chemistry that was at work on the primitive Earth, before the appearance of life some 3.8 Gyr ago. Observations from Cassini-Huygens confirmed that Titan resembles the Earth in many ways.

Huygens was designed for a detailed *in situ* study of Titan's atmosphere and to characterise the surface of the satellite near the Probe's landing site. The objectives were to make detailed *in situ* measurements of the atmosphere's structure, composition and dynamics. Images and spectroscopic measurements of the surface were made during the atmospheric descent. Since it was hoped that the Probe would survive after impact for at least a few minutes, the payload included the capability for making *in situ* measurements for a direct characterisation of the surface at the landing site.

## The payload

On 10 October 1989, NASA and ESA simultaneously released coordinated Announcements of Opportunity (AOs) calling respectively for investigations to be performed with the Saturn Orbiter and the Huygens Probe. The NASA AO called for four types of proposals:

— Principal Investigator (PI) Instruments;
— Orbiter facility team leader (TL);

— Orbiter facility team member (TM);
— Interdisciplinary Scientist (IDS) investigation.

The ESA AO called for two types of proposals:
— PI Instrument;
— Interdisciplinary Scientist investigation.

The ESA Huygens selection, which comprised six PI Instruments (Table 2.4.1) and three IDS investigations (Table 2.4.2), was announced in September 1990. The NASA Saturn Orbiter selection, which comprised seven PI Instruments, four Team Leaders, 52 Team Members and seven IDS investigations, was announced in November 1990. During the selection process, NASA included the additional INMS facility instrument on the Orbiter, for which a call for Team Leader and Team Member investigation proposals was released in August 1991. The INMS investigation selection was announced in February 1992. The NASA-selected IDS is shown in Table 2.4.2 and the Orbiter Payload in Table 2.4.3.

## Cassini/Huygens mission overview

The Cassini/Huygens spacecraft arrived at Saturn in late June 2004. The Saturn Orbit Insertion (SOI) manoeuvre was executed while above the ring plane on 1 July; two ring plane crossings occurred around the main engine burn. SOI established a 119-day orbit, which included the first targeted Titan flyby. The second (48-day) orbit, which also included a targeted Titan flyby, shaped the trajectory so that the Huygens mission could be carried out on the third (32-day) orbit using an Orbiter flyby altitude of 60 000 km. The Huygens mission trajectory was changed in 2001 to accommodate a new geometry requirement during the Probe relay phase that reduced the Doppler shift of the radio signal received by the Orbiter. This change was necessary to cope with a design flaw of the Huygens radio receiver discovered during in-flight testing in 2000. The onboard software of the Probe and several instruments was also modified in December 2003 to optimise the mission recovery. The Probe was released on 25 December 2004, about 20 days and 7 h before Titan encounter. Within 48 h of release, the Orbiter took three series of images of the Probe moving away. They were used to refine the knowledge of Huygens' trajectory and to confirm that it was well on target for entry 3 weeks later.

Three days after release, the Orbiter performed a deflection manoeuvre to avoid Titan impact. This manoeuvre also set up the Probe-Orbiter radio communication geometry for the descent. Huygens entered Titan's atmosphere on 14 January 2005 at 09:06 UTC. The Orbiter received the data on its High Gain Antenna (HGA) for more than 3.5 h. The Probe transmitted data on two channels, but, owing to a missing command in the mission sequence aboard the Orbiter, one receiver was not configured to receive the data. The other channel worked flawlessly. The data were stored in the Orbiter's two solid-state recorders for later transmission to Earth after completion of the Probe mission. The main events of the Probe entry and descent are illustrated in Fig. 2.4.2. The Probe data were received on Earth within 3 h of the Orbiter stopping listening to Huygens and reorienting its HGA towards Earth.

After completion of the Probe mission, the Orbiter continued its 4-year satellite tour of the Saturnian system. This consists of 75 Saturn-centred orbits, connected by Titan gravity-assist flybys or propulsive manoeuvres. The size of these orbits, their orientation to the Sun/Saturn line and their inclination to Saturn's equator are dictated by the various scientific requirements, which include: Probe landing site ground-track coverage, icy-satellite flybys, Saturn, Titan or ring occultation, magnetosphere

**Table 2.4.3. Saturn Orbiter payload.**

| *Instrument*<br>*PI* | *Measurement* | *Technique* | *Mass (kg)* | *Power (W)* | *Countries* |
|---|---|---|---|---|---|
| *Optical Remote Sensing* | | | | | |
| Composite Infrared Spectrometer (CIRS)<br>V. Kunde, NASA/GSFC, USA | High-resolution spectra, 7-1000 μm | Spectroscopy using 3 interferometric spectrometers | 43 | 43.3 | USA, F, D, I, UK |
| Imaging Science Subsystem (ISS)<br>C. Porco, U. Arizona, USA | Photometric images through filters, 0.2-1.1 μm | Imaging with CCD detectors;<br>1 wide-angle camera (61.2 mrad FOV);<br>1 narrow-angle camera (6.1 mrad FOV) | 56.5 | 59.3 | USA, F, D, UK |
| Ultraviolet Imaging Spectrometer (UVIS)<br>L. Esposito, U. Colorado, Boulder, USA | Spectral images, 55-190 nm; occultation photometry, 2 ms; H and D spectroscopy, 0.0002 μm resolution | Imaging spectroscopy, 2 spectrometers; hydrogen-deuterium absorption cell | 15.5 | 14.6 | USA, F, D |
| Visible and Infrared Mapper Spectrometer (VIMS)<br>R. Brown, U. Arizona, Tucson, USA | Spectral images, 0.35-1.05 μm (0.073 μm resolution); 0.85-5.1 μm (0.166 μm resolution); occultation photometry | Imaging spectroscopy; 2 spectrometers | 37.1 | 24.6 | USA, F, D, I |
| *Radio Remote Sensing* | | | | | |
| Cassini Radar (RADAR)<br>C. Elachi, JPL, USA | Ku-band radar images (13.8 GHz); radiometry, <0.5K resolution | Synthetic aperture radar; radiometry with a microwave receiver | 43.3 | 108.4 | USA, F, I, UK |
| Radio-Science Instrument (RSS)<br>A. Kliore, JPL, USA | Ka/S/X-bands; frequency, phase, timing and amplitude | X/Ka-band uplink;<br>Ka/X/S-band downlink | 14.4 | 82.3 | USA, I |
| *Particle Remote Sensing & In-Situ Measurement* | | | | | |
| Magnetospheric Imaging Instrument (MIMI)<br>S.T. Krimigis, Johns Hopkins Univ, Baltimore, USA | 1. Image energetic neutrals and ions at <10 keV to 8 MeV per nucleon; composition. 2. 10-265 keV/e ions; charge state; composition; directional flux; 3. mass range: 20 keV to 130 MeV ions; 15 keV to >11 MeV electrons; directional flux | 1. Particle detection and imaging; ion-neutral camera (time-of-flight, total energy detector); 2. charge energy mass spectrometer; 3. solid-state detectors with magnetic focusing telescope and aperture-controlled ~45° FOV | 29 | 23.4 | USA, F, D |
| *In-Situ Measurement* | | | | | |
| Cassini Plasma Spectrometer (CAPS)<br>D.T. Young, SWRI, San Antonio, USA | Particle energy/charge:<br>1. 0.7-30 000 eV/e;<br>2. 1-50 000 eV/e<br>3. 1-50 000 eV/e | Particle detection and spectroscopy:<br>1. electron spectrometer;<br>2. ion-mass spectrometer;<br>3. ion-beam spectrometer | 23.8 | 19.2 | USA, SF, F, H, N, UK |
| Cosmic Dust Analyser (CDA)<br>E. Gruen, MPI Heidelberg, D | Directional flux and mass of dust particles in the range $10^{-16}$-$10^{-6}$ g; chemical composition | Impact-induced currents | 16.8 | 19.3 | D, CZ, F, ESA/RSSD, N, UK, USA |
| Dual Technique Magnetometer (MAG)<br>D. Southwood, IC, UK | B: DC to 4 Hz up to 256 nT; scalar field DC to 20 Hz up to 44 000 nT | Magnetic field measurement; flux gate magnetometer; vector-scalar magnetometer | 8.8 | 12.4 | UK, D, USA |
| Ion and Neutral Mass Spectrometer (INMS)<br>J.H. Waite, SWRI, San Antonio, USA | Fluxes of +ions and neutrals in mass range 2-66 amu | Mass spectrometery; closed source and open source | 10.3 | 26.6 | USA, D |
| Radio and Plasma Wave Science (RPWS)<br>D. Gurnett, U. Iowa, USA | E: 10 Hz-2 MHz; B: 1 Hz-20 kHz; plasma density and temperature | Radio frequency receivers; 3 electric monopole antennas; 3 magnetic search coils; Langmuir Probe | 37.7 | 17.5 | USA, A, F, S, UK, N |

**Table 2.4.4. Mass breakdown of the Cassini/Huygens spacecraft.**

| | |
|---|---|
| Orbiter (dry, inc. payload) | 2068 kg |
| Probe (inc. 44 kg payload) | 318 kg |
| Probe Support Equipment | 30 kg |
| Launch adaptor | 135 kg |
| Bipropellant | 3000 kg |
| Monopropellant | 132 kg |
| Launch mass | 5683 kg |

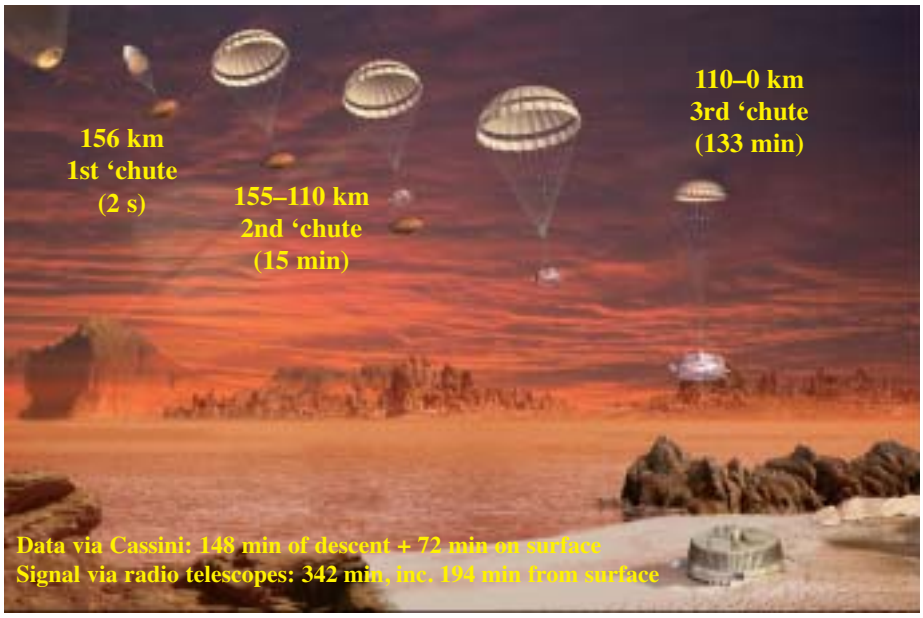


**Figure 2.4.2. The entry and descent sequence for the Huygens Probe.**

coverage, orbit inclinations and ring-plane crossings. Titan is also a principal target for the Orbiter; it is being observed during each of the 45 targeted Titan flybys.

The Orbiter science instruments are mounted on two body-fixed platforms: the remote-sensing pallet and the particle & field pallet; the magnetometer is mounted at the tip of an 11 m-long boom; the magnetic and electric antennas of the RPWS experiment are mounted on the body; both the radar and the radio-science instrument use the HGA. The mass budget of the spacecraft is shown in Table 2.4.4.

## Scientific highlights

Huygens successfully entered Titan's atmosphere and descended by parachute to Titan's surface. Even though one of the radio receivers on Cassini was not switched on properly, an excellent dataset was delivered to Earth thanks to redundancy. The descent lasted 148 min. Huygens survived the landing and continued to operate on the surface for more than 3 h. The Orbiter received data transmitted from the surface for 72 min until it passed below the landing site horizon.

The carrier frequency signal of the channel not properly received on the Orbiter was tracked on Earth by an array of radio telescopes. Doppler tracking was achieved by the Green Bank Telescope in West Virginia, USA, and at the Parkes telescope in Australia. These and 15 other radio telescopes were part of a Very Long Baseline Interferometry (VLBI) network that was tracking Huygens. The network achieved precise VLBI tracking during the whole descent and for 3 h 14 min on the surface. Huygens was still transmitting at the end of the planned radio observation period. Post-flight analysis of the telemetry indicated that the Probe's batteries were fully discharged about 15 min after the last radio signal was received on ground.

The data provides a rich harvest of scientific information about Titan. The ground-based radio observations are an excellent complement. In addition, a coordinated campaign of many optical telescopes observed Titan around the time of, and during, the Probe's descent. The detailed *in situ* data also complement the impressive set of data acquired by Cassini during its Titan flybys. The Huygens results were published

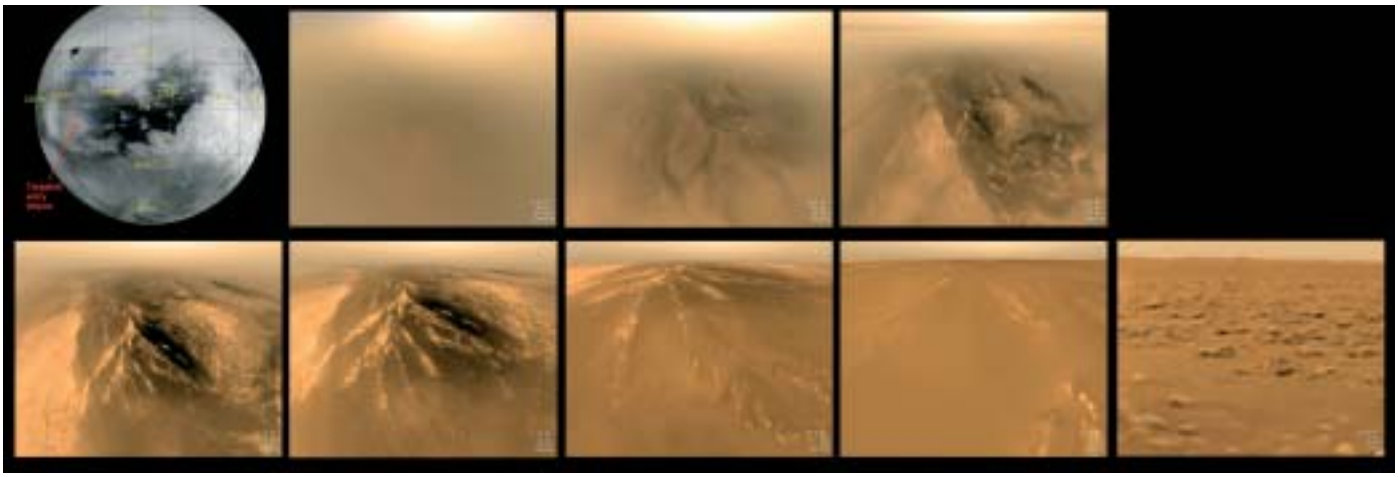

**Figure 2.4.3. Huygens' view of Titan, based on DISR images. Original black and white images are 'colourised' based on the spectral data. The bright area near the centre top is the bright part of Titan's haze below the Sun. Surface features appear as Huygens descends through the haze. At 21 km (top right), it passes through a thin haze layer. Below 7 km (bottom left), the forward, eastward motion reverses, before reversing again at 1 km (centre bottom). On landing, the view is to the southern horizon with ice rocks visible below, with nearby rocks of some 20 cm. (Frames extracted from DISR movie available at http://saturn.esa.int) (Background of top left image courtesy NASA/JPL/SSI/ISS Team)**

in *Nature* (8 December 2005). Most of the results from the ground campaign will appear in a special issue of the *Journal of Geophysical Research* in 2006.

The structure of the upper atmosphere was inferred from accelerometry measurements during entry from about 1400 km down to 160 km by HASI. Pressure and temperature were measured directly by HASI below 155 km. Huygens confirmed the troposphere temperature profile obtained by Voyager using radio occultation. The surface temperature is –179ºC. The physical and optical properties of the organic haze that prevented Voyager's camera from seeing the surface through the atmosphere was well characterised by the DISR, which made measurements during the whole descent. Although the haze did not clear below the tropopause, the camera obtained clear views of the surface below about 50 km. Extraordinary panoramas were reconstructed from a series of images taken at different altitudes and azimuth angles, taking advantage of the fact that the Probe was spinning under its parachute. Examples are shown in Fig. 2.4.3, which reveal a complex surface with river networks cut into an icy landscape. Huygens landed in what appears to be a dry lake or riverbed. The most detailed surface image was obtained after landing (Fig. 2.4.3, bottom right) and shows a surface covered with ice pebbles and cobbles mixed with organic material.

The composition of haze particles was measured using the combination of the ACP and GCMS. GCMS also measured the composition of the atmosphere during the descent and obtained the methane concentration profile down to the surface. The methane mole fraction, as measured by GCMS, has a constant value of $1.41\pm0.07\times10^{-2}$ in the stratosphere. It increases below about 32 km down to 8 km to $4.92\pm0.25\times10^{-2}$, then remains constant down to the surface. Upon impact, the GCMS inlet was heated to facilitate evaporation of surface material into the mass spectrometer. Impact measurements by the SSP provided evidence that Titan soil has the consistency of wet sand. The methane model fraction measured on the surface rose to about 7% (40% increase) and then remained constant for the rest of the time that GCMS collected data. Methane measurements, complemented by data from Cassini, provide a new understanding of the methane cycle on Titan. Researchers are now suggesting a subsurface reservoir of methane. DISR and GCMS data provide good evidence that there is intense geological activity, substantiated by observations made by the Orbiter VIMS and radar.

The DWE, using the Doppler tracking and VLBI observations from the start of the

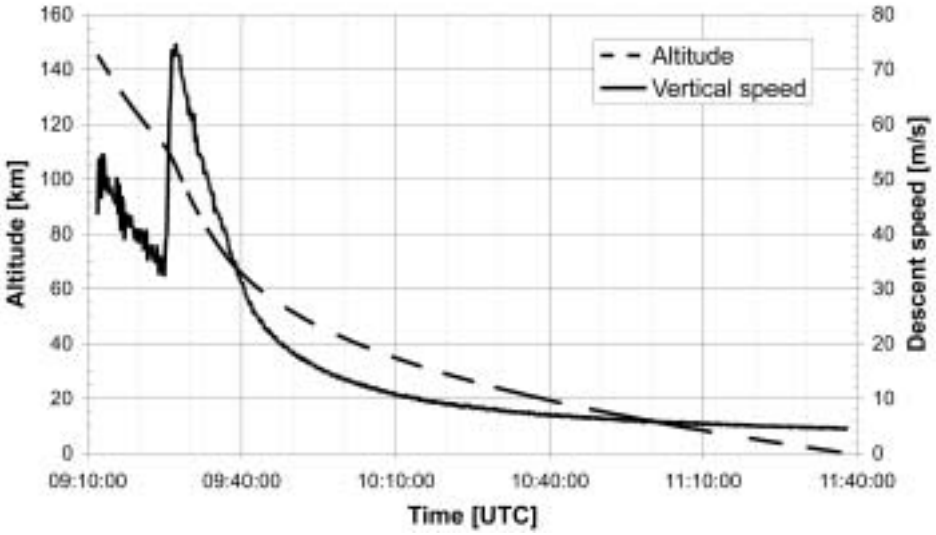


**Figure 2.4.4. The reconstructed altitude and descent speed.**

descent, inferred wind properties. Below about 50 km, winds were independently measured by DISR, which tracked surface features. Prograde (west to east) winds as high as 120 m/s were observed above 120 km. The winds generally followed the profile predicted from Voyager observations with two major exceptions: a weak wind layer was detected around 80 km, with strong wind gradients above and below it. The wind reversed below 8 km, becoming westerly. Wind speeds of ~1 m/s were observed near the surface, sufficient to explain the formation of dunes of sand-like material observed by the Cassini radar. Dune-like features were also spotted by DISR, and used as landmarks to reposition the Huygens landing site in overall radar, ISS and VIMS surface images. This allowed independent confirmation (to an accuracy of a few tens of km) of the coordinates of the landing site determined by the Huygens Descent Trajectory working group using data from all Huygens investigations (Fig. 2.4.4).

## Data archive

Data from the Orbiter investigations are regularly archived and made available to the wide scientific community and the public through the NASA Planetary Data System (PDS). Data from the Huygens investigations are being archived in the ESA Planetary Science Archive (PSA) and mirrored in the PDS. The plan is to make the data publicly available on 15 July 2006. High-level data products will be reworked once a full characterisation of the Probe entry and descent performance is achieved, taking into account the measured atmosphere profile. It is planned to redeliver an updated Huygens data archive in 2007/2008.

# 2.5 XMM-Newton

## Introduction

The XMM-Newton observatory was launched on 10 December 1999 from Kourou on the first commercial Ariane-5 (V504). The mission is routinely producing high-quality data and has effectively completed its guaranteed time, AO-1, AO-2 and AO-3 programmes and 75% of its AO-4 programme. In AO-3, for the first time, proposals were accepted in a special, large-programmes, category. Starting in 2004, annual calls for proposals have been issued on around 1 September. The mission, designed for a 10-year life, was approved in November 2005 by the SPC for operations up to end-March 2010.

## Mission status

XMM-Newton is a 3-axis-stabilised spacecraft with a mass of about 4 t. The satellite is dominated by a large carbon-fibre telescope tube attached to the Service Module (SVM) at one end and to the Focal Plane Assembly (FPA) at the other. The SVM is a platform that carries all the equipment for the power, data handling, and attitude and orbit control subsystems, including the structure to support the solar arrays and antennas. The attitude control loop uses a star tracker and momentum wheels, which allow for a slew rate of 90° per hour and a pointing reconstruction accuracy of a few arcsec. Gyros are used only in cases of eclipses or anomalies.

The operations efficiency at maximum allows for a maximum of 132 ks of science observations per revolution; the remaining 40 ks are spent inside the radiation belts. The mission routinely responds to Targets of Opportunity (ToO) with a very short response time – as fast as 5 h. This has been put to good use a number of times when XMM-Newton has performed rapid follow-up of Gamma-Ray Bursts (GRBs).

The status of the satellite and the instruments is excellent, and well in line with the 10-year design goal. Onboard consumables are sufficient to operate for at least another 10 years. On the hardware side, the spacecraft is being operated on all its prime hardware chains, and no redundancy has had to be used yet. The radiation-induced performance degradation of the instruments is in line with pre-launch expectations, and has recently been largely ameliorated by allowing the X-ray detectors to operate at lower temperatures. Based on current knowledge, the instruments will be within specification at least for the designed mission lifetime.

**European Photon Imaging Cameras** (PI M. Turner, Leicester University, UK)
An EPIC detector is positioned behind each of the three X-ray mirror modules. Two MOS-CCD cameras share the mirrors with the grating array, and the PN-CCD detector is located behind the fully open telescope position. The in-orbit performance of the EPIC cameras is excellent, and the degradation of the camera owing to irradiation by (mostly solar) protons is as predicted pre-launch. A decision to lower the temperature of the detectors was taken at end-2002 in order to ameliorate the radiation damage. This has been very successful: not only has more than 75% of the performance degradation since launch been recovered, but the rate of degradation has also decreased considerably. The EPIC cameras are particularly powerful for those sources that show weak extended X-ray emission, such as clusters of galaxies.

**Reflection Grating Spectrometer** (PI J. Kaastra, SRON, NL)
RGS is a powerful, large-area detector that allows XMM-Newton to take X-ray spectra with an $E/\Delta E$ of 300–700 (1st order) in the 5-35 Å (0.35–2.4 keV) soft X-ray band. The effective area for the two grating arrays is in the range of 40–200 $cm^2$ over this wavelength band. The instrument's performance is as predicted. It was decided at the end of 2002 to cool the detectors to a lower operational temperature. This exercise was as successful as with EPIC, ameliorating a lot of the incurred radiation damage

*For further information, see http://sci.esa.int/xmm*

and, most importantly, dramatically decreasing the number of hot columns and hot pixels.

**Optical Monitor** (PI K. Mason, MSSL, UK)
OM is a powerful telescope in the 170–600 nm wavelength band, and can detect sources down to 24th magnitude in a few ks (depending on spectral type). This camera is powerful enough, both in sensitivity and positional accuracy, to allow identification of counterparts of many of the new X-ray sources detected with XMM-Newton.

XMM-Newton operations are carried out via a Mission Operations Centre (MOC) in Darmstadt, D (ESOC) and a Science Operations Centre (SOC) at the European Space Astronomy Centre (ESAC) near Villafranca, E. The design of the spacecraft and its instruments is such that continuous real-time supervision of the operations is necessary. The ground segment also involves the Survey Science Consortium (SSC; PI M. Watson, Leicester Univ., UK), an AO-selected, nationally-funded, multi-national consortium. The SSC, among others, pipeline processes raw science data and converts them into first-level science files and results. The PI teams, who designed and built the instruments, support the SOC in the areas of calibration and validation of changes to the onboard software. Both the PI teams and the SSC collaborate with ESA in the creation of the widely used Science Analysis Software (SAS).

The analysis of XMM-Newton data is supported by the SAS software package, now at version 6.5, being released approximately once a year. It allows data users to derive reliable and calibrated results for further analysis with standard X-ray astronomy spectral analysis packages. The derivation of accurate calibration data, and the proper incorporation of this knowledge into the SAS software, is a continuing process. The status of the calibration is now such that most (spectral) parameters can be derived to an absolute accuracy around 2–5%, depending on the quantity.

The XMM-Newton Science Archive (XSA), based on reusing technology from the ISO archive, was released in March 2002. The archive allows for flexible querying and retrieving of all XMM-Newton (public) data in a highly flexible and configurable way.

In April 2003, the first version of the XMM-Newton serendipitous source catalogue (1XMM), generated by the SSC was released. The release of the second version of this catalogue (2XMM) is expected in early 2006. More than 80% of the entries of the first catalogue had not previously been reported as X-ray sources. The 2XMM catalogue is expected to become a significant astronomical resource, as it is the largest catalogue of X-ray sources derived from observations with CCD energy resolution over the full 0.2–12 keV energy band. It is expected to contain detailed information on some 200 000 sources with a positional accuracy of ~0.5–2 arcsec (68% confidence radius).

## Science results

XMM-Newton results continue to impact many areas of science. This is illustrated below by examples. Exciting challenges lie ahead for the mission, such as the identification and characterisation of newly detected TeV sources, time- and phase-resolved spectroscopy of compact objects, especially of neutron stars and accreting stellar and super-massive black holes, and studies of high redshift clusters of galaxies in the areas of cluster formation history and cosmology. Proposals for further investigation of these and other exciting topics have been accepted for AO-4 and AO-5. Some 15% of the available observing time is allocated to large programmes, which have proved to be an invaluable addition to the XMM-Newton observations.

**Stars**
XMM-Newton has shed new light on many important properties of stars over a wide range of masses, spectral types and evolutionary stages. Concerning very young stars, for example, it has been possible to characterise the X-ray spectra and light curves of extremely embedded protostars of class 0 and I for the first time. The finding that X-ray emission in classical T Tauri pre-main sequence stars arises from a hot spot suggests that accretion shocks are common features during this evolutionary phase. A major highlight was the first detection of a cyclic X-ray variation synchronised with the star-spot cycle, similar to that of the Sun, in another solar-type star. In a similar context, a high-resolution spectroscopy survey of a sample of nearby G dwarfs with ages 0.1–1.6 Gyr provided unprecedented insight into the long-term evolution of X-ray coronae of solar analogues. This is especially important in view of the impact X-rays could have on the atmospheres of newly formed planets.

**Gamma-ray bursts**
The rapid response time of XMM-Newton to GRBs has led to the first detection of a time-dependent dust-scattered X-ray halo around a GRB, where the halo appeared as concentric time-dependent ring-like structures centred on the burst location and allowed accurate, direct distance measurement of the intervening dust slabs.

**Supernova remnants**
The importance of synchrotron continuum X-ray radiation in supernova remnants has only recently been recognised. The sensitivity and energy range covered by EPIC now makes it possible to study this component in many remnants, both spatially and spectrally, and to establish its relation to the TeV emission. Using RGS observations of the rims of bright supernova remnants such as SN 1006, it has been possible to measure ion temperatures directly from line broadening of oxygen lines; this opens opportunities to test shock equilibration models directly from the observations.

**Neutron stars**
The discovery of bow shocks aligned with the neutron star Geminga's supersonic motion, and the discovery of a ~60 m-radius rotating hot spot on its surface through phase-resolved spectroscopy, were exciting results, both of which were published in *Science*. The two discoveries together are of fundamental importance, as they identify the missing link between the X-ray and gamma-ray emission from neutron stars. Phase-resolved spectroscopy allowed the detection of hot spots on two further neutron stars, demonstrating that the magnetic field configurations and surface temperature distributions are significantly more complex than previously anticipated.

**Active Galactic Nuclei**
The innermost regions of AGN, where the bulk of the energy produced through accretion-driven processes is released, can only be investigated by sensitive X-ray observations. The intensity and the profile of the iron emission line (Fe Ka) provide unique diagnostic tools to understand accretion processes in the vicinity of the black hole where the effects of strong gravity, such as gravitational redshift and light-bending in curved space-time, are important. One of the most recent results is the detection of a transient redshifted emission feature in the X-ray spectra of a few bright highly variable Seyfert galaxies (e.g. Mrk 766 and NGC 3516), showing flux modulation over time intervals of the same order as, or shorter than, the XMM-Newton exposure (a few tens of ks). The evolution of such a feature agrees with iron emission from a spot in the innermost (a few Schwarzschild radii) regions of an

accretion disc illuminated by a corotating flare. Such observations offer the opportunity to estimate the black hole mass and spin directly.

**Clusters of galaxies**

The unique combination of high spectral resolution, throughput and sensitivity offered by XMM-Newton provided the basis for significant improvement in the understanding of the dynamical process of hierarchical formation of clusters. Important results in this context were the discovery of turbulence in Coma and observations of merging clusters, which confirm the importance of the large-scale environment on cluster formation. Another highlight was the mapping of the dark matter profiles of relaxed clusters over wide ranges of mass and radius. Quantitative comparisons with predictions from numerical simulations provided strong support for the Cold Dark Matter cosmological scenario. In parallel, new clusters are being serendipitously discovered by XMM-Newton, up to very high redshift. Recently, the most distant well-formed cluster ever known was discovered by XMM-Newton at a redshift of 1.4; more than 1000 cluster candidates have been discovered by the XMM-Newton Cluster Survey (XCS).

**X-ray background**

XMM-Newton's large collecting area, relatively wide FOV and broad bandpass are crucial for progress in the study of the X-ray background. One of the most outstanding recent results is the detection, in the summed spectra of the sources in the deep Lockman hole observation, of broad iron lines. This indicates that this feature is present in AGN out to $z > 1$ and that the average super-massive black hole has significant spin. Another highlight was the first significant detection of the correlation function of hard X-ray selected AGN, allowing their use as a tracer of dark matter on large scales. Further progress will come from the large solid-angle deep XMM-Newton surveys (e.g. COSMOS) that are currently being performed. These will allow measurement of the 3-D correlation function of AGN, its evolution with redshift, and the evolution of AGN activity compared to the growth of cosmic structure.

The large number of serendipitous objects in the new XMM-Newton catalogue will make possible the first measurement of the properties of large numbers of sources in the range $10^{-13}$–$10^{-12}$ ergs/cm$^2$/s. While not making a major contribution to the X-ray background, the measurement and identification of these objects will be a major step forward in our understanding of the evolution of AGN over cosmic time.

## Highlights

A number of papers on XMM-Newton results were of such importance that they were also issued as press and/or news releases, and were picked up by the international media.

An article published in *A&A* reported on the determination of the mass and angular momentum of the central super-massive black hole in the centre of our Galaxy based on frequencies found in XMM-Newton, Chandra and IR data. The authors determined the mass and angular momentum with an error of only 5.7% and 0.5%, respectively. If the measurements can be confirmed independently then this is the first measurement that cannot be described with the weak-field or post-Newtonian approximation of the General Theory of Relativity.

A paper in *MNRAS* reported on the tentative detection of the modulation of a transient, redshifted Fe K$\alpha$ emission feature in the X-ray spectrum of the Seyfert galaxy NGC 3516. The spectral feature at 6.1 keV, in addition to a stable 6.4 keV line, has been reported previously. The authors found that the feature varies systematically

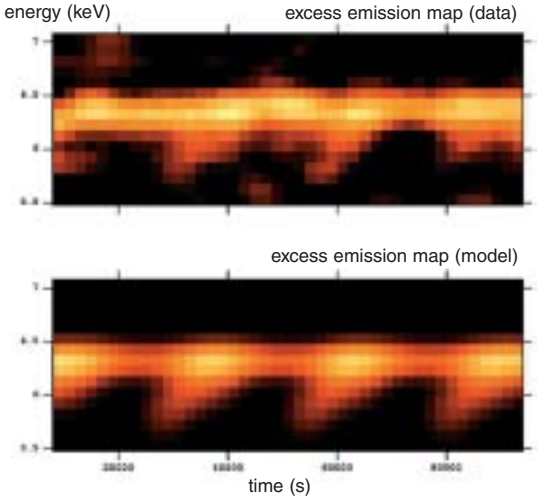


**Figure 2.5.1 The upper panel shows the smoothed excess emission map on the time-energy plane for the Fe Kα as measured for NGC 3516. The resolution is 100 eV in energy and 2 ks in time. The colour-coding is according to a 'blackbody' with the brightest pixels correspond to about 15 excess counts. The spectral evolution agrees with emission arising from a spot on the accretion disc, illuminated by a corotating flare located at a radius of 3.5–8 Rs (Schwarzschild radii). The lower panel shows a theoretical picture for comparison.**

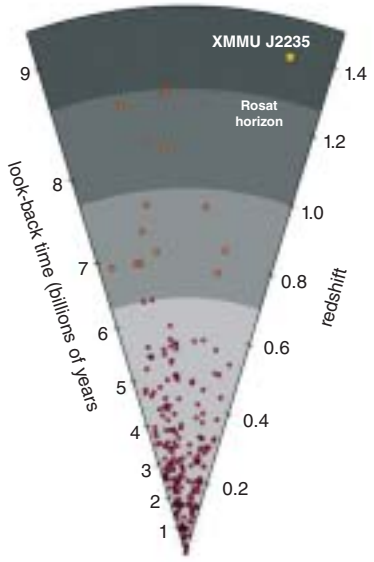


**Figure 2.5.2 The distribution of known galaxy clusters in space. As Earth-bound observers look out from the apex of the cone, they see an increasingly more distant and earlier Universe. Distance is marked on the right side in units of redshift, while the corresponding cosmic look-back time is indicated on the left axis. The newly discovered cluster, labelled XMMU J2235, falls in a remote regime, well beyond the horizon of previous studies (labelled 'Rosat horizon').**

in flux at intervals of 25 ks. The peak moves in energy between 5.7 keV and 6.5 keV. The spectral evolution of the feature agrees with Fe K emission arising from a spot on the accretion disc, illuminated by a corotating flare located at a radius of 3.5–8 Rs (Schwarzschild radii), modulated by Doppler and gravitational effects as the flare orbits the black hole (Fig. 2.5.1). Combining the orbital timescale and the location of the orbiting flare, the mass of the black hole is estimated to be (1–5)x$10^7$ $M_{Sun}$, which is in good agreement with values obtained from other techniques.

A letter in *ApJ* reported the discovery of a massive, X-ray-luminous cluster of galaxies at $z = 1.393$, which is the most distant (X-ray-selected) cluster found to date (Fig. 2.5.2). XMMU J2235.3-2557 (Fig. 2.5.3) was serendipitously detected as an extended X-ray source in an archival XMM-Newton observation. VLT-FORS2 R and *z*-band snapshot imaging reveals an over-density of red galaxies in both angular and colour spaces coincident in the sky with the X-ray emission. Subsequent VLT-FORS2 multi-object spectroscopy unambiguously confirms the presence of a massive cluster

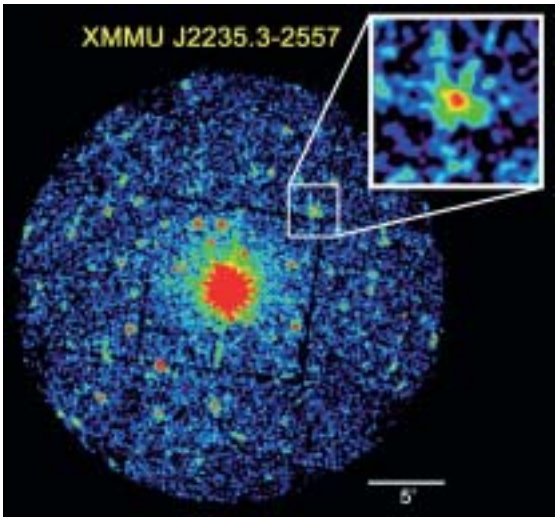


**Figure 2.5.3. The XMM-Newton observation of the nearby galaxy NGC 7314 (bright object at centre) from which the distant cluster XMMU J2235.3-2557 was serendipitously identified (white box). The inset covers a 2.8x2.8 arcmin region of the sky and shows the diffuse X-ray emission from XMMU J2235.3-2557, coming from a distance of 9 billion light-years. Note that the circular FOV of XMM-Newton has the same angular size as the full Moon.**

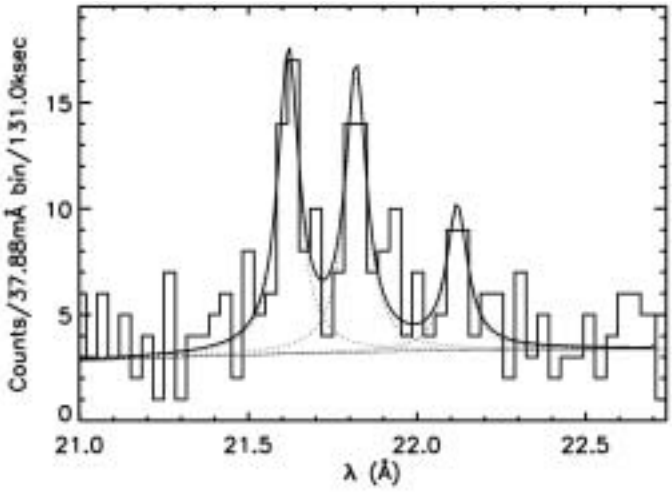


**Figure 2.5.4. RGS spectrum of BP Tau. Shown is the best fit model, overlaid on the OVII region spectrum.**

based on 12 concordant redshifts in the interval $1.38 < z < 1.40$. The cluster has an aperture-corrected, unabsorbed X-ray flux of $f_X = (3.6\pm0.3)$ x $10^{-14}$ erg/cm$^2$/s, a rest-frame X-ray luminosity of $L_X = (3.0\pm0.2)$ x $10^{44}\, h_{70}^{-2}$ erg/s (0.5–2.0 keV), and a temperature of kT = 6.0 (+2.5, –1.8) keV. Though XMMU J2235.3-2557 is likely to be the first confirmed $z > 1$ cluster found with XMM-Newton, the relative ease and efficiency of the discovery demonstrates that it should be possible to build large samples of $z > 1$ clusters through the joint use of XMM-Newton and large, ground-based telescopes.

A letter in *A&A* reported on the classical T Tauri star BP Tau. In the XMM-Newton RGS spectrum (Fig. 2.5.4), the O VII triplet is clearly detected with a very weak forbidden line indicating high plasma densities and/or a high UV flux environment. At the same time, concurrent XMM-Newton OM UV data point to a small hot-spot filling factor, suggesting an accretion funnel shock as the site of the X-ray and UV emission. Together with the X-ray data on TW Hya, these new observations suggest such funnels to be a general feature in classical T Tauri stars.

# 2.6 Cluster

## Introduction

After 5 years of operations, the four Cluster spacecraft are making great advances in magnetospheric physics by looking for the first time at plasma structures in three dimensions. This is the first time that the Earth's magnetic field and its environment have been explored by a constellation of four identical spacecraft. Results show that, with four, a detailed 3-D view of the Sun-Earth connection processes taking place at the interface between the solar wind and Earth's magnetic field can be obtained.

Cluster and SOHO together constitute the Solar Terrestrial Science Programme (STSP), the first Cornerstone of ESA's Horizon 2000 Programme. Cluster was proposed in November 1982 in response to an ESA call for proposals for the next series of scientific missions. After the failure of Ariane-5 on 4 June 1996 and the destruction of the four original satellites, Cluster was rebuilt and launched in pairs in July and August 2000 aboard two Soyuz rockets.

In February 2005 the ESA SPC agreed to a second extension of the mission for a period of 4 years (up to end-2009), with a mid-term review at the end of 2007.

## Mission status

The four satellites and 41 instruments (Table 2.6.1) have worked normally since the beginning of the mission. The payload consists of magnetometers (flux gate for the static magnetic field and search coil for the magnetic waves), wire booms and electron guns to measure electric fields, and particle detectors to measure electrons and ions from a few eV to a few MeV. The mission goal is to measure the magnetospheric structures at different scales. To achieve that, about half of the spacecraft mass consisted of propellant: about 450 kg of the 600 kg was used to achieve the operational orbit of 4 x 19.6 Earth-radii. The remainder is being used to modify the satellite separations (Fig. 2.6.1). Seven constellation manoeuvres have been made so far to create separations of 600, 2000, 100, 5000, 250, 1000 and, since the summer of 2005, 10 000 km.

The latter is known as a multi-scale configuration. Instead of a perfect tetrahedron with the same distance between each satellite, a 'flat-tetrahedron' was formed with three satellites (C1, C2 and C3) separated by 10 000 km and two (C3 and C4) by 1000 km. This configuration allows the study of detailed plasma boundaries that are usually smaller in one direction, such as the magnetotail plasma sheet, or the magnetopause and bow shock.

The satellites are in a polar orbit that is influenced by solar and lunar perturbations. A direct consequence is a drift of the apogee towards the southern hemisphere. This natural evolution will improve the science return, since new regions will be visited, such as the magnetopause at the sub-solar point, the near-Earth plasma sheet and the auroral acceleration region (Fig. 2.6.2).

## Science highlights

Some of the major advances in magnetospheric physics with Cluster have come from the first measurements of surface waves. These waves can be produced when two plasmas of different origins encounter each other, or when a catastrophic explosion, such as magnetic reconnection, changes the magnetic configuration of a plasma region. With four satellites, the waves can be fully characterised for the first time (speed, direction, wave mode). A statistical study using Cluster data has revealed the main characteristics of the waves observed in the magnetotail. The flapping motions of the Earth's plasma sheet are of internal origin, according to a large set of observations from Cluster. This dataset includes 58 rapid plasma sheet crossings, observed near the magnetotail flanks.

Rapid, large-amplitude magnetic variations are frequently observed in the centre of

*For further information, see http://sci.esa.int/cluster*

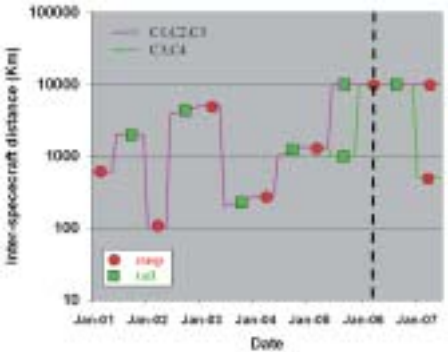


**Figure 2.6.1. Inter-spacecraft distances from launch to mid-2007.**

**Table 2.6.1. The Cluster payload.**

| *Acronym/Instrument* | *Principal Investigator* |
|---|---|
| FGM/Fluxgate Magnetometer | E. Lucek (IC, UK) |
| STAFF*/Spatio-Temporal Analysis of Field Fluctuation experiment | N. Cornilleau-Wehrlin (CETP, France) |
| EFW*/Electric Field and Wave experiment | M. André (IRFU, Sweden) |
| WHISPER*/Waves of High Frequency and Sounder for Probing of Electron density by Relaxation | P.M.E. Décréau (LPCE, France) |
| WBD*/Wide Band Data | J. Pickett (Iowa U., USA) |
| DWP*/Digital Wave Processing experiment | H. Alleyne (Sheffield U., UK) |
| EDI/Electron Drift Instrument | R. Torbert (U. New Hampshire, USA) |
| CIS/Cluster-II Ion Spectrometry | H. Rème (CESR, France) |
| PEACE/Plasma Electron and Current Experiment | A. Fazakerley (MSSL, UK) |
| RAPID/Research with Adaptive Imaging Particle Detectors | P. Daly (MPAe, Germany) |
| ASPOC/Active Spacecraft Potential Control | K. Torkar (IWF, Austria) |

* Members of the Wave Experiment Consortium (WEC)

the magnetotail (Fig. 2.6.3). These variations indicate up-down (north-south) oscillating current sheet motions, known as current sheet flapping. Two possible origins of these motions were proposed in the past: external (caused by inhomogeneous solar wind) or internal (large-scale waves, emitted in the current sheet and/or propagating in the tail).

Before Cluster, no final conclusion could be drawn, owing to the difficulties of separating spatial and temporal effects. Now, a systematic analysis of tens of rapid plasma sheet crossings suggests that the flapping motions are of internal origin. Kink-like waves are emitted in the centre of the tail and propagate toward the tail flanks (Fig. 2.6.3, top). The properties of these waves (phase velocity, direction of propagation) cannot be explained by any local excitation mechanism discussed so far in the literature.

In addition to waves, high-speed flows of plasma, or bursty bulk flows (BBFs), are often observed in the magnetotail. BBFs propagate from the magnetotail to the Earth at speeds higher than 300 km/s and are the carriers of significant amounts of mass, energy and magnetic flux. A statistical study, based on multipoint measurements by Cluster, revealed their typical spatial scale for the first time. More than 1600 data points of Earthward flow events were used to deduce the size of the BBFs around 2–3 $R_E$ in the dawn-dusk direction and 1.5–2 $R_E$ in the north-south direction.

The Earth's magnetic field acts as a shield against the solar wind, which itself carries the Sun's magnetic field to the edge of the heliosphere. Sometimes the magnetic field in the solar wind lines up with that of the Earth, and sometimes it points in the opposite direction. When the two fields are opposed, they can undergo magnetic reconnection, allowing the solar wind to flow into the magnetosphere and collect in a reservoir known as the boundary layer. On the other hand, if the fields are aligned, they should present an impenetrable barrier to the flow.

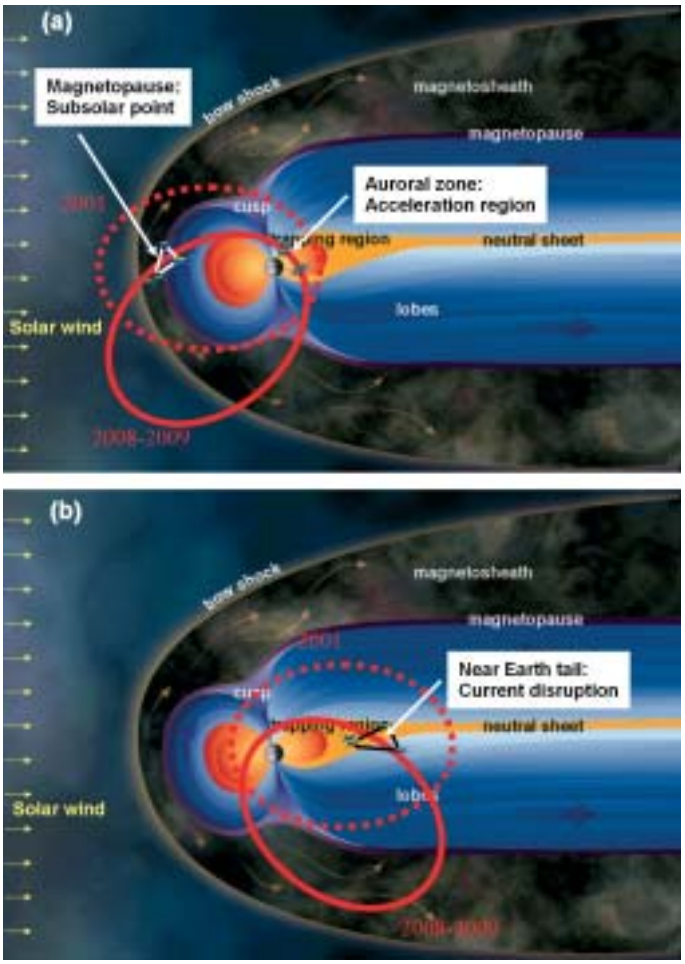


**Figure 2.6.2. Cluster orbit evolution between 2001 and 2009 in (a) winter and (b) summer.**

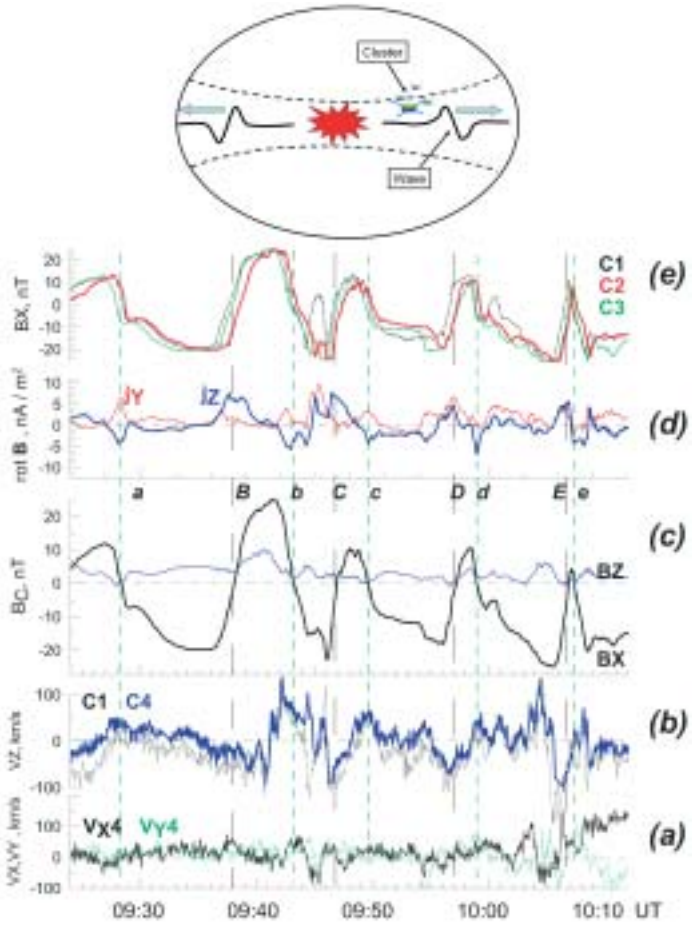


**Figure 2.6.3. Top: the surface waves propagating from the centre of the magnetotail to the flanks. Bottom: overview of Cluster observations on 20 October 2001, including ion plasma flows from CIS-CODIF (a, b), Bx-components at spacecraft C1, C2 and C3 (e), magnetic field x- and z-components computed at the Cluster baricentre, (c) Bx estimates by the curlometer technique (panel d, only samples with $|\bar{v}\cdot B|/|\bar{v}\times B| < 0.2$ are included). (From Sergeev et al., 2004)**

Satellite measurements dating back to 1987 present a puzzle, however, because they clearly show that the boundary layer contains more solar wind plasma when the fields are aligned than when they are not. So how is the solar wind getting in?

On 20 November 2001, the Cluster flotilla was heading around from behind Earth and had just arrived at the dusk side of the planet, where the solar wind slides past the magnetosphere. There it began to encounter vortices of plasma at the magnetopause, the outer edge of the magnetosphere. These vortices were large structures, about 6 $R_E$ (38 000 km) across.

Such vortices are known to be products of Kelvin-Helmholtz instabilities (KHIs), and can occur when two adjacent flows are travelling at different speeds, so that one slips past the other. Good examples of KHIs are the waves whipped up by the wind

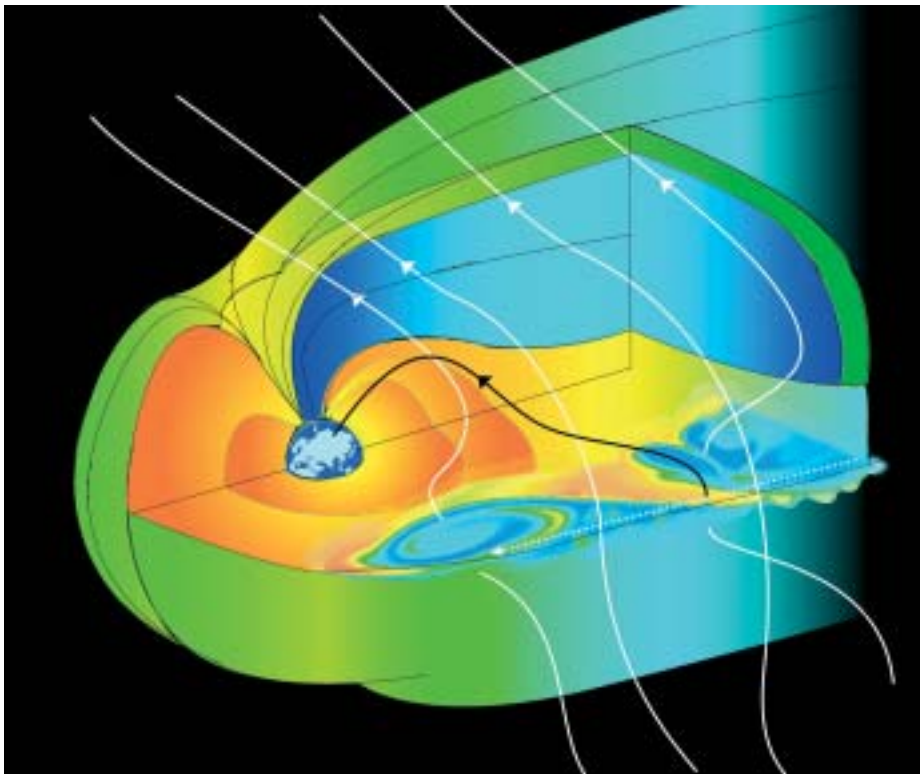

**Figure 2.6.4. A 3-D cutaway of Earth's magnetosphere. The curly features sketched on the boundary layer are the Kelvin-Helmholtz vortices discovered by Cluster. They originate where two adjacent flows travel at different speeds. In this case, one of the flows is the heated gas inside the boundary layer of the magnetosphere, the other the solar wind just outside it. The arrows show the direction of the magnetic field; white is associated with the solar wind and black inside the magnetosphere. The white arrows show the trajectories followed by Cluster. (From Hasegawa et al., 2004)**

slipping across the surface of the ocean. Although KHI-waves had been observed before, this was the first time that vortices were actually detected.

When a KHI-wave rolls up into a vortex, it becomes known as a 'Kelvin cat's eye'. The data collected by Cluster have shown density variations of the plasma, right at the magnetopause, precisely like those expected when travelling through a Kelvin cat's eye. Scientists had postulated that, if these structures were to form at the magnetopause, they might be able to pull large quantities of the solar wind inside the boundary layer as they collapse.

Cluster is shedding light on other aspects of magnetic reconnection. Complex geometrical properties of a transient and spatially confined type of reconnection have been observed in the past, but have remained unexplained owing to the high velocity of the magnetopause and the use of single-satellite measurements. Multipoint measurements from Cluster have provided the first direct observation of a 3-D magnetic field topology at the magnetopause, resulting from magnetic reconnection at multiple sites, that could explain these geometrical properties. They have also provided a direct view of the entry of particles through the magnetopause.

Cluster has made the first direct measurement of the 'ring current' that is part of the radiation belts, and which increases dramatically during geomagnetic storms. The curlometer method (involving measurement of the magnetic field at the four satellites and computation of the electric current) was not expected to give good results for the ring current because the satellite tetrahedron is greatly deformed at this location. When the separation of the four satellites was below 200 km, however, the current could be estimated with sufficient accuracy.

Finally, a study of the changes to the radiation belts during the October-November

2003 solar storms has revealed a new process that could produce energetic particles. On 29 October, the radiation belts disappeared from their usual location and then reformed much closer to the Earth, in a region where high-energy particles are usually not found. Combining data from Cluster with ground-based measurements from Antarctica, it was found that a 'chorus' electromagnetic emission was responsible for the acceleration of electrons. Radiation belts can be a hazard to satellites and humans in space, and such studies are crucial to understanding their formation.

## Cluster Science Data System and Active Archive

The Cluster Science Data System (CSDS) is a distributed system of eight nationally-funded and -operated data centres. It makes possible the joint scientific analysis of data from all 41 instruments. The general approach is to have national data centres located near the Principal Investigators (PIs) and thus near the expertise required for processing the data. A major task of CSDS is to offer products routinely, such as the Summary Parameter Data Base and the Prime Parameter Data Base. CSDS also serves to some extent as the infrastructure for the Joint Science Operations Centre (JSOC), which is a staffed facility at the Rutherford Appleton Laboratory (UK), to support the scientific payload operations.

In most cases, the data centres produce data products on behalf of the national PI teams. Members of the Cluster science community wishing to access CSDS do so via their national data centres. In those countries without a national data centre, members can ask the relevant PI to determine which data centre should be contacted. It should be noted that all data centres offer the same data products. Scientists from outside the Cluster community also have access to CSDS, according to the policy on data rights as agreed by the PIs. Full access can be granted to the Summary Parameters and CSDSweb.

CSDS data access has been steadily increasing since its opening on 1 February 2001. The download rate for summary and prime parameters data is now above 7 Gb per month and above 2.5 Gb per month for CSDSweb. More information and data access can be found at: http://sci2.estec.esa.nl/cluster/csds/csds.html

CSDS was established to exchange data from different instruments soon after acquisition and to facilitate data browsing to identify interesting events. For that purpose, CSDS contains low- and medium-resolution data. Once events have been identified, the detailed data analysis requires high-resolution data. These data are processed and validated at the PI institute. Owing to limited manpower in the PI teams, this is done on an event-by-event basis. To maximise the scientific return of the mission, it is necessary to make all Cluster high-resolution data available to the wide scientific community. To facilitate this, the Cluster Active Archive (CAA) was created.

The CAA is a database of high-resolution data (and allied products and services) that was established and is maintained under the overall control of ESA. A small team, led by the Archive Project Manager, runs the CAA. In view of the shortage of manpower in most institutes where Cluster data are processed, ESA provides support to manpower deployed in institutes where the relevant expertise exists, to assist in the preparation, validation, and documentation of the high-resolution data deposited in the archive. The web page of the CAA is at: http://caa.estec.esa.int/

After successfully passing the implementation review in June 2005, and beta testing during autumn 2005, the CAA was opened to the public on 1 February 2005. Initially, the database will contain data from the first few years of Cluster, with data from the following years being added progressively.

# 2.7 Integral

## Introduction

Integral was launched on 17 October 2002 into a highly elliptical 72 h orbit with an initial perigee of 9000 km, apogee of 154 000 km and inclination of 52°. Scientific observations are performed above nominal altitudes of 60 000 km (approaching the radiation belts) and 40 000 km (leaving the radiation belts). This ESA-led mission includes contributions from Russia (Proton launch) and NASA (Goldstone ground station). Integral is currently delivering gamma-ray observations at high spatial and spectral resolution in the 15 keV to 10 MeV energy range using two main instruments: the SPI spectrometer and the IBIS imager. Both instruments provide spectral and spatial information, with SPI optimised for high spectral resolution ($E/\Delta E \sim 500$) in the energy range 20 keV to 8 MeV, and IBIS for high spatial resolution (a source location accuracy of < 1 arcmin). SPI has of 19 cooled Ge detectors, while IBIS has an array of 16 384 CdTe detectors (ISGRI) sensitive at 15 keV to 1 MeV located above 4096 CsI crystals (PICsIT) working at 175 keV to 10 MeV. In addition, simultaneous X-ray (JEM-X; 3-35 keV) and V-band (OMC) optical monitoring is provided. All three high-energy instruments use the coded mask principle to provide imaging information over large fields of view. The Integral Science Operations Centre (ISOC) is located in ESAC, Madrid. Mission operations are conducted from ESOC, Darmstadt and the nationally-provided science data centre (ISDC) in Versoix, near Geneva. The main ground station is at Redu, Belgium.

## Mission status

Integral was originally approved for 2.2 years of operation with a design lifetime of 5 years. The SPC has approved a 4-year extension, to December 2010, subject to the usual performance and mission status review after 2 years. Operations continue smoothly, with all systems and the ground segment performing nominally. At the current rate of consumption there is ample propellant for the approved lifetime. There has been no unexpected degradation of the solar arrays, batteries or any other system and there has been no loss of redundancy. The particle background experienced by Integral is monitored via a dedicated counter (IREM). On the payload side, 2 of the 19 SPI detectors have failed (in 2003 December and 2004 July) resulting in, to first order, a reduction in observing efficiency of ~10%. The SPI detectors are annealed (baked) about every 6 months to maintain the instrument's very high spectral resolution. Owing to a slow change in performance, only one of the two identical JEM-X units is operated at any one time, thereby ensuring a suitably long lifetime. The other instruments are working as expected, with performances in line with those predicted before launch.

The majority of observing time is made available to the general astronomical community via calls for observing proposals. AO-3 was issued in September 2004 and covered 75% of the available observing time for an interval of 18 months. 108 proposals were received, resulting in an annualised over-subscription factor of 4.1. Approximately half concerned compact galactic sources, a quarter extragalactic objects, and the remainder nucleosynthesis studies and miscellaneous objects. The remaining observing time is provided to the Integral Science Working Team (ISWT) in return for their contributions to the mission. The ISWT comprises the instrument and data centre principal investigators, mission scientists, the project scientist and representatives of the US and Russian scientific communities. This core programme observing time has been used mainly for survey-type activities, including regular scans along the galactic plane and deep exposures of the central parts of the Galaxy.

The on-line data archive at the ISDC (http://isdc.unige.ch/?Data+browse) is regularly updated as new observations enter the public domain (1 year after they are received by the observer). In collaboration with the ISDC, the ISOC Science Data

*For further information, see http://integral.esa.int/*

**Table 2.7.1. Principal characteristics of the Integral scientific payload.**

| | *SPI* | *IBIS* | *JEM-X* | *OMC* |
|---|---|---|---|---|
| Energy range | 20 keV - 8 MeV | 15 keV - 10 MeV | 3-35 keV | 500-850 nm |
| Detectors/characteristics | 19 Ge (each 6x7 cm) cooled @ 85K | 16384 CdTe (each 4x4x2 mm); 4096 CsI (each 9x9x30 mm) | Microstrip Xe-gas detector (1.5 bar) | CCD + V-filter |
| Detector area ($cm^2$) | 500 | 2600 (CdTe) 3100 (CsI) | 2 x 500 | 2048 x 1024 pix |
| Spectral resolution | 2.2 keV @ 1.33 MeV | 9 keV @ 100 keV | 1.3 keV @ 10 keV | – |
| FOV (fully coded) | 16° | 9x9° | 4.8° | 5x5° |
| Angular res (FWHM) | 2° | 12 arcmin | 3 arcmin | 17.6 arcsec/pix |
| 10σ source location | 1.3° | < 1 arcmin | < 30 arcsec | 6 arcsec |
| Continuum sensitivity* | $3x10^{-6}$ @ 1 MeV | $3x10^{-6}$ @ 100 keV | $1.2x10^{-4}$ @ 6 keV | $18.2^{m}$ ($10^{-3}$ s) |
| Line sensitivity* | $5x10^{-6}$ @ 1 MeV | $2x10^{-5}$ @ 100 keV | $1.7x10^{-5}$ @ 6 keV | – |
| Timing accuracy (3σ) | 129 μs | 62 μs - 30 min | 122 μs | var. in units of 1 s |
| Mass (kg) | 1309 | 628 | 65 | 17 |
| Power (W) | 250 | 220 | 52 | 12 |
| Telemetry allocation (kbit/s) | 45 | 57 | 4 | 2 |

*sensitivities are 3σ in $10^5$ s and $\Delta E/E = 0.5$, units ph $cm^{-2}$ $s^{-1}$ $keV^{-1}$ (continuum) and ph $cm^{-2}$ $s^{-1}$ (line)

Archive (ISDA) (http://Integral.esac.esa.int/isda) was made publicly available in July 2005. The ISDA is based on the technology used to create the ISO and XMM-Newton ESA archives and provides users experienced with, for example, the XMM-Newton archive with a familiar interface to access Integral science products. Offline scientific analysis software for all the instruments (currently OSA 5.1) can be downloaded from the ISDC and installed on the users' own computers.

## Scientific highlights

There have been many important scientific achievements obtained during the first 3 years of the mission. There are currently around six refereed papers per month appearing in the scientific literature containing results from Integral. A selection of interesting results is given below.

**Origin of soft Galactic gamma-ray emission**

Integral has solved a key problem concerning the contribution of discrete point sources to the galactic diffuse soft gamma-ray background. At energies below 10 keV, it is believed that there is a truly diffuse component that accounts for 80% of the unresolved emission detected in small sky regions that do not contain bright sources. At higher energies, previous observations by SIGMA and CGRO/OSSE were unable to separate reliably point sources from diffuse emission, and 50% of the emission in the 50–500 keV range was attributed to point sources. It was difficult to explain the

**Table 2.7.2. Principal characteristics of the Integral mission.**

*Launch:* 17 October 2002 by Proton into orbit of 72 h, 51.6° inclination, 9 000 km perigee height, 153 000 km apogee height. Start of science operations December 2002 (nominal duration 2 years, extended mission to December 2010 approved).

*Science goals:* compact objects; extragalactic astronomy; stellar nucleosynthesis; galactic structure; particle processes and acceleration; identification of high-energy sources.

*Science operations:*
Integral Science Operations Centre (ISOC) at ESAC (Vilspa);
Integral Science Data Centre (ISDC) in Versoix (CH);
distribution of observing time:
1st mission year: 35% guaranteed time, 65% open time (via AO)
2nd mission year: 30% guaranteed time, 70% open time (via AO)
3rd-5th mission years: 25% guaranteed time, 75% open time (via AO)
6th mission year: 20% guaranteed time, 80% open time (via AO)

*Spacecraft:*
3-axis stabilised (all errors 3σ; instruments point along x-axis, y-axis is along length of solar arrays):
absolute pointing error: 5 arcmin (y,z), 15 arcmin (x)
absolute pointing drift ($10^5$ s): 0.6 arcmin (y,z), 2 arcmin (x)
relative pointing error ($10^3$ s) : 0.3 arcmin (y,z), 1 arcmin (x)
absolute measurement error : 1 arcmin (y,z), 3 arcmin (x)
Data rate: 108 kbit/s (science telemetry)
Power (payload): 690 W
Spacecraft size: 3x4x5 m (solar arrays stowed; 16 m span deployed)
Mass: about 4000 kg at launch; 3500 kg dry; 520 kg hydrazine propellant

*Operations:*
Operations Centre: Mission Operations Centre (Darmstadt, D), ISOC (ESTEC)
Data transmission: S-Band, ground stations: Redu (B), Goldstone (USA)
Mission lifetime: 2 years nominal, 5 years technical design life

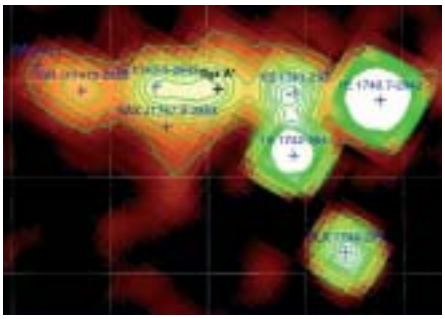

**Figure 2.7.1. IBIS/ISGRI map in the 20–40 keV range of the galactic centre region (4.7 Ms). The orientation is in galactic coordinates, the image size is ~2.5° x 1.7° (Bélanger et al., *ApJ* 636, 275, 2006).**

remaining emission, which was assumed to be diffuse, because inverse Compton scattering of very energetic cosmic ray electrons would also produce a substantial radio-synchrotron emission at much higher level than observed. An alternative explanation (electron Bremsstrahlung in the interstellar medium) was difficult to reconcile with those observations, because the associated power of $10^{43}$ erg/s would affect the ionisation equilibrium and dissociation of molecules in the interstellar medium.

Integral was able to solve this long-standing problem by combining accurate imaging with good sensitivity at 20–220 keV. The energy output from 91 individual point sources detected in the inner Galaxy accounts for around 90% of the diffuse continuum emission. The truly diffuse component contributes only 10–25% (depending on energy) of the total Galactic ridge emission.

### The Galactic Centre

The Galactic Centre is a prime target for Integral because it harbours many compact objects and sources of diffuse emission, as well as a 3 million solar-mass black hole that is surprisingly weak at high energies.

The centre of our Galaxy was observed with IBIS/ISGRI above 20 keV. A new source (Fig. 2.7.1) coincident to within 0.9 arcmin of the Galactic nucleus Sgr A* (believed to be the counterpart of the massive black hole) was detected at energies up to 120 keV. The 20–120 keV luminosity is only $5x10^{35}$ erg $s^{-1}$, approximately 8 orders

of magnitude lower than expected from a maximally accreting black hole of this mass. Contemporaneous XMM-Newton and Integral observations did not reveal any significant variability. This new source is the first example of persistent hard X-ray emission from within the central 10 arcmin of the Galaxy. There is a distinct possibility that we are seeing hard X-ray emission from the supermassive black hole at the centre for the first time. These measurements are providing new insights into the broadband spectra of massive, weakly accreting, black holes.

Is it possible that Sgr A* was much brighter in the past? This hypothesis has been tested assuming scattering of X-rays by molecular clouds. Integral observations of the molecular cloud Sgr B2 revealed this source for the first time above 20 keV. The observed hard X-ray continuum, a hard power-law with a photon index of 1.8, together with a cut-off above 100 keV and a strong fluorescence line at 6.4 keV as observed by ASCA, were used to model the input spectrum of Sgr A*. It was concluded that, about 350 years ago (corresponding to the light travel time between Sgr A* and Sgr B2), Sgr A* was about 10 000 times more luminous than it is today. This conclusion is supported by the observation that the 6.4 keV line has remained stable over the last 10 years, ruling out any close stellar transient X-ray binary as the illuminating source

**A new class of high-mass X-ray binaries**

The second Integral source catalogue identified 55 gamma-ray sources (IGR), of which only 20% had been classified. These new sources are located around the Galactic Centre and in the Norma and Scutum spiral arms. Most are highly absorbed below 5 keV, many are X-ray pulsars, and the intrinsic absorption is very high ($N_H > 10^{23}$ cm$^{-2}$). A 'typical' IGR-source can be characterised as a 'cocooned' compact object residing in a binary system with accretion/wind from a massive companion. These sources escaped previous detection in soft X-rays. By detecting a new class of super-giant, high-mass X-ray binaries (HMXBs) with Integral, their known population in the inner Galaxy has more than doubled, opening new insights into HMXBs and their relation to star formation and galactic structure.

Another interesting group of objects studied by Integral are Fast X-ray Transients. These are sources that flare up for just hours instead of weeks or months, and thus are easily missed. Integral data, combined with other X-ray satellite observations, indicate that again these are systems with supergiant companions, forming a wide class that lies hidden throughout the Galaxy and probably much more abundant in our Galaxy than previously thought.

**Accreting ms-pulsar IGR J00291+5934**

The high-energy sky is highly variable and Targets of Opportunity (ToO) observations are crucial for every high-energy mission. Up until August 2005, Integral had performed 23 TOO observations (about 5 Ms in total). One of the most interesting sources observed is the new ms pulsar IGR J00291+5934. Detected in December 2004, it turned out to be the fastest known accreting X-ray pulsar (period: 1.67 ms) and is considered to be the missing link between normal radio pulsars and isolated radio ms-pulsars. Accurate imaging with IBIS isolated the pulsar from the nearby (20 arcmin) cataclysmic variable V709 Cas and allowed the observation of the high-energy emission during the entire outburst. For the first time, IBIS detected pulsed emission up to 150 keV. The total spectrum is characterised by thermal emission from the disc in soft X-rays (from contemporaneous RXTE data), while at energies above 20 keV, the spectrum is dominated by a 40 keV thermally Comptonised spectrum, considerably hotter than measured previously. Matter is thought to accrete along

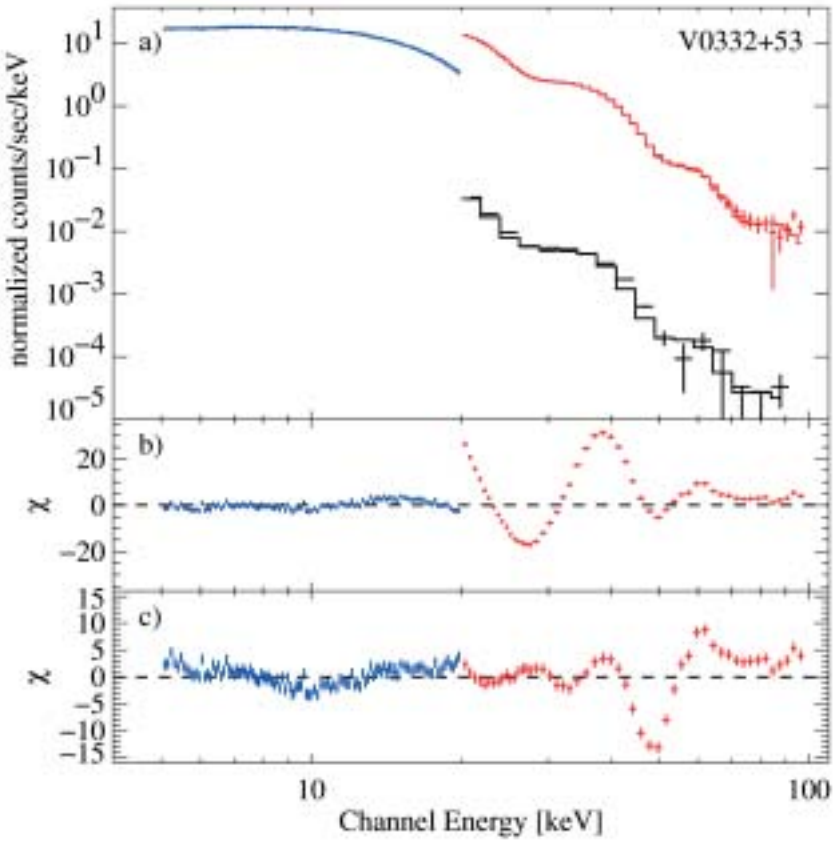


**Figure 2.7.2. Integral spectra of V 0332+53 with broad cyclotron line features at ~25, ~50 and ~72 keV. Panel (a) shows detector spectra of JEM-X (blue), ISGRI (red) and SPI (black); panels (b) and (c) show residuals of fits with no line and a line at ~25 keV included, respectively. (Kreykenbohm et al., *A&A* 433, L45, 2005).**

magnetic field lines toward the poles of the neutron star and be heated by an accretion shock. Thermal (1 keV) seed photons from the hot spot are scattered in the 40 keV plasma. As pulsed emission is also observed, a large fraction of the hard tail emission must come from the poles, not from the disc. The observations further showed, for the first time, that the pulsed emission becomes (much) harder than the total spectrum with increasing energy – consistent with Doppler boosting from the emitting polar region – and also that the pulsed fraction of the emission increases with energy: up to 20% at 100 keV.

**Anomalous X-ray pulsars**

Another surprise was the detection of very hard emission from anomalous X-ray pulsars (AXPs). Before Integral, these systems were known to be young pulsars with soft spectra and very strong magnetic fields of order $10^{15}$ G. Integral showed that AXP spectra are surprisingly hard at energies above 10–20 keV. The hard spectra most probably indicate a magnetospheric origin, i.e. they are not powered by the spin-down mechanism. In order to be consistent with higher energy observations by CGRO, these spectra must show a break, or bend, at higher energies, to be detected by Integral in the future.

**Cyclotron lines**

Cyclotron lines are often observed in the spectra of accreting X-ray pulsars as broad absorption features typically with energies of 10-50 keV. They arise as a result of

resonant scattering of photons by electrons whose energies are quantised into Landau levels by the magnetic field, offering a direct measure of the field strength in accreting neutron stars and, less directly, other parameters of the emission region. A major strength of Integral for studying these features is the good energy resolution of the instruments combined with the broad spectral coverage, allowing more precise line parameter determinations than previously.

In January 2005, Integral observed the transient X-ray pulsar V 0332+53 during an outburst. In the source spectra, three broad line features at ~25, ~50 and ~72 keV (Fig. 2.7.2) are immediately visible. A more detailed study shows that the line parameters vary significantly during the outburst decay – both the line energies and depths increase with decreasing source brightness, while the line widths decrease. These changes indicate a scattering region diminishing in size and moving closer to the polar cap as the accretion rate decreases.

Another interesting cyclotron line source is the X-ray binary 1A 0535+262 that, after 11 years of quiescence, erupted again in a giant outburst. The line-of-sight was too close to the Sun for most satellites, however. A subsequent (weaker) outburst was observed by Integral. This showed a strong line feature at ~45 keV, not at 110 keV as expected from CGRO observations of the last giant outburst in 1994. Besides halving the accepted magnetic field strength of this object from ~$10^{13}$ G to ~$4 \times 10^{12}$ G (still the strongest field measured directly), these observations again clearly indicate a scattering region changing with overall luminosity.

**Electron-positron annihilation (511 keV) emission**

The 511 keV line, resulting from annihilation of electrons with their antimatter particles (positrons), is the brightest gamma-ray line in the Galaxy. The principal source of the positrons is unknown, however. Current theories include explosive nucleosynthesis products from supernovae, novae, Wolf-Rayet stars; cosmic ray interaction with the interstellar medium; black holes and pulsars; gamma-ray bursts; hypernovae and light dark-matter particles. On theoretical grounds, it is difficult to disentangle the primary positron source owing to the highly uncertain yields and the uncertain source distribution and frequency. Mapping of a large part of the entire sky by Integral showed for the first time that the diffuse 511 keV emission is located only towards the galactic centre (Fig. 2.7.3). The emission is almost symmetrical with a FWHM of 8°. The flux from the bulge is $10^{-3}$ cm$^{-2}$ s$^{-1}$. The results are compatible with a weak disc component (70% of the bulge flux) that can be fully explained by the $\beta^+$-decay of $^{26}$Al and $^{44}$Ti. However, the bulge/disc luminosity ratio of 3–9 imposes severe constraints on the principal positron source: the 511 keV sky map has a unique morphology not fully matched by any counterpart tracer map. Likely counterparts could be the old stellar population (SNIa, novae, low-mass X-ray binaries) or light dark-matter particles, all having a weak or no disc component. No point sources contribute to a level of $10^{-4}$ cm$^{-2}$ s$^{-1}$ and the local annihilation fountain of 511 keV emission reported by CGRO/OSSE from a region about 8° north of the Galactic centre could not be confirmed.

The spectral line with energy 510.954±0.075 keV and width (FWHM) 2.37±0.25 keV is unshifted and no fast expansion can be seen. The narrow line is compatible with a single-phase warm (8000K), weakly ionised (0.1) interstellar medium with an electron density of ~0.3 cm$^{-3}$. Very recently, the existence of a broad (FWHM 5.4±1.2 keV) component, resulting from in-flight annihilation in warm neutral interstellar medium, could be identified with a flux of ~50% of the narrow line flux. The observed continuum emission owing to the decay of ortho-positronium below 511 keV results in a positronium fraction of about 96%.

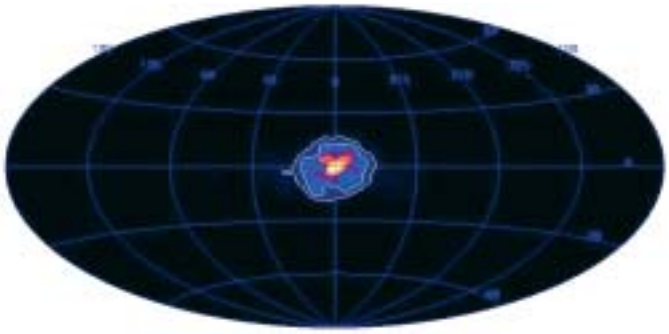

**Figure 2.7.3. All-sky map of the 511 keV annihilation emission in galactic coordinates. (Knödlseder et al., *A&A* 441, 513, 2005).**

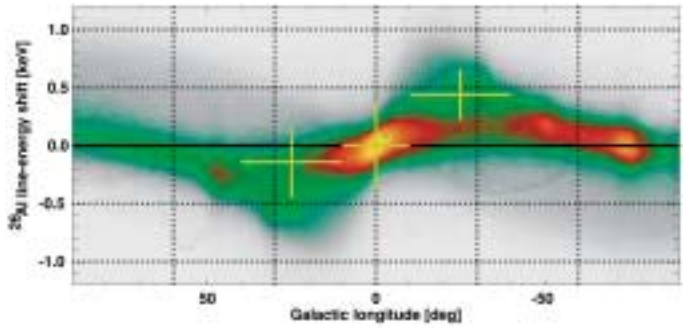


**Figure 2.7.4. Integral measurements of the $^{26}$Al line emission at 1809 keV in three longitude intervals superposed on the modelled 3-D distribution of $^{26}$Al sources combined with the galactic rotation. (Diehl et al., *Nature* 439, 45, 2006).**

**Gamma-ray line emission from Cas A, the inner Galaxy and Cygnus region**

Cas A, the youngest known Galactic supernova remnant (320 yr, at a distance of 3.4 kpc), was observed and IBIS detected a line at 67.8 keV associated with $^{44}$Ti, a key tracer for core-collapse supernovae. The flux is $(2.3\pm0.8)\times10^{-5}$ cm$^{-2}$ s$^{-1}$. The 78.4 keV line 3σ upper limit is $2.3\times10^{-5}$ cm$^{-2}$ s$^{-1}$. Accurate imaging excludes possible source contamination of the signal during earlier BeppoSax observations. The uncertainty in the determination of the continuum below 100 keV needs to be further reduced by future observations. With SPI, the 3σ upper limit is $3.1\times10^{-5}$ cm$^{-2}$ s$^{-1}$ for a 4 keV (1000 km s$^{-1}$) -wide line, compatible with the CGRO Comptel detection at 1.1 MeV; a narrow line can now almost be excluded. This may create a conflict with theoretical models because $^{44}$Ti is thought to be formed close to the mass cut, hence small velocities (≤ 1000 km s$^{-1}$) should be expected.

1809 keV emission from $^{26}$Al is a key tracer for nucleosynthesis from massive stars. Accurate spectroscopy using SPI has revealed that the emission from the longitude range 10–40° is redshifted by about 0.2 keV, while emission from the longitude range –10–40° is blueshifted by about 0.4 keV, with respect to the 1809 keV emission observed from the Galactic centre (Fig. 2.7.4). These results confirm the global nature of the observed $^{26}$Al emission and are compatible with the expected shifts due to galactic rotation in the inner Galaxy. Interestingly, this implies that we are observing the entire Al-emission throughout the Galaxy (with a half-life of about $10^6$ yr, covering many supernova events), so this provides an independent method to determine the current core-collapse supernovae rate in the Galaxy of 1.9±1.1 per century. This also allows the derivation of the Galactic star formation rate of ~4 solar masses per year (or ~7.5 stars per year) in the Galaxy.

The Cygnus region is the most active nearby star-forming region in the Galaxy; a large number of massive stars should enrich the interstellar medium with

nucleosynthesis products. Integral observations of the 1809 keV line from $^{26}$Al show that the line is much broader (FWHM 3.3 keV) than in the inner Galaxy (1.6 keV). This can be attributed to the observation of turbulent motions in hot superbubbles.

Gamma-ray lines at 1173 keV and 1333 keV are produced by $^{60}$Fe, another tracer of nucleosynthesis in massive stars. As the lifetime is similar to that of $^{26}$Al, a steady state abundance along the Galactic plane is expected because the time difference between galactic supernova events is much smaller. Integral detected a flux (combined for the two lines) of $3.7 \times 10^{-5}$ cm$^{-2}$ s$^{-1}$ from the inner Galaxy. The flux ratio $^{60}$Fe/$^{26}$Al is $0.11 \pm 0.03$, substantially below predictions ($\geq 0.40$). Present uncertainties in theoretical modelling include insufficient knowledge of the cross-sections involved, and possibly also the need for another large source for $^{26}$Al emission other than core-collapse SN – possibly massive winds during the Wolf-Rayet phase. Future mapping should cast a light on this because the spatial distribution of Wolf-Rayet stars might be quite different (mass, metallicity) from the spatial distribution of the average supernova progenitor.

**Active galactic nuclei**

AGN are important targets for Integral: of the 209 sources in the second IBIS soft gamma-ray catalogue, 33 are extragalactic. The inner regions of AGN consist of a central supermassive black hole surrounded by accreting matter. Using Integral and XMM-Newton, more evidence has been found that supermassive black holes are surrounded by a toroidal gas cloud. Depending on our line-of-sight, the torus can block the view to the central black hole. Looking edge on into this doughnut for NGC 4388, it is possible to see features never before revealed with such clarity. For example, some of the gamma-rays produced close to the black hole are absorbed by iron atoms in the torus and are re-emitted at a lower energy, proof of seeing 'reprocessed' light farther out. Also, because of the line-of-sight towards NGC 4388, we know this iron is in the torus in the same plane as the accretion disc, and not from gas clouds above or below the accretion disc.

**Gamma-ray bursts**

Integral observes about one gamma-ray burst (GRB) each month as a serendipitous source in the large field of view. An automatic software system on-ground detects the GRB within seconds and automatically alerts the worldwide science community, allowing crucial follow-up observations at other wavelengths. In this way, a GRB that occurred on 3 December 2003 has been thoroughly studied by Integral and an armada of space- and ground-based observatories. It has been concluded that this event, GRB 031203, is the closest cosmic gamma-ray burst on record, and also the faintest. This important detection suggests that a large population of sub-energetic GRBs exists that had so far gone unnoticed.

# 2.8 Mars Express

## Introduction

Mars Express was launched on 2 June 2003 from Baikonur Cosmodrome aboard a Soyuz-Fregat vehicle. In addition to global studies of the surface, subsurface, atmosphere and space environment of Mars at unprecedented spatial and spectral resolution, the unifying theme of the mission is the search for water in its various states everywhere on the planet. The highly elliptical orbit is optimised to study all of this over the various Martian seasons, allowing for high-resolution observations near pericentre and global observations from higher altitude. Mars Express is the first European mission to orbit another planet in our Solar System.

Mars Express is on its way to providing a quantum leap in our understanding of the geological evolution of Mars, complemented by ground truth being provided by the NASA Mars Exploration Rovers (MERs). The nominal mission lifetime of 1 Martian year has already been extended by another Martian year. During the extended mission, priority will be given to fulfilling the remaining goals of the nominal mission (such as gravity measurements and seasonal coverage), to catching up with delayed MARSIS measurements, to completing global coverage of high-resolution imaging and spectroscopy, as well as subsurface sounding with the radar, to observing atmospheric and variable phenomena, and to revisiting areas where discoveries were made. Also, an effort to enlarge the scope of existing cooperation will be made, in particular with respect to other missions to Mars such as Mars Global Surveyor (MGS), MER, Mars Reconnaissance Orbiter (MRO), and missions to other planets carrying the same instruments as Mars Express (Venus Express).

## Status

The spacecraft platform performance has been as expected since the end of the commissioning phase. The primary areas on which work focused during the reporting period were:

- the power situation: with only 70% of the pre-launch expected values being available, careful power management is needed, especially during eclipse seasons;
- the solid-state mass memory and some of its anomalies: an entirely new version of the onboard software, removing almost all known anomalies, was uplinked in May 2005;
- the solar conjunction season at the end of 2004: this required careful management of spacecraft communications over a period of about a month, during which no science observations (except for radio science) were possible. The lessons-learnt will be applied to the next solar conjunction period in 2006;
- deployment of the MARSIS antenna booms.

The overall behaviour of the spacecraft is well understood, and allows execution of the required scientific observations, albeit with considerable constraints during eclipse seasons. Solar array degradation is slightly less than predicted, and the degradation of the batteries is in line with pre-launch predictions. Performing orbit maintenance of the 'frozen' orbit through carefully planned reaction-wheel off-loading manoeuvres keeps the fuel consumption low (6 g/day), with about 28 kg remaining. This is sufficient for several mission extension phases.

The status of the science instruments is good. The health of the OMEGA cryocoolers remains excellent. Most of the actual cooling is being performed at low power, and no problems are expected because there are independent cryocoolers for the two channels.

*For further information, see http://sci.esa.int/marsexpress*

**Table 2.8.1. The scientific objectives of Mars Express.**

*Orbiter science*
Global high-resolution photogeology and super-resolution of selected areas
Global high-resolution mineralogical mapping
Global atmospheric circulation and composition studies
Subsurface structure profiles a few km down to permafrost
Surface-atmosphere interaction studies
Interaction of upper atmosphere with the solar wind
Radio science of ionosphere, atmosphere, surface and interior

*Common threads to all payloads*
Inventory of water in atmosphere, subsurface and throughout history
Search for past or present traces of biological activity

*Global coverage*
Global studies of surface, subsurface, atmosphere and space environment
Geoscience database: high-resolution images, digital terrain models, hyperspectral data, subsurface sounding

**Table 2.8.2. The Mars Express orbiter scientific experiments.**

| *Expt. Code* | *Instrument* | *Principal Investigator* | *Participating Countries* |
|---|---|---|---|
| HRSC | Super/High-Resolution Stereo Colour Imager | G. Neukum | D, F, RU, US, FIN, I, UK |
| OMEGA | IR Mineralogical Mapping Spectrometer | J.P. Bibring | F, I, RU |
| PFS | Atmospheric Fourier Spectrometer | V. Formisano | I, RU, PL, D, F, E, US |
| MARSIS | Subsurface-Sounding Radar/Altimeter | G. Picardi & J. Plaut | I, US, D, CH, UK, DK |
| ASPERA | Energetic Neutral Atoms Analyzer | R. Lundin & S. Barabash | S, D, UK, F, FIN, I, US, RU |
| SPICAM | UV and IR Atmospheric Spectrometer | J.L. Bertaux | F, B, RU, US |
| MaRS | Radio Science Experiment | M. Paetzold | D, F, US, A |

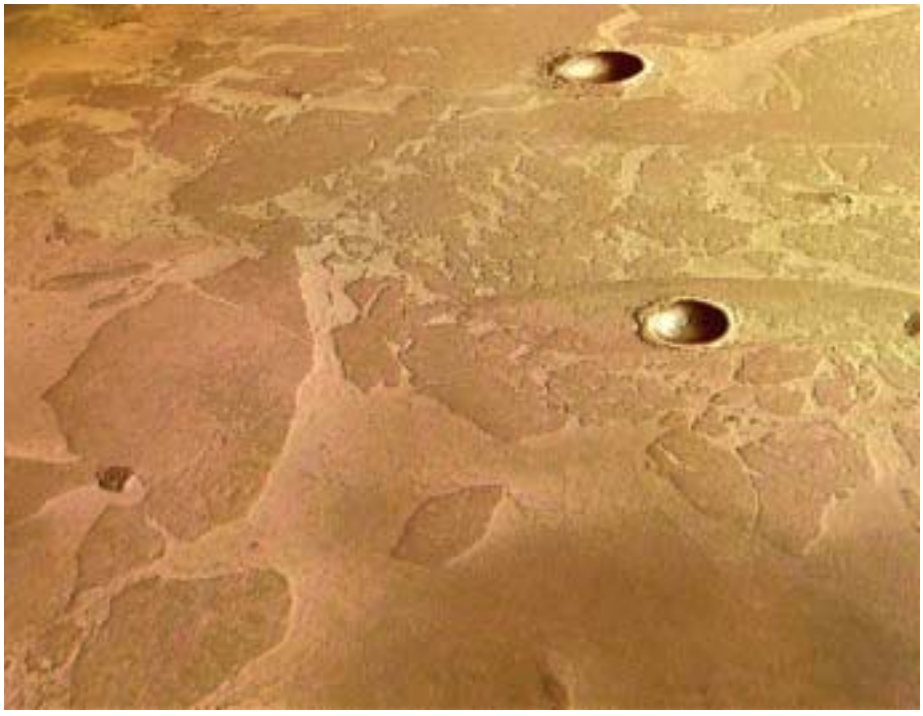

**Figure 2.8.1. Remnants of a frozen sea near the Martian equator. This HRSC image shows a flat plain, part of the Elysium Planitia, covered with irregular blocky shapes. They look just like the rafts of fragmented sea ice that lie off the coast of Antarctica on Earth. This scene is a few tens of km across, and is centred at 5°N/150°E.**
**(ESA/DLR/FU Berlin; G. Neukem)**

The Mars Express ground segment is made up of the following elements:

— Mission Operations Centre at ESOC;
— Science Operations Team at ESTEC;
— instrument operations planning, data analysis and archiving support by the PI teams;
— Deep Space Network support at JPL;
— contractor support:
— Payload Operations Service (POS) at RAL, UK
— spacecraft support at Astrium, Toulouse.

The orbit is such that orbits *n* and *n*+11 overlap in surface coverage, in order to achieve global mapping of the planet. The separation in time between such orbits is not an integer multiple of the Earth day, however. This implies a continuously changing pattern of interleaved science observations, data downlink, command uplink and spacecraft maintenance operations. Adding in other mission characteristics and the scientific requirements leads to Mars Express being operated with two shifts per day. The intricate and manpower-intensive operations activities at ESOC therefore require extensive engineering, planning and flight dynamics support. This level of support will remain almost constant over the extended mission.

The science operations team at ESTEC performs the core task of iterating the mission planning cycles with the PIs, the POS and ESOC, until solutions are achieved. This is a task requiring detailed knowledge of the science to be achieved and the spacecraft limitations in different mission phases (eclipse, conjunction, solar distance/power, etc). The team is also involved in data archiving and distributing support data to the Mars Express users.

**Table 2.8.3. Mars Express Interdisciplinary Scientists.**

| |
|---|
| Space environment<br>K. Maezawa, ISAS, JPN |
| Atmosphere and surface-atmosphere interactions<br>F. Forget, LMD/CNRS, Paris, F |
| Geological evolution<br>G.G. Ori, Int. Research School of Planetary Sciences, Università d'Annunzio, Pescara, I |
| Geodesy and cartography<br>T.C. Duxbury, JPL, USA |
| Astrobiology<br>R. Amils, CAB-Centro de Astrobiologia Torrejon de Ardoz, E |
| Geochemistry<br>E.K. Gibson, NASA Johnson Space Center, Houston, TX, USA |

## Scientific highlights

After 1.5 years of operations around Mars and the impressive scientific data received, the mission can be regarded as an enormous success. All the instruments have made significant and unexpected discoveries in the various fields of Mars science, representing a big step forward in our understanding of the planet. In addition, Mars Express is building up a dataset for global coverage of the surface, subsurface and atmosphere. In fact, a new Mars is emerging day by day. These discoveries were debated by the scientific community at the First Mars Express Science Workshop, held 21-25 February 2005 at ESTEC. Furthermore, dedicated sessions on Mars Express science have taken place (for several years running) at both the Lunar & Planetary Science Conference (Houston) and the European Geosciences Union general assembly (Vienna).

A brief list of the scientific achievements to date includes:

— much more recent geological ages than previously estimated (an order of magnitude) for volcanic processes and glacial processes, which means that the planet is still basically 'active' today (HRSC);
— confirmation of glacial processes in current equatorial regions (HRSC; Fig. 2.8.1);
— mapping of various types of ice ($H_2O$ and $CO_2$), either mixed or distinct, in polar regions (OMEGA; Fig. 2.8.2);
— lack of aqueous alteration of mafic minerals (olivine), which suggests that large bodies of water, such as lakes or seas, have not existed for long on the surface (OMEGA);

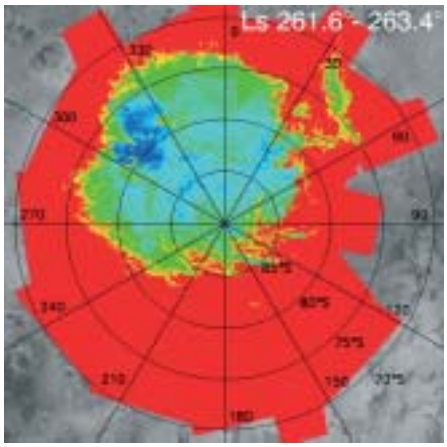


**Figure 2.8.2. Average of the southern cap by seasonal $CO_2$ at the end of the local spring (from red: no $CO_2$, to blue: high $CO_2$). The recess is highly asymmetrical, in contrast to what is observed for the northern cap: the seasonal evolution of the surface ices is tied to the complex dynamics of the atmosphere.**

— determination that the alteration products (phyllosilicates) in the early history of Mars correspond to abundant liquid water, while the post-Noachian products (sulphates) suggest a colder, drier planet with only episodic water on the surface (OMEGA);
— the presence of methane in the atmosphere (concurrent with ground observations) that, together with the detection of formaldehyde (oxidation product of methane), indicates that Mars either bears volcanic activity or biological processes today (PFS);
— the clear correlation between water vapour in the boundary layer and methane concentrations observed from orbit, further illustrating the volcanism *vs*. life debate (PFS);
— the complete atmospheric profiles between 10 km and 100 km altitude through limb observations, which for the first time include both density and temperature (SPICAM);
— the presence of nightglow and its implications for atmospheric transport (SPICAM);
— the discovery of auroras due to remnant magnetic anomalies on the surface (SPICAM; Fig. 2.8.3);
— the characterisation of the planetary wind composition ($O^+$) away from the solar wind (ASPERA);
— solar wind scavenging of the atmosphere down to 270 km altitude, representing a major mechanism in neutral atmospheric degassing and past climate change (ASPERA);
— build-up of the ionosphere shortly before dawn (MaRS);
— the first bistatic radar experiment, by pointing the high-gain antenna towards Mars to determine dielectric properties in regions of geological interest (MaRS);
— the indication of strong echoes from the surface and the subsurface, allowing the identification of buried craters and tectonic structures (Fig. 2.8.4). Probing of the ionosphere reveals a variety of echoes originating in areas of remnant magnetism (MARSIS).

Mars Express is providing a combined set of data that is uniquely suitable for geological mapping of the surface and subsurface. HRSC is providing the high-resolution surface images combined with surface topography from the stereo images and derived Digital Terrain Models. OMEGA is providing the surface mineralogical information that can be matched with the HRSC information to provide a compositional and structural geological surface map of unprecedented detail and reliability. To obtain a full 3-D set of geological information, the HRSC and OMEGA surface data should be merged with the subsurface information, which MARSIS is providing during the night season at the start of the extended mission. MARSIS is giving information on the subsurface structure (layering, compositional boundaries, faults and potentially subsurface aquifers) of the crust down to about 5 km. Radio science gravity measurements are an additional source of information on the interior. The atmospheric instruments are building up seasonal and global 3-D coverage of a variety of atmospheric parameters, including composition, pressure and temperature.

Mars Express has successfully cooperated with NASA orbiters and rovers, both in terms of joint operations (e.g. MER communications to test potential data relay) and collaborative scientific investigations with the MER rovers. Further scientific collaboration with MER and Mars Odyssey is expected during the rest of the nominal mission and the extended mission, and with MRO during the extended mission.

In spite of these first-class scientific achievements from the first European

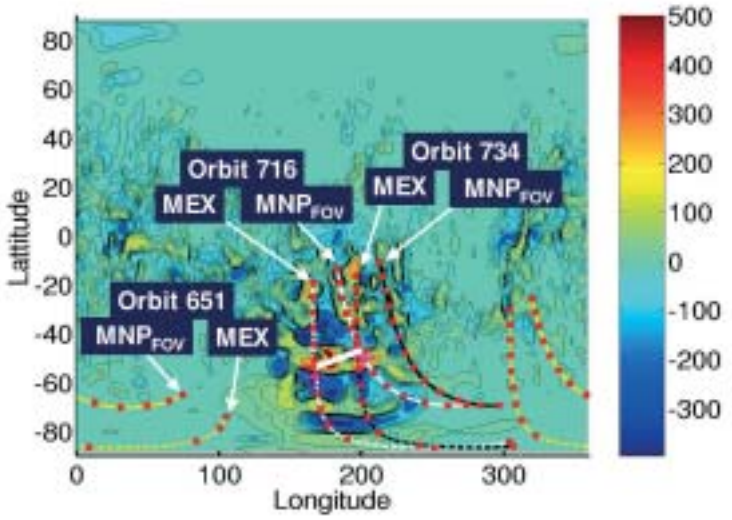


**Figure 2.8.3. Non-polar auroras on Mars. SPICAM has discovered auroras over regions with paleomagnetic signatures.**

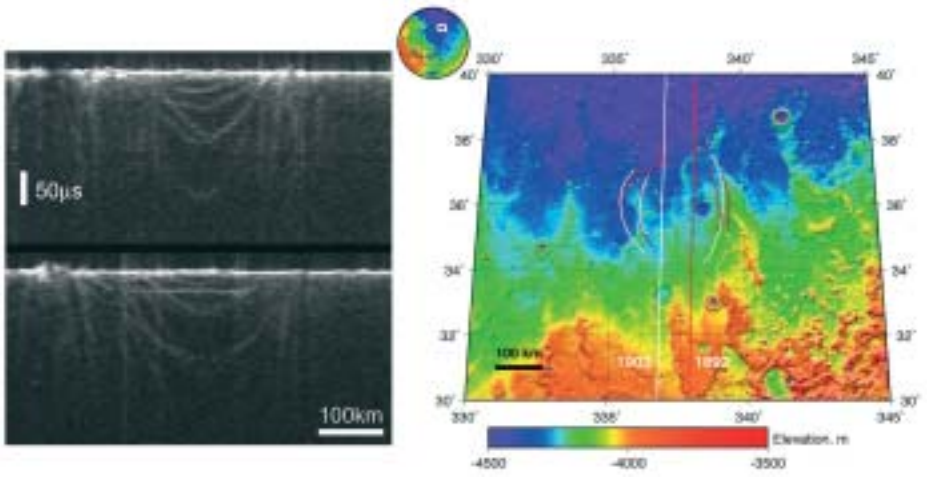


**Figure 2.8.4. MARSIS has discovered circular structures, typically 200–300 km in diameter, with no obvious surface expression. They are ancient craters buried in the northern lowlands. The bright planar reflector 2–2.5 km deep (left diagram) implies low loss in volume, which could be interpreted as ice-rich.**

planetary mission, a lot more science remains to be done to fulfil the original scientific objectives of the mission included in its Announcement of Opportunity. Given more time, all the instruments will continue to make discoveries in the areas of geology, atmosphere and the environment of Mars, including their evolution in time. There are, however, four key areas of investigations that are intrinsically linked to time (thus requiring an extended mission). These are:

— the MARSIS subsurface sounding radar: this is one of the major elements of the mission that is set to bring an unprecedented view of the geological structure underground, and more specifically, is bound to provide an estimate of the inventory of ice/liquid water below the surface to be added to the visible water ice of the polar regions. The two dipole booms and the monopole were deployed in time to observe the northern regions of the planet briefly, but the extended mission is necessary to observe the planet during conditions appropriate for subsurface sounding (i.e. night-time observations);
— HRSC global coverage: this is not only a major mission objective from the AO,

but represents an outstanding legacy of ESA, Mars Express and HRSC to future generations of scientists. Not since the Viking missions of the mid-1970's has the planetary community had at its disposal a global view of the planet that allows global phenomena to be studied in their entirety (tectonics, volcanism, dating by crater counting, wind patterns, glacial processes, etc). HRSC is providing an exciting new data set in colour, 3-D and unprecedented resolution to replace Viking. However, at present only about 15% of the planet has been covered at 20 m or better resolution. The extended mission is thus needed to image new areas as well as to recover those areas that were missed during the nominal mission owing to technical constraints;

— seasonal and time variations: these are another key area of observations that depends on the duration of the mission. This concerns all the instruments, but especially the atmospheric ones (PFS, SPICAM) studying the daily, seasonal or annual variability of the atmosphere. It also applies to those instruments observing variable phenomena such as frost, fog or ice (OMEGA), or studying the variability throughout the year of the interaction of the solar wind with the upper atmosphere (ASPERA, MaRS).
— follow-up observations of areas where discoveries have been made (e.g., new volcanic structures, sedimentary layering, methane sources, nightglow, auroras): revisiting those areas can be done only during the extended mission, however, because the spacecraft flies over the same location under the same illumination conditions only months or even years later.

In summary, by combining the datasets for the surface and subsurface, we can obtain the first 3-D and compositional model of the upper crust. This will represent a major step forward in our understanding of past and present geological processes on Mars. In addition, such a reliable 3-D geological dataset is a prerequisite for the preparation of an exploration lander mission to Mars.

# 2.9 SMART-1

## Introduction

SMART-1 was launched by Ariane-5 on 27 September 2003. After a 13.5-month cruise using solar electric propulsion, it attained lunar orbit (Fig. 2.9.1) in November 2004, and lunar science orbit in March 2005. The SMART missions were introduced into ESA's Scientific Programme to prepare the technology for future Cornerstone missions. SMART-1 is designed mainly to demonstrate innovative and key technologies for future deep-space science missions, with the potential to reduce the size and cost of propulsion systems while increasing manoeuvring flexibility and the mass available for scientific instrumentation. The first technology demonstrated on SMART-1 is Solar Electric Primary Propulsion (SEPP), a highly efficient and lightweight propulsion system that is ideal for long-duration deep-space missions. The propulsion system consists of a single ion engine fuelled by 82 kg of xenon gas and powered by solar energy. The 70 mN of thrust is delivered with a specific impulse 5-10 times better than traditional chemical thrusters. The low thrust levels are compensated for by very long thrust intervals – months to years instead of the minutes for typical chemical engines.

A wide range of other new technologies have been also demonstrated: a Li-Ion modular battery package, new-generation high-data-rate deep-space communications in X- and Ka-bands, and techniques enabling spacecraft to determine their position autonomously in space as a step towards fully autonomous navigation

## Scientific objectives

In synergy with the technology objectives, the science objectives for the lunar investigations include studies of the origin of the Earth-Moon system, accretional processes that led to the formation of planets, the chemical composition and evolution of the Moon, geophysical processes (volcanism, tectonics, cratering, erosion, deposition of ices and volatiles) for comparative planetology, and high-resolution mapping. SMART-1 carries seven instruments (Table 2.9.1) to perform 10 experiments. Part of the payload monitored the electric propulsion and spacecraft environment during the cruise, and tested novel spacecraft and instrument technologies:

**Figure 2.9.1. SMART-1 in lunar orbit.**

*For further information, see http://sci.esa.int/smart-1/*

**Table 2.9.1. The SMART-1 payload experiments.**

| *Expt. Code* | *Investigation Type* | *Main Investigator* | *Team Co-Is* | *Description of Experiment* |
|---|---|---|---|---|
| AMIE | Principal Investigator | J.L. Josset (CH) | F, NL, I, ESA | 5.3° FOV miniaturised CCD-camera, with 4 fixed filters and micro-Data Processing Unit for Moon multi-band imaging. 1.8 kg, 9 W |
| Laser-link | Guest Technology Investigator | Z. Sodnik (ESA) | | Demonstration of a deep-space laser link with ESA Optical Ground Station; sub-aperturing techniques for mitigating atmospheric distortion. Uses AMIE |
| OBAN | Guest Technology Investigator | F. Ankersen (ESA) | | Validation of On-Board Autonomous Navigation algorithm by planetary bodies tracking. Uses star trackers and AMIE images |
| SPEDE | Principal Investigator | W. Schmidt (FIN) A. Malkki (FIN) | FIN, S, ESA, USA | Langmuir probes measure spacecraft potential and plasma environment. Support to Electric Propulsion monitoring. 0.7 kg,1.2 W |
| RSIS | Guest Science Investigator | L. Iess (I) | USA, D, UK, F, ESA, S | Radio-science experiment monitors the Electric Propulsion. Uses KATE and AMIE |
| SIR | Technology Investigator | U. Keller (D) | D, UK, CH, I, IRL | Miniaturised near-IR (0.9-2.4 $\mu$m) grating spectrometer for lunar surface mineralogy studies. 1.7 kg, 2.5 W |
| D-CIXS/ XSM | Technology Investigator | M. Grande (UK) J. Huovelin (FIN) | FIN, S, E, I, F, ESA, USA | Compact X-ray spectrometer for mapping lunar chemical and variations of X-ray objects. 3.3 kg, 13 W |
| EPDP | Technology Investigator | G. Noci (I) | I, ESA, FIN, A | Multi-sensor package for monitoring the Electric Propulsion; plasma environment characterisation. 2.3 kg, 18 W |
| KATE | Technology Investigator | R. Birkl (D) P. MacMannamon (ESA) | ESA, UK | X/Ka-band Telemetry, Tracking & Control package, demonstrates telecommunication and tracking 5.2 kg, 18 W |

**Table 2.9.2. Principal characteristics of the SMART-1 spacecraft.**

*Stabilisation:* 3-axis, zero momentum
*Attitude control:* autonomous star tracker, Sun sensor, rate sensor gyro, reaction wheels, reaction control hydrazine system, thruster engine gimbals
*Mass:* 350 kg at launch
*Size:* 1 m cube, 14 m from tip-to-tip of solar arrays
*Propellants:* 82 kg of xenon and 4 kg of hydrazine
*Power:* two solar wings of three panels each; total area 10 $m^2$, generating 1950 W @ 1 AU. Supported by 5 Li-ion batteries totalling 600 Wh storage
*Telemetry data rate:* S-band 62 Kbit $s^{-1}$, X-band: 2 Kbit $s^{-1}$ (from lunar orbit), Ka-band 120 Kbit $s^{-1}$
*Onboard memory:* redundant 4 Gbit solid-state mass memory
*Primary propulsion:* Stationary Plasma Thruster PPS-1350, nominal 70 mN thrust at 1350 W inlet power and Specific Impulse of 16 000 Ns $kg^{-1}$


**Figure 2.9.2. The Moon as seen by SMART-1. This is the first view of the lunar north pole and farside by SMART-1, and only the second in the history of lunar exploration. (ESA/SMART-1/AMIE).**

— the diagnostic instruments include SPEDE, to characterise the spacecraft and its environment, together with EPDP, a suite of sensors monitoring secondary thrustions, charging and deposition effects;
— KaTE supports radio science (RSIS) to monitor the acceleration provided by the electric propulsion and has been used as a testbed for turbo-code techniques to improve the return of scientific data;
— RSIS, aimed at characterising the X/Ka-band deep-space communication channels, has been used to demonstrate a method for measuring the libration of the Moon from orbit by using high-resolution images from AMIE and accurate orbit determination by tracking in Ka-band, as preparation for BepiColombo.

The remote-sensing instruments for imaging and spectrometry are all highly miniaturised:
— D-CIXS, a compact X-ray spectrometer based on novel Swept Charge Device detectors and micro-collimator optics, to perform lunar geochemistry, by fluorescence mapping of the major rock-forming elements (Mg, Si, Al, O, Fe) and to monitor bright X-ray sources during cruise;
— XSM, an X-ray solar monitor, to observe variations of the Sun owing to activity and flares, and to serve in the calibration of the D-CIXS determination of absolute lunar elemental abundances;
— SIR, a miniaturised quasi-monolithic point-spectrometer, is the first near-IR lunar spectrometer to survey the distribution of the main minerals in the lunar crust;
— AMIE, a miniature camera based on 3-D integrated electronics, imaging the Moon in four spectral bands defined by thin-film filters, and supporting three guest investigations: Laser-Link, a demonstration of acquisition of a deep-space laser-link from the ESA Optical Ground Station at Tenerife; OBAN, the demonstration of an autonomous navigation tool; and RSIS for the in-orbit measurement of lunar libration.

## Results

Bulk crustal composition has a bearing on theories of the origin and evolution of the Moon. D-CIXS is producing the first global view of the lunar surface in X-ray fluorescence (XRF), elemental abundances of Mg, Al and Si (and Fe plus others if

solar activity permits) across the whole Moon. The South Pole-Aitken Basin and large lunar impact basins are being mapped with D-CIXS. These are the first XRF measurements of the lunar surface since the Apollo 15 and 16 missions, which covered only 9% of the Moon and were restricted to equatorial regions. More importantly, rather than the elemental ratios as derived by Apollo, D-CIXS is deriving absolute elemental abundances by measuring (with XSM) the incident solar spectrum that causes the lunar surface to fluoresce in X-rays.

D-CIXS is providing a global distribution of Mg and permitting the production of global magnesium numbers (Mg# = Mg/Mg+Fe). The mapping of Mg# is a key to studying the evidence of a primitive source, the relations of Mg-suite rocks *vs*. ferroan anorthosites or KREEP, and the constraints on the magma ocean model/evolution.

SIR has sufficient spectral resolution to separate the pyroxene and olivine signatures in lunar soils. This is a key to understanding the evolution of crustal materials, because the distribution of olivine is poorly constrained in current models. Olivine is considered to be a common mineral in the lunar mantle, so its distribution throughout the crust and across the surface is of critical importance to models of crustal differentiation and evolution. SIR data are helping to refine compositional analyses from Clementine/Lunar Prospector data. IR spectrometry, with spatial resolution as high as 400 m, permits units to be distinguished on central peaks, walls, rims and ejecta blankets of large impact craters, allowing stratigraphic studies of the crust. Observations of small craters showing a wide age range is aiding studies of the influence of space weathering on reflectance spectra. Furthermore, SMART-1's target pointing allows SIR to take near-continuous spectra as the phase angle changes. The data allow the extraction of phase angle influences.

The AMIE camera obtained demonstration images of the Earth and Moon during the cruise and final approach before lunar capture. AMIE includes filters deposited on the CCD in white light + three filters for colour analyses, with bands at 750, 900 and 950 nm. These provide data on the 1 mm absorption of pyroxene and olivine. The camera has a resolution of 40 m/pixel for a perilune of 400 km, and 80 m/pixel for a large part of the southern hemisphere. Imaging has been obtained in survey mode to cover adjacent parts of the Moon along one orbit (Fig. 2.9.3), and in targeted mode for detailed studies of specific sites. AMIE is providing images for the study of impact crater physics (Fig. 2.9.4), volcanic processes and tectonics. They provide a geological context for SIR and D-CIXS data, and complementary colour or multi-phase angle data.

Repeated high-resolution images of the poles have been obtained. SMART-1 has mapped potential sites of 'eternal light' and 'eternal shadow', sites important for future exploration (bases, power supplies). Long exposures using target-tracking are studying multi-angle texture effects and identifying shadowed or double-shadowed areas in the search for potential water-ice traps.

## Operations

SMART-1 is operated from the Mission Operations Centre (MOC) at ESOC. The Science and Technology Coordination (STOC) effort is located at ESTEC. STOC provides inputs to the Flight Operation Plan for payload commanding at the spacecraft level. It implements joint payload operations, following priorities defined by science themes. The Experiment Operation Facilities are located at each Principle Investigator site. They are connected to STOC and MOC via the network and remotely operate the experiments. The scientific activities are coordinated within the Science and Technology Working Team (STWT) chaired by the Project Scientist, and via STOC. Experiment requests for operations, commands and data delivery are routed via the STOC.

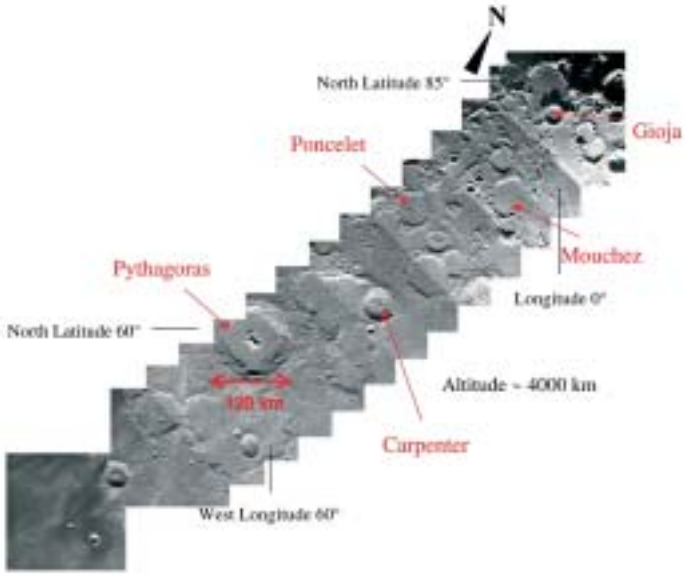


**Figure 2.9.3 (left). Mosaic of successive images taken by AMIE in survey mode at distances of 1000–5000 km prior to the science phase. (ESA/SMART-1/AMIE/Space-X Space Exploration Institute)**

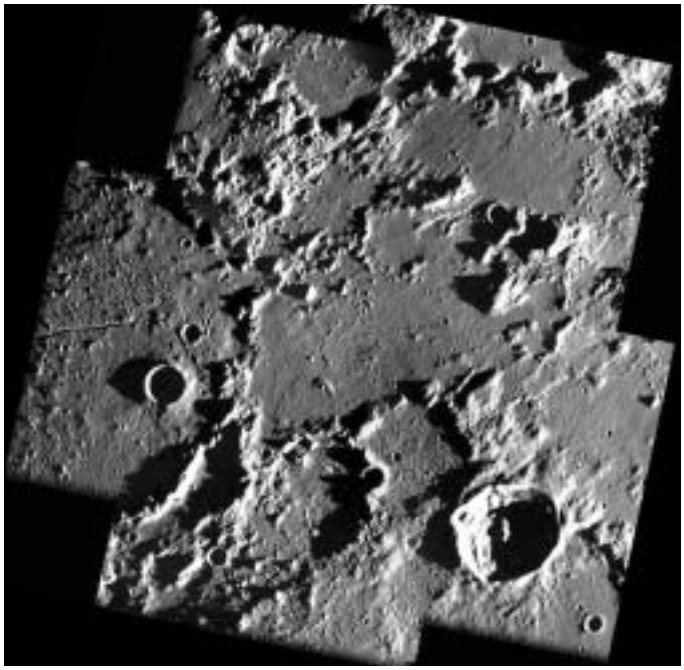

**Figure 2.9.4 (right). AMIE view of craters north of Mare Frigoris (near 64ºN). Pre-Nectarian old crater W. Bond (left, diameter 156 km) has been eroded and reshaped, and covered by debris from the Imbrium basin impact ejecta, and its centre plain has been cut by a volcanic rille. Crater Mayer (lower right, diameter 38 km) is a young crater. Clearly visible are its central peak, formed by impact rebound, the surrounding ejecta, and terraces formed during crater collapse.**
**(ESA/SMART-1/AMIE/Space-X Space Exploration Institute)**

SMART-1 data are archived according to the Planetary Data System Standards. There will be an inter-calibration and integration of the SMART-1 data between the instruments and with existing data from previous missions such as Clementine and Lunar Prospector. The SMART-1 team is cooperating with the teams from upcoming missions (Japan's Selene and Lunar-A, India's Chandrayaan-1, China's Chang'E-1, and the US Lunar Reconnaissance Orbiter) and will study sites for future landers and rovers.

## Status

Owing to the efficiency of the electric propulsion system and the higher level of electric power available, lunar capture occurred on 15 November 2004 with a propellant reserve that allowed the apolune to be lowered from 10 000 km to 3000 km. During the following weeks, the ion engine gradually reduced the size and duration of the orbit, reaching the final polar science orbit (period 4.98 h, 400–3000 km from surface) on 15 March 2005. The engine was used again in July-August to boost the orbit and extend the mission lifetime until mid-August 2006, thereby avoiding surface impact in September 2005. This manoeuvre consumed almost all the available xenon propellant.

At the end of February 2006, the spacecraft had performed about 2000 lunar orbits.

Using a hydrazine-thruster manoeuvre at the end of June 2006, the low-perilune mission will last until the impact on the lunar near side predicted for 1–3 September 2006. This will provide conditions for coordinated ground-based observations; the science community has been asked to contribute predictions, observations and outreach opportunities for the impact.

Some 30 refereed papers and 130 proceedings papers have been published on the mission, and several are in press on the first year results.

# 2.10 Double Star

## Introduction

The collaboration between China and ESA on Cluster began in 1992 when China proposed to set up a Data Centre to distribute Cluster data. Since then, several Chinese scientists have been hosted in Europe at ESA establishments and in Principal Investigator (PI) institutes and become Co-Investigators on the Cluster mission. In 1997, the Chinese Centre for Space Science and Applied Research (CSSAR) presented its new magnetospheric Double Star Programme (DSP) to the Cluster Science Working Team (SWT) and invited the Cluster PIs to participate in the payload; six Cluster PIs provided their instrument flight spare models.

A major milestone was reached in July 2001 when ESA and the Chinese National Space Agency (CNSA) signed the DSP agreement of cooperation. ESA's aims in this first collaboration with China are to provide unique opportunities for European space plasma scientists, to increase the scientific return of DSP by acquiring 4 h of data per day, to support the refurbishment/rebuilding of the European instruments, to coordinate the scientific operations of the European instruments on DSP, and to help in the pre-integration of the European instruments in Europe.

Within 2.5 years, TC-1 (Tan Ce: Explorer) was launched from Xichang in Southern China, on 29 December 2003 into a 570 x 78 970 km, 28.5° orbit. Owing to over-performance by the upper stage, the apogee is about 12 000 km higher than planned. This has not had an adverse effect on the mission's scientific performance, however; Earth's bow shock, not included in the original mission goals, can now be observed by TC-1, with crossings occurring February-May.

TC-2 was launched on 25 July 2004 into a polar orbit of 680 x 38 300 km. Its measurements focus on the physical processes taking place over the magnetic poles, and the development of auroras.

## Mission status

The TC instruments (Table 2.10.1) are operating nominally. As a result of enhanced geomagnetic activity during the initial stages of the mission, however, both satellites have lost their attitude computers. In the absence of system-level attitude control, the data from the magnetometers are now used to derive the attitude. Fortunately, this has not affected the projected mission lifetime (initially 1.5 years), and the SPC has approved a mission extension from July 2005 to December 2006.

## Scientific highlights

The two orbits were designed to complement the Cluster mission by maximising the time when both Cluster and Double Star are in the same scientifically interesting region. In this way, the two missions can simultaneously observe the Earth's magnetosphere from six points in space, providing a unique capability for investigating space plasma phenomena such as magnetic reconnection.

In early 2005, TC-1 and the four Clusters observed a flux transfer event (FTE). The small-scale structure was probed by the Cluster tetrahedron, and the large-scale structure and FTE evolution were revealed by TC-1, located over 15 000 km from the position of Cluster. The observations were consistent with models of magnetic reconnection. Combined observations revealed that flapping motions of the Earth's magnetotail are of internal origin, generated in the central part of the tail, as close as 11 Earth-radii (70 000 km) to the Earth. The unique capabilities of Double Star and Cluster were demonstrated in an unusual way on 27 December 2004, when many astrophysical instruments, including Integral, detected a giant gamma-ray flare from soft gamma repeater (SGR) 1806-20. For the first 200 ms, however, most gamma-ray detectors were saturated. The PEACE electron instruments aboard Cluster and TC-2,

*For further information, see http://sci.esa.int/doublestar*

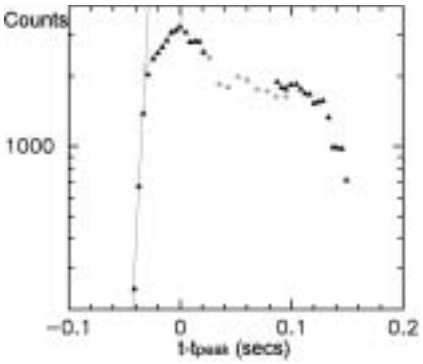


**Figure 2.10.1. The combined Double Star (triangles) and Cluster (grey circles) of electron count rates during the initial rise and decay of the gamma-ray flare expanding from SGR 1806-20, 27 December 2004. (S.J. Schwartz et al., 2005)**

**Table 2.10.1. Double Star payload.**

| *Instrument* | *PI* |
|---|---|
| *Equatorial satellite* | |
| Active Spacecraft Potential Control (ASPOC) | K. Torkar, IWF, Graz, A |
| Fluxgate Magnetometer (FGM) | C. Carr IC, UK |
| Plasma Electron and Current Exp. (PEACE) | A. Fazakerley, MSSL, Dorking, UK |
| Hot Ion Analyser (HIA), sensor 2 of CIS | H. Reme, CESR, Toulouse, F |
| part of Spatio-Temporal Analysis of Field Fluct.(STAFF) + Digital Wave Processor (DWP) | N. Cornilleau/H. Alleyne, CETP, Velizy, F & Sheffield U., UK |
| High Energy Electron Detector (HEED)* | W. Zhang & J.B. Cao, CSSAR, China |
| High Energy Proton Detector (HEPD)* | J. Liang & J.B. Cao, CSSAR, China |
| Heavy ion detector (HID)* | Y. Zhai & J.B. Cao, CSSAR, China |
| *Polar satellite* | |
| Neutral Atom Imager (NUADU) | S. McKenna-Lawlor, Ireland U., IRL |
| Fluxgate Magnetometer (FGM) | T. Zhang, IWF, A |
| Plasma Electron and Current Exp. (PEACE) | A. Fazakerley, MSSL, Dorking, UK |
| Low Energy Ion Detector (LEID)* | Q. Ren & J.B. Cao, CSSAR,China |
| Low Frequency Electromagnetic Wave detector (LFEW)* | Z. Wang & J.B. Cao, CSSAR, China |
| High Energy Electron Detector (HEED)* | W. Zhang & J.B. Cao, CSSAR, China |
| High Energy Proton Detector (HEPD)* | J. Liang & J.B. Cao, CSSAR, China |
| Heavy ion detector (HID)* | Y. Zhai & J.B. Cao, CSSAR, China |

*instrument built by China

although designed for thermal electron detection, were able to observe the initial rise of the flare without going into saturation. They provided the first observational evidence of three separate timescales within the first 100 ms of the event.

## Operations and data distribution system

The European Payload Operation Services (EPOS) at RAL coordinates the scientific operation of the European instruments aboard DSP (except NUADU, which is operated by China). EPOS also distributes planning data to the scientific community and developed the DSP data management system. A new contract for an extended EPOS has been signed that will combine the operations of Cluster, DSP and Mars Express.

The Double Star Data System (DSDS), which consists of five data centres (Austria, China, France, The Netherlands, UK), distributes the data from the instruments to all scientific users. The ESA ground station at Villafranca (E) and the Chinese stations in Beijing and Shanghai track the satellites. The data acquired at Villafranca (3 h per day on average) are then decommutated in China and sent to the PI teams via the Austrian data centre. A dedicated VPN line is used for the data traffic between Europe and China. Once in the PI institutes, the raw data are processed and calibrated and then distributed to the five data centres for access by the scientific community.

# 2.11 Rosetta

## Introduction

Rosetta was launched on 2 March 2004, when Ariane V158 placed in orbit for the start of its 10-year journey to comet 67P/Churyumov-Gerasimenko. The injection was so precise that approval was given to include flybys of two asteroids, Steins and Lutetia, in the baseline mission profile. The principal mission milestones are:

| | |
|---|---|
| Launch | 2 March 2004 |
| Earth Gravity Assist #1 | 4 March 2005 |
| Mars Gravity Assist | March 2007 |
| Earth Gravity Assist #2 | November 2007 |
| Asteroid Steins flyby | 5 September 2008 |
| Earth Gravity Assist #3 | November 2009 |
| Asteroid Lutetia flyby | 10 July 2010 |
| Enter/exit hibernation | July 2011/January 2014 |
| Rendezvous manoeuvre | May 2014 |
| Start global mapping phase | August 2014 |
| Lander delivery | November 2014 |
| Perihelion passage | August 2015 |
| End of mission | 31 December 2015 |

## Background

The International Rosetta Mission was approved in November 1993 by ESA's Science Programme Committee as the Planetary Cornerstone Mission in the Agency's Horizon 2000 long-term space science programme. The prime scientific objective of the mission is to study the origin of comets, the relationship between cometary and interstellar material, and its implications with regard to the origin of the Solar System. The measurements to be made in support of this objective are:

- global characterisation of the nucleus, determination of dynamic properties, surface morphology and composition;
- determination of the chemical, mineralogical and isotopic compositions of volatiles and refractories in a cometary nucleus;
- determination of the physical properties and interrelation of volatiles and refractories in a cometary nucleus;
- study of the development of cometary activity and the processes in the surface layer of the nucleus and the inner coma (dust/gas interaction);
- global characterisation of asteroids, including the determination of dynamic properties, surface morphology and composition.

## Science operations

Rosetta is a Principal Investigator (PI)-type mission, i.e. the individual Experiment Teams are responsible for defining the science operations timelines for their individual instruments (Tables 2.11.1 & 2.11.2). These requests are coordinated and merged into the Science Operations Plans by the Rosetta Science Operations Centre (RSOC), in ESA's Research & Scientific Support Department in ESTEC, Noordwijk, The Netherlands. For key mission phases (commissioning, nucleus rendezvous, lander delivery), RSOC is collocated with the Rosetta Mission Operations Centre (RMOC) at ESOC, in Darmstadt, Germany (Fig. 2.11.1). ESOC is operating and controlling the spacecraft throughout the mission, working through the Agency's 35 m Deep Space Antenna at New Norcia in Western Australia (Fig. 2.11.2).

The Rosetta Science Data Archive will be prepared by RSOC in collaboration with the Primitive Bodies Node of the Planetary Data System at the University of Maryland.

*For further information, see http://sci.esa.int/rosetta*

**Table 2.11.1. The Rosetta Orbiter payload.**

| *Acronym* | *Objective* | *Principal Investigator* |
|---|---|---|
| *Remote Sensing* | | |
| OSIRIS | Multi-colour imaging<br>NAC (Narrow Angle Camera) 2.35×2.35°<br>WAC (Wide Angle Camera) 12×12° (250-1000 nm) | H.U. Keller, MPI for Solar System Research, Katlenburg-Lindau, Germany |
| ALICE | UV spectroscopy (70-205 nm) | A. Stern, Southwest Research Institute, Boulder, Colorado, USA |
| VIRTIS | VIS/IR mapping spectroscopy (0.25–5 $\mu$m) | A. Coradini, IASFC-CNR, Rome, Italy |
| MIRO | Microwave spectroscopy (1.3 & 0.5 mm) | S. Gulkis, NASA-JPL, Pasadena, CA, USA |
| *Composition Analysis* | | |
| ROSINA | Neutral gas and ion mass spectroscopy. Double-focusing, 12–200 amu, m/Δm~3000. Time-of-flight, 12–350 amu, m/Δm~2500 including Neutral Dynamics Monitor | H. Balsiger, Univ. of Bern, Switzerland |
| COSIMA | Dust mass spectrometer (SIMS, m/Δm~2000) | M. Hilchenbach, MPI for Solar System Research, Katlenburg-Lindau, Germany |
| MIDAS | Grain morphology (Atomic Force Microscope, nm resolution) | W. Riedler, Space Research Inst., Graz, Austria |
| *Nucleus Large-scale Structure* | | |
| CONSERT | Radio sounding, nucleus tomography | W. Kofman, LPG, Grenoble, France |
| *Dust Flux, Dust Mass Distribution* | | |
| GIADA | Dust velocity and impact momentum measurement, contamination monitor | L. Colangeli, Oss. Astronomico di CapodiMonte Naples, Italy |
| *Comet Plasma Environment, Solar Wind Interaction* | | |
| RPC | Langmuir probe, ion and electron sensor, flux-gate magnetometer, ion composition analyser, mutual impedance probe | A. Eriksson, Swedish Inst. of Space Physics, Uppsala, Sweden; J. Burch, Southwest Research Inst., San Antonio, Texas, USA; K-H. Glassmeier, TU Braunschweig, Germany; R. Lundin, Swedish Inst. of Space Physics, Kiruna, Sweden; J.G. Trotignon, LPCE/CNRS, Orleans, France; C. Carr, Imperial College London, UK |
| RSI | Radio science experiment | M. Pätzold, Univ. of Cologne, Germany |

**Table 2.11.3. Rosetta spacecraft characteristics.**

*Spacecraft*
3-axis stabilisation
Highly autonomous (two star trackers, Sun sensors, navigation cameras)
Three laser-gyro packages
S/X-band up and downlink
Data transmission rates: 5–20 kbit/s (depending on geocentric distance)
Solid-state mass memory: 25 Gbit
Solar arrays (LILT-cells, low-intensity, low-temperature cells) to provide 400 W @ 5.2 AU
Size: box shaped, 2.5×2.5×2 m, all instruments body-mounted

*Launch mass:* ~3000 kg

*Propellant:* ~1670 kg bipropellant monomethyl hydrazine (MMH), nitrogen tetroxide (NTO)

*Mission lifetime:* 11 years

**Table 2.11.2. The Rosetta Lander payload.**

| *Acronym* | *Instrument* | *Principal Investigator* |
|---|---|---|
| APXS | Alpha-p-X-ray Spectrometer | R. Rieder, MPI Chemistry, Mainz, D |
| SD2 | Sample Acquisition System | A. Ercoli-Finzi, Polytecnico, Milano, I |
| COSAC | Gas Chromatograph/Mass Spectrometer | H. Rosenbauer, MPS, Lindau, D |
| PTOLEMY | Evolved gas analyser | I. Wright, Open Univ., UK |
| CIVA<br>ROLIS | Rosetta Lander imaging system | J.P. Bibring, IAS, Orsay, F;<br>S. Mottola, DLR Berlin, D |
| SESAME | Surface Electrical and Acoustic Monitoring Experiment,<br>Dust Impact Monitor | D. Möhlmann, DLR Cologne, D;<br>W. Schmidt, FMI, SF;<br>I. Apathy, KFKI, H |
| MUPUS | Multi-Purpose Sensor for Surface and Sub-surface Science | T. Spohn, Univ. of Münster, D |
| ROMAP | RoLand Magnetometer and Plasma Monitor | U. Auster, DLR Berlin, D;<br>I. Apathy, KFKI, H |
| CONSERT | Comet nucleus sounding | W. Kofman, LPG, Grenoble, F |

**Figure 2.11.2. ESA's 35 m Deep Space Antenna at New Norcia, Australia.**

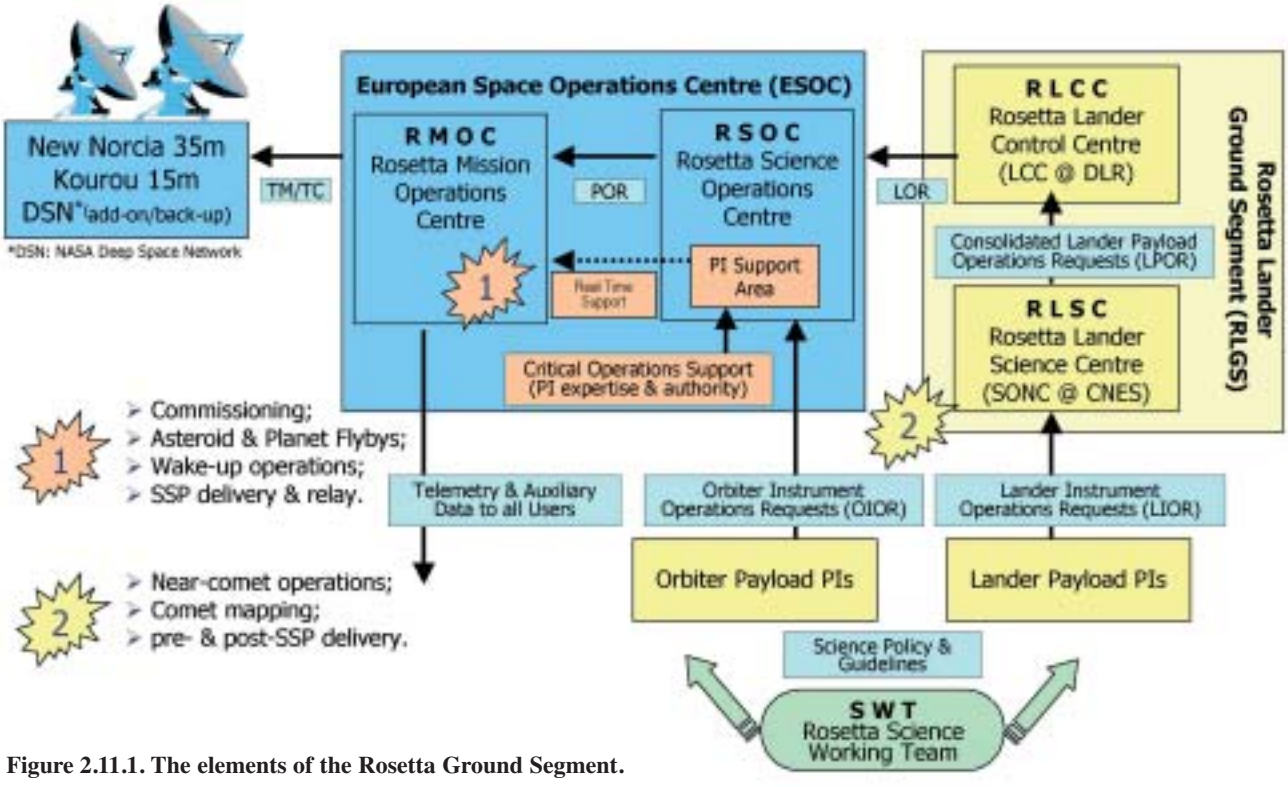


**Figure 2.11.1. The elements of the Rosetta Ground Segment.**

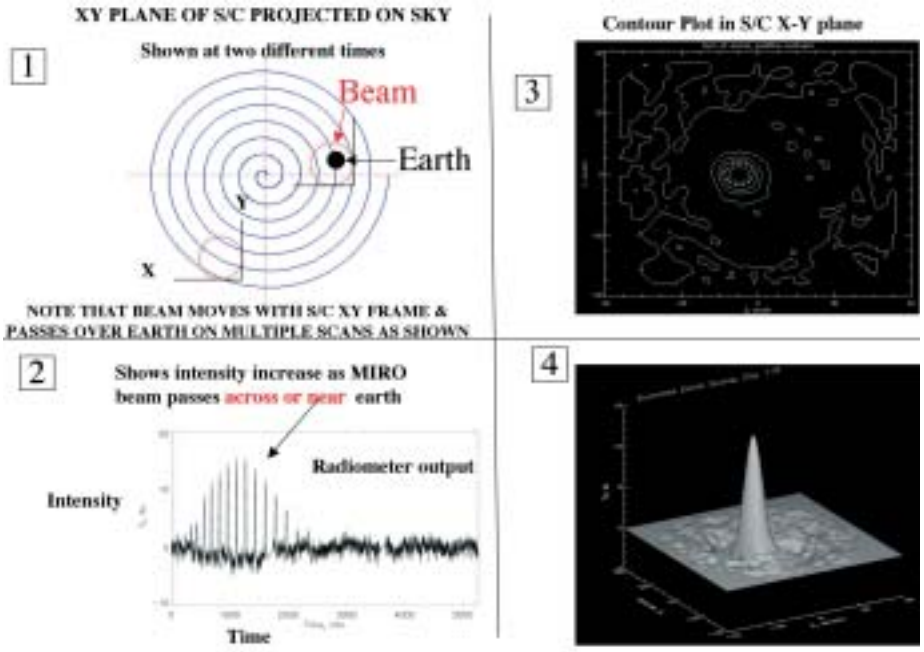


**Figure 2.11.3. The observation pattern for MIRO's in-orbit calibration.**

Five Interdisciplinary Scientists have been nominated for a limited period to support the mission's implementation:

- M. Fulchignoni, DESPA, Observatoire de Paris, France, to develop physico-chemical models of the possible target asteroids in order to provide the Rosetta Project and the Rosetta Science Working Team with a reference data set;
- P. Weissman, NASA-JPL, Pasadena, California, USA, to provide thermo-physical modelling of the cometary nucleus and of the inner coma of comets;
- R. Schulz, ESA RSSD, to liaise with the astronomical community and to derive a basic characterisation of the target comet from ground-based observations;
- E. Grün, MPI für Kernphysik, Heidelberg, Germany and M. Fulle, Trieste Astronomical Observatory, Italy, to provide empirical 'engineering models' for the nucleus dust environment in order to establish a reference data set for the Rosetta Project and the Rosetta Science Teams.

## Status

After the successful launch, spacecraft commissioning operations began immediately. The first instrument to be switched on was COSIMA, on 7 March 2004. As Rosetta had to share usage of ESA's Deep Space Antenna in New Norcia with Mars Express, the payload commissioning was divided into three periods: two immediately after launch until early June, and the Pointing and Interference Campaigns in September and October 2004. For this last period, RSOC took the full responsibility in preparing the payload operations for the first time. This required close interaction and collaboration with the Experiment Teams. The system worked flawlessly and proved the readiness of RSOC. An example is given in Fig. 2.11.3, showing the complicated observation pattern that had to be implemented for MIRO's in-orbit calibration.

The Mission Commissioning Results Review, held on 3 December 2004 at ESOC,

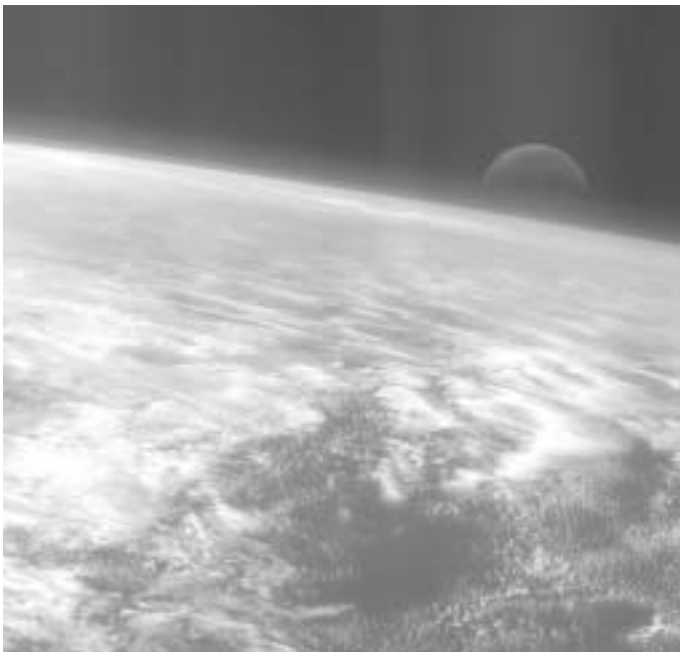

**Figure 2.11.4. The Moon rising behind the Earth, as seen by Rosetta's navigation camera during the gravity-assist swingby of 4 March 2005.**

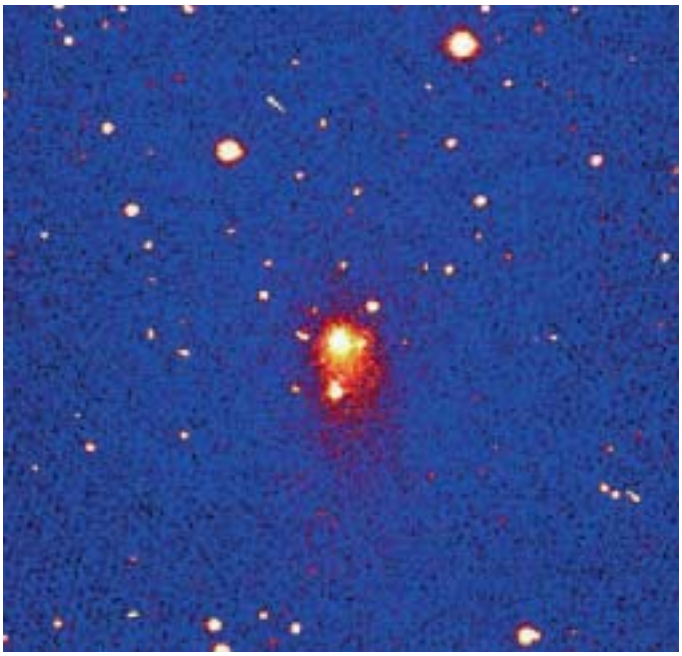

**Figure 2.11.5. A still from the OSIRIS/NAC sequence showing how the brightness of comet 9P/Tempel-1 developed after the strike by Deep Impact. (ESA/OSIRIS Consortium)**

formally completed these activities. It was concluded that all the goals of the spacecraft and payload commissioning had been achieved and that the mission was operational. Subsequently, for the operational phase of the mission, the management of Rosetta was transferred from the Projects Department to the Research & Scientific Support Department.

In mid-October 2004, Rosetta was put in quiet cruise mode and preparations began for the first big mission event, the first Earth gravity assist on 4 March 2005 (Fig. 2.11.4). The asteroid-tracking mode was tested during the Earth flyby, using the Moon as the target. As all systems performed extremely well, it was decided to join the monitoring campaign of NASA's Deep Impact mission to comet Tempel-1 on 4 July 2005. The science operations sequences were worked out jointly between the participating Experiment Teams and RSOC and the Mission Operations Team at ESOC. A 2-week sequence was uploaded and executed successfully. This again was an excellent test demonstrating that the science ground segment for Rosetta meets the operational requirements. An example of the excellent results from OSIRIS is shown in Fig. 2.11.5. Since then, the spacecraft has been in quiet cruise mode, with basically one tracking pass per week for monitoring and small onboard software updates.

The small RSOC team has interacted closely with the Mission Operations and Flight Dynamics Teams at ESOC, and the Rosetta Orbiter and Lander Instrument Teams, to ensure that the science operations schemes for the asteroid flybys and the comet phase fit into a general framework of specific, pre-defined science themes. In the coming years, these themes will be translated into detailed operational scenarios that will help to optimise the actual operations planning when the spacecraft reaches

the comet in 2014. Onboard operational procedures have been reviewed based on the initial operational experience, and this will be reflected in the final versions of the specific User Manuals.

Considerable effort went into the preparation of the Rosetta science data archive as part of ESA's Planetary Science Archive. The data from the commissioning campaign have already been ingested into the archive and made available to the wide scientific community.

# 2.12 Venus Express

## Introduction

Venus Express was launched from Baikonur Cosmodrome on 9 November 2005. A Soyuz-Fregat rocket put the 1200 kg spacecraft almost perfectly on the ideal trajectory towards Earth's twin planet, where it will arrive 11 April 2006 (Figs. 2.12.1 and 2.12.2).

The mission, originally proposed to ESA in response to a March 2001 Call for Ideas for reuse of the Mars Express platform, is aimed at the study of the atmosphere, plasma environment and surface of Venus. It was developed in a record time of less than 4 years, starting with a 3-month Mission Definition Study in 2001 in competition with two other mission proposals. At the end of this study, Venus Express was selected by the science programme advisory committees on the strength of its excellent scientific value. In July 2002 the Science Programme Committee (SPC) provisionally approved the start of work on Venus Express pending an agreement on the funding of parts of the payload. In November 2002 ESA made its final decision on the payload complement and to proceed with the mission. The demanding schedule set out at the very beginning of the project has been strictly followed and Venus Express was ready for launch on the first day of the launch window. An anomaly with a small patch of thermal insulation material on the launcher delayed departure by 2 weeks but allowed the launch to take place close to the optimum day within the window.

## Mission overview

The duration of the transfer to Venus is 153 days. An orbit insertion manoeuvre will place the spacecraft in a highly elliptical 9 day-period orbit around Venus. A series of apocentre-lowering manoeuvres will then establish the final 24 h-period polar orbit, with a pericentre altitude of 250–400 km and an apocentre altitude of 66 000 km. The pericentre will be located at around 80°N latitude at the start of the orbital phase. Scientific observations will be shared between the pericentre region, where high-resolution studies of small-scale features will be carried out, and near apocentre and intermediate regions, where global features will be studied. The acquired data will be transmitted to Earth each orbit during the 8 h following the pericentre pass. ESA's new deep-space tracking station at Cebreros (E), finished just in time for the launch, will be the nominal ground station for spacecraft control and data downlink. The other 35 m station, at New Norcia, Australia, is used during mission-critical operations and for radio-science support during dedicated campaigns at certain phases of the mission. A nominal mission duration of two Venus sidereal days (486 Earth days) is foreseen, with the possibility of extending the mission for another two Venus days.

## Scientific goals

The main goal of the mission is to conduct a comprehensive study of the atmosphere of Venus and to study to some detail the plasma environment and the interaction between the upper atmosphere and the solar wind. Several aspects of the surface and surface-atmosphere interactions will also be studied. In order to organise properly the topics to be studied and to ensure that the full potential of the mission is exploited, seven Science Themes have been defined, where each theme has its own detailed set of objectives:

— atmospheric dynamics;
— atmospheric structure;
— atmospheric composition and chemistry;
— cloud layers and hazes;
— radiative balance;

*For further information, see http://sci.esa.int/venusexpress*

**Figure 2.12.1. Venus Express lifts off from Baikonur at 03:33 UT on 9 November 2005.**

**Figure 2.12.2. Venus Express separates from its upper stage after the second burn of the Fregat engine that has injected the combination into a heliocentric orbit towards Venus. The solar panels were deployed a few minutes later.**

— surface properties and geology;
— plasma environment and escape processes.

Addressing these themes to a proper depth will enable solutions to many of the fundamental questions still open for Venus. These include the following: what is the mechanism of the global atmospheric circulation; what are the mechanisms and the driving force behind the atmospheric super-rotation; what are the chemical composition and its spatial and temporal variations on the short- and long-term; what is the role of the cloud layers and the trace gasses in the thermal balance of the planet; what is the importance of the greenhouse effect; how can the origin and the evolution of the atmosphere be described; what has been and what is the role of atmospheric escape for the present state of the atmosphere; what role does the solar wind play in the evolution of the atmosphere; and is there still active volcanism and seismic activity on Venus? Resolving these issues is of crucial importance for understanding the long-term evolution of climatic processes on the sister planets Venus, Earth and Mars, and will significantly contribute to general comparative planetology.

Venus Express will provide a breakthrough by fully exploiting the near-IR spectral windows, discovered by accident in the 1980s, through which radiation from the lower atmosphere and even the surface escapes to space (Fig. 2.12.3). The mission will also tackle open questions on the plasma environment, focusing on non-thermal atmospheric escape.

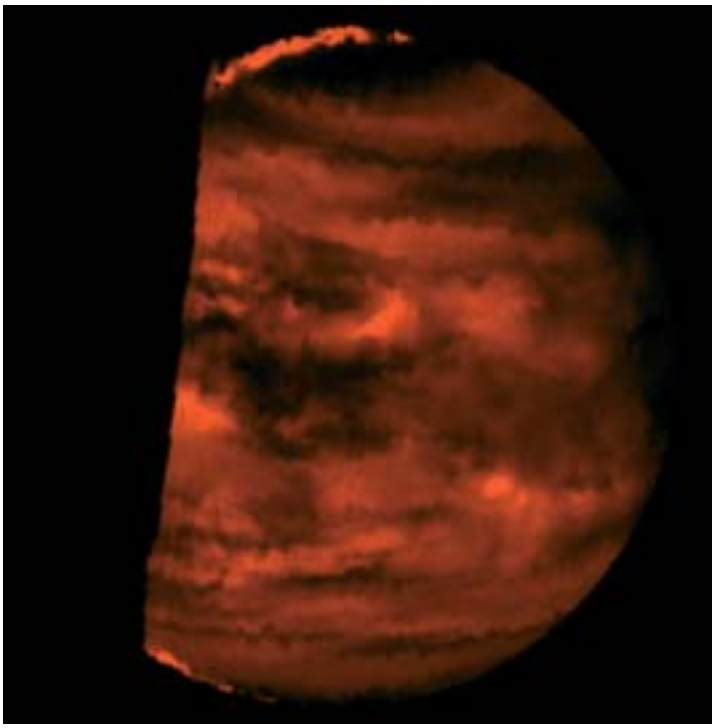

**Figure 2.12.3. Venus at 2.3 $\mu$m, as seen by Galileo's NIMS instrument during the flyby of Venus en route to Jupiter. This image shows the dark side of Venus and visualises the IR radiation from the hot lower atmosphere penetrating the upper clouds. A strong variability in the cloud cover can be seen: bright patches indicate thin cloud cover, and the dark areas thick cloud cover. These IR windows will be exploited by Venus Express to probe the atmosphere in three dimensions and to map the surface temperature.**

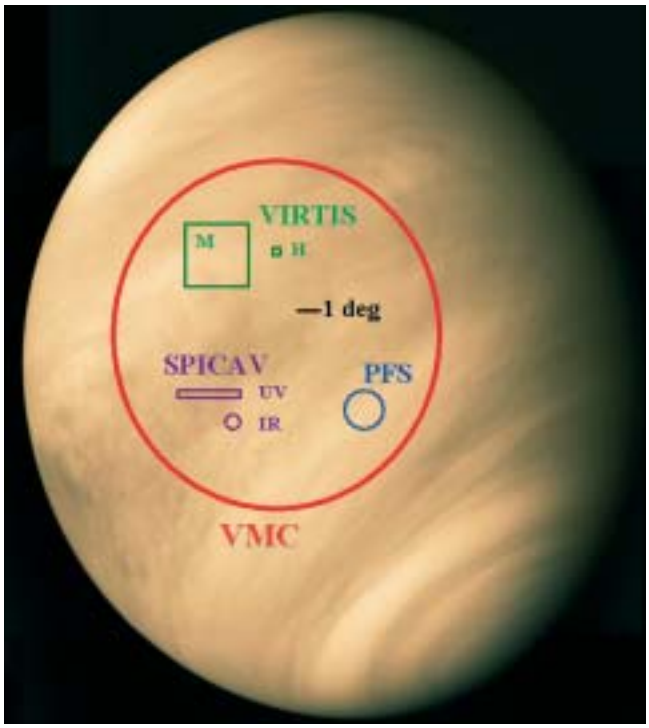


**Figure 2.12.4. The instruments' fields of view (assuming a planet distance of 20 000 km), plotted on to a UV image of Venus from Mariner 10. At apocentre, the VMC FOV will cover the planet's full disc. The instruments together provide a balanced combination of high spatial resolution data for detailed studies and large-scale data for global features.**

## Scientific payload

Great challenges were presented to the team defining the set of instruments to be carried by Venus Express. Since the schedule was postulated *a priori*, the choice of instruments was naturally restricted to units not requiring significant new development; existing qualified designs from previous projects were clearly preferred. The obvious candidates were the instruments developed for Mars Express and Rosetta. After a detailed assessment, three Mars Express instruments were chosen together with two Rosetta instruments, enhanced with a new, miniaturised 4-band camera and a new Magnetometer (with heritage from the Rosetta lander). In addition, a very high-resolution IR solar occultation spectrometer was added to the SPICAM instrument from Mars Express to make SPICAV/SOIR for Venus Express. This new instrument, with a spectral resolution of more than 20 000, will be able to identify a number of isotopes and be particularly important for studying the escape of hydrogen from the planet and so contribute to a better understanding of the evolution of water on Venus.

The resulting instrument complement thus includes a combination of two spectrometers, an imaging spectrometer and a camera, covering the range from UV to thermal-IR, along with a plasma analyser and a magnetometer. These instruments

**Table 2.12.1. The Venus Express scientific payload.**

| *Code* | *Technique* | *Principal Investigator* |
|---|---|---|
| ASPERA | Plasma analyser.<br>Energetic neutral atom imager | S. Barabash (IRF-Kiruna, Sweden) |
| MAG | Magnetometer | T. Zhang (IFW, Graz, Austria) |
| PFS | High-resolution IR Fourier spectrometer | V. Formisano (IFSI-INAF, Rome, Italy) |
| SPICAV/ SOIR | UV & IR atmospheric spectrometer for solar/stellar occultations and nadir observations | J.-L. Bertaux (SA/CNRS, Verrières-le-Buisson, France)<br>D. Nevejans (BIRA-IASB, Brussels, Belgium) |
| VeRa | Radio occultation instrument | B. Häusler (Universität der Bundeswehr, München, Germany) |
| VIRTIS | UV-visible-IR imaging and high-resolution spectrometer | P. Drossart (CNRS/LESIA & Observatoire de Paris, France)<br>G. Piccioni (IASF-INAF, Rome, Italy) |
| VMC | Wide-angle Venus Monitoring Camera | W. Markiewicz (MPAe, Katlenburg-Lindau, Germany) |

together have the capability of sounding the entire atmosphere from the surface to above 200 km altitude (Fig. 2.12.4). Radio science will use the communication link to Earth enhanced with an ultra-stable oscillator, to make high vertical resolution investigations by occultation and to carry out surface studies by bistatic radar techniques.

The elements of the scientific payload are listed in Table 2.12.1 and their locations aboard the spacecraft are shown in Fig. 2.12.5. As it turns out, despite the limitations in the freedom of choice, the payload is a first-class set of instruments well optimised for the mission, and all aspects of the scientific objectives will be addressed to a proper depth.

## Spacecraft

The spacecraft is derived from the Mars Express spacecraft, reusing most subsystems without major modifications. The important differences are found in the thermal control system, which had to be redesigned in order to cope with the much higher heat input from the Sun at Venus and the higher albedo of the planet itself. For the same reason, the solar panels were completely redesigned: they are based on high-temperature GaAs cells and have a total area about half that on Mars Express.

The X-band telemetry rate will vary according to the Venus-Earth distance, with a minimum rate giving at least 500 Mbit of science data per orbit. An S-band channel was provided for near-Earth communications and enhanced radio-science investigations.

The main spacecraft dimensions, excluding the solar panels, are 1.7x1.7x1.4 m; the total mass is 1203 kg, of which 570 kg is propellant.

The spacecraft and its subsystems and scientific instruments were subjected to a full testing programme and those elements not previously qualified for other projects went through a qualification programme. A final test of the fully integrated spacecraft included exposure to a representative solar input at Venus of 2600 W/m$^2$.

The spacecraft prime contractor was Astrium-EADS, Toulouse (F), while the assembly, integration and verification were performed by Alenia Spazio, Turin (I).

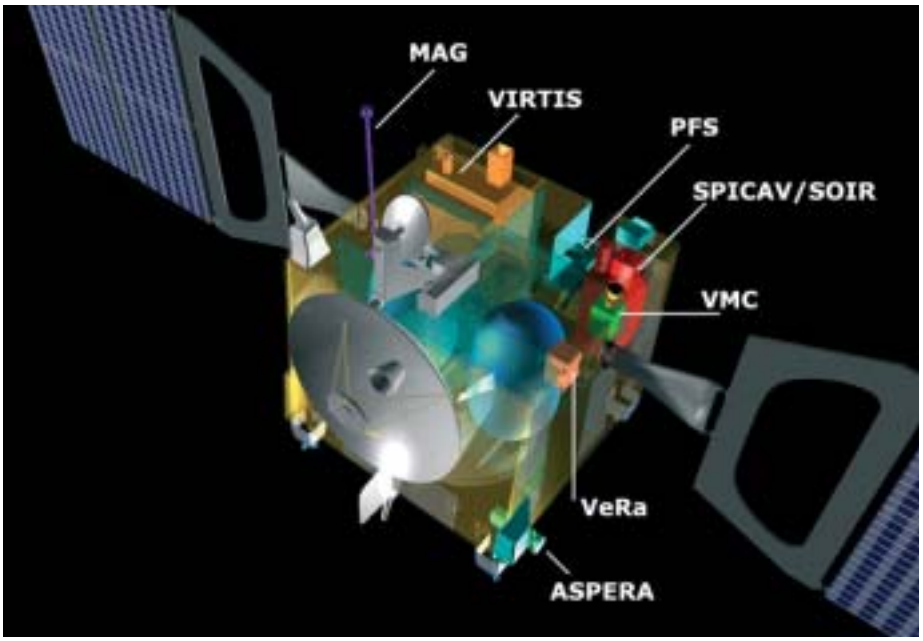


**Figure 2.12.5. Accommodation of the scientific instruments. Most apertures are on the upper platform, which faces Venus during observations. The thermal design allows the Sun to illuminate only the upper platform and the side with the HGA; strict time limits apply if observations force solar illumination on any other panel. The nominal attitude while not observing is with the HGA pointing towards Earth and the solar panels oriented north-south.**

## Status

The Launch and Early Operations Phase went very smoothly and was finished in only 3 days. Then in-orbit testing continued with the Near-Earth Commissioning Phase, when all instruments were switched on and checked out. VMC and VIRTIS proved their capabilities by taking images of the Earth and Moon from a distance of 3.5 million km. All instruments have been coaligned internally and the offsets to the spacecraft star trackers and the spacecraft reference system have been established. An interference campaign, with all instruments running in their noisiest modes, was carried out without revealing any significant problem. One anomaly still to be solved relates to the PFS scanner mechanism, which does not appear to be operating properly. Two tests have been performed, supported by laboratory tests on a spare model, and the results are being investigated. Further tests will be performed on the spacecraft after orbit-insertion.

The Mission Operations Centre and the related ground system are fully operational. Seven simulations of the Venus orbit-insertion activities have been performed in order to ensure a safe and smooth operation. The Science Operations Centre is fully operational and all staff and equipment are prepared for the in-orbit commissioning and the first routine operations. A long-term plan for scientific observations is ready, and medium- and short-term plans for the first phases of science activities have been established. All systems are green for operation in orbit around Venus.

# 3. Missions in Post-Operations/Archival Phase

# 3.1 ISO

## Introduction

ESA's Infrared Space Observatory (ISO) made almost 30 000 scientific observations in its 2.5-year operational lifetime, which ended in May 1998. Employing its four sophisticated and versatile scientific instruments ISO provided astronomers with diverse data of unprecedented sensitivity at IR wavelengths of 2.5–240 $\mu$m. Infrared light penetrates the obscuring dust that hides much of the Universe from inspection at visible wavelengths; light of these wavelengths originates from bodies and material that are cool and distinct from the energetic sources of visible light, like stars. These cool sources are of fundamental importance. A rich variety of atomic, ionic, molecular and solid-state spectral features trace the chemistry and evolution of the cold gas and dust from which stars form, and which they in turn enrich with the heavy elements produced during their nuclear burning and terminal phases. New generations of stars and planets form from the enriched interstellar medium, revealing their presence first through the IR emission associated with proto-stellar and proto-planetary sources. Most of the star formation in the history of the Universe is revealed through the IR emission of the heated dust clouds that would otherwise hide it from view.

The mission resulted from a proposal made to ESA in 1979. After a number of studies, ISO was selected in 1983 as the next new start in the ESA Scientific Programme. Following a Call for Experiment and Mission Scientist Proposals, the scientific instruments were selected in mid-1985. The two spectrometers, a camera and an imaging photo-polarimeter jointly covered wavelengths from 2.5 $\mu$m to around 240 $\mu$m with spatial resolutions ranging from 1.5 arcsec (at the shortest wavelengths) to 90 arcsec (at the longer wavelengths). The satellite design and main development phases started in 1986 and 1988, respectively, with Alcatel (Cannes, F; formerly Aerospatiale) as prime contractor. ISO was launched perfectly in November 1995 by an Ariane-44P and all went very smoothly in orbit. At 12 $\mu$m, ISO was a thousand times more sensitive and had a hundred times better angular resolution than IRAS. Routine scientific operations began in February 1996 and continued until April 1998, with limited operations continuing through May. All data were reprocessed with the end-of-mission calibration to populate the first homogeneous ISO Data Archive, which opened to the community in December 1998. By August 1999, all data had entered the public domain.

Through the ensuing 4 years of the post-operations phase, ESA's ISO Data Centre developed and refined the ISO Data Archive to offer the ISO data to the worldwide astronomical community, and, together with the National Data Centres in various member states and in the US (Table 3.1.1), worked to fill the archive with the best systematically processed and calibrated data products that could be achieved for the huge ISO database. These products allow users to select data sets of interest for deeper study with interactive analysis tools. ISO's Legacy Archive, containing this reference product set, was released at the end of February 2002.

During ISO's Active Archive Phase, which is running from January 2002 to December 2006, the ISO Data Centre continues to work with active National Data Centres in The Netherlands, Germany and the UK to support the community in its use of the ISO data and to leave behind an enhanced archive as a legacy to future generations of astronomers, especially those preparing and interpreting Herschel observations. Particular focus is placed on systematic and interactive processing of the ISO data in order to purge further instrumental effects and to prepare the ISO archive for its role as part of a system of interoperable archives forming the 'virtual telescopes' of the future.

*For further information, see http://iso.esac.esa.int/*

**Table 3.1.1. Principal characteristics of the ISO instruments.**

| *Instrument/ PI* | *Participating countries* | *Main function* | *Wavelength ($\mu$m)* | *Spectral resolution* | *Spatial resolution* | *Outline description* |
|---|---|---|---|---|---|---|
| ISOCAM (C. Cesarsky, CEN-Saclay, F) | F, GB, I, S, USA | Camera and polarimetry | 2.5–17 | Broadband, narrow-band and circular variable filters | Pixels of 1.5, 3, 6 & 12 arcsec | Two channels, each with a 32×32-element detector array |
| ISOPHOT (D. Lemke, MPI für Astronomie, Heidelberg, D) | D, DK, E, GB, IRL, SF, USA | Imaging photopolarimeter | 2.5–240 | Broadband and narrowband filters<br><br>Near-IR grating spectrometer (R~90) | Variable from diffraction-limited to wide-beam | Three subsystems:<br>1. multi--band, multi-aperture photopolarimeter (3-125 $\mu$m)<br>2. far-IR camera (50–240 $\mu$m)<br>3. spectrophotometer (2.5–12 $\mu$m) |
| SWS (Th. de Graauw, Lab. for Space Research, Groningen, NL | B, D, NL, USA | Short-wavelength spectrometer | 2.5–45 | 1000 across wavelength range and $2\times10^4$ for 12–44 $\mu$m | 14×20 and 20×44 arcsec | Two gratings and two Fabry-Perot interferometers |
| LWS (P. Clegg, Queen Mary College, London, UK | F, GB, I, USA | Long-wavelength spectrometer | 43–195 | 200 and $10^4$ across wavelength range | 1.65 arcmin | Grating and two Fabry-Perot interferometers |

The Data Centres responsible for ISO User Support were or are (Centres continuing to operate into the Active Archive Phase are marked with *): ISO Data Centre at ESA/ESAC in Spain*; Five Specialist National Data Centres (NDCs): French ISO Centres, SAp/Saclay and IAS/Orsay, France; ISOPHOT Data Centre at MPIA, Heidelberg, D*; Dutch ISO Data Analysis Centre at SRON, Groningen, NL* (now part of the HIFI Operation Centre); ISO Spectrometer Data Centre at MPE in Munich, D*; UK ISO Data Centre at RAL, Oxford, UK*. In the USA: ISO Support Center at NASA's IPAC, on CalTech campus.

**Table 3.1.2. Principal characteristics of the ISO mission.**

*Launch:* 17 November 1995 by Ariane-4 into an elliptical orbit of 24 h, 5° inclination, 1000 km perigee height, 70 600 km apogee height. Routine operational phase lasted from 4 February 1996 to 8 April 1998.

*Science goals:* IR astronomy (using imaging, photometry, polarimetry and spectroscopy), from comets to cosmology.

*Science operations:*

ISO Science Operations Centre at Vilspa (E);
Distribution of observing time: 45% guaranteed time, 55% open time (via AO).

*Spacecraft:*

3-axis stabilised (all errors $2\sigma$; half-cone, instruments point along x-axis, y-axis is along length of solar arrays):
absolute pointing error: 1.5 arcsec
absolute pointing drift (1 h): < 0.1 arcsec
relative pointing error: 0.5 arcsec
Data rate: 24 kbit/s (science telemetry)
Power (payload): 600 W
Spacecraft size: 5.3 x 2.3 m
Mass: about 2300 kg at launch

*Operations:*

ISO Spacecraft Control Centre at Vilspa (E)
Data transmission: S-band, ground stations: Vilspa (E), Goldstone (USA)
Mission lifetime: 18 months nominal, 30 months effective

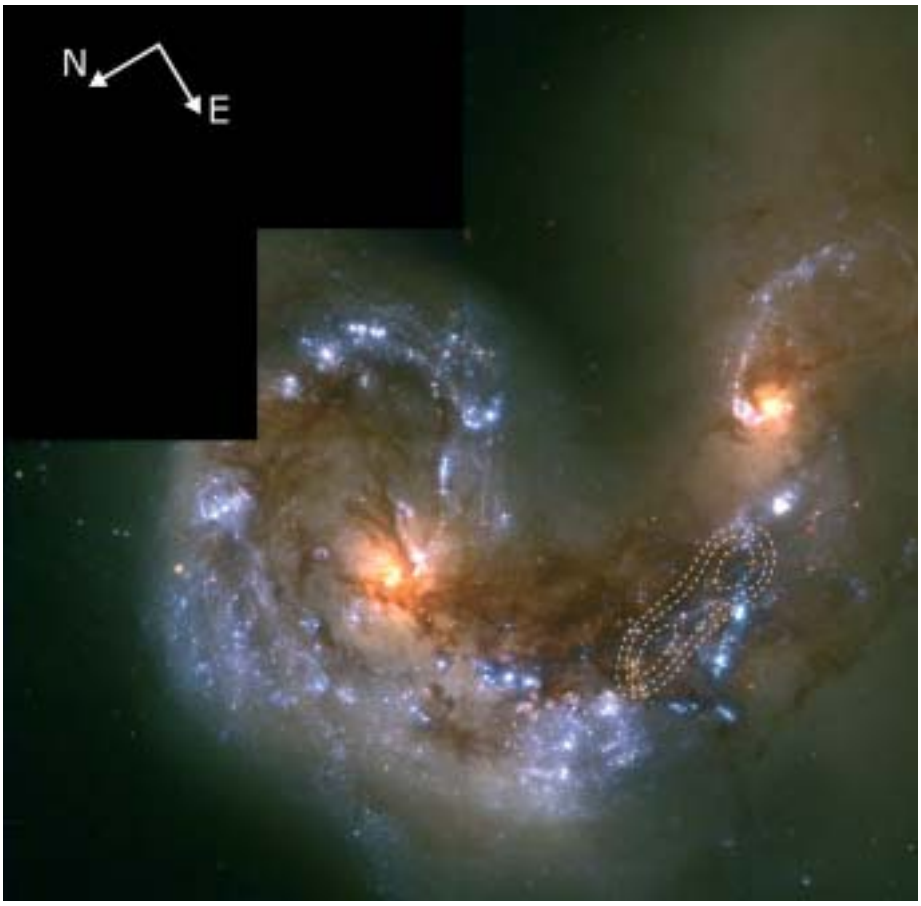


**Figure 3.1.1. The pair of colliding galaxies known as Antennae (NGC 4038/4039), 60 million light years away in Corvus. Early in the mission, ISOCAM images revealed that the region of collision harbours violent star-formation processes, obscured by the dust and visible only in the IR. Further studies provided the direct evidence that shock waves generated by the collisions excite the gas from which new stars will form. This was revealed by the exceptional molecular hydrogen rotational line emission detected (shown as contours). There are too few supernova explosions or regions of intense star-formation there to explain the observed molecular hydrogen emission. So, the excitation of the molecular hydrogen must be the signature of that observationally rare pre-star birth phase in which hydrogen is excited by the mechanical energy produced in the collision and transported by shock waves. In other words, these results provide the first direct evidence of the missing link between gas collision and the birth of the first stars. In the course of the next million years, the new stars will make the Antennae galaxies twice as bright in the IR. (Haas et al., 2005)**

## ISO science

ISO continues to deliver ground-breaking results in all areas of astronomy. Over 1300 papers have appeared in the refereed literature based on ISO data (at an average rate of 110/year in the last 2 years). The results produced to late 2004 were reviewed in a special issue of *Space Science Reviews* (volume 119, 2005). The 450-page book, entitled *ISO Science Legacy – A Compact Review of ISO Major Achievements*, consists of four general articles reviewing four major themes investigated by ISO (crystalline silicates, molecular hydrogen, water in the Universe, deep surveys), followed by 13 papers reviewing ISO science from the Solar System to the distant Universe.

Crystalline silicates have been discovered by ISO outside the Solar System and were shown to be ubiquitous throughout the Galaxy wherever matter is dense (while not occurring in significant amounts in the diffuse interstellar medium). They sometimes appear in very large quantities (>50% of the small dust particles). Previously, it was generally assumed that all cosmic silicates in space were of amorphous structure! The diagnostic potential of direct detection of $H_2$ rotational lines is also demonstrated by ISO observations, such as those shown in Fig. 3.1.1. We have learned about such diverse astrophysical sources as photon-dominated regions, shocks, young stellar objects, planetary nebulae and starburst galaxies, inferring important physical quantities such as the gas temperature, gas density and strength of the radiation field. ISO found water to be ubiquitous in the Universe, and provided a wealth of data on its abundance and spatial distribution in the direction of molecular

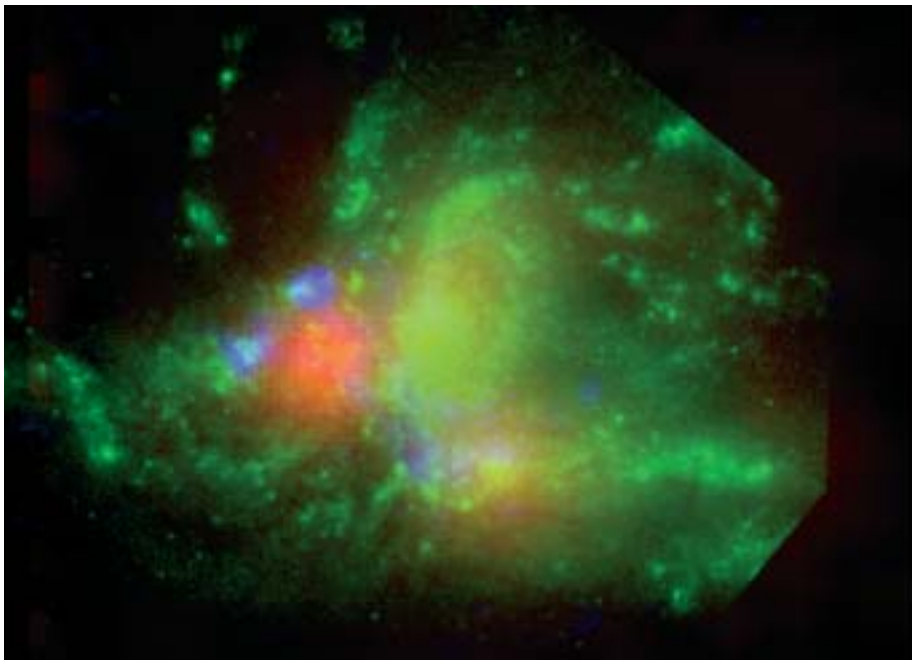

**Figure 3.1.2. Hidden starburst detected in the colliding galaxy pair Mkn297, using visible (HST F555W, green), 15 $\mu$m (ISOCAM, red) and 6 cm radio (blue) data. The hidden starburst appears strongly red. At 15 $\mu$m, it is, respectively, 14.6 and 3.8 times more luminous than the hidden sources in the Antennae and Stephan's Quintet. The total IR luminosity is some $10^{11}$ solar luminosities, which (marginally) classifies the system as a luminous IR galaxy. A supernova that exploded in 1979 (SN 1982aa) gave rise to one of the most powerful known radio remnants (blue), which falls close to the strongest mid-IR source. Another radio source, appearing in blue, is a star cluster, at the location of the near-IR peak detected by the 2MASS survey. The optically detectable material is green. (Metcalfe et al., 2005)**

clouds, evolved stars, galaxies and in the bodies of our Solar System. IRAS revealed the existence of galaxies forming stars at a rate of a few tens (in the case of luminous IR galaxies) or even hundreds (in the case of ultraluminous IR galaxies) of solar masses per year in the local Universe. ISO followed up by not only studying samples of such galaxies (Fig. 3.1.2) out to redshifts of 1 and beyond, but also by showing that they are not the exceptional objects that we once believed. Instead, they appear to have played a dominant role in shaping present-day galaxies, skewing the cosmic history of star formation and producing the cosmic IR background detected by the COBE satellite in the far-IR to sub-mm range.

Recent papers continue to develop these themes and address a number of important questions in all areas of astronomy, either based on the study of particular objects or, more frequently, on samples of targets extracted from the ISO archive, often in combination with data from other facilities. ISO data also feed back into modelling and/or laboratory research activities.

New results have been published: on comet Hale-Bopp, with precise determination of constituent crystalline dust size and mass; on Saturn's moon Titan via observations in its 3 $\mu$m methane window, giving the first surface albedo spectrum and demonstrating the presence of water ice and other compounds (Fig. 3.1.3); and on the association between asteroids and meteorites from comparison of their spectra with laboratory spectra.

Recent papers discuss the absence of crystalline silicates in the interstellar medium and the high formation rate of molecular hydrogen in photo-dissociation regions, the latter possibly arising on polycyclic aromatic hydrocarbons (PAHs). Maps of dust grain distributions were obtained in molecular clouds, showing their destruction into clusters of PAHs away from the generating star. Several hundreds of Young Stellar Objects and their outflows have been studied through their far-IR fine-structure lines and expanded inventories of ices. PAHs and properties of dust found in discs around Herbig Ae/Be stars are also discussed. Of interest is the inferred

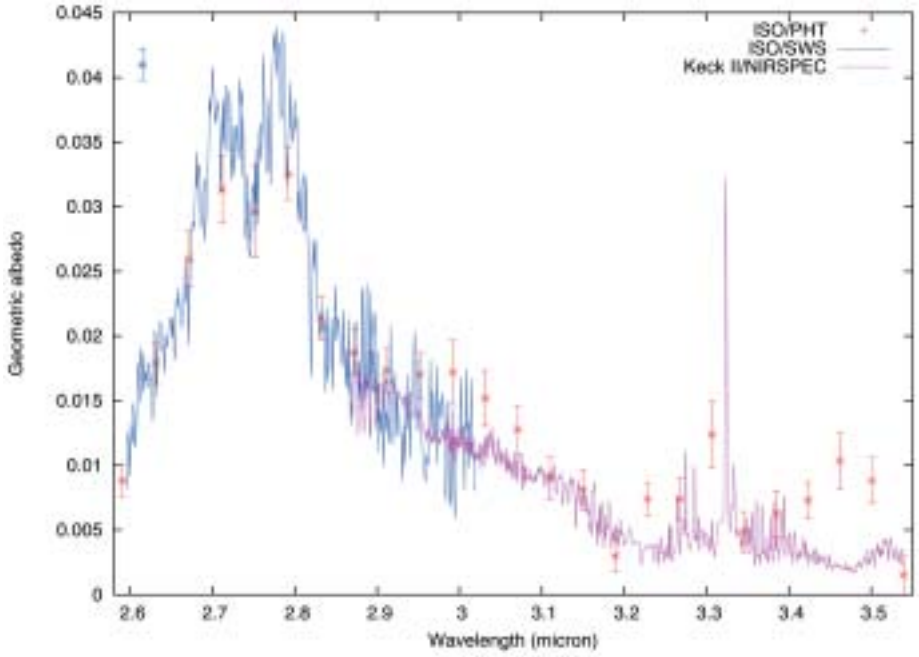


**Figure 3.1.3. Titan surface albedo spectrum in the 3 $\mu$m methane window. ISO SWS (continuum line), ISOPHOT-S (red dots) and Keck II/NIRSPEC spectra are shown for comparison. Atmosphere models indicate water ice (and other components). The surface methane abundance is derived to be of the order or less than 3%. (Coustenis et al., 2006)**

presence of calcite in protostars, complementing its detection reported previously in a planetary nebula and suggesting a formation mechanism for carbonates in the absence of water. Particular spectral features detected in samples of hundreds of Asymptotic Giant Branch (AGB) stars aid in defining scenarios for their evolution. Detections of cold dust are reported in a number of galaxies and in their surrounding halos. The interplay of PAHs and very small grains in galaxies is discussed, as well as the roles of starbursts and Active Galactic Nuceli (AGN) as prevailing sources of IR emission in large samples of IR galaxies.

New results emerging from the various ISO surveys (ELAIS, FIRBACK, Lockman Hole) in the form of catalogues, source counts and multi-wavelength cross-identifications, continue to confirm that only evolutionary models can explain the ISO data. The ISOPHOT 170 $\mu$m Serendipity Survey catalogue has been published, listing more than 1900 galaxies observed serendipitously while the spacecraft was moving from one object to the other in the observing programme. Very cold and massive cores have been measured near one of the detected sources, with implications for initial conditions of high-mass star formation.

## ISO Data Archive (IDA)

ISO performed around 30 000 science observations. Allowing for observations made in the parallel and serendipity modes (observational modes in which an instrument could observe while another instrument was prime), almost 150 000 data sets were recorded. Since ISO was operated as an observatory with four complex instruments, the resulting data are very heterogeneous. The data underwent extensive processing, including validation and accuracy analysis. In total, around 400 GBytes of data are stored on magnetic disks. These data are served to the user community via a unique state-of-the-art astronomical data archive. In addition to the observational data products, the archive also contains satellite housekeeping data, software tools, documentation and externally derived products.

The IDA is based on an open and flexible three-tier architecture: Data Products and Database: Business Logic: and User Interface. An important consideration was to separate the stored data from their final presentation to the user. The Business Logic and the User Interface were developed entirely in JAVA and XML, which allows the IDA to be accessible from any platform and from the most popular web browsers. This has facilitated its reuse for other ESA archive projects (such as XMM-Newton, Integral and Planetary Missions).

A textual and visual presentation of the data is offered to users to aid them in selecting observations for retrieval through FTP. One of the main features is the provision of browse products or quick-look data associated with each observation. These enable users to make informed decisions as to which observations they want to download for detailed astronomical analysis.

By December 2005, IDA counted nearly 2000 users and was queried about 2500 times per month. Forty different users retrieve data each month. IDA supports easy-to-make but powerful queries against all ISO data. The quick-look images and online visualisation tools aid users in the selection of products for data retrieval through a 'shopping basket' mechanism familiar to anyone who has made commercial purchases via the web. After email notification that their request has been serviced, users make fast data retrieval by FTP. A direct download facility is also available.

Three major versions of the IDA were released during 2004–2005. Enhanced quality information of ISO observations is thoroughly documented in queriable Data Quality reports, specifying the remaining caveats on the pipeline processing and flagging specific real-time or processing problems (Version 7, June 2004). The documentation strategy is also injected in the emerging Virtual Observatories. Version 8, released in May 2005, incorporates functionalities that were developed for other science archives at ESAC, via a Common User Interface, thus simplifying its maintenance after the end of the ISO project in 2006. Version 9, released in July 2005, incorporates the option to retrieve the most reliable dataset associated with a given observation. This is called the 'Default Dataset' and can be generated by the legacy automatic pipeline software or by advanced interactive processing (Highly Processed Data Product).

**Off-line products**

Every ISO observation has been run through an automatic data-analysis pipeline called Off-Line Processing (OLP), to generate standard data products. The automatic data products passed through several generations, until at the end of ISO Post Operations and in the first months of the Active Archive Phase in early 2002 a final full reprocessing of all ISO data was performed, producing the ISO Legacy Archive. All products were put on hard disk, superseding previous product versions.

**Interactive analysis tools**

All interactive analysis tools, including a number of software packages offered to the community for reduction and analysis of ISO data, are archived. These include: ISOCAM Interactive Analysis (CIA); ISOPHOT Interactive Analysis (PIA); Observers' SWS Interactive Analysis (OSIA); LWS Interactive Analysis (LIA); and ISO Spectroscopic Analysis Package (ISAP). They are obtainable through the ISO WWW page or directly from the responsible software groups.

**Documentation**

Extensive explanatory and technical support documentation is archived. This includes the five volumes of the *ISO Handbook* (released in their final form as SP-1262),

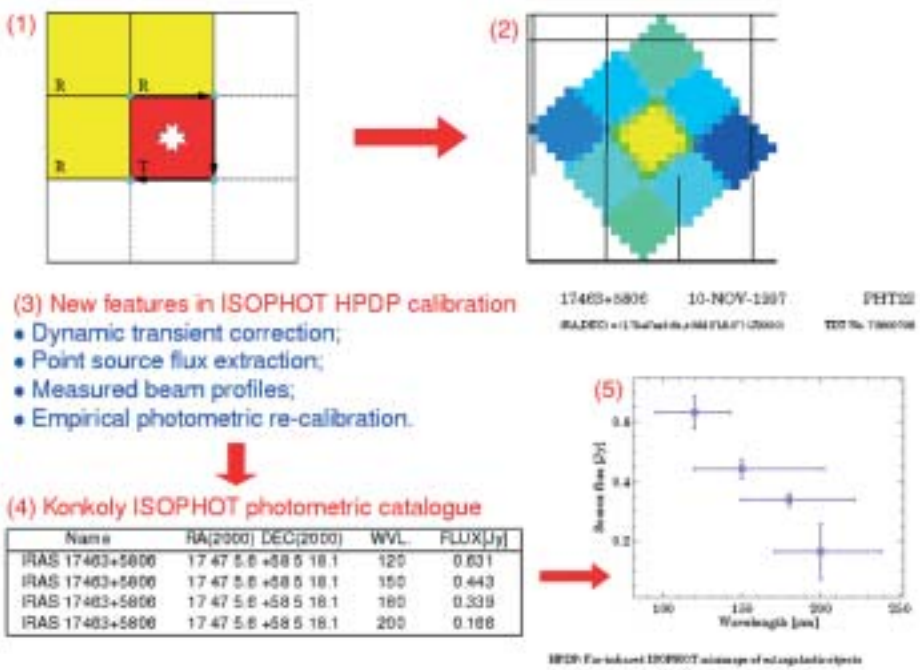


**Figure 3.1.4. Highly Processed Data Products are produced in the ISO Active Archive Phase as readily usable products. These include photometric catalogues produced within a dedicated 4-year project run at the Konkoly Observatory, in Budapest (Hungary). Most are derived from small maps performed around compact sources with ISOPHOT. The catalogues are produced after correction for residual instrumental artifacts present in the automatic pipeline products (drift and transient correction, empirical correction for systematic trends, background determination and flux correction). Survey products, icon and postcards generated by the Off-Line Processing Legacy Pipeline are replaced by those created from the HPDP (photometric points). The catalogues can be queried and retrieved from the archive.**

gathering all the information needed to make efficient use of ISO data, and extensive technical documentation, tracing and explaining the experience of the instrument teams as they worked to understand the calibration of their instruments. Together with the ISO Data Products, the body of explanatory and support documentation is called the ISO Explanatory Library. The calibration legacy of ISO is extensively documented in ESA SP-481.

**Highly Processed Data Products (HPDP)**

HPDP are the result of further processing beyond the pipeline and/or using new, refined algorithms mainly contributed by ISO instrument experts. They include processed images and spectra, object catalogues and spectral and image atlases (Fig. 3.1.4). A number of instrument-mode or object-type specific projects have been carried out, and many more are in progress or foreseen to be completed in 2006.

**Virtual Observatory**

ISO has played a key role in the last 2 years in the definition of standards for interoperability within the International Virtual Observatory Alliance (IVOA, *http://ivoa.net*), providing access to its spectral data through the IVOA Simple Spectrum Access Protocol (SSAP). It has become a reference implementation and testbed for the proper specification and improvement of the protocol. Image data have been provided through the IVOA Simple Image Access Protocol (SIAP). ISO has also been a pioneer in Europe by implementing access to its products using Basic SkyNode (another IVOA standard).

The ESAVO-VOSpec (*http://esavo.esac.esa.int/vospec/*) tool has been used on the spectral data from ISO, becoming the first-ever Virtual Observatory-compatible tool fuelled by IVOA standards. Through this tool, these data have been exposed to the world in an unprecedented manner.

## Conclusions

ISO has made, and continues to make, ground-breaking contributions to all areas of astronomy, from Solar System studies, to the limits of cosmology and the history of the Universe. The mission itself was technically extremely successful, with several key aspects of the technology substantially outperforming their specifications (e.g. cryostat hold time, and attitude and orbit control accuracy and stability). Beyond that, the challenge of serving the huge body of ISO results to the astronomical community in a user-friendly way stimulated the development of an innovative data archive, pioneering many aspects of interoperability, and leading the way towards the virtual observatories of the future. Its contents are being constantly upgraded, with more 'readily-usable' products. The extended post-operational activities have enabled the community to get the most out of ISO and, additionally, have built a bridge towards new ESA missions, especially Herschel.

# 4. Projects Under Development

# 4.1 Herschel

## Introduction

The Herschel Space Observatory, the fourth of the original Cornerstone missions in the ESA Horizon 2000 science plan, is a multi-user observatory-type mission that will provide unrivalled observing opportunities for the general astronomical community in the relatively poorly explored 57-670 $\mu$m part of the far-IR and sub-mm range. It will bridge the wavelength gap between earlier IR missions such as IRAS, ISO, Astro-F and Spitzer, and ground-based observatories.

## Scientific objectives

Herschel (Fig. 4.1.1) is the only space facility dedicated to the far-IR and sub-mm part of the spectrum. It has the potential for discovering the earliest epoch proto-galaxies, revealing the cosmologically evolving AGN/starburst symbiosis, and unravelling the mechanisms involved in the formation of stars and planetary system bodies.

The major strengths of Herschel are its photometric mapping capability for performing unbiased surveys related to galaxy and star formation and its spectral coverage for follow-up observations. Redshifted ultraluminous IR-dominated galaxies, with spectral energy density functions (SEDs) that 'peak' in the 50-100 $\mu$m range in their rest frames, as well as class 0 proto-stars and pre-stellar objects in our own and nearby galaxies, have SEDs that peak in the Herschel 'prime' band. Herschel is also well-equipped to perform spectroscopic follow-up observations to characterise further particularly interesting individual objects.

The key science objectives emphasise the formation of stars and galaxies, and their interrelation. Example observing programmes with Herschel will include:

— deep extragalactic broadband photometric surveys in six colours spanning the Herschel wavelength coverage and related research. The main goals include further resolving the IR background into discrete sources, performing a detailed investigation of the formation and evolution of galaxy bulges and elliptical galaxies in the first third of the present age of the Universe, and determining how the star-formation rate and galaxy luminosity functions evolve with cosmic time;
— follow-up spectroscopy of especially interesting objects discovered in the survey. The far-IR/sub-mm band contains the brightest cooling lines of interstellar gas, which give important information on the physical processes and energy-production mechanisms (for example, AGN *vs*. star formation) in galaxies;
— detailed studies of the physics and chemistry of the interstellar medium in galaxies, both locally in our own Galaxy as well as in external galaxies, by means of photometric and spectroscopic surveys and detailed observations. This includes implicitly the important question of how stars form out of molecular clouds in various environments using galaxies as 'laboratories' providing, for example, different levels of metallicity;
— observational astrochemistry (of gas and dust) as a quantitative tool for understanding the stellar/interstellar lifecycle and investigating the physical and chemical processes involved in star formation and in both early and late stages stellar evolution in our own Galaxy. Herschel will provide unique information on most phases of this lifecycle, including the study of the evolution of circumstellar disks during the planet-forming era;
— detailed high-resolution spectroscopy of a number of comets and the atmospheres of the cool outer planets and their satellites;
— studies of Kuiper belt objects, and comparisons with the global properties of those observed around nearby stars.

From experience, it is also clear that the discovery potential is significant when a

*For further information, see http://www.rssd.esa.int/herschel/*

**Figure 4.1.1. Herschel during the mechanical qualification campaign in the ESTEC Test Centre. The cryostat (with the black radiator in the centre), six of the eight side panels plus the top and bottom panels of the service module, the thermal shield and the upper half of the sunshade are flight hardware. The photograph was taken on 1 February 2006 during a Herschel Science Team meeting.**

**Figure 4.1.2. The Herschel telescope, shown during warm alignment activities at Astrium in Toulouse (F) in summer 2005. (EADS Astrium)**

**Table 4.1.1. Herschel scientific payload.**

| *Acronym* | *Instrument* | *Principal Investigator* |
|---|---|---|
| PACS | imaging camera & grating spectrometer, spectral coverage ~57-205 $\mu$m | A. Poglitsch, MPE, Garching (D) |
| SPIRE | imaging camera & FTS spectrometer, spectral coverage ~200-670 $\mu$m | M. Griffin, U. Cardiff (UK) |
| HIFI | high-res heterodyne spectrometer; spectral coverage 157-212 & 240-625 $\mu$m | Th. de Graauw, SRON, Groningen (NL) |

**Table 4.1.2. Principal characteristics of the Herschel mission.**

*Type of mission:* far-IR and sub-mm observatory; ~2/3 open time available to the general user community; 4th ESA Cornerstone mission
*Science goals:* star and galaxy formation, interstellar medium physics and chemistry, solar system body studies
*Telescope:* 3.5 m-diameter Cassegrain telescope of silicon carbide
*Spacecraft:* 3-axis spacecraft with superfluid helium cryostat for instrument focal plane unit cooling
*Size:* height 7.5 m x width 4 m, launch mass 3 t
*Science data rate:* 130 kbit/s average production rate
*Lifetime:* 3 years of routine science operations
*Operational orbit:* Lissajous orbit around L2
*Launch:* dual launch (with Planck) on Ariane-5 ECA in 2008

new capability is being implemented for the first time. Observations have never been performed in space in the prime band of Herschel. The total absence of (even residual) atmospheric effects – enabling both a much lower background for photometry and full wavelength coverage for spectroscopy – and a cool low-emissivity telescope open up a new part of the phase-space of observations. Thus, a space facility is essential in this wavelength range and Herschel will be breaking new ground.

## Telescope and science payload

In order to exploit fully the favourable conditions offered by being in space, Herschel has a precise, stable, low-background telescope, and a complement of capable scientific instruments. The telescope (Fig. 4.1.2) is passively cooled (placing it outside the cryostat maximises its size), while the instrument focal plane units are mounted on a common optical bench housed inside a cryostat containing superfluid helium below 1.7K. The bolometer arrays in PACS and SPIRE are cooled to ~300mK using dedicated instrument-provided sorption coolers.

During operations, the telescope must have a total wavefront error (WFE) of no more than 6 $\mu$m, corresponding to diffraction-limited operation at about 85 $\mu$m. It also has a very low emissivity to minimise the background signal, and the whole optical chain is optimised for high straylight rejection. Protected by a fixed sunshade, the telescope will radiatively cool to an operational temperature of around 80K. The design is a classical Cassegrain with a 3.5 m-diameter primary and an 'undersized' secondary. The telescope, manufactured by EADS Astrium (Toulouse, F), is made almost entirely of silicon carbide (SiC). The primary mirror blank was made out of 12

segments brazed together to form a monolithic mirror. This was then ground, lapped and polished to the required accuracy, and finally metallised to provide the required high reflectivity and low emissivity. The secondary was machined out of a single piece of SiC, including an integrated scattercone in its centre for standing-wave suppression, and metallised in the same way as the primary. The secondary support structure, consisting of a hexapod and a barrel-like structure, is also made of SiC, carries the launch loads and is optimised for adequate straylight and standing-wave performance.

The scientific payload consists of three instruments (Table 4.1.1), provided by consortia led by Principal Investigators (PIs) in return for guaranteed observing time.

PACS (Photodetector Array Camera and Spectrometer) is a short-wavelength camera and low- to medium-resolution spectrometer covering wavelengths up to about 205 $\mu$m. It employs four detector arrays: two bolometer arrays for photometry, and two photoconductor arrays for spectroscopy. PACS can be operated either as a photometer, fully sampling an FOV of 1.75x3.5 arcmin on the sky simultaneously in two broadband colours (either of the 60–85 or 85–130 $\mu$m bands plus the 130–210 $\mu$m band), or as an integral field line spectrometer covering just under 1 arcmin square on the sky with a resolution in the range 1000–4000 depending on wavelength.

SPIRE (Spectral and Photometric Imaging REceiver) is a long-wavelength camera and low- to medium-resolution spectrometer covering wavelengths longer than 200 $\mu$m. It comprises an imaging photometer and a Fourier Transform Spectrometer (FTS), both of which use bolometer detector arrays with individual feedhorns for each detector. There are five arrays in total: three dedicated to photometry, and two for spectroscopy and spectrophotometry. As a photometer, SPIRE covers a large 4x8 arcmin field on the sky that is imaged in three colours (centred on 250, 360, 520 $\mu$m simultaneously), and in spectroscopy a field approximately 2.6 arcmin across with a resolution of order 100.

HIFI (Heterodyne Instrument for the Far Infrared) is a heterodyne spectrometer. It offers very high velocity-resolution spectroscopy using auto-correlator and acousto-optical spectrometers, combined with low noise detection using superconductor-insulator-superconductor (SIS) and hot electron bolometer (HEB) mixers. Five dual polarisation SIS mixer bands cover the frequency range 490–1250 GHz, and two HEB bands cover 1410–1910 GHz. HIFI covers a single pixel on the sky, and builds up images either by raster scanning or by on-the-fly mapping.

## Spacecraft and in-orbit operations

Herschel is based on the well-proven ISO cryostat technology. It is modular, consisting of the 'extended payload module' (EPLM) comprising the superfluid helium cryostat (housing the optical bench with the instrument focal plane units) that supports the telescope, the sunshield/shade, and payload associated equipment; and the service module (SVM), which provides the infrastructure and houses the warm payload electronics. Herschel is about 7.5 m high and 4 m wide, and has a launch mass of around 3000 kg.

An industrial consortium led by Alcatel Space Industries (Cannes, F) as prime, with EADS Astrium (Friedrichshafen, D), responsible for the EPLM, and Alenia Spazio (Torino, I) for the SVM, and a host of subcontractors from all over Europe, are building the spacecraft. Arianespace will provide the launch services in Kourou. For a summary of principal mission characteristics see Table 4.1.2.

An Ariane-5 ECA launcher, shared with Planck, will inject both satellites into a transfer trajectory towards the second Lagrangian point (L2) in the Sun- Earth system. They will then separate from the launcher, and subsequently operate independently,

from orbits of different amplitudes around L2. It offers a stable thermal environment with good sky visibility. Since Herschel will be in a large orbit around L2, which has the advantage of not costing any orbit injection delta-V, its distance to Earth will vary by 1.2–1.8 million km. Herschel will take about 4 months to reach the operational orbit. For the first 2 weeks after launch, while cooldown and outgassing take place, the telescope will be kept warm by heaters to prevent it acting as a cold trap for the outgassing products. It will then cool, for the opening of the cryostat door (thus providing 'first light') about 5-6 weeks after launch. Commissioning and performance verification will take place enroute to L2, followed by a science demonstration phase. Once these crucial mission phases have been accomplished, Herschel will begin routine science operations.

## Science operations

Herschel will be a multi-user observatory open to the general astronomical community. It will perform routine science operations for a minimum of 3 years, until depletion of the helium. The available observation time will be shared between guaranteed time (one third) owned by contributors to the Herschel mission (mainly by the PI instrument consortia), and open time allocated to the general community (including the guaranteed time holders) on the basis of calls for observing time. The initial call for observing proposals is planned to be issued in the second half 2006.

The scientific operations of Herschel will be conducted in a decentralised manner. The operational ground segment comprises six elements:

— the Herschel Science Centre (HSC), provided by ESA;
— three dedicated Instrument Control Centres (ICCs), one for each instrument, provided by the respective PIs;
— the Mission Operations Centre (MOC), provided by ESA;
— the NASA Herschel Science Center (NHSC), provided by NASA.

The HSC acts as the interface to the science community and outside world in general, supported by the NHSC (primarily) for the US science community. The HSC provides information and user support related to the entire life-cycle of an observation, from calls for observing time, the proposing procedure, proposal tracking, data access and data processing, as well as general and specific information about using Herschel and its instruments.

All scientific data will be archived and made available to the data owners. After the proprietary time has expired for a given dataset, these data will be available to the entire astronomical community in the same manner they were previously available only to the original owner. The accumulated experience from earlier observatory missions (particularly ISO and XMM-Newton) is being used in the implementation of the infrastructure by ESA and the PIs together. An important conclusion is to build one single system that evolves over time, rather than having separate systems for different mission phases. The first functional version of this system is already being used in connection with instrument-level tests.

## Status and schedule

The Pls and science payload were provisionally selected in 1998 and confirmed a year later. The focal plane unit cryogenic qualification models were delivered in late 2004 for integration and testing in the engineering qualification model (EQM), and avionics models for testing together with the SVM. The instrument flight models will be tested, characterised, and calibrated before delivery in the second half of 2006.

The telescope activity began in mid-2001, and the Mid-Term Review was held in November 2001, paving the way for the telescope Critical Design Review (CDR) in April 2002. The telescope was aligned and characterised in warm conditions in summer 2005, immediately followed by successful mechanical qualification. An extensive cryogenic test campaign was underway in early 2006 in Centre Spatial de Liège (B).

The industrial contract for the Herschel spacecraft for Phases-B, C/D and E1 was awarded in April 2001, marking the start of Phase-B. The System Requirements Review took place in autumn 2001, after which the industrial consortium was formed by the selection of subcontractors, involving in excess of 100 procurement activities. The next major step, the Preliminary Design Review took place a year later. The mission-level CDR was held in early 2005.

The first spacecraft hardware to arrive for testing in the ESTEC Test Centre was the SVM structural thermal model (STM), in spring 2005. It was followed by the proto-flight model cryostat, which was tested the Large Space Simulator in late autumn. The entire spacececraft in STM configuration underwent mechanical qualification in early 2006.

Current planning foresees milestones that include instrument and telescope flight model deliveries to ESA and the issue of the first call for observing proposals in 2006. This will be followed by spacecraft integration and extensive system-level spacecraft testing, science ground segment testing (including proposal evaluation and the awarding of observing time), and end-to-end ground testing and simulations, leading to the launch in 2008. Routine science operations are planned to begins about 6 months after launch.

# 4.2 Planck

## Scientific goals

In late 1992, the COBE team announced the detection of intrinsic temperature fluctuations in the Cosmic Background Radiation Field (CBRF),observed on the sky at angular scales larger than ~10°, and at a brightness level $\Delta T/T \sim 10^{-5}$. In February 2003, the WMAP team announced results on scales of about 15 arcmin with a similar sensitivity (see *http://lambda.gsfc.nasa.gov* for detailed descriptions of COBE and WMAP). These fluctuations have been interpreted as due to differential gravitational redshift of photons scattered out of an inhomogeneously dense medium, thus mapping the spectrum of density fluctuations in the Universe at a very early epoch. This long-sought result established the Inflationary Big Bang model of the origin and evolution of the Universe as the theoretical paradigm. However, in spite of the importance of the COBE and WMAP measurements (and those made by many other ground- or balloon-based experiments), many fundamental cosmological questions remain open. Building on the pioneering work of COBE and WMAP, the main objective of the Planck mission is to map the fluctuations of the CBRF with an accuracy that is set by fundamental astrophysical limits, allowing these fundamental questions to be effectively addressed.

Mapping the fluctuations of the CBRF with high angular resolution and high sensitivity would give credible answers to such issues as: the initial conditions for structure evolution, the origin of primordial fluctuations, the type of potential that drove inflation, the existence of topological defects, the nature and amount of dark matter, and the nature of dark energy. Planck will set constraints on theories of particle physics at energies greater than $10^{15}$ GeV, which cannot be reached by any conceivable experiment on Earth. Finally, the ability to measure to high accuracy the angular power spectrum of the CBRF fluctuations will allow the determination of fundamental cosmological parameters such as the density parameter $\Omega_0$ and the Hubble constant $H_0$, with an uncertainty of order a few percent.

The mission's observational goal is to mount a single space-based experiment that will survey the whole sky with an angular resolution as high as 5 arcmin, a sensitivity approaching $\Delta T/T \sim 10^{-6}$, and covering a frequency range that is wide enough to encompass and deconvolve all possible foreground sources of emission. The main scientific result will be an all-sky map of the fluctuations of the CBRF. In addition, the sky survey will be used to study in detail the very sources of emission that contaminate the cosmological signal, and will result in a wealth of information on the dust and gas in both our own Galaxy and extragalactic sources. One specific notable result will be the measurement of the Sunyaev-Zeldovich effect in many thousands of galaxy clusters.

## Planck payload

The Planck payload consists of a 1.5 m-diameter offset telescope, with a focal plane shared by clusters of detectors in nine frequency bands covering the range 30–900 GHz. The three lowest frequency bands (up to ~70 GHz) consist of HEMT-based receivers actively cooled to ~20K by an $H_2$ sorption cooler. The higher frequency bands consist of arrays of bolometers cooled to ~100mK; the $H_2$ sorption cooler provides precooling for a Joule-Thomson 4K stage, to which a dilution refrigerator is coupled. The main elements of the Planck satellite are shown in Fig. 4.2.1, and the characteristics and goal performance of the instruments are given in Table 4.2.1.

The satellite will be placed into a Lissajous orbit around the L2 point of the Earth-Sun system. At this location, the payload can point continuously in the anti-Sun direction, thus minimising potentially confusing signals due to thermal fluctuations and straylight entering the detectors through far side-lobes. From L2, Planck will carry out two complete surveys of the full sky, for which it requires about 14 months

*For further information, see http://www.rssd.esa.int/Planck*

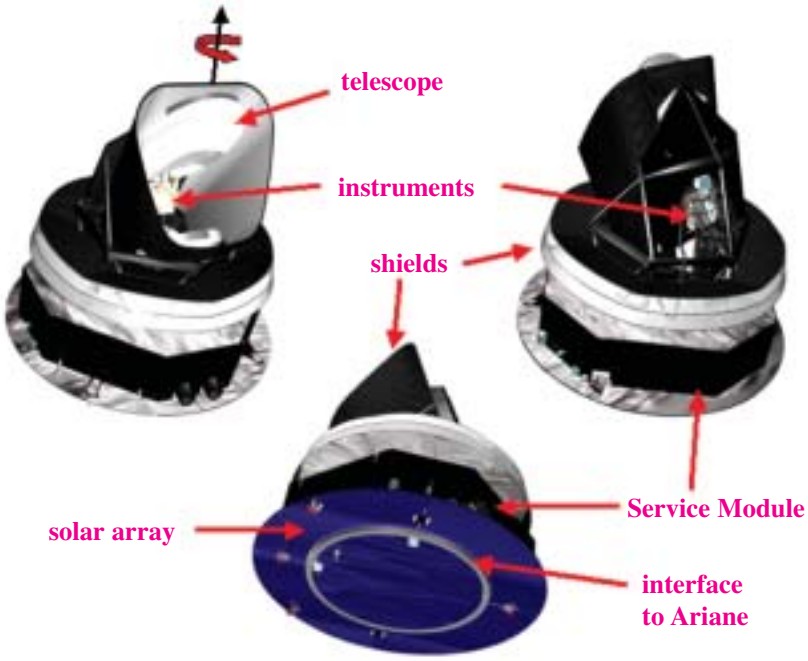


**Figure 4.2.1 (left). The main elements of the Planck satellite.**
**Figure 4.2.2 (right). The Qualification Model ready to be integrated into the cryogenic facility at the Centre Spatial de Liège. This model does not include telescope reflectors.**

of observing time. The spacecraft will be spin-stabilised at 1 rpm. The viewing direction of the telescope will be offset by 85° from the spin axis, so that the observed sky patch will trace a large circle on the sky.

Planck is a survey-type project, developed and operated as a PI mission. The payload will be provided by two PI teams, who will also man and operate two Data Processing Centres, which will process and monitor the data during operations, and reduce the final data set into the science products of the mission. All-sky maps in the nine frequency bands will be made publicly available 1 year after completion of the mission, as well as a first-generation set of maps of the CBRF, Sunyaev-Zeldovich effect and dust, free-free and synchrotron emission. The time-series of observations (after calibration and position reconstruction) will also eventually be made available as an on-line archive.

## Status

Planck was selected in late 1996 as the third Medium Mission (M3) of ESA's Horizon 2000 Scientific Programme, and is now part of its Cosmic Vision Programme. At the time of its selection, Planck was called COBRAS/SAMBA; after the mission was approved, it was renamed in honor of the German scientist Max Planck (1858–1947), winner of the Nobel Prize for Physics in 1918. Planck will be launched together with the Herschel far-IR and sub-mm observatory.

Starting in 1993, a number of technical studies laid the basis for the issue in September 2000 of an Invitation to Tender to European industry for the procurement of the Herschel and Planck spacecraft. From the submitted proposals, a single prime contractor, Alcatel Space (F), was selected in early 2001 to develop both spacecraft. Alcatel Space is supported by two major subcontractors: Alenia Spazio (Torino, I) for the Service Module, and Astrium GmbH (Friedrichshafen, D) for the Herschel Payload Module; and by many other industrial subcontractors from all ESA member states. The detailed definition work began in June 2001.

**Table 4.2.1. Planck instrument performance goals.**

| | | | | | | | | | | |
|---|---|---|---|---|---|---|---|---|---|---|
| Telescope | 1.5 m (projected aperture) offset; shared focal plane; system emissivity ~1%<br>Viewing direction offset 85° from spin axis; field of view 8° | | | | | | | | | |
| Instrument | LFI | | | HFI | | | | | | |
| Centre Frequency (GHz) | 30 | 44 | 70 | 100 | 143 | 217 | 353 | 545 | 857 | |
| Detector Technology | HEMT LNA arrays | | | Bolometer arrays | | | | | | |
| Detector Temperature | ~20K | | | 0.1K | | | | | | |
| Cooling Requirements | $H_2$ sorption cooler | | | $H_2$ sorption + 4K J-T stage + Dilution cooler | | | | | | |
| Number of Detectors | 4 | 6 | 12 | 8 | 12 | 12 | 12 | 4 | 4 | |
| Bandwidth (GHz) | 6 | 8.8 | 14 | 33 | 47 | 72 | 116 | 180 | 283 | |
| Angular Resolution (FWHM arcmin) | 33 | 24 | 14 | 9.5 | 7.1 | 5 | 5 | 5 | 5 | |
| Average ΔT/T per pixel (14 months, 1σ, $10^{-6}$ units) | 2.0 | 2.7 | 4.7 | 2.5 | 2.2 | 4.8 | 14.7 | 147 | 6700 | |
| Average ΔT/T (polarisation) per pixel (14 months, 1σ, $10^{-6}$ units) | 2.8 | 3.9 | 6.7 | 4.0 | 4.2 | 9.8 | 29.8 | | | |

During 2003–2005, industry concentrated on qualifying the satellite design. This phase culminated in major environmental tests on purpose-built qualification models, including a full thermal-vacuum test in a specially constructed chamber at the Centre Spatial de Liège (B); Fig. 4.2.2 shows the qualification model used in this test. This successful test validated the passive thermal behaviour of the satellite and of most of the active cryogenic cooler chain. These two aspects were considered among the most critical in the satellite design.

As of early 2006, most of the flight hardware has been manufactured and assembled. The complete flight satellite will undergo a flight-representative end-to-end test in early 2007.

In early 1999, ESA selected two Consortia of scientific institutes to provide the two Planck instruments: the Low Frequency Instrument (LFI) by a consortium led by R. Mandolesi of the Istituto di Astrofisica Spaziale e Fisica Cosmica (CNR) in Bologna (I); the High Frequency Instrument (HFI) by a consortium led by J.-L. Puget of the Institut d'Astrophysique Spatiale (CNRS) in Orsay (F). More than 40 European institutes, and some from the USA, are collaborating on the development, testing and operation of these instruments, as well as the ensuing data analysis and exploitation. The capabilities of the instruments are described in Table 4.2.1.

In the last 2 years, the instrument development has advanced in parallel with that of the satellite. Qualification programmes were completed in 2005, with tests of complete qualification models. The HFI qualification model was integrated into the

satellite-level qualification model, with which it was submitted to a complete (and successful) series of end-to-end tests. The flight models have been assembled, with test and calibration campaigns beginning in early 2006. The instruments will be delivered to ESA by mid-2006, to be integrated into the flight-model satellite.

In early 2000, ESA and the Danish Space Research Institute (DSRI, Copenhagen) signed an Agreement for the provision of the two reflectors that constitute the Planck telescope. DSRI leads a consortium of Danish institutes, and together with ESA subcontracted the development to Astrium GmbH (Friedrichshafen), who manufactured the reflectors using state-of-the-art carbon fibre technology. They have been subjected to a complete qualification programme, including characterisation of the surface accuracy at cryogenic temperatures. The flight models are now undergoing a similar suite of characterisation tests, both at reflector and at assembled telescope level.

In addition, the reflectors used for qualification have been assembled into a telescope model that will be characterised at radio frequencies of 30–320 GHz, in order to validate the mathematical models that will generate detailed predictions of the optical behaviour of Planck in flight. This is critical to the scientific return of the mission.

The development of the Planck ground segment is developing at a similar pace to the flight segment. The first series of Integration Tests is expected to take place in the second half of 2006. In parallel, detailed planning is taking place to carry out end-to-end tests of the scientific pipelines within each of the two Data Processing Centres, starting in the summer of 2006.

The launch date is driven by many factors that have been evolving over the last 2 years. Currently, it is not expected to launch Planck before the end of February 2008.

A detailed and updated version of the scientific case for Planck can be downloaded from *http://www.rssd.esa.int/Planck*

# 4.3 LISA Pathfinder

## Introduction

LISA Pathfinder (formerly known as SMART-2, the second of the ESA Small Missions for Advanced Research in Technology), is a dedicated technology demonstrator for the joint ESA/NASA Laser Interferometer Space Antenna (LISA) mission. The technologies required for LISA are many and extremely challenging. Coupled with the fact that some flight hardware cannot be tested on the ground because of the Earth-induced noise, this led to the LISA Pathfinder (LPF) mission being implemented to test the critical LISA technologies in a flight environment. The scientific objective of the LISA Pathfinder mission consists then of the first in-flight test of gravitational-wave detection metrology.

LPF carries two payloads, the European-provided LISA Technology Package (LTP) and the NASA-provided Disturbance Reduction System Precision Flight Control Validation (DRS PCFV), formerly known as the DRS.

## Mission goals

The mission goals of the LTP are:

- to demonstrate that a test-mass can be put in pure gravitational free-fall within one order of magnitude of the requirement for LISA. The one order of magnitude rule applies also to frequency. Thus the flight test is considered satisfactory if free-fall of one test-mass is demonstrated to within $3\times10^{-14}$ ms$^{-2}/\sqrt{\text{Hz}}$ 1 mHz, rising as $f^2$ between 3 mHz and 30 mHz;
- to demonstrate laser interferometry with a free-falling mirror (LTP test-mass) with displacement sensitivity meeting the LISA requirements over the LTP measurement bandwidth. Thus the flight test of LTP is considered satisfactory if the laser metrology resolution is demonstrated to within $9\times10^{-12}$ m/$\sqrt{\text{Hz}}$ between 3 mHz and 30 mHz, rising as $1/f^2$ down to 1 mHz;
- to assess the lifetime and reliability of the $\mu$N thrusters, lasers and optics in a space environment.

## LISA Technology Package

The basic idea behind the LTP is to reduce the size of one arm of LISA from $5\times10^6$ km to a few cm and place it onboard a single spacecraft. The key elements are two nominally free-flying test-masses and a laser interferometer to read the distance between the TMs (Fig. 4.3.1).

The two test-masses are surrounded by position-sensing electrodes. These provide the information to a drag-free control loop that, via a series of $\mu$N thrusters, keeps the spacecraft centred with respect to some fiducial point.

In LISA, as in LPF, each spacecraft hosts two test-masses; they belong to different interferometer arms, however. This has an important consequence for the spacecraft control logic. The baseline for LISA foresees a control logic whereby the spacecraft is simultaneously centred on both test-masses. The spacecraft follows each test-mass only along the axis defined by the incoming laser beam, however; the remaining axes have to be controlled by a capacitive suspension (or by some other controlled actuation scheme). On LPF, in order to be able to measure differential acceleration, the sensitive axes of the two test-masses have to be aligned. This requires the development of a capacitive suspension scheme that carries one or both test-masses along with the spacecraft (including along the measurement axis), while ensuring the meaningfulness of the test.

In LISA, the proper distance between the two free-falling test-masses at the end of the interferometer arms is measured via a three step process: by measuring the distance between one test-mass and the optical bench (known as the local

*For further information, see http://sci.esa.int/lisa*

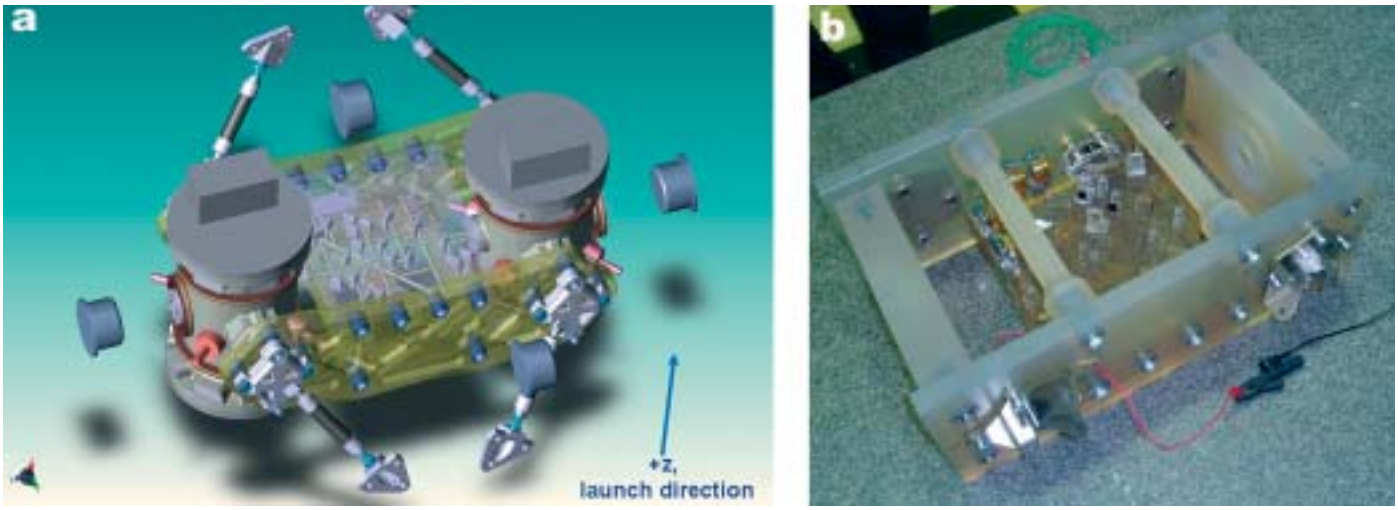


**Figure 4.3.1. Left: drawing of the LISA Technology Package, showing the two vacuum enclosures housing the test masses, and the optical bench interferometer (OBI). Right: the OBI Engineering Model, with the vacuum enclosures replaced by end plates.**

measurement), by measuring the distance between optical benches (separated by 5 million km), and finally by measuring the distance between the other test-mass and its optical bench. In LPF, the optical metrology system essentially makes two measurements: the separation of the test masses, and the position of one test-mass with respect to the optical bench. The latter is identical to the LISA local measurement interferometer, thereby providing a flight demonstration of precision laser metrology directly applicable to LISA.

In both LISA and LPF, charging by cosmic rays is a major source of disturbance. Each test-mass therefore carries a non-contacting charge measurement and neutralisation system based on UV photoelectron extraction. A flight test of this device is a key element of the overall LPF test.

## DRS-PCFV

The DRS-PCFV is a NASA-provided payload. When proposed, the DRS payload closely resembled the LTP, in that it consisted of two inertial sensors with associated interferometric readout, as well as the drag-free control laws and $\mu$N colloidal thrusters. The technologies employed were different from the LTP, however. Owing to budgetary constraints, the DRS was descoped, and now consists of the $\mu$N colloidal thrusters, drag-free and attitude control system (DFACS), and a micro-processor. The DRS-PCFV will now use the LTP inertial sensors as its drag-free sensors.

The primary goal of the DRS-PCFV is to maintain the position of the spacecraft with respect to the proof mass to within 10 nm/$\sqrt{\text{Hz}}$ over the frequency range of 1–30 mHz.

## Launch & orbit

LISA Pathfinder is due to be launched in October 2009 on a dedicated launcher. Rockot is the baseline vehicle, although Vega is the target vehicle that will be used if available. The spacecraft and propulsion module (Fig. 4.3.2) are injected into LEO (200 x 900 km), from which, after a series of apogee-raising burns, they enter a transfer orbit towards the first Sun-Earth Lagrange point (L1). After separation from the propulsion module, the LISA Pathfinder spacecraft is stabilised using the $\mu$N, entering a Lissajous orbit around L1 (500 000 x 800 000 km).

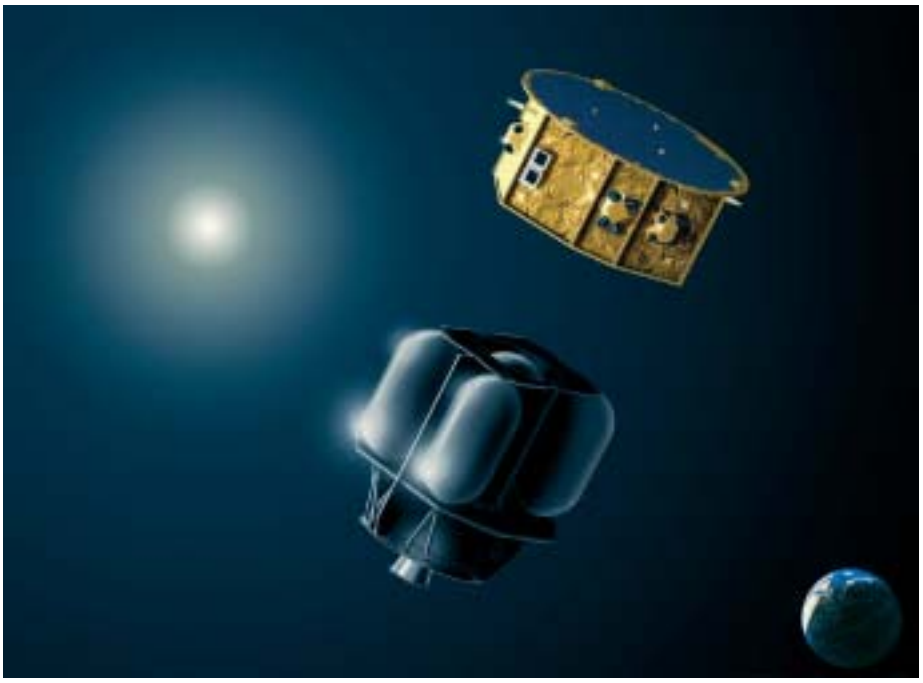

**Figure 4.3.2. LISA Pathfinder separating from its propulsion module. (Astrium Ltd)**

Following the initial checkout and instrument calibration, the flight demonstration of the LISA technology will take place in the first half of 2010. The nominal lifetime of the mission is 180 days, and includes LTP operations, DRS operations and a period of joint operations when the LTP will control the DRS thrusters.

## Status

LISA Pathfinder is in its Implementation Phase. The contract with the prime industrial contractor, Astrium UK, was signed in May 2004. During the last year, all ITTs for spacecraft subcontractors have been issued. In October 2004, SPC approved the LTP Multi-Lateral Agreement, detailing the national agency responsibilities for the construction of the LTP. All subcontracts for the LTP are under way. The project has completed a number of significant Agency-level reviews over the last 2 years, including the Systems Requirements Review, Technology Readiness Review, the LTP Preliminary Design Review, System Preliminary Design Review, and the Mission Preliminary Design Review. In addition, all the LTP subsystems have undergone PDR within the last year. The first LTP subsystem flight hardware is due to be delivered to the LTP Architect (Astrium GmbH) during the third quarter 2006.

With the deletion of the gravitational reference sensor from the DRS, it was recommended that the DRS undergo a joint ESA/NASA delta-Critical Design Review Risk Review. This was completed in January 2006.

# 4.4 Gaia

## Introduction

After a detailed concept and technology study during 1998-2000, Gaia was selected as a confirmed mission within ESA's scientific programme in October 2000, with a launch date of 'not later than 2012'. It was confirmed by ESA's Science Programme Committee following a re-evaluation of the science programme in June 2002, and reconfirmed following another re-evaluation of the programme in November 2003. The project entered Phase-B2/C/D in February 2006. A launch date of mid-2011 is currently targeted.

## Scientific goals

Gaia will rely on the proven principles of ESA's Hipparcos mission to solve one of the most difficult yet deeply fundamental challenges in modern astronomy: to create an extraordinarily precise 3-D map of about a billion stars throughout our Galaxy and beyond. In the process, it will map their motions, which encode the origin and subsequent evolution of the Galaxy. Through comprehensive photometric classification, it will provide the detailed physical properties of each star observed: characterising their luminosity, temperature, gravity and elemental composition. This massive stellar census will provide the basic observational data to tackle an enormous range of important problems related to the origin, structure and evolutionary history of our Galaxy – a kind of 'Humane Genome Project' for astronomy.

Gaia will achieve this by repeatedly measuring the positions of all objects down to V = 20 mag. Onboard object detection will ensure that variable stars, supernovae, burst sources, micro-lensed events and minor planets will all be detected and catalogued to this faint limit. Final accuracies of 12-25 $\mu$arcsec at 15 mag, comparable to the diameter of a human hair at a distance of 1000 km, will provide distances accurate to 10% as far as the Galactic Centre, 30 000 light years away. Stellar motions will be measured even in the Andromeda Galaxy.

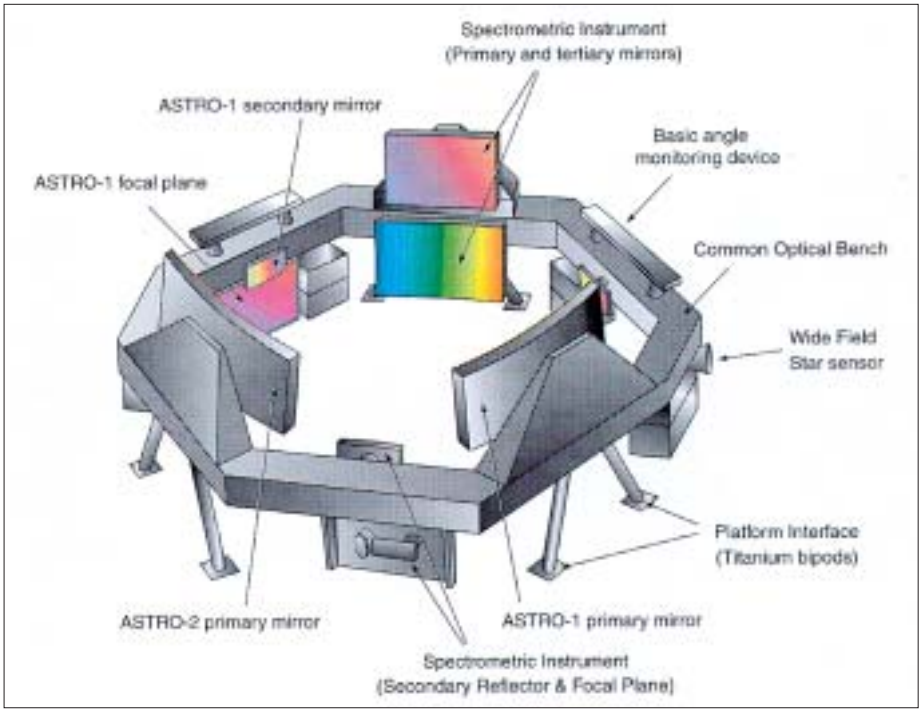


**Figure 4.4.1. The Gaia payload comprises two astrometric viewing directions, and the radial velocity/spectroscopic instrument, suspended on a common stable platform. The instrument scans the sky by spinning about an axis perpendicular to the supporting ring structure. The actual design will differ in detail somewhat according to the selection of the industrial prime contractor.**

*For further information, see http://www.rssd.esa.int/Gaia*

**Table 4.4.1. Gaia vs. Hipparcos capabilities.**

| | *Hipparcos* | *GAIA* |
|---|---|---|
| Magnitude limit | 12 | 20 mag |
| Completeness | 7.3 - 9.0 | ~20 mag |
| Bright limit | ~ 0 | ~3-7 mag |
| Number of objects | 120 000 | 26 million to V = 15 |
| | | 250 million to V = 18 |
| | | 1000 million to V = 20 |
| Effective distance limit | 1 kpc | 1 Mpc |
| Quasars | none | ~500 000 |
| Galaxies | none | $10^6$ - $10^7$ |
| Accuracy | ~1 milliarcsec | 7 $\mu$arcsec at V = 10 |
| | | 12-25 $\mu$arcsec at V = 15 |
| | | 100-300 $\mu$arcsec at V = 20 |
| Broadband photometry | 2-colour | 4-colour to V = 20 |
| Medium band photometry | none | 11-colour to V = 20 |
| Radial velocity | none | 1-10 km/s to V = 16-17 |
| Observing programme | pre-selected | onboard and unbiased |

Gaia's expected scientific harvest is of almost inconceivable extent and implication. Its main goal is to clarify the origin and history of our Galaxy, by providing tests of the various formation theories, and of star formation and evolution. This is possible because low-mass stars live for much longer than the present age of the Universe, and therefore retain in their atmospheres a fossil record of their detailed origin. The Gaia results will precisely identify relics of tidally-disrupted accretion debris, probe the distribution of dark matter, establish the luminosity function for pre-main sequence stars, detect and categorise rapid evolutionary stellar phases, place unprecedented constraints on the age, internal structure and evolution of all stellar types, establish a rigorous distance-scale framework throughout the Galaxy and beyond, and classify star-formation and kinematical and dynamical behaviour within the Local Group of galaxies.

Gaia will pinpoint exotic objects in colossal and almost unimaginable numbers: many thousands of extrasolar planets will be discovered, and their detailed orbits and masses determined; tens of thousands of brown dwarfs and white dwarfs will be identified; some 100 000 extragalactic supernovae will be discovered and details passed to ground-based observers for follow-up observations; Solar System studies will receive a massive impetus through the detection of many tens of thousands of new minor planets; inner Trojans and even new trans-Neptunian objects, including Plutinos, may be discovered. Gaia will follow the bending of starlight by the Sun and major planets, over the entire celestial sphere, and therefore directly observe the structure of space-time (the accuracy of its measurement of General Relativistic light bending may reveal the long-sought scalar correction to its tensor form). The PPN parameters gamma and beta will be determined with unprecedented precision.

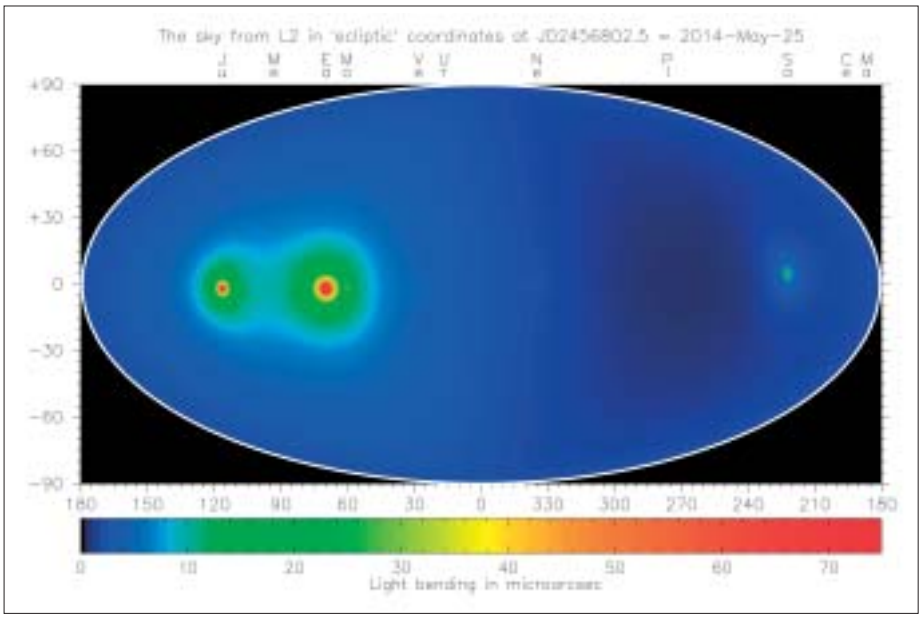


**Figure 4.4.2. The amplitude of the relativistic light bending terms due to the presence of the various Solar System objects, as seen by Gaia from its L2 orbit. The sky is shown in ecliptic coordinates, and the dominant effect of the Sun's gravitational field has been suppressed. At the epoch simulated (May 2014), the effects of Jupiter, the Earth, Moon and Saturn can be clearly seen. All planets as well as other Solar System objects, including the four Galilean moons of Jupiter, and the most massive minor planets, will have a measurable effect on the Gaia observations. (Courtesy J. de Bruijne).**

## The spacecraft

Gaia will carry the demonstrated Hipparcos principles into orders of magnitude improvement in terms of accuracy, number of objects, and limiting magnitude, by combining them with state-of-the-art technology. It will be a continuously scanning spacecraft, accurately measuring 1-D coordinates along great circles, and in two simultaneous fields of view, separated by a well-defined and well-known angle. These 1-D coordinates are then converted into the astrometric parameters in a global data analysis, in which distances and proper motions 'fall out' of the processing, as does information on double and multiple systems, photometry, variability, metric, planetary systems, etc. The payload is based on a large CCD focal plane assembly, with passive thermal control, and natural short-term (3 h) instrument stability arising from the sunshield, selected orbit and robust payload design.

The telescopes are of moderate size (1.45x0.5 m) manufactured from SiC, with no specific design or manufacturing complexity. The system fits within a Soyuz-Fregat launch configuration, without deployment of any payload elements (moving from an Ariane to a Soyuz launch was one of the results of the 2002 redesign effort). A Lissajous orbit at L2 is the adopted operational orbit, from where about 1 Mbit/s of data is returned to the single ground station throughout the 5-year mission. The final astrometric accuracies are evaluated through a comprehensive accuracy assessment programme; $\mu$arcsec accuracies are possible partly by virtue of the (unusual) instrumental self-calibration achieved through the data analysis on-ground. This ensures that final accuracies essentially reflect the photon noise limit for localisation accuracy, exactly as achieved with Hipparcos.

One of the objectives of the Concept and Technology Study completed in 2000 was to identify the areas of technology where further development was required before moving into Phase-B2, starting in early 2006. About 15 well-identified key technology areas were identified, including the CCD/focal plane development, silicon carbide mirrors, onboard data handling, and antenna design. All of these activities are now underway, and should lead to full confidence in the required technology by the end of 2004. Noteworthy progress in 2003 was the detailed design review of the

primary mirror, leading to the start of the manufacturing of a prototype SiC primary mirror in early 2004. Detailed design of the focal plane assembly is proceeding intensively, with the first custom-made Gaia CCDs being manufactured by e2v in late 2003.

## Scientific organisation and progress

During 2001, a scientific organisation structure was put in place for the period until the start of Phase-B2. About 280 European scientists participated in various preparatory aspects of Gaia, ranging from the instrument design, through to the data processing, the treatment of specific objects (such as variable and multiple stars), and the optimisation of the photometric and radial velocity instruments. A group of about 12 scientists forms the Gaia Science Team, charged with advising ESA on all aspects of the scientific development and conduct of Gaia, and chaired by the ESA Project Scientist.

About 16 working groups, under the direction of leaders and coordinated by the science team, were responsible for the study and development of the various scientific aspects of the mission. Considerable progress was made in many areas during the last 2 years. One very challenging task was the completed design of the photometric system capable of classifying and physically characterising the billion objects observed: for example, determining their temperatures, surface gravity, reddening and metallicity. One working group was charged with the optimisation and development of the radial velocity instrument, where the challenge was to establish the characteristics of an instrument optimally designed to determine radial velocities for as many objects as possible (down to 17-18 mag), and to derive spectral characteristics at the same time. The relativity working group has defined the principles underlying the derivation of a reference system deeply affected by gravitational light bending where, for example, effects due to the Sun, Jupiter, the other planets and even the more massive minor planets, will be observable at the microarcsec level. One group assessed the observability and detectability of Solar System objects, including Near-Earth Objects; another assessed the detectability of transient events such as microlensing, supernova and gamma ray bursts.

A key activity where much early effort was devoted was to establish the feasibility of the Gaia data analysis procedure. The task is large and daunting: over its 5-year mission, Gaia will deliver some 100 TByte of data, and will require processing power of order $10^{20}$–$10^{21}$ floating point operations. Given that the data are effectively 'tangled' in time and position on the sphere, the data analysis problem is extremely challenging, even taking realistic assumptions about data processing capabilities extrapolated 5–10 years into the future. A prototype system has been set up, which is capable of ingesting a realistic but simplified telemetry stream, detecting and matching up observations of the same objects observed days, weeks or months apart, and subjecting them to an iterative adjustment in which the stellar parameters, satellite attitude and calibration parameters are estimated. A prototype operating with 1 million simulated objects was successfully run in 2005.

During 2005, an ESA announcement for Letters of Intent to participate in the Gaia data processing was issued. Based on the results, a Data Analysis Coordination Committee has been working during late 2005 and early 2006 to put together a structure of the Gaia Data Processing and Analysis Consortium.

In early 2006 the project entered Phase-B2 with the selection of the chosen industrial prime contractor, progress in the formation of the data processing consortium will continue, and large-scale simulations of the data processing will commence.

# 4.5 JWST

## Introduction

NASA, ESA and the Canadian Space Agency (CSA) have since 1996 collaborated on the definition of a successor to the Hubble Space Telescope (HST). Known initially as the Next Generation Space Telescope (NGST), in 2002 the project was renamed the James Webb Space Telescope (JWST) in honour of NASA's second Administrator, who led the agency during the Apollo programme.

The JWST observatory consists of a passively cooled, 6.55 m-aperture telescope, optimised for diffraction-limited performance in the near-IR (1-5 $\mu$m) region, but with extensions to either side into the visible (0.6-1 $\mu$m) and mid-IR (5-28 $\mu$m) regions. The large aperture and shift to the IR embodied by JWST is first and foremost driven scientifically by the desire to follow the contents of the faint extragalactic Universe back in time and redshift to the epoch of 'First Light' and the ignition of the very first stars. Nonetheless, like its predecessor, JWST will be a general-purpose observatory and carry a suite of astronomical instruments capable of addressing a very broad spectrum of outstanding problems in galactic and extragalactic astronomy. In contrast to HST, however, JWST will be placed into a Sun-Earth L2 halo orbit and will not be serviceable after launch.

## Science

The scientific goals of the JWST mission can be sorted into four broad themes:

— First Light (after the Big Bang);
— Assembly of galaxies;
— Birth of stars and proto-planetary systems;
— Planetary systems and the origins of life.

The first two themes are extragalactic and concerned with exploring the formation of stars and galaxies in the remote Universe at the earliest times. They are nonetheless

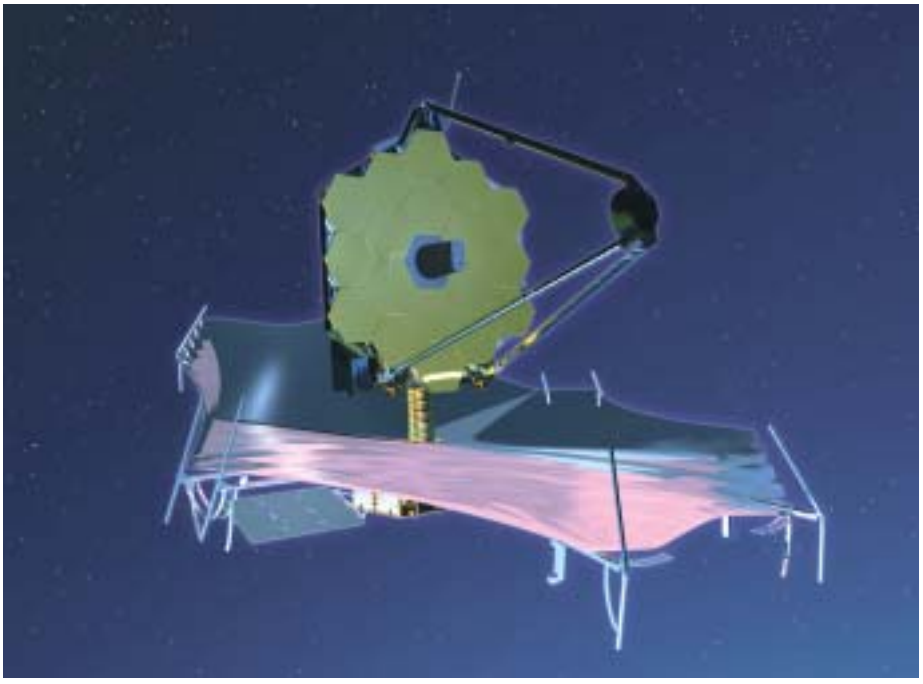

**Figure 4.5.1. JWST observatory in orbit, showing the deployed 6.55 m-diameter telescope and the large sunshade (Northrop Grumman/Ball).**

*For further information, see http://sci.esa.int/jwst*

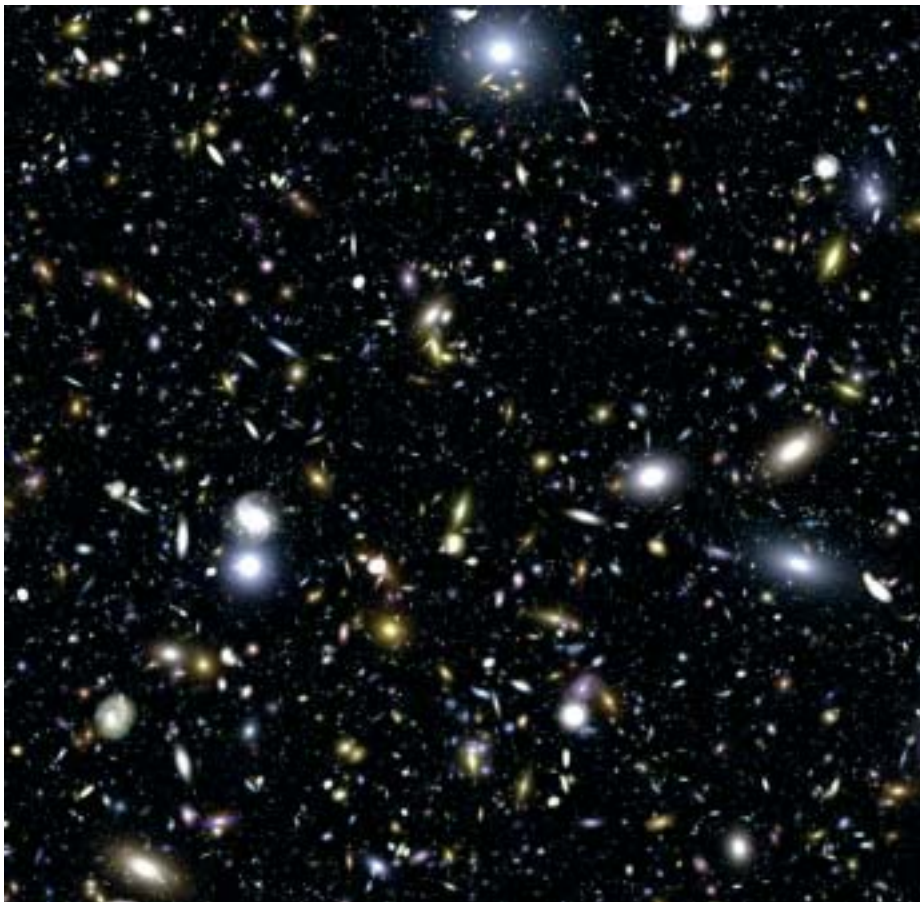

**Figure 4.5.2. Simulated deep JWST image. (STScI)**

intimately linked to the latter two, mainly galactic, themes, which aim at understanding the detailed process of star- and planet-formation in our own Galaxy.

ESA's participation in JWST was initially approved by the Science Programme Committee in November 2000 at the level of a Flexi-mission. This level will secure ESA a 15% partnership as well as a continuation of its present participation in HST to the end of that observatory's operational life.

In 2002, NASA selected Northrop Grumman Space Technology as the prime contractor for the observatory. The JWST project is entering its final design phase. Launch is currently scheduled for 2013.

JWST will carry four main instruments:

— NIRCam: a wide-field (2.2 x 4.4 arcmin) near-IR camera covering wavelengths 0.6-5$\mu$m;
— NIRSpec: a wide-field (3.5 x 3.5 arcmin) multi-object near-IR spectrometer covering wavelengths 0.6-5 $\mu$m at spectral resolutions of $R$~100, $R$~1000 and $R$~7000;
— MIRI: a combined mid-IR camera (1.4 x 1.9 arcmin) and spectrograph ($R$~3000) covering wavelengths 5-27 $\mu$m;
— FGS/TF: a fine guidance camera that includes a near-IR tunable filter imaging capability (2.3 x 2.3 arcmin; $R$~100).

The JWST telescope proper and its associated instruments will be cooled in bulk to 35–40K, a temperature range determined by the operating temperature of the HgCdTe detector arrays employed by NIRCam, NIRSpec and FGS. Cooling is to be attained passively by placing the observatory at L2 and keeping the telescope and its instrumentation in perpetual shadow under a large deployable sunshade. The telescope is made up of 18 hexagonal segments, and is specified to yield diffraction-limited performance at wavelengths above 2 $\mu$m in the near-IR. In order to fit into the fairing of the Ariane-5 launcher, the 6.55 m primary mirror needs to be folded and deployed along with the secondary mirror in orbit. Fine pointing will be achieved by deflecting the beam by means of a fast steering mirror controlled by the FGS (to be provided by Canada) located in the telescope focal plane.

The 0.6 $\mu$m visible wavelength limit allows the use of gold as the reflecting coating in the telescope and instruments. For reasons of cost, diffraction-limited performance will not be obtained at wavelengths in the region of overlap with HST below 2 $\mu$m. Nonetheless, depending on the character of the residual aberrations, the image quality is expected to match that of HST (which is less than half the size) in terms of resolving power.

The performance at longer wavelengths in the mid-IR is a slightly more complex story. The primary sources of stray light in the mid-IR are thermal radiation emitted by the backside of the sunshield and scattered off the largely unbaffled telescope, and thermal emission from the telescope structure. Provided the temperature of the sunshield can be kept below ~110K and the dust contamination of the JWST optics can be kept sufficiently low, the intensity of this stray light contribution can be kept below that of the zodiacal light at wavelengths shorter than ~10 $\mu$m. The JWST specifications are designed to assure such sky-limited performance throughout the core 1-5 $\mu$m region and out to at least 10 $\mu$m.

The telescope will be fully diffraction-limited throughout the mid-IR. However, the candidate Si:As detector arrays needed to reach wavelengths beyond 5 $\mu$m require an operating temperature of ~7K, which is significantly below the ~30-50K ambient environment of the telescope and instrument module. Active cooling by means of a mechanical cryocooler is therefore called for as part of the mid-IR instrument.

Although observations beyond 10 $\mu$m will not be sky-limited and subject to thermal self-emission from the observatory, the sheer size and location of the telescope assures that its performance will be vastly superior to anything that can be done from the ground at these wavelengths. The extreme long wavelength cut-off of JWST is expected to fall just shortward of ~28 $\mu$m, a limit dictated by the sensitivity cut-off of the baseline Si:As detectors.

The components of Europe's contributions to JWST were approved by the SPC in February 2003. The level of participation closely follows the HST model, and consists of three main elements: scientific instrumentation, non-instrument flight hardware and contributions to operations.

ESA will provide NIRSpec and, through special contributions from its member states, the optics module of MIRI (be developed jointly with NASA). These instruments are undergoing their final designs.

As its non-instrument contribution, ESA will provide the Ariane-5 ECA launcher that will place the observatory in an orbit around the anti-Sun Earth-Sun Lagrangian point, L2.

Responsibility for scientific operation of JWST lies with the Space Telescope Science Institute (STScI) in Baltimore, working under contract to NASA. A yet-to-be negotiated number of ESA staff will be posted at STScI in support of the European payload components. The observing programme will be determined by the

astronomical community on the basis of periodic competitive peer reviews organised by the STScI. The overriding motivation for ESA's partnership in the mission is to secure full access for member-state scientists to compete for time on JWST on an equal footing with their US and Canadian counterparts.

# 4.6 BepiColombo

## Introduction

BepiColombo is the planetary Cornerstone of ESA's Cosmic Vision Programme, and is devoted to the thorough exploration of Mercury and its environment. It will be carried out as a joint project between ESA and the Japanese Aerospace Exploration Agency (JAXA). The mission consists of two orbiters, the Mercury Planetary Orbiter (MPO), which is 3-axis-stabilised and nadir pointing, and the Mercury Magnetospheric Orbiter (MMO), a spinning spacecraft. ESA is responsible for the overall BepiColombo mission design, including launcher, spacecraft composite, propulsion modules, ground segment and the delivery of both spacecraft into their dedicated orbits, as well as for the MPO and its operations. JAXA is responsible for the procurement of the MMO and for its mission and science operation at Mercury. The mission scenario foresees a launch of both spacecraft on a single Soyuz-Fregat 2-1B in August 2013 and an arrival at Mercury in August 2019. The 6-year cruise phase is achieved using a combination of seven flybys (Moon, 2 Venus, 4 Mercury) and electric propulsion. The launch configuration is a stack consisting of the two spacecraft and the chemical and electrical propulsion modules. The MPO will carry the MMO during launch and cruise. Mercury orbit capture and the subsequent lowering to the operational orbits will be done with chemical propulsion. Both orbits are elliptical, with eccentricity and inclination optimised for the study of Mercury (MPO orbit: 400 x 1500 km) and its magnetosphere (MMO orbit: 400 x 12 000 km). Being as close as 0.3 AU to the Sun, the spacecraft have to withstand extremely high temperatures and radiation doses, which necessitates the inclusion of radiators and extensive shielding in their design. The MPO employs lightweight technologies and materials able to cope with the aggressive thermal environment at Mercury. The current baseline is for 1 Earth-year of science operations in Mercury orbit, with the possibility to extend the mission for another year.

## Scientific objectives

With its two-spacecraft, interdisciplinary approach, the BepiColombo mission will provide the detailed information necessary to understand the process of planetary formation and evolution in the hottest part of the proto-planetary nebula, as well as the similarities and differences between the magnetospheres of Mercury and Earth. To accomplish this, a global characterisation of Mercury is required, which can be achieved through the investigation of its interior, surface, exosphere and magnetosphere. In addition, the mission offers unique possibilities for testing Einstein's theory of general relativity. The mission's scientific objectives are:

- origin and evolution of a planet close to its parent star;
- Mercury's figure, interior structure and composition;
- interior dynamics and origin of its magnetic field;
- exogenic and endogenic surface modifications, cratering, tectonics, volcanism;
- composition, origin and dynamics of Mercury's exosphere and polar deposits;
- structure and dynamics of Mercury's magnetosphere;
- test of Einstein's theory of general relativity.

The MPO will perform a global mapping of the surface morphology, composition and temperature of Mercury, study its extremely thin atmosphere (exosphere) and investigate its interior structure and magnetic field. Initially, the onboard cameras will provide a global mapping of the surface morphology at a spatial scale of 100 m, and then image areas of specific interest with spatial resolutions better than 5 m. The near-IR and thermal-IR spectrometers will obtain the global mineralogical surface composition with a spatial resolution of 500 m, comparable to the regolith mixing

*For further information, see http://sci.esa.int/bepicolombo*

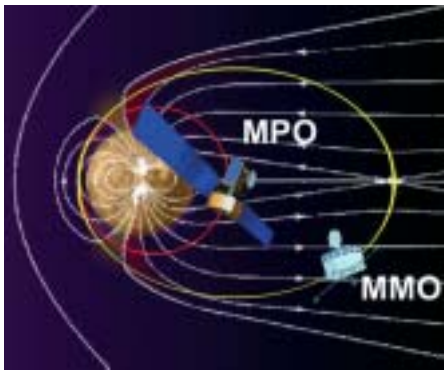


**Figure 4.6.1. MPO and MMO in orbit around Mercury.**

length. The X-ray spectrometer will provide a global mapping of the elemental surface composition at a scale of about 50 km. During higher solar activity, a spatial resolution of up to 500 m will be achieved. The combination of these five instruments allows the morphological and compositional characterisation of individual surface features, and hence the identification of compositional variations. Knowledge of the surface composition will provide a key test of competing models for the formation and evolution of Mercury and all the terrestrial planets. Elements not accessible through X-ray spectroscopy, as well as the subsurface elemental composition, will be measured by the gamma-ray-neutron spectrometer, albeit at lower spatial resolution. In addition, the neutron spectrometer will take measurements of the radar-bright spots observed from ground in the polar regions to identify their composition.

Mercury's interior will be investigated by the radio science experiment in combination with the laser altimeter and the high-resolution camera. Together, these instruments will provide an accurate determination of the global gravity field and the rotational state of the planet, as well as the amplitude of the physical libration. These parameters place constraints on its internal structure. The question of whether the solid crust of the planet is decoupled from the inner core by some liquid layer will also be addressed using the magnetic field measurements.

The exosphere will be studied using remote-sensing spectrometers in the visible and UV to provide large-scale measurements of its composition, vertical structure and dynamics. In addition, the neutral and ion particle analyser will perform an *in situ* analysis of the exosphere and its interactions with the surface and the magnetosphere to understand the surface release processes and the source/sink balance.

The MMO will focus on the investigation of the magnetic field, waves and particles in the environment of Mercury, which will result in a complete characterisation of the planet's magnetosphere. It will also provide information on the exosphere to complement the MPO investigations and determine the interplanetary dust environment around Mercury.

Simultaneous measurements by the two spacecraft will resolve spatial and temporal ambiguities in the exosphere and magnetosphere that would arise from single-point observations. For instance, parallel measurements of the magnetic flux by the magnetometers on both spacecraft will enable the separation of the contributions from the magnetosphere and the planetary magnetic field.

In summary, BepiColombo will perform a complete, in-depth exploration of Mercury and its magnetospheric environment.

## Status

The mission definition has been completed and the scientific payload of both spacecraft (Table 4.6.1) has been selected. The MPO payload comprises 11 instruments/instrument packages; the MMO payload consists of 5 instruments/instrument packages.

**Table 4.6.1. BepiColombo scientific instruments.**

| | *Instrument* | | *Measurements* |
|---|---|---|---|
| **MPO** | | | |
| Co-PI: N. Thomas, CH<br>Co-PI: T. Spohn, D | BepiColombo Laser Altimeter | BELA | Topographic mapping |
| PI: V. Iafolla, I | Italian Spring Accelerometer | ISA | Non-gravitational accelerations of MPO |
| PI: K.H. Glassmeier | Magnetic Field Investigation | MERMAG | Detailed description of planetary magnetic field, its source and interaction with the solar wind |
| PI: E.K. Jessberger, D | Mercury Radiometer and Thermal Imaging Spectrometer | MERTIS | Global mineralogical mapping (7-14 $\mu$m), surface temperatures and thermal inertia |
| PI: I. Mitrofanov, RUS | Mercury Gamma-Ray and Neutron Spectrometer | MGNS | Elemental surface and subsurface composition, volatile deposits on polar areas |
| PI: G. Fraser, UK | Mercury Imaging X-ray Spectrometer | MIXS | Elemental surface composition, global mapping and composition of surface features |
| PI: L. Iess, I | Mercury Orbiter Radio Science Experiment | MORE | Core and mantle structure, Mercury orbit, fundamental science, gravity field |
| PI: E. Chassefière, F | Probing of Hermean Exosphere by UV Spectroscopy | PHEBUS | UV spectral mapping of the exosphere |
| PI: S. Orsini, I | Search for Exospheric Refilling and Emitted Natural Abundances | SERENA: Elena, MIPA, PICAM, Strofio | *In situ* study of composition, vertical structure and source and sink processes of the exosphere |
| PI: J. Huovelin, FIN | Solar Intensity X-ray and particle Spectrometer | SIXS | Monitor solar X-ray intensity and solar particles in support of MIXS |
| PI: E. Flamini, I | Spectrometers and Imagers for MPO BepiColombo Integrated Observatory | SIMBIO-SYS: HIRC, STC, VIHI | Optical high resolution and stereo imaging, near-IR (< 2.0 $\mu$m) imaging spectroscopy for global mineralogical mapping |
| **MMO** | | | |
| PI: W. Baumjohann, A | Mercury Magnetometer | MERMAG -M/MGF | Detailed description of magnetosphere and relation and interaction with solar wind and planetary magnetic field |
| PI: Y. Saito, JPN | Mercury Plasma Particle Experiment | MPPE: MEA, MIA, MSA, HEP, ENA | Study of low- and high-energy particles in the magnetosphere |
| PI: H. Matsumoto, JPN | Plasma Wave Instrument | PWI: OFA/ WFC/EFD, SORBET, AM2P, WPANT, MEFISTO, LF-SC, DB-SC | Detailed analysis of the structure and dynamics of the magnetosphere |
| PI: I. Yoshikawa, JPN | Mercury Sodium Atmospheric Spectral Imager | MSASI | Abundance, distribution and dynamics of sodium in the exosphere |
| PI: K. Nogami, JPN | Mercury Dust Monitor | MDM | Distribution of interplanetary dust in Mercury orbit |

# 4.7 Contributions to Nationally-Led Missions

## 4.7.1 COROT

COROT is a small mission for asteroseismology and extrasolar planet-finding funded mainly by CNES, with substantial contributions from the ESA Science Programme, Austria, Belgium, Germany, Italy, Spain, ESA/RSSD and Brazil. COROT is the third mission in the CNES small-mission series based upon the Proteus multi-mission platform, and is due to be launched in October 2006. It is the first attempt to perform accurate asteroseismic observations, as well as to detect rocky planets. Both goals require the accuracy of space-based photometry.

The COROT payload consists of an off-axis afocal parabolic telescope of 27 cm aperture, with a 2.8 x 2.8º FOV. The camera has two separate focal planes, one for asteroseismic observations, the other for planet-finding. The latter includes a dispersive element (a grism) that allows colour-resolved light curves to be obtained. The ESA contribution to the programme includes the telescope optics (comprising an afocal dioptric telescope with two mirrors and a refractive objective assembly) and support to the payload AIV. ESA/RSSD provided the payload Data Processing Unit as part of its internal research activities.

The observing programme includes the detailed asteroseismic study (with very high frequency resolution) of a limited number of bright stars (V = 6–9), the asteroseismic study (with lower accuracy) of some hundred fainter stars, and the search for planets around a much larger number (some 10 000) of fainter stars (V = 11–16.5). In addition, a number of shorter observations (around 1 month in duration) will address a number of different science goals, including stellar rotation and activity, accretion in pre-main sequence stars, and variability in extra-galactic objects.

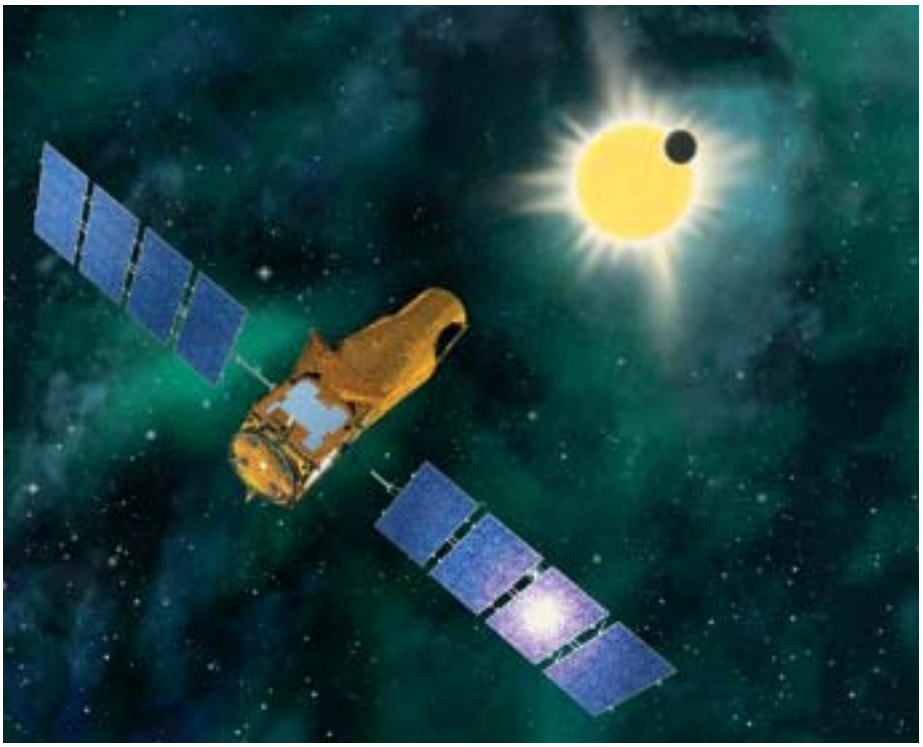

**Figure 4.7.1.1. The COROT spacecraft in orbit, pointed towards a planetary transit.**

*For further information, see http://corot.astrsp-mrs.fr*

ESA's participation in COROT was approved by the SPC in October 2000. In return for the ESA contribution, scientists in ESA member countries have received access to the COROT observing programme and scientific data. This happened first through an open Announcement of Opportunity in 2002 that resulted in the selection of a number of new COROT Co-Is and associated scientists. In 2005, a Call for Proposals for the 'COROT Additional Programmes' was issued that also elicited a strong response from scientists in ESA member states not otherwise contributing to the COROT programme.

## 4.7.2 Microscope

Microscope (MICROSatellite à traînée Compensée pour l'Observation du Principe d'Equivalence) will be the first mission to test the Equivalence Principle (EP) in space. It is aimed at testing the EP to 1 part in $10^{15}$, 2-3 orders of magnitude more precise than is possible with a torsion pendulum on the ground or with lunar-laser ranging. This test is of fundamental importance for our understanding of gravity. A violation of the EP would place severe restrictions on the validity of General Relativity; a confirmation of the EP up to the level of 1 part in $10^{15}$ would provide strong constraints for theories that attempt to unify General Relativity with the other fundamental interactions.

The payload comprises two differential electrostatic accelerometers, one testing a pair of materials A-A (to provide an upper limit for systematic errors), the other testing a pair of materials A-B (the EP test proper). The test masses are freely-floating concentric cylinders of about 500 g each; material A is platinum, material B is titanium. As the satellite orbits the Earth, the Earth's gravity pulls on the test masses. According to the EP, the acceleration felt by A and B should be identical. Because the test masses are constrained to one-dimensional motion, any EP violation signal would be periodic at orbital frequency. The signal is the force that is required to keep the test masses in a pair centred on each other. During flight, the spacecraft rotates about its long axis at a small multiple of the orbital frequency in order to spectrally shift the science signal from orbit-fixed systematic error sources. One major error source for an EP test in space is test-mass charging due to penetrating charged particles (cosmic rays, solar protons, radiation belt particles in particular as the satellite traverses the South Atlantic Anomaly). In the Microscope experiment, the problem of test-mass charging has been eliminated by grounding the test masses through a thin gold wire.

The 3-axis stablised 200 kg satellite is planned for launch in March 2009 on a shared Dnepr rocket into a Sun-synchronous, quasi-circular orbit at about 700 km altitude. The drag by the residual atmosphere at orbital altitude and solar radiation pressure will be compensated by a system of proportional Field Emission Electric Propulsion (FEEP) thrusters. A total of 12 thrusters (four 3-thruster clusters), each with a thrust authority of 150 $\mu$N will be employed. Their noise level must not exceed 0.1 $\mu N/Hz^{1/2}$ at frequencies $> 0.1$ Hz to provide the required drag-free performance of $3x10^{-10}$ m $s^{-2}$ $Hz^{-1/2}$ in the measurement bandwidth. The FEEP thrusters also serve as actuators for fine attitude control. After the nominal mission of up to one year, prolonged lifetime tests with eventually degrading FEEP thrusters are proposed to maximise the in-orbit operational experience with this novel electric propulsion system.

Microscope is a CNES/ESA collaboration: ESA's share is the procurement of the FEEP thrusters. In return, ESA will have full access to all FEEP thruster flight data, which provide a valuable technology test in space for a whole suite of future science missions, in particular LISA and Gaia.

On 24 June, the CNES board of administration decided to proceed with Phase-B, C, D & E.. The Electric Propulsion System (EPS, which includes the FEEP thrusters) passed its Preliminary Design Review (PDR) in June 2005. The PDR of the accelerometric T-SAGE instrument in December 2005 was also successful and the programme was on track for the satellite-level PDR in February 2006. The second long-duration test of the ion emitter – critical component of the FEEP thrusters – took place successfully in 2005, thereby accumulating more than 1200 h of continuous operation and achieving a total impulse of 400 N-s.

## 4.7.3 Akari

Astro-F, developed by ISAS/JAXA, is the second Japanese space mission for IR astronomy. It will make an all-sky survey with better sensitivity, spatial resolution and wider wavelength coverage than IRAS. Akari has a 68.5 cm-diameter telescope cooled to 6K to observe in the wavelength range 2–180 $\mu$m from a Sun-synchronous polar orbit at 745 km altitude. It was launched on 21 February 2006 by an M-V rocket and renamed Akari ('light').

It is expected that the all-sky survey will: detect about a million galaxies, tracing the large-scale structure of the Universe to $z = 1$; detect exotic extraordinarily luminous objects at high redshift (including the most luminous objects within the observable Universe); map the Galactic plane, tracing the large-scale structure of nearby star-forming regions; and detect brown dwarfs in the solar neighbourhood as well as protostars. Akari will also perform pointed observations within 2-180 $\mu$m in 13 bands, providing comprehensive, multi-wavelength photometric and spectroscopic coverage of a wide variety of astronomical sources. These range from nearby Solar System objects, the zodiacal light, brown dwarfs and young stars, to debris discs and evolved stars in our Galaxy and in other galaxies of the Local Group, including complete coverage of the Magellanic Clouds. High-resolution imaging and spectroscopy of nearby galaxies are also planned.

ESA is collaborating with JAXA/ISAS in order to increase the scientific output of the mission by capturing all of the possible data (impossible with the baselined single ground station in Japan), to make observing opportunities available to the European astronomical community, and to accelerate the production of the sky catalogues, which will be extremely valuable in the exploitation of the Herschel and Planck missions. In brief, the cooperation involves ESA provision of tracking and scientific data processing support in return for observation time and accelerating public access to the mission's IR sky catalogues. Tracking support is provided via ESA's Kiruna ground station, which is equipped to receive the 4 Mbit/s X-band data stream. The European Call for Observing Proposals was released on 20 September 2005 and resulted in 50 proposals from 42 different PIs from 32 institutes in 9 European countries, plus ESO and ESA. The oversubscription factor was 7. Following the usual peer-review process, successful European proposals were merged in January 2006 with those resulting from the parallel Japanese call (48 proposals).

**Figure 4.7.3.1. The launch of Akari from Japan. (JAXA)**

## 4.7.4 Suzaku

Suzaku, previously called Astro-E2, is Japan's fifth X-ray astronomy satellite and was successfully launched in July 2005. The mission was developed at ISAS, which is now part of JAXA, together with a number of US and Japanese institutes. The

payload consists of three instruments: an imaging X-ray micro-calorimeter (XRS) and four CCD detectors (XIS) to provide high-sensitivity imaging in the 0.5–10 keV energy range. Above 10 keV, the non-imaging hard-X-ray detector (HXD) provides spectral and timing information. Unfortunately, during the course of commissioning all the helium cryogen was lost from the XRS, the highest resolution spectrometer flown to date.

Although observing proposals for Suzaku had been solicited, selected and announced in 2004, the selection process emphasised the use of the XRS. Since the selected proposals may therefore not provide for the best use of the XIS and HXD, it was decided to announce a new solicitation. This covers 1 year of observations starting around April 2006. JAXA/ISAS kindly offered to allocate 8% of the observing time to successful proposals from scientists in ESA Member States. The European announcement closed in January 2006 in parallel with those from JAXA and NASA. A total of 52 proposals from 49 different PIs in 29 institutes located in 10 different member states and ESA were received. The over-subscription factor in time was a very high 6.7. The proposals will be peer-reviewed by an ESA-appointed Time Allocation Committee and the recommended proposals will be forwarded to JAXA for merging with those resulting from the parallel Japanese and US calls. More information can be found on RSSD's Suzaku website at *www.rssd.esa.int/Suzaku*

## 4.7.5 Solar-B

Solar-B is the follow-up to the highly successful Japan/UK/US Yohkoh mission. Using a combination of optical, EUV and X-ray instrumentation, it will study the interaction between the Sun's magnetic field and corona, with the goal of increasing our understanding of the causes of solar variability. The launch is planned for late 2006, into a dusk-dawn, polar, Sun-synchronous orbit.

The satellite consists of a Sun-pointing platform with three major instrument packages:

— Solar Optical Telescope (SOT), a high-resolution (0.25 arcsec) visual imaging system with a vector magnetograph and spectrograph;
— X-ray Telescope (XRT), providing full- or partial-disc imaging with 1.0–2.5 arcsec resolution in the wavelength range 0.2–6 nm;
— EUV Imaging Spectrometer (EIS), with wavelength ranges 17–21 nm and 25–29 nm, 2.0 arcsec resolution and FOV 360x512 arcsec.

Data from the 8 Gbit solid-state recorder will be downlinked at 4 Mbit/s via X-band and in real time at up to 256 kbit/s in S-band. The planned ground coverage used a station in Japan (4 passess daily) and NASA Fairbanks (several per day). Since the amount of scientific data that can be transmitted is limited by the downlink bandwidth, this arrangement would have allowed less than half the data recorder content to be downlinked per orbit. Increasing the number of downlinks per orbit increases the observation cadence accordingly, which is crucial for the study of solar activity. ESA has therefore decided to support the mission with additional downlink capacity from a European high-latitude station for each of the 15 daily orbits: a contract has been agreed with the Norwegian Space Centre, for the provision of a ground station on Svalbard and a European Solar-B data centre in Oslo (N).

# 5. Missions under Definition

# 5.1 LISA

## Scientific goals

Gravitational waves are a necessary consequence of Einstein's theory of General Relativity. They cause a shrinking and stretching of space-time and therefore modify the distance between freely-falling test masses. Their strength can be expressed in terms of the strain, the relative change in distance caused by a gravitational wave. In contrast to the familiar electromagnetic waves, they are by nature quadrupole waves.

Predicted in 1916 by Einstein and proved in the late 1950s to be observable, there is no direct evidence for their existence, although there is indirect evidence from the Hulse-Taylor binary pulsar (PSR1913+16): its orbital period is decaying due to the loss of orbital energy to gravitational waves at exactly the rate predicted by General Relativity. Efforts to detect gravitational waves in the high-frequency range (frequencies from 10 Hz to the kHz range) on the ground with bar detectors and small interferometers have been made since the 1960s. The construction of several large ground-based interferometers with increased sensitivity is now well underway; four are fully operational (TAMA, in Japan; LIGO, a US project with two sites in Hanford, Washington and Livingston, Louisiana; GEO600, a British-German collaboration, near Hannover, D) and one is in the final stages of construction (VIRGO, an Italian-French project near Pisa, I).

The primary objective of the LISA (Laser Interferometer Space Antenna) mission is the detection and observation of gravitational waves from massive black holes (MBHs) and galactic binaries in the frequency range $10^{-4}$-$10^{-1}$ Hz (Fig. 5.1.1). This low-frequency range is inaccessible to ground-based interferometers because of the background of local gravitational noise and because ground-based interferometers are limited in length to a few kilometres.

Ground-based interferometers can in principle observe the bursts of gravitational radiation emitted by galactic binaries during the final stages (lasting minutes or seconds) of coalescence when the frequencies are high and the amplitudes and frequencies both increase quickly with time. However, the improvement of theoretical knowledge over the last few years has shown that the signal-to-noise ratio, though still slightly uncertain, is expected to be marginal for first-generation detectors. Only second-generation detectors, to be operational in 2013, are expected to achieve

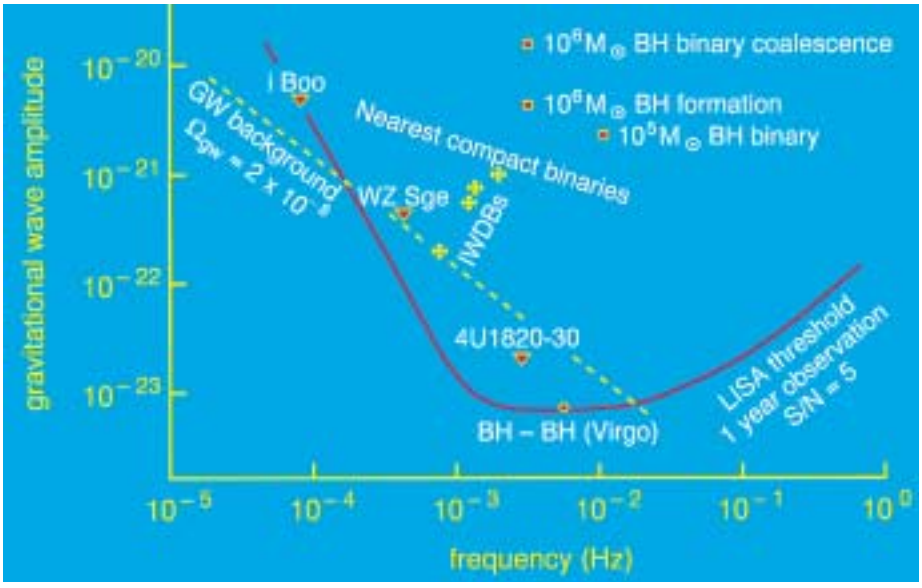


**Figure 5.1.1. The target sensitivity curve of LISA and the strengths of expected gravitational-wave sources.**

*For further information, see http://sci.esa.int/lisa*

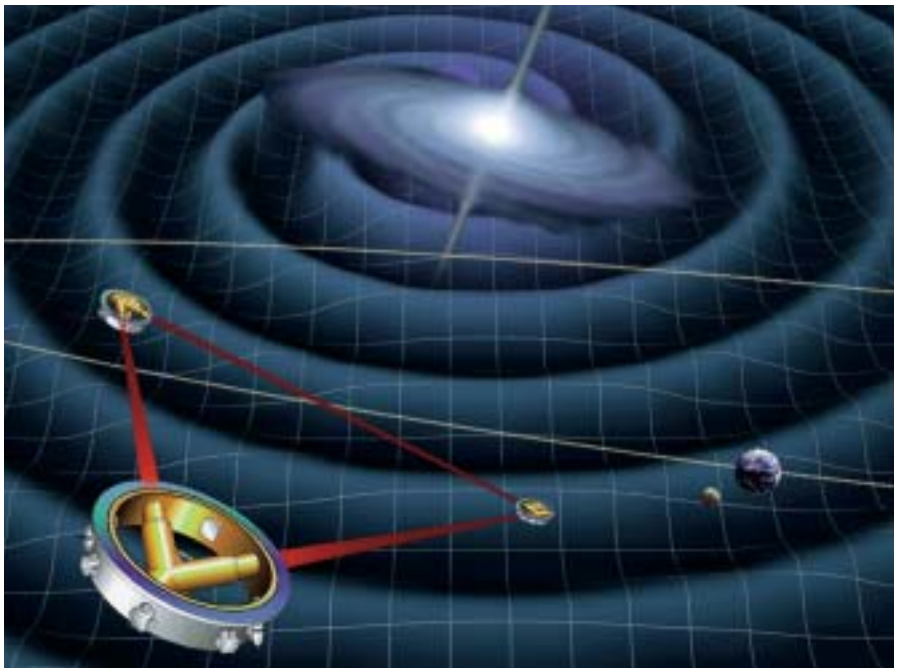

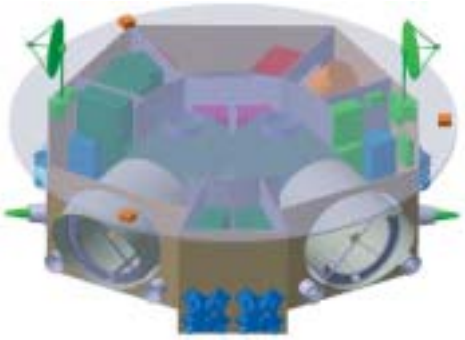

**Figure 5.1.2 (left). Orbital configuration of the three LISA spacecraft.**

**Figure 5.1.3 (above). Cutaway view of one of the three identical LISA spacecraft. The main structure is a ring with a diameter of 2.7 m and a height of 0.8 m. The top of the spacecraft is covered by a solar cell array, removed here to allow a view of the Y-shaped payload.**

reliable detection of those important astrophysical sources. Coalescences of MBHs are detectable only in space owing to the very low frequencies involved.

In the low-frequency band of LISA, sources are well-known and signals are stable over long periods (many months to thousands of years). LISA will detect signals from numerous sources with signal-to-noise ratios of 50-1000 for MBHs, which will allow determination of the internal parameters of their sources, such as position, orientation, mass and distance. LISA will complement the operation of the second-generation ground-based interferometers, giving a full coverage of the frequency spectrum, from a tenth of a mHz to the kHz region.

## Configuration

The LISA mission comprises three identical spacecraft positioned 5 million km apart in an equilateral triangle. The centre of the triangular formation is in the plane of the ecliptic, 1 AU from the Sun and trailing the Earth by approximately 20°. The plane of the triangle is inclined at 60° with respect to the ecliptic, resulting in a stable formation throughout the projected mission life. Owing to orbital mechanics, the formation appears to counter-rotate about its centre once per year (Fig. 5.1.2). Despite the stability of the formation, the spacecraft will oscillate around their nominal position which will cause the inter-spacecraft distance to change by many thousands of km, resulting in relative velocities of up to 15 m/s. This oscillation is partly inherent to the chosen orbits, partly caused by the gravitational pull of the Earth-Moon system.

The position of the formation at 20° behind the Earth is a result of a trade-off between minimising the gravitational disturbances from the Earth-Moon system and the communication needs. While going farther away would further reduce the disturbances, the larger distance would require larger antennas or higher transmitter power.

## Measurement principle

While LISA provides interferometric measurements, the measurement principle is somewhat different from a ground-based interferometer. The laser light going from one spacecraft to another cannot be reflected directly back, because diffraction and the large separation would attenuate the beam by a factor of $10^{10}$. In an analogy with an RF-transponder scheme, the laser on the receiving spacecraft is phase-locked to the incoming light, effectively providing a copy of the incoming light with full intensity to be sent back.

The transponded light from the far spacecraft is received and superposed with the onboard laser light that serves as the local oscillator in a heterodyne detection. This way, the change in armlength is measured individually for each arm. Heterodyne detection is chosen because the relative velocities of the spacecraft will cause a Doppler-shift of the received light of up to 15 MHz, which does not allow for a homodyne detection. Additionally, heterodyne detection is self-calibrating. Subsequent data processing makes it possible to reduce greatly the effects of laser frequency noise and to synthesise the responses of different interferometric architectures, such as Michelson- and Sagnac-interferometers, in order to assess the instrumental noise of LISA.

## Spacecraft

Each spacecraft has a launch mass of about 1600 kg (including margin), of which 550 kg is allocated to the 'sciencecraft', 350 kg to a propulsion module with about 400 kg of chemical bipropellants. After launch by an Atlas-V, the trio separate and use their propulsion modules to reach their operational orbits in 13 months. There, they jettison their propulsion modules and attitude and drag-free control is left to $\mu$N thrusters.

Each spacecraft carries two 30 cm-diameter steerable high-gain antennas for communication with Earth. Using the 34 m antennas of the Deep Space Network and 25 W transmitter power, data can be transmitted in the Ka-band at 148 kbit/s. Data are transmitted for 4 h every 2 days and stored onboard in a solid-state mass memory of 1 Gb capacity during times of no communication. Only one spacecraft is used to transmit data to Earth; the other two transmit their data to the 'master spacecraft' via the laser link between the trio. The nominal mission lifetime is 5 years once the spacecraft reached their operational orbits.

## Payload

Each spacecraft contains two optical assemblies (Fig. 5.1.3). The two on one spacecraft point towards an identical assembly on the other two spacecraft. A 1 W IR laser beam (1064 nm wavelength) is transmitted to the corresponding remote spacecraft via a 40 cm-aperture Dall-Kirkham telescope. The same telescope is used to focus the very weak beam (about 100 pW) coming from the distant spacecraft and to direct the light to a sensitive photodetector (a quadrant photodiode), where it is superimposed with a fraction of the original local light. At the heart of each assembly is a vacuum enclosure containing a free-flying polished platinum-gold 40 mm cube (the proof mass) that serves as an optical reference (mirror) for the light beams. A passing gravitational wave will change the length of the optical path between the proof masses of one arm of the interferometer relative to the other arm. The distance fluctuations are measured to a precision of 20 pm (averaged over 1 s) which, when combined with the large separation between the spacecraft, allows LISA to detect gravitational wave strains down to a level of order $\Delta l/l = 10^{-23}$ in 1 year of observation with a signal-to-noise ratio of 5.

The spacecraft serves mainly to shield the proof masses from the adverse effects of

solar radiation pressure so that they follow a purely gravitational orbit. Although the position of the spacecraft does not enter directly into the measurement, it is nevertheless necessary to keep all spacecraft moderately accurately centred on their proof masses to reduce spurious local noise forces. This is achieved by a drag-free control system consisting of an accelerometer (or inertial sensor) and a system of $\mu$N thrusters.

Capacitive sensing in three dimensions is used to measure the displacements of the proof masses relative to the spacecraft. These position signals are used in a feedback loop to command Field Emission Electric Propulsion (FEEP) thrusters to follow the proof masses precisely. As a reference point for the drag-free system, one or the other mass (or any point in between) can be chosen. The FEEP thrusters are also used to control the attitude of the spacecraft relative to the incoming optical wavefronts using signals derived from the quadrant photodiodes.

Although the spacecraft shields its proof masses from non-gravitational forces, cosmic rays and solar flare particles can cause a significant charging of the proof masses. A discharging system, consisting of a fibre-coupled UV light source, will be operated at regular intervals.

As the 3-spacecraft constellation orbits the Sun in the course of a year, the observed gravitational waves are Doppler-shifted by the orbital motion and amplitude-modulated by the non-isotropic antenna pattern of the detector. This allows determination of the direction of the source and assessment of some of its characteristics, e.g. its orientation, the mass and the distance. Depending on the strength of the source, a precision for determining the position of up to an arcminute can be achieved.

## Status

LISA and its LISA Pathfinder technology-demonstrating precursor form an ESA/NASA collaborative project, selected as an ESA Cornerstone and included in NASA's 'Beyond Einstein' initiative, with a launch in the 2015 time frame. LISA is in its formulation phase, undergoing a 2-year industrial study that started in January 2005. Preliminary agreement has been reached with NASA concerning the share of responsibilities and hardware between the agencies, with ESA taking responsibility for the payload, and NASA the spacecraft, the integration and the launch vehicle. About half of the payload hardware will be provided by NASA, the other half by European institutes.

# 5.2 Solar Orbiter

## Introduction

The Sun's atmosphere and the heliosphere are uniquely accessible domains of space, where fundamental physical processes common to solar, astrophysical and laboratory plasmas can be studied in detail and under conditions impossible to reproduce on Earth or to study from astronomical distances.

The results from missions such as Helios, Ulysses, Yohkoh, SOHO, TRACE and RHESSI have significantly advanced our understanding of the solar corona, the associated solar wind and the 3-D heliosphere. Further progress is to be expected with the launch of STEREO, Solar-B, and the first of NASA's Living With a Star (LWS) missions, the Solar Dynamics Observatory (SDO). Each of these missions has a specific focus, being part of an overall strategy of coordinated solar and heliospheric research. An important element of this strategy, however, has yet to be implemented. We have reached the point where further *in situ* measurements, now much closer to the Sun, together with high-resolution imaging and spectroscopy from a near-Sun and out-of-ecliptic perspective, promise to bring about major breakthroughs in solar and heliospheric physics. Solar Orbiter will, through a novel orbital design and an advanced suite of scientific instruments, provide the required observations. The unique mission profile of Solar Orbiter will, for the first time, make it possible to:

— explore the uncharted innermost regions of the Solar System;
— study the Sun from close by (48 solar radii, or 0.22 AU);
— examine the solar surface and the space above from a quasi-heliosynchronous vantage point during the close perihelion passes;
— provide images of the Sun's polar regions from heliographic latitudes as high as 34°.

## Scientific goals

Within the framework of the global strategy outlined above, the top-level scientific goals of the Solar Orbiter mission are to:

— determine the properties, dynamics and interactions of plasma, fields and particles in the near-Sun heliosphere;
— investigate the links between the solar surface, corona and inner heliosphere;
— explore, at all latitudes, the energetics, dynamics and fine-scale structure of the Sun's magnetised atmosphere;
— probe the solar dynamo by observing the Sun's high-latitude field, flows and seismic waves.

The near-Sun interplanetary measurements together with simultaneous remote-sensing observations of the Sun will permit us to disentangle spatial and temporal variations during the quasi-heliosynchronous phases. They will allow us to understand the characteristics of the solar wind and energetic particles in close linkage with the plasma conditions in their source regions on the Sun. By approaching as close as 48 solar radii, Solar Orbiter will view the solar atmosphere with unprecedented spatial resolution (0.5 arcsec pixels, equivalent to ~80 km at 0.22 AU). Over extended periods, Solar Orbiter will deliver images and data of the polar regions and the side of the Sun not visible from Earth. This latter aspect of the mission is a key factor in Solar Orbiter's envisaged role as a Solar Sentinel within the framework of the International Living With a Star (ILWS) initiative.

The scientific goals listed above have been translated into detailed science requirements that have in turn been used to define a baseline reference payload comprising the following instruments:

*For further information, see http://sci.esa.int/solarorbiter*

**Fig. 5.2.1. Solar Orbiter near perihelion.**

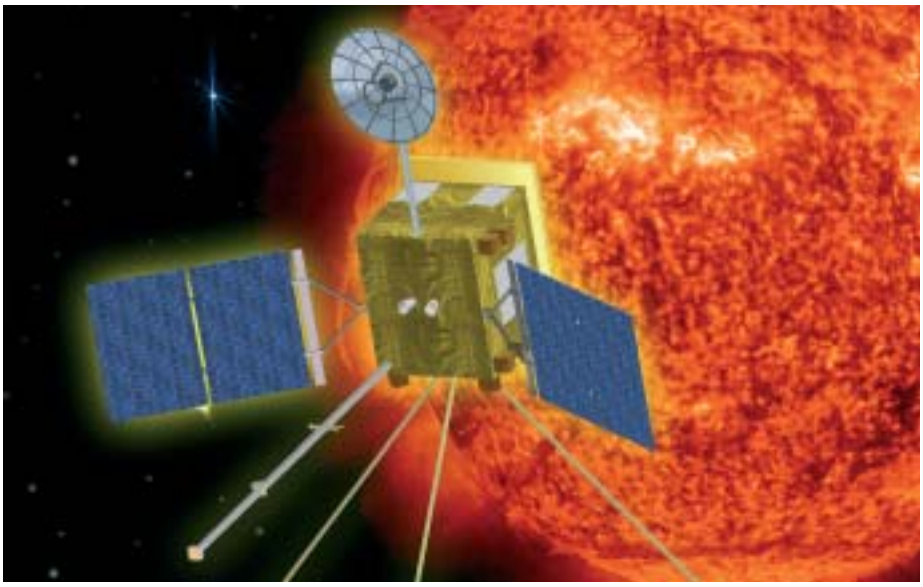

— heliospheric *in situ* instruments: plasma package (solar wind analyser); fields package (radio and plasma wave analyser, magnetometer, coronal sounding); particles package (energetic particle detectors, interplanetary dust detector, neutral particle detector, solar gamma-ray and neutron detector);
— solar remote-sensing instruments: Visible-light imager and magnetograph; EUV full-Sun and high-resolution imager; EUV spectrometer; X-ray spectrometer/telescope; coronagraph.

## Status

Solar Orbiter was selected as an ESA Flexi-mission in October 2000, and reconfirmed in 2002 as a common development with the BepiColombo mission. Assessment by ESA and in industry has continued during the reporting period, with particular emphasis on further refinement of the reference payload and detailed study of a chemical mission profile. The latter was introduced as an alternative to the solar-electric propulsion (SEP) option that was originally foreseen in view of the higher risk and smaller system-level margins associated with the SEP option. The chemical option, now the recommended baseline, has a longer cruise phase than the SEP option (3.4 years compared with 1.8 years), but would allow science operations to start earlier. The remainder of the mission profile, in particular the use of Venus flybys to achieve a low perihelion distance and subsequent increase in inclination, is very similar. Launch opportunities for Solar Orbiter occur every 19 months because of the need to encounter Venus. For the purpose of assessment, launches in November 2013, May 2015 and January 2017 have been considered. The system-level studies have confirmed that a single spacecraft design can accommodate all these opportunities. The present baseline is for a launch in 2015.

Final presentations of the respective assessment studies by the two industrial contractors were given at the end of September 2005, and the completed Assessment Study documentation package delivered to the ESA executive in December. The Announcement of Opportunity for the scientific payload is planned to be issued early in 2007.

# 6. Missions under Study

# 6.1 Darwin

## Introduction

Darwin is an ESA mission aimed at the search for, and the study of, terrestrial exoplanets. Darwin was already under study when the Cosmic Vision exercise was launched; a large number of proposals concerning the science of exoplanets, terrestrial exoplanets and the possibility of life elsewhere in the Universe were received. These subsequently matured into Theme 1 of the Cosmic Vision 2015-2025 plan. It is clear that the Darwin mission as currently envisaged would address significant parts of this theme, including the existence of terrestrial exoplanets in the Sun's vicinity, their properties and the possibility for them to host life, as well as the study of how planets form and how this process relates to the formation of the parental stars. The mission's interest received a large boost with the discovery in 2005 (through a microlensing detection) of the first truly rocky exoplanet.

## Status

During the reporting period, the technology development carried out under ESA contract achieved a number of satisfying results, while two system-level studies of the current concept were initiated. Darwin comprises a nulling (destructive) interferometer combining the light from three or four telescopes in the 3–4 m-diameter class, each free-flying on its own spacecraft. The light is combined in an optical bench on a separate beam-combiner spacecraft. Baselines of between 30 m and a few 100 m are required to search for and study terrestrial exoplanets out to about 25 pc. Darwin operates in the wavelength range 6-20 $\mu$m, making it a mid-IR mission. Its capabilities include obtaining spectra with a resolution sufficient to measure accurately the signatures of water, ozone, methane and carbon dioxide, found in our own atmosphere, out to distances of 25–30 pc. These elements, in combination and when found in the 'Habitable Zone' (HZ, where one would expect liquid water on a planetary surface or atmosphere), are generally considered to be true biomarkers.

A Darwin target star catalogue has been completed and will be published during 2006. It contains about 800 possible F-, G-, K- and M-class targets. Since the input databases are incomplete regarding late K and M dwarf stars, it is expected that the catalogue will increase by several hundred objects ~1.5 years into the mission of Gaia, ESA's astrometric satellite (i.e., by mid-2013).

Among the technological studies that have been completed are:

— integrated optics, the possibility to combine beams on the equivalent of an integrated circuit, a technology that promises significant benefits in mass, complexity, reliability and thus cost;
— 10 $\mu$m monomode fibres and waveguides, a technology that enables the injection of beams into combiners in interferometric systems such that low spatial frequency disturbances are eliminated, thereby lowering the requirements on the precision of optical components and alignments.

A number of simulators are under development:

— FINCH (Flexible Interferometer Characterisation): a free-flying scenario simulation, including servo-loop control and thruster for a given interferometer geometry, spectral bandwidth, polarisation that produces as an output the optical performance in terms of sensitivity, polarisation, etc;
— RESSP (Reconstruction of Exo-Solar System Properties): generates the dynamical source scenery around Darwin targets. This is used as input data for FINCH;
— FITTEST: will recover the input data from the simulation of Darwin science and housekeeping data, test the reconstruction algorithms, and provide a baseline for

*For further information, see http://sci.esa.int/darwin*

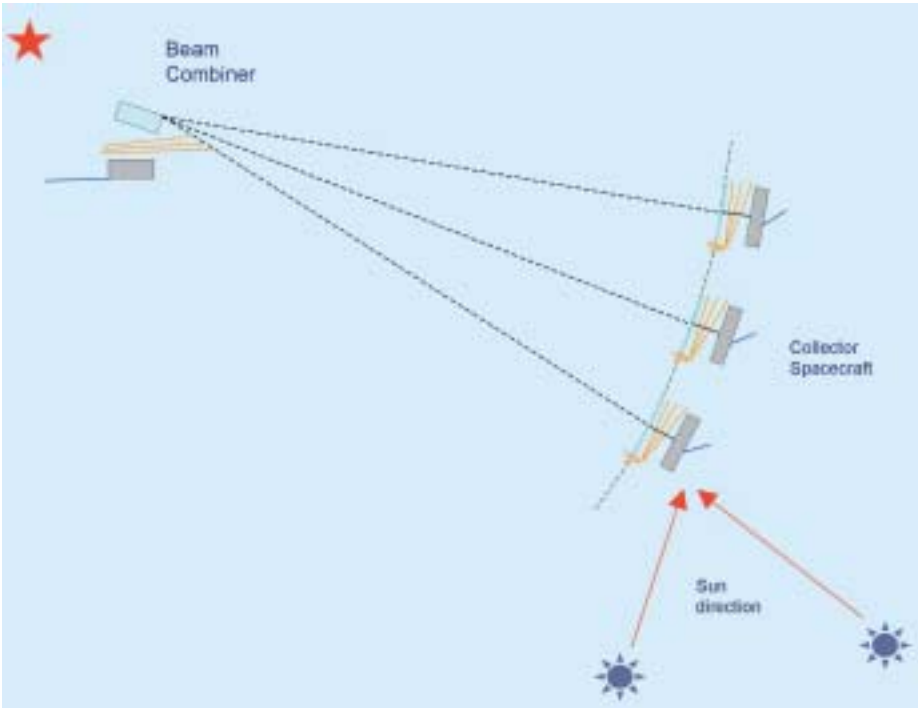


**Figure 6.1.1. The Emma configuration. The three Collector Spacecraft (CS) are located on a parabolic 3-D surface; the Beam Combiner Spacecraft (BCS) is at the focus of the paraboloid. The CS are located along a circle of radius variable between 15 m and 100 m, forming a triangle or a trapezoid. The CS-BCS range is about 1 km.**

reconstruction efficiency. It will be used as a precursor of the eventual data reduction pipeline process;

— DarwinSim: evaluates the science performance and allows the number of target stars and candidates for spectroscopy follow-up observations to be ascertained. For a given interferometer architecture, the program searches the candidate target catalogue of nearby stars within 25 pc, selects the stars to be observed and assumes three visits for detection, sets the integration times, and also selects the observed stars that are optimum for spectroscopy. One of the conclusions of DarwinSim is that one visit will provide 90% confidence as to the presence of a planet.

Three of these simulators are being developed by industry, while DarwinSim is being developed by ESA.

The study of the ground-based technological precursor, GENIE (Ground-based European Nulling Interferometry Experiment), carried out by industry under the auspices of ESA and the European Southern Observatory (ESO), has been completed. It shows clearly that GENIE is feasible, with the capability of detecting zodiacal clouds 20–30 times more massive than our own around Darwin target stars. A caveat is, however, that it must be possible to control differential polarisation in the two arms of the interferometer to a level of better than 0.5–1%. Currently, measurements of the polarisation properties of the Very Large Telescope Interferometer are lacking; the next step is to carry out such measurements.

The goal of the two system-level studies is to mature the mission concept further, as well as to provide input for the selection of the interferometric configuration best suited to carrying out the mission that fulfils the scientific objectives in a complete and affordable way. Several concepts, in which the number of apertures is constrained

to be four or fewer, are being explored in these studies. These include the Emma (named after Charles Darwin's wife) arrangement, a novel concept in which three low-curvature mirrors (collector spacecraft) fly on the surface of a parabola, while injecting their beams directly into a beam combiner flying about 1 km away from the collectors (Fig. 6.1.1).

A study of a limited exoplanetary mission that would answer only part of the full Theme 1 objectives will begin in 2006. The rationale is that Darwin as envisaged will doubtless be both complicated and costly. Indeed, the mission may be the most technically ambitious ever attempted by any space agency. Given such constraints, it makes sense to investigate whether it can be simplified or divided into several missions. The fact that we do not currently know which stars – if any – in the solar vicinity have terrestrial planets, also suggests a natural division into first, a planet-finding mission, followed (if successful) by a mission dedicated to direct studies. Such a division immediately suggests several areas of simplification.

Firstly, significant savings can be made by limiting the spectral range to 9–15 $\mu$m. The thermal requirements relax from 40K on the optics to 60–70K or higher, which can probably be achieved through simple passive means. By discarding the 6–9 $\mu$m range, the requirements on the precision in the beam combination, as well as the stability of the spacecraft, are significantly relaxed. In that case, what is directly lost from the scientific case is the detection of water. A limited mission, carrying out photometry through 3–5 filters in the 9–15 $\mu$m range still has the capability of detecting Earth-like planets and determining if they possess atmospheres. In addition, for planets of exactly the same type and age as the Earth, the detection of ozone (and via that, of free molecular oxygen) is possible.

Secondly, the telescopes can be smaller. This limits the reach of the search for Earth-like planets, and by doing so, limits the number of stars available for search. There are at least 447 prime Darwin target stars out to 25 pc (and several hundred M- and late K-dwarfs are still missing from this sample), while there are only 45 target stars out to 10 pc and a further 97 if the range is extended to 15 pc. It is not known today, however, how many stars possess terrestrial planets. On the other hand, 5% of all solar-type stars (and about 15% if we sample only metal-rich stars) are known to have giant planets orbiting them. Gas giants have even been found around a few red dwarfs and in multiple systems. Only two Earth-like systems are known, however: one found around a relatively nearby red dwarf using the radial velocity method (after sampling 8 years of data) with a mass at least 7.5 times that of the Earth, and the other (found by the microlensing method) of about 5 Earth masses, orbiting 3 AU from a red dwarf star. Clearly, these statistics are very poor.

The situation will improve with the launch of the CNES-ESA COROT mission (2006) and NASA's Kepler mission (2008). Both are capable of detecting rocky planets. Kepler even has the possibility of detecting HZ planets around G-type stars. Neither mission can observe nearby stars, however. NASA's astrometric Space Interferometry Mission (SIM; launch about 2015) will have the possibility of detecting exoplanets of 1 or a few Earth masses orbiting some of the nearest stars; of course, those results will not be available for a long time.

In short, although a down-scoped Darwin may be able to find planets like our own out to a certain (limited) distance, it will not be able to measure their spectra. Furthermore, there is a risk of not detecting anything, even if this risk ought to be alleviated by the precursor missions.

The near-term activities for the Darwin programme are:

— first, the system-level industrial studies will continue well into 2007. These will

have to react to any changes brought about by the continuous evolution of the Cosmic Vision programme;

— secondly, the precursor activities will continue. Polarisation measurements are being planned at the Very Large Telescope Interferometer to determine the final capabilities of the GENIE experiment. Planning of observations of Darwin targets by the Herschel space observatory will continue;

— third, the ground-based programme will continue to evolve.

# 6.2 XEUS

## Introduction

The X-ray Evolving Universe Spectroscopy (XEUS) mission is the potential follow-on to XMM-Newton and aims to provide an X-ray capability comparable in sensitivity to the future generation of ground- and space-based observatories such as ALMA and JWST. XEUS is being jointly studied by ESA and JAXA. A proposal outlining the science goals of a mission such as XEUS was submitted to ESA's Cosmic Vision 2015-2025 programme and the science has been identified as one of the highest priorities of the future ESA Science Programme.

The main goals of XEUS are to study the formation of large-scale structure and the growth of galaxies and their massive black holes. It is now believed that 96% of the energy density of the Universe exists in the form of Dark Matter and Dark Energy that governs the structure and evolution of the Universe on the largest possible scales. Clusters of galaxies are the largest collapsed objects in the Universe. Their formation and evolution is dominated by gravity, i.e. Dark Matter, while their large-scale distribution and number density depend on the geometry of the Universe, i.e. Dark Energy. Clusters are filled with hot baryonic gas enriched with elements through star formation and stellar explosions and is most easily detected by its high-energy radiation. X-ray observations of clusters provide information on the Dark Matter and Dark Energy content of the Universe, on the amplitude of primordial density fluctuations, on the complex physics governing the formation and evolution of structures in the Universe, and on the history of metal synthesis. While nearby clusters of galaxies have been studied in great detail with existing X-ray satellites, very little is known about their formation and evolution in the early Universe. In addition, the fate of almost 50% of the baryons in the Universe, believed to reside in warm/hot filamentary structures observable through X-ray absorption spectroscopy, is still a mystery. XEUS will study the genesis of groups and clusters of galaxies and the filamentary structure at redshifts of $< 2$, and the evolution of the physical state and chemical abundances of the intergalactic medium.

XEUS will also study the coeval growth of galaxies and their massive black holes. The first stars and galaxies formed where gravity overpowered the pressure of the ambient baryons. The first generation of stellar mass black holes then formed, resulting probably in gamma-ray burst explosions. Such black holes then grew through cataclysmic feeding events, with the highest redshift accreting black holes known being at around a redshift of 6.5. The fact that practically all galaxy bulges in the local Universe contain massive black holes, with a tight relation between black hole mass and the stellar velocity dispersion, indicates a coexistence and coevolution of stars and central black holes early in the history of the Universe. Massive black holes must therefore be an important constituent of the evolving Universe. Only recently has the importance of feedback of stellar explosions and accreting black holes into the intergalactic and interstellar medium, and thus their role in subsequent star and galaxy formation, been realised.

## Spacecraft and science

The study of these topics requires an unprecedented combination in the X-ray regime of large spectral throughput, high angular resolving power (2-5 arcsec HEW) large fields of view and a good bandpass. Meeting such demanding requirements is only possible due to the development of a novel, high-performance, lightweight silicon mirror technology and a new approach to assembling an X-ray telescope using modular High-performance Pore Optics (HPO). This will provide the largest X-ray mirror flown so far, with outstanding spatial resolution. HPO technology provides the single critical element in the construction of a feasible mission and has many wider applications in other areas of high-energy astrophysics, such as a large-area collector

*For further information, see http://sci.esa.int/xeus/*

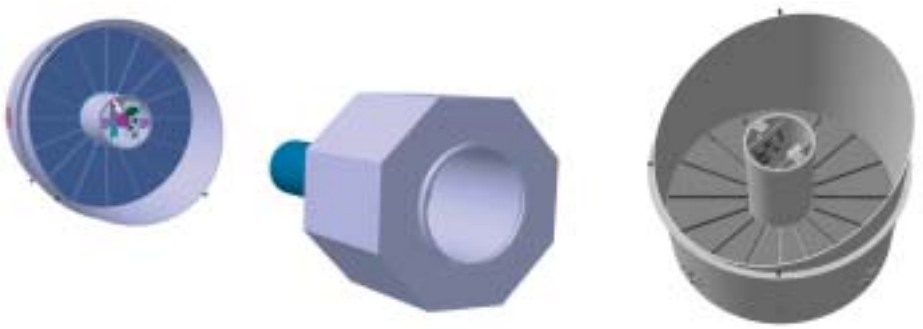

**Figure 6.2.1 (left). Formation-flying: the mirror spacecraft (left) and the detector spacecraft (right) are separated by the 35 m focal length of the XEUS optics. The cylindrical baffle extending in front of the detector spacecraft blocks the direct view of the X-ray sky by the instruments.**

**Figure 6.2.2 (right). The mirror spacecraft. The central column houses the spacecraft subsystems. The 16 mirror petals are arranged in a circular configuration, with a sunshield around the outer circumference. A thin skirt helps to block the unfocused X-ray sky from the instruments.**

for timing studies. The starting points for the new optics are incredibly flat, highly polished, Si wafers. These are then chemically treated to form a rib-structure. The ribbed plates are then robotically stacked under interferometric control. The stacked modules are assembled into mirror modules that include baffles and then integrated into petal segments that make up the mirror. In tests at a synchrotron facility, pencil-beam scanning of a representative 2 $cm^2$ area has demonstrated a resolution of 6 arcsec HEW.

Work has continued within ESA on evaluating mission designs based around two formation- flying spacecraft (Fig. 6.2.1) placed into halo orbits around the Earth-Sun L2 point by an Ariane-5-class launcher. One spacecraft would carry optics based on the new HPO technology (Fig. 6.2.2), and the other new-generation detectors. The optimum mirror spacecraft and optics configurations (the two are closely linked) are still being evaluated in order to maximise the mirror area over the key energy ranges below 2 keV and above 6 keV, while reducing complexity and cost by avoiding critical deployment mechanisms. A number of platform- and payload-related technology-development activities are being conducted to support the future mission development. Specific work is being carried out on formation- flying and cryogenic technologies, as well as on advanced focal plane detectors.

Two sorts of imaging instruments are envisaged: spectrometers based on cryogenic technology, optimised for high-spectral resolution but with small FOVs, and Wide-Field Imagers (WFI) with lower spectral resolution and 7 arcmin FOVs. It is possible that two high-resolution devices will be needed to provide the required spectral resolution over the entire 0.1-10 keV energy range. The initial goal of the European Cryogenic Array (EURECA) consortium is to build a 5x5 array of Transition Edge sensors with 1-2 eV FWHM energy resolution as a prototype of an instrument that could be developed for XEUS. The array will be read-out by four SQUID-amplifier chains making use of frequency domain multiplexing. The sensors and SQUID-amplifiers would be cooled down to about 50mK making use of a space-qualified ADR being developed by ESA. The WFI could be an Active Pixel Sensor which would provide for a large FOV with CCD-like spectral resolution and a much higher count rate capability than the XMM-Newton EPIC detectors. In addition, a number of auxiliary science instruments are being considered to take advantage of the large mirror area and good quality imaging. These include a hard X-ray camera to view the obscured Universe and non-thermal components, a fast timing detector to probe General Relativity in strong gravitational fields, an extended FOV for the WFI, and a highly sensitive X-ray polarimeter.

# 6.3 ROSITA and Lobster

## Introduction

ROSITA (ROentgen Survey with an Imaging Telescope Array) and Lobster were originally studied by ESA's Science and Human Space Flight Directorates as potential external payloads on the International Space Station (ISS). The X-ray all-sky monitor Lobster successfully completed a Phase-A study that showed that the payload could be accommodated on the zenith platform of the External Payload Facility of ESA's Columbus module. Owing to concerns about contamination and uncertainties brought about by the likely retirement of the Shuttle fleet around 2010, however, it was decided to seek alternative mission scenarios for both instruments. In collaboration with the Space Research Institute (IKI) in Moscow, the two instruments have been accepted for study as part of the payload of the Russian Spectrum-Rontgen-Gamma (SRG) mission. This is being completely revised from the original concept, and developed for a launch around 2009-2010 on a Soyuz rocket from Kourou into a 600 km equatorial orbit. The payload would be complemented by a Russian-led coded-mask hard X-ray imager (ART) and a gamma-ray burst monitor. The revised SRG mission would be a highly significant scientific and technological step between today's X-ray observatories (Chandra, Suzaku and XMM-Newton) and the next generation of giant observatories such as XEUS. SRG will conduct the first all-sky survey with an imaging telescope in the 2-12 keV energy range to discover the hidden population of < 170 000 obscured massive black holes and the first all-sky imaging X-ray time-variability survey. In addition to the all-sky survey, it is foreseen to perform wide (20 000 square deg) and deep (200 square deg) sky surveys. These should allow for the detection of 50 000–100 000 clusters of galaxies and permit follow-up pointed observations of selected sources in order to investigate the nature of Dark Matter and Dark Energy.

## ROSITA

The ROSITA telescopes are based on an existing design that was launched on the German ABRIXAS national mission that failed soon after launch as a result of a power conditioning problem. ROSITA will continue the pioneering work performed by European scientists on X-ray surveys using the German/US/UK ROSAT observatory that completed the first X-ray all-sky imaging survey. In order to optimise ROSITA for Dark Energy studies, it is planned increase the low-energy grasp and angular resolution of the X-ray telescopes. The group at MPE, under the PI leadership of G. Hasinger, is undertaking a feasibility study for such improvements. ROSITA will consist of seven individual Wolter-I X-ray telescopes operating at 0.2-12 keV, with an effective area of 2500 $cm^2$ and a grasp of ~700 $cm^2$ $deg^2$ at 1 keV. Each telescope will have a CCD detector at the focus. These detectors are a development of the highly successful pn camera on XMM-Newton and are a potential prototype of those to be flown on XEUS.

## Lobster

Lobster will use a novel form of micro-channel plate X-ray optics developed under the ESA Technology Research Programme to provide an unprecedented 0.1-3.0 keV sensitivity. It will provide the first true imaging X-ray all-sky monitor (ASM) and be able to locate X-ray sources to within 1 arcmin to allow the rapid identification of new transient sources. The high sensitivity will allow many topics to be studied, including the long-term variability of active galactic nuclei and stars, X-ray bursts and superbursts, supersoft sources, black holes in X-ray binaries, X-ray afterglows of gamma-ray bursts, X-ray flashes and the sources of gravitational waves. The advantage of this type of optics for an X-ray ASM is its extremely large simultaneous FOV. This is achieved by accurately bending the thousands of tiny glass pores that

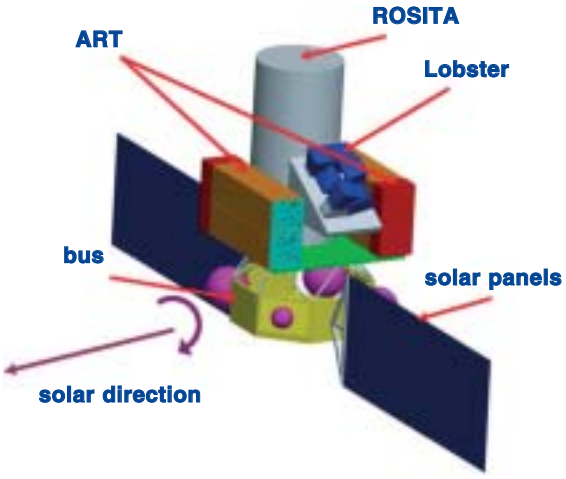


**Figure 6.3.1. SRG showing the main payload elements (ART, ROSITA and Lobster). The satellite bus consists of a medium-class 3-axis spacecraft such as a Yamal (RSC Energia) or Navigator (Lavochkin Association) platform.**

make up each micro-channel plate by exactly the right amount, in order to focus incident X-rays. This explains the name Lobster, since this is similar to how the eye of a crustacean works. The design of Lobster was optimised for accommodation on the Columbus external platform. The PI, G. Fraser (Leicester University, UK), is investigating the use of reflectivity coating and increases in the focal length of the X-ray optics to improve the effective area and energy range.

When the current studies have been completed, the instrument teams and Russian colleagues plan to submit, through their respective funding agencies, a proposal for ESA funding of certain programme elements in response to the expected 2006 Announcement of Opportunity for support to nationally-led projects.

# 6.4 ACES

## Introduction

The Atomic Clock Ensemble in Space (ACES) is a challenging mission in fundamental physics and time and frequency metrology. ACES will demonstrate the performances of a new generation of space clocks in the microgravity environment of the International Space Station (ISS) and the possibility of achieving accurate time and frequency transfer with stability better than $10^{-16}$. The ISS orbit will allow ground users to compare and synchronise their own clocks to the space clock signal, leading to a worldwide access to the ultra-stable frequency reference of ACES. The results of clock-to-clock comparisons at the $10^{-16}$ level will provide new tests of General Relativity, such as an improved measurement of Einstein's gravitational redshift, a search for a possible anisotropy of the speed of light, tests of the Standard Model Extension (SME), and the measurement of space-time variations of fundamental physical constants.

## Scientific goals

The mission has three main objectives:

— to demonstrate the high performances of a new generation of clocks for space applications: the cold caesium atomic clock 'Projet d'Horloge Atomique par Refroidissement d'Atomes en Orbit' (PHARAO) will allow fractional frequency instabilities below $10^{-13}\,\tau^{-1/2}$ ($\tau$ is the integration time) to be reached with an accuracy at the $10^{-16}$ level; the Space Hydrogen Maser (SHM) will ensure mid-term frequency stabilities at the $10^{-15}$ level;

— to deliver a global atomic time scale and perform direct comparisons of ultra-stable clocks at the $10^{-16}$ level on a worldwide basis;

— to perform fundamental physics tests:

*accurate measurement of the gravitational redshift*. The comparison between the space clock and ground-based atomic clocks will allow the measurement of the frequency variation due to the gravitational redshift with a relative frequency uncertainty of $3\times10^{-6}$;

*measurement of time variations of the fine structure constant*. This experiment is based on the direct comparison of clocks working with different atomic species as a function of time. The measurement will establish strong constraints on the time variations of $\alpha$, allowing a direct test of Einstein's Equivalence Principle ($1/\alpha \times \delta\alpha/\delta t < 10^{-16}$/yr);

*SME tests*. The measurement of the propagation delay of electromagnetic signals between the ISS and the ground stations around the Earth will test the validity of Special Relativity. Using ultra-stable atomic clocks, it will be possible to detect relative variations of the speed of light at the level $\delta c/c \sim 10^{-10}$.

Other applications of the stable and accurate ACES clock signal are under investigation. ACES will improve the accuracy of the atomic time and will contribute to the definition of global time scales. Third-generation navigation systems will benefit from the technology development related to the ACES mission, both in terms of more stable and accurate clocks, and of high-performance time- and frequency-transfer techniques. New concepts for global positioning systems based on a reduced set of ultra-stable space clocks in orbit associated with simple transponding satellites could be studied. Moreover, a new kind of gravimetry and geodesy based on the accurate measurement of Einstein's gravitational redshift will be demonstrated.

## ACES payload

The heart of the ACES payload (Fig. 6.4.1) is an atomic clock using laser-cooled caesium atoms. The performance of the caesium frequency standard (Fig. 6.4.2) PHARAO is combined with the characteristics of the SHM. The ACES clock signal

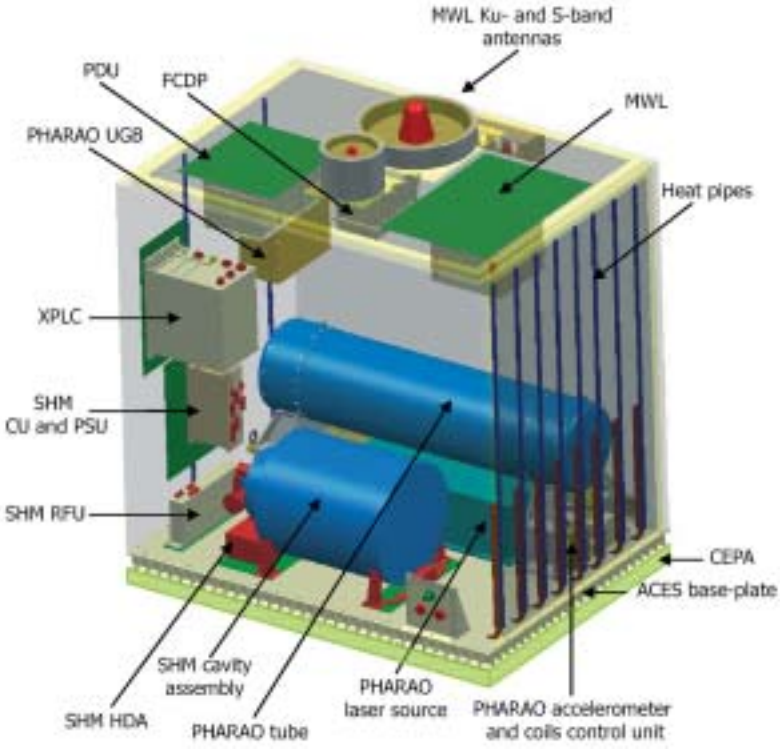


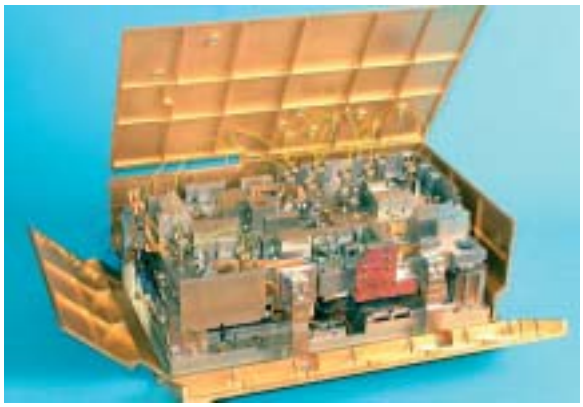

**Figure 6.4.1 (left). The ACES payload. The two atomic clocks (PHARAO and SHM), the frequency comparison and distribution package (FCDP), and the microwave link (MWL) fit into a thermally regulated payload with a total mass of 227 kg and a power consumption of 450 W. ACES will be accommodated aboard the ISS, on the Columbus External Payload Facility.**

**Figure 6.4.2 (above). Engineering model of the PHARAO optical bench. PHARAO subsystems are under test in CNES (Toulouse, F).**

will therefore merge the good short- and medium-term frequency stability of hydrogen masers with the long-term stability and accuracy of a primary frequency standard. The onboard clock-to-clock comparison (PHARAO-SHM) and the distribution of the clock signal are ensured by the Frequency Comparison and Distribution Package (FCDP), while all data-handling processes are controlled by the eXternal PayLoad Computer. A major objective is to maintain a stable and accurate onboard time scale that can be used for space-to-ground and ground-to-ground comparisons of frequency standards. Stable and accurate time and frequency transfer is achieved using a microwave link (MWL), that is necessary to characterise the ACES clock ensemble and to perform General Relativity tests of high scientific relevance.

## Status

The ACES project is under the responsibility of ESA's Directorate of Human Spaceflight, Microgravity and Exploration, with a small contribution from the Directorate of Science in the form of scientific expertise. The mission is now in Phae-C/D. Development, implementation and test activities on payload, instruments and subsystems are under way. During 2006, all the instruments and subsystems will be tested and their design concepts demonstrated by fully developed engineering models. The FCDP engineering model is under test. The feasibility demonstration of PHARAO, the end-to-end verification of SHM, and the tests of the MWL time and frequency link are the next important milestones. The Preliminary Design Review will be held in 2006.

# Acronyms

| | |
|---|---|
| AAT | Anglo-Australian Telescope |
| ACES | Atomic Clock Ensemble in Space |
| ACS | Advanced Camera for Surveys (HST) |
| ADS | Astrophysics Data System (NASA) |
| AFM | Atomic Force Microscope |
| AGB | Asymptotic Giant Branch |
| AGN | Active Galactic Nuclei |
| AGU | American Geophysical Union |
| AIV | Assembly, Integration & Verification |
| ALICE | Rosetta Orbiter UV imaging spectrometer |
| ALMA | Atacama Large Millimetre Array |
| AMIE | Asteroid Moon micro-Imager Experiment (SMART-1) |
| AO | Announcement of Opportunity |
| APXS | Alpha-Proton-X-ray Spectrometer (Rosetta) |
| ASCA | Advanced Satellite for Cosmology and Astrophysics (Japan) |
| ASI | Italian Space Agency |
| ASIC | Application Specific Integrated Circuit |
| ASM | All-Sky Monitor |
| ASPOC | Active Spacecraft Potential Control (Cluster) |
| ASU | Atomic Sagnac Unit |
| AU | Astronomical Unit |
| AXPS | anomalous X-ray pulsar |
| BBF | bursty bulk flow |
| *c* | speed of light |
| CAA | Cluster Active Archive |
| CBRF | Cosmic Background Radiation Field |
| CCD | Charge Coupled Device |
| CDMS | Cluster Data Management System |
| CDR | critical design review |
| CDS | Coronal Diagnostics Spectrometer (SOHO) |
| CDS | Command & Data Subsystem |
| CDS | Centre de Données astronomiques de Strasbourg |
| CdTe | cadmium telluride |
| CELIAS | Charge, Element and Isotope Analysis System (SOHO) |
| CEPHAG | Centre d'Etude des Phenomenes Aleatoires et Geophysiques (France) |
| CERN | Centre Européen de Recherches Nucléaires (France) |
| CESR | Centre d'Etude Spatial des Rayonnements (France) |
| CFHT | Canadian-French-Hawaiian Telescope |
| CGRO | Compton Gamma Ray Observatory (NASA) |
| CIR | Corotating Interaction Region |
| CIS | Cluster Ion Spectrometry |
| CIVA | Comet Infrared and Visible Analyser (Rosetta) |
| CMB | Cosmic Microwave Background |
| CMD | colour magnitude diagram |
| CME | Coronal Mass Ejection |
| CMOS | Complementary Metal Oxide Semiconductor |
| CNES | Centre National d'Etudes Spatiales |
| CNR | Consiglio Nazionale della Ricercha (Italy) |
| CNRS | Centre National de la Recherche Scientifique (France) |
| CNSA | China National Space Administration |
| CODIF | (Cluster) Composition and Distribution Function analyser |
| Co-I | Co-Investigator |
| COBE | Cosmic Background Explorer (NASA) |
| COMPTEL | Compton Telescope (CGRO) |
| CONSERT | Comet Nucleus Sounding Experiment by Radiowave Transmission (Rosetta) |
| COPUOS | Committee for the Peaceful Use of Outer Space (United Nations) |
| COROT | COnvection, ROtation and planetary Transits |
| COS | Cosmic Origins Spectrograph (HST) |
| COSAC | Comet Sampling and Composition Experiment (Rosetta) |
| COSIMA | Cometary Secondary Ion Mass Analyser (Rosetta) |
| COSPAR | Committee on Space Research |
| COSPIN | Cosmic Ray & Solar Charged Particles Investigation (Ulysses) |
| COSTEP | Comprehensive Measurements of the Supra-Thermal and Energetic Particles Populations (SOHO) |
| CP | Charge Parity |
| CPM | Chemical Propulsion Module (BepiColombo) |
| CQM | Cryogenic Qualification Model |
| CR | Carrington Rotation |
| CSA | Canadian Space Agency |
| CSDS | Cluster Science Data System |
| CsI | caesium iodide |
| CSSAR | Centre for Space Science and Applied Research (China) |
| D-CIXS | Demonstration of a Compact Imaging X-ray Spectrometer (SMART-1) |
| DESPA | Observatoire de Paris, Département Spatial |
| DFACS | drag-free attitude control system |
| DISR | Descent Imager/Spectral Radiometer (Huygens) |
| DLR | Deutsches Zentrum für Luft- und Raumfahrt |
| DPC | Data Processing Centre |
| DROID | distributed readout architecture |
| DRS | Disturbance Reduction System (LISA) |
| DSDS | Double Star Data System |
| DSN | Deep Space Network |
| DSP | Double Star Programme |
| DSP | Digital Signal Processor |
| DSRI | Danish Space Research Institute |

| | |
|---|---|
| EAS | European Astronomical Society |
| ECF | European Coordinating Facility |
| EFW | Electric Field and Wave experiment (Cluster) |
| EGS | European Geophysical Society |
| EIS | EUV Imaging Spectrometer (Solar-B) |
| EIT | Extreme UV Imaging Telescope (SOHO) |
| EQM | Electrical Qualification Model; Engineering Qualification Model |
| EM | Electrical Model, Engineering Model |
| EOF | Experiment Operations Facility (SOHO) |
| EP | Equivalence Principle |
| EPAC | energetic particle instrument (Ulysses) |
| EPDP | Electric Propulsion Diagnostic Package (SMART-1) |
| EPF | External Payload Facility (Columbus) |
| EPIC | European Photon Imaging Camera (XMM) |
| EPOS | European Payload Operation Services (Double Star) |
| EPS | European Physical Society |
| ERNE | Energetic and Relativistic Nuclei and Electron experiment (SOHO) |
| ERO | Early Release Observation |
| ESA | European Space Agency |
| ESAC | European Space Astronomy Centre (ESA) |
| ESLAB | European Space Laboratory (former name of RSSD) |
| ESO | European Southern Observatory |
| ESOC | European Space Operations Centre, Darmstadt (Germany) |
| ESRIN | ESA's Documentation and Information Centre (Italy) |
| ESRO | European Space Research Organisation |
| ESTEC | European Space Research and Technology Centre, Noordwijk (The Netherlands) |
| EURECA | European Cryogenic Array |
| EUSO | Extreme Universe Space Observatory |
| EUV | Extreme Ultra-Violet |
| Exosat | European X-ray Observatory Satellite (ESA) |
| FEEP | Field Emission Electric Propulsion |
| FES | Fine Error Sensor |
| FGS | Fine Guidance Sensor; Fine Guidance System |
| FINCH | Flexible Interferometer Characterisation |
| FIRST | Far Infrared and Submillimetre Space Telescope (now Herschel) |
| FM | Flight Model |
| FMI | Finnish Meteorological Institute |
| FOS | Faint Object Spectrograph (HST) |
| FOV | Field of View |
| FP | Fabry-Pérot |
| FPA | Focal Plane Assembly |
| FPAG | Fundamental Physics Advisory Group |
| FTE | flux transfer event |
| FTS | Fourier Transform Spectrometer |
| FUV | far-ultraviolet |
| FWHM | Full Width at Half Maximum |
| GaAs | gallium arsenide |
| GC | Galactic Centre |
| GENIE | Ground-based European Nulling Interferometry Experiment |
| GI | Guest Investigator |
| GIADA | Grain Impact Analyser and Dust Accumulator (Rosetta) |
| GMT | Greenwich Mean Time |
| GOODS | Great Observatories Origins Deep Survey |
| GONG | Global Oscillation Network Group |
| GR | General Relativity |
| GRB | Gamma Ray Burst |
| GSE | Ground Support Equipment |
| GSFC | Goddard Space Flight Center (NASA) |
| GSTP | General Support & Technology Programme (ESA) |
| GTO | Geostationary Transfer Orbit |
| HASI | Huygens Atmospheric Structure Instrument |
| HCS | Heliospheric Current Sheet |
| HDF | Hubble Deep Field |
| HEB | Hot Electron Bolometer |
| HEMT | High Electron Mobility Transistor |
| HEW | Half Energy Width |
| HFI | High Frequency Instrument (Planck) |
| HGA | High-Gain Antenna |
| HIFI | Heterodyne Instrument for the Far-IR (Herschel) |
| HMXB | high-mass X-ray binary |
| HPDP | Highly Processed Data Product |
| HPO | High-performance Pore Optics |
| HPOC | Huygens Probe Operations Centre |
| HR | Hertzsprung-Russell |
| HSC | Herschel Science Centre |
| HST | Hubble Space Telescope |
| HUDF | Hubble Ultra Deep Field |
| HZ | Habitable Zone |
| IAC | Instituto de Astrofisica de Canarias |
| IAS | Institut d'Astrophysique Spatiale, Orsay (France) |
| IAU | International Astronomical Union |
| IBIS | Integral imager |
| ICC | Instrument Control Centre (Herschel) |
| ICME | Interplanetary Coronal Mass Ejection |
| IDA | ISO Data Archive |
| IDC | ISO Data Centre |
| IDS | Interdisciplinary Scientist |
| IFTS | Imaging Fourier Transform Spectrometer |
| IKI | Space Research Institute (Moscow) |

| | |
|---|---|
| ILWS | International Living With a Star |
| IMF | Initial Mass Function |
| IMF | Interplanetary Magnetic Field |
| INT | Isaac Newton Telescope |
| INTA | Instituto Nacional de Técnica Aerospacial (Spain) |
| IOA | Institute of Astronomy (Cambridge, UK) |
| IPAC | Infrared Processing Analysis Centre |
| IR | Infrared |
| IRAS | Infrared Astronomy Satellite |
| IREM | Integral Radiation Environment Monitor |
| IRF-U | Institute for Space Physics-Uppsala (Sweden) |
| ISAAC | Infrared Spectrometer and Array Camera |
| ISAS | Institute of Space and Astronautical Science (Japan), now part of JAXA |
| ISDA | ISOC Science Data Archive |
| ISDC | Integral Science Data Centre |
| ISGRI | Integral Soft Gamma Ray Imager |
| ISM | Interstellar Medium |
| ISO | Infrared Space Observatory (ESA) |
| ISOC | Integral Science Operations Centre |
| ISS | International Space Station |
| ISSI | International Space Science Institute, Bern (Switzerland) |
| ISWT | Integral Science Working Team |
| ITT | Invitation to Tender |
| IUE | International Ultraviolet Explorer |
| IUS | Inertial Upper Stage |
| IVOA | International Virtual Observatory Alliance |
| JAXA | Japan Aerospace Exploration Agency |
| JCMT | James Clark Maxwell Telescope |
| JEM-X | Integral X-ray monitor |
| JPL | Jet Propulsion Laboratory (NASA) |
| JWST | James Webb Space Telescope; previously Next Generation Space Telescope |
| KATE | X/Ka-band Telemetry & Telecommand Experiment (SMART-1) |
| KBO | Kuiper Belt Object |
| KHI | Kelvin-Helmholtz Instability |
| KPNO | Kitt Peak National Observatory (USA) |
| KSC | Kennedy Space Center (NASA) |
| LAEFF | Laboratory for Space Astrophysics and Fundamental Physics |
| LAP | Langmuir Probe (Rosetta) |
| LAPP | Laboratoire d'Annecy-Le-Vieux de Physique des Particules (CNRS, France) |
| LASCO | Large Angle Spectroscopic Coronagraph (SOHO) |
| LASP | Laboratory for Astronomy and Solar Physics (NASA) |
| LET | Low Energy Telescope (Ulysses) |
| LFI | Low Frequency Instrument (Planck) |
| LIM | local interstellar medium |
| LISA | Laser Interferometer Space Antenna |
| LMC | Large Magellanic Cloud |
| LOI | Luminosity Oscillation Imager (SOHO) |
| LOWL | Ground-based instrument for observing solar low *p*-modes, High Altitude Observatory, USA |
| LPCE | Laboratoire de Physique et Chemie, de l'Environnement (France) |
| LPF | LISA Pathfinder |
| LPSP | Laboratoire de Physique Stellaire et Planétaire (France) |
| LTP | LISA Technology Package |
| LWS | Long Wavelength Spectrometer (ISO); Living With a Star |
| MBH | massive black hole |
| MCP | Microchannel Plate |
| MDI | Michelson Doppler Imager (SOHO) |
| MER | Mars Exploration Rover (NASA) |
| MGS | Mars Global Surveyor (NASA) |
| Microscope | MICROSatellite à traînée Compensée pour l'Observaton du Principe d'Equivalence (CNES) |
| MIDAS | Micro-Imaging Dust Analysing System (Rosetta) |
| MIP | Mutual Impedance Probe (Rosetta) |
| MIRO | Microwave Instrument for the Rosetta Orbiter |
| MMO | Mercury Magnetospheric Orbiter (BepiColombo) |
| MOC | Mission Operations Centre |
| MOS-CCD | Metal Oxide Semiconductor - Charge Coupled Device |
| MoU | Memorandum of Understanding |
| MPE | Max-Planck-Institut für Extraterrestrische Physik |
| MPI | Max-Planck Institut (Germany) |
| MPIA | Max-Planck-Institut für Astronomie |
| MPIK | Max-Planck-Institut für Kernphysik |
| MPO | Mercury Planetary Orbiter (BepiColombo) |
| MPS | Max-Planck-Institut für Sonnensystemforschung |
| MRO | Mars Recconnaissance Orbiter (NASA) |
| MSSL | Mullard Space Science Laboratory (UK) |
| MTR | mid-term review |
| MUPUS | Multi-Purpose Sensors for Surface and Subsurface Science (Rosetta) |
| MUSICOS | Multi-Site Continuous Spectroscopy |
| MWL | MicroWave Link (ACES) |
| NAC | Narrow Angle Camera (OSIRIS) |
| NASA | National Aeronautics & Space Administration (USA) |
| NGST | Next Generation Space Telescope; now James Webb Space Telescope |

| | |
|---|---|
| NHSC | NASA Herschel Science Centre |
| NICMOS | Near-Infrared Camera and Multi-Object Spectrometer (HST) |
| NIS | normal incidence spectrometer |
| NLR | Narrow Line Region |
| NOT | Nordic Optical Telescope |
| NRAO | National Radio Astronomy Observatory (USA) |
| NSSDC | National Space Science Data Center (at GSFC, USA) |
| NTT | New Technology Telescope |
| OHP | Observatoire de Haute-Provence |
| OLP | off-line processing |
| OM | Optical Monitor (XMM-Newton) |
| OMC | Optical Monitor Camera (Integral) |
| OSSE | Oriented Scintillation Spectrometer Experiment (CGRO, NASA) |
| OSIRIS | Optical and Spectroscopic Remote Imaging System (Rosetta) |
| PACS | Photodetector Array Camera and Spectrometer (Herschel) |
| PAH | Polycyclic Aromatic Hydrocarbon |
| PAM | Payload Assist Module |
| pc | parsec |
| PCA | Proportional Counter Array |
| PCD | Photon Counting Detector |
| PDB | Project Data Base |
| PDR | preliminary design review |
| PDS | Planetary Data System |
| PEN | penetrator |
| PHARAO | Projet d'Horloge Atomique par Refroidissement d'Atomes en Orbit) |
| PI | Principal Investigator |
| PIA | (ISO)PHOT Interactive Analysis |
| PLM | Payload Module |
| PN | Planetary Nebula |
| POS | Payload Operations Service |
| PP | Permittivity Probe (SESAME on Rosetta) |
| PPDB | Primary Parameter Data Base (Cluster) |
| ppm | parts per million |
| PPN | Parameterised Post-Newtonian |
| PROM | Programmable Read-Only Memory |
| PS | Project Scientist |
| PSA | Planetary Science Archive |
| PSE | Probe Support Equipment (Huygens) |
| PSF | Point Spread Function |
| PST | Project Science Team |
| PWA | Permitivity, Waves and Altimetry (part of HASI on Huygens) |
| QM | Qualification Model |
| QPO | Quasi Periodic Oscillations |
| QSO | Quasi Stellar Object |
| R&D | Research and Development |
| RAL | Rutherford Appleton Laboratory (UK) |
| RD | Requirements Document |
| RESSP | Reconstruction of Exo-Solar System Properties |
| RF | Radio Frequency |
| RGB | red giant branch |
| RGS | Reflection Grating Spectrometer (XMM-Newton) |
| RHESSI | Reuven Ramaty High Energy Solar Spectroscopic Imager |
| RMOC | Rosetta Mission Operations Centre |
| ROLIS | Rosetta Lander Imaging System |
| ROMAP | RoLand Magnetometer & Plasma Monitor (Rosetta) |
| ROSINA | Rosetta Orbiter Spectrometer for Ion and Neutral Analysis (Rosetta) |
| ROSITA | Roentgen Survey with an Imaging Telescope Array |
| RPC | Rosetta Plasma Consortium |
| RSI | Radio Science Investigation |
| RTG | Radioisotope Thermoelectric Generator |
| RSOC | Rosetta Science Operations Centre |
| RXTE | Rossi X-ray Timing Explorer (NASA) |
| SAO | Smithsonian Astrophysical Observatory (US) |
| SAp/Saclay | Service d'Astrophysique (Commissariat à l'Energie Atomique; Saclay, France) |
| SAS | Scientific Analysis Software (XMM-Newton) |
| SAX | Satellite per Astronomia in raggi X (Italy/The Netherlands) |
| SCD | Swept Charge Device |
| SCUBA | Submillimetre Common User Bolometer Array |
| SDO | Solar Dynamics Observatory (NASA) |
| SDT | Science Definition Team |
| SED | Spectral Energy Distribution |
| SEP | solar energetic particle |
| SEPP | Solar Electric Primary Propulsion |
| SESAME | Surface Electric, Seismic and Acoustic Monitoring Experiment (Rosetta) |
| SGR | soft gamma repeater |
| SHM | Space Hydrogen Maser |
| SiC | silicon carbide |
| SIM | Space Interferometry Mission (NASA) |
| SIS | Superconductor-Insulator-Superconductor |
| SLP | Segmented Langmuir Probe |
| SMART | Small Mission for Advanced Research in Technology (ESA) |
| SMC | Small Magellanic Cloud |
| SMOG | Survey of Molecular Oxygen in the Galaxy (SMART-1) |

| | |
|---|---|
| SN | Supernova |
| SNR | Supernova Remnant |
| SOC | Science Operations Centre |
| SOHO | Solar and Heliospheric Observatory |
| SOI | Saturn Orbit Insertion |
| SOPC | Science Operations & Planning Computer |
| SOS | Silicon-on-Sapphire |
| SOT | Science Operations Team; Solar Optical Telescope |
| SPC | Science Programme Committee (ESA) |
| SPDB | Secondary Parameter Data Base (Cluster) |
| SPEDE | Spacecraft Potential, Electron & Dust Experiment (SMART-1) |
| SPI | Integral spectrometer |
| SPIRE | Spectral and Photometric Imaging Receiver (Herschel) |
| SQUID | superconducting quantum interference device |
| SRG | Spectrum-Roentgen-Gamma |
| SRON | Space Research Organisation Netherlands |
| SRR | system requirements review |
| SSAC | Space Science Advisory Committee (ESA) |
| SSP | Surface Science Package (Huygens and Rosetta) |
| SSWG | Solar System Working Group |
| ST | Science Team; Space Technology (NASA) |
| ST-ECF | Space Telescope European Coordinating Facility |
| STEP | Satellite Test of the Equivalence Principle |
| STEREO | Solar-Terrestrial Relations Observatory |
| STIS | Space Telescope Imaging Spectrograph |
| STJ | Superconducting Tunnel Junction |
| STOC | Science and Technology Coordination |
| STScI | Space Telescope Science Institute |
| STSP | Solar Terrestrial Science Programme |
| STWT | Science & Technology Working Team |
| SUMER | Solar UV Measurements of Emitted Radiation (SOHO) |
| SVM | Service Module |
| SWAN | Solar Wind Anisotropies (SOHO) |
| SWG | Science Working Group |
| SWS | Short Wavelength Spectrometer (ISO) |
| SWT | Science Working Team |
| TC | Tan Ce (‘Explorer’, China) |
| TF | tunable filter |
| ToO | Target of Opportunity |
| TRACE | Transition Region & Coronal Explorer (NASA) |
| TRP | Technology Research Programme (ESA) |
| TWTA | Travelling Wave Tube Amplifier |
| UCB | University of California Berkeley |
| UCLA | University of California Los Angeles |
| ULIRG | Utra-Luminous IR Galaxy |
| UV | Ultraviolet |
| UVCS | Ultraviolet Coronal Spectrometer (SOHO) |
| VILSPA | Villafranca Satellite Tracking Station |
| VIRGO | Variability of Irradiance and Gravity Oscillations (SOHO) |
| VIRTIS | Visible Infra Red Thermal Imaging Spectrometer (Rosetta) |
| VLA | Very Large Array |
| VLBI | Very Long Baseline Interferometry |
| VLT | Very Large Telescope |
| VO | Virtual Observatory |
| WAC | Wide Angle Camera (OSIRIS on Rosetta) |
| WEC | Wave Experiment Consortium (Cluster) |
| WFC | Wide-Field Camera |
| WFE | wavefront error |
| WFI | Wide-Field Imager |
| WFPC | Wide-Field Planetary Camera (HST) |
| WHT | William Herschel Telescope |
| WMAP | Wilkinson Microwave Anisotropy Probe (NASA) |
| WWW | World Wide Web |
| XEUS | X-ray Evolving Universe Spectroscopy mission (ESA) |
| XMM | X-ray Multi-Mirror Mission (ESA) |
| XRT | X-ray Telescope |
| XSA | XMM-Newton Science Archive |
| XSM | X-ray Solar Monitor (SMART-1) |